Swansea University
Prifysgol Abertawe

Investigation into the Mechanical Properties and Microstructure of Stainless Steel 316L Additively Manufactured Parts

Bethan Hannah Girling MEng
Swansea University

Submitted to Swansea University in fulfilment of the requirements for the Degree of Doctor of Philosophy

March 2026

Summary

This thesis investigates Additive Manufactured (AM) Stainless Steel (SS) 316L parts using detailed experimentation and optical microscopy. Additive Layer Manufacturing (ALM) is a process of manufacturing parts by building them up layer by layer. Selective Laser Melting (SLM), which is the method investigated in this work, is a method by which consecutive thin layers of powder are melted by a laser in a pattern pre-defined by a CAD forming the cross section of a component. Although it's a technology that is becoming mainstream in industry, there are still certain areas, which are not fully understood. The research here is aimed at finding out more on how built parts are affected by the process. This has been carried out by building a selection of parts using the same CAD designs but changing the parameters and powder used and subsequently measuring and testing these. Different laser powers, exposure times, laser patterns, layer rotations and heat treatment have been explored along with 'virgin' and 'aged' powder. A number of experimental tests including tensile, density and hardness were carried out, to investigate the variation seen in the properties of the manufactured AM parts due to the changing build parameters and due to powder reuse. These properties are then compared to conventional SS316L. In cases, parts with inadequate properties were found along with a majority more cases where parts with comparable properties to conventional SS316L were found. In addition to the properties of the parts, the microstructure has also been studied to see how this compares to conventional SS316L. It was found that parts produced by AM vary in microstructure and properties when compared to conventional SS316L.

Declarations

This work has not previously been accepted in substance for any degree and is not being concurrently submitted in candidature for any degree.

Signed ..... [redacted] ..... (candidate)

Date .....31st March 2026.....

This thesis is the result of my own investigations, except where otherwise stated. Other sources are acknowledged by footnotes giving explicit references. A bibliography is appended.

Signed ... [redacted] ..... (candidate)

Date .....31st March 2026.....

I hereby give consent for my thesis, if accepted, to be available for electronic sharing.

Signed .... [redacted] ..... (candidate)

Date .....31st March 2026.....

The University's ethical procedures have been followed and, where appropriate, that ethical approval has been granted.

Signed .... [redacted] ..... (candidate)

Date .....31st March 2026.....

Acknowledgements

Firstly, I would like to thank my supervisor Professor Sienz for giving me the opportunity to undertake this PhD and all of his help with it including help with checking my thesis.

I would also like to thank, Dr Helen Davis for her help with my experimental and microstructure work, Dr John Cherry for his help with using the AM machine and running the experimental tests and Dr Liz Sacket for all of her help with my experimental and microstructure study and for helping me with checking the corresponding chapters for me, thanks go to Dr Ben Cockings for his help with the residual stress test preparation and testing.

I would also like to thank Dr Nick P. Lavery for his help with my experimental work and Dr Sha Mehraban for all of his help with the tensile testing and both of their extensive help during the resubmission of this thesis.

Thanks also go to AWE, all my line managers during this work, Greg McNally, Mark Carne, and the rest of the AM team, Lucy Cowley and Dave Richards, for all of their support and time allowances whilst I have been writing my thesis and the hands-on experience I have gained through my work in AM.

Finally, I would like to thank, my partner George Valvona and son Oliver for all of their support and being so understanding while I have been completing and writing up my PhD, along with the rest of my family for all of their support whilst I have been studying for my degree and PhD, it has been gratefully received.

Table of Contents

Table of Tables

Table of Figures

Abbreviations

ALM – Additive Layer Manufacturing

AM – Additive Manufacturing

ASTM – American Society for Testing and Materials

BP – Build Programme

CAD – Computer Aided Design

CIP – Cold Isostatic Pressing

CNC – Computer Number Control

CoCr – Cobalt Chromium

CT – Computerised Tomography

DMLS – Direct Metal Laser Sintering

EBM – Electron Beam Melting

EDM – Electrical Discharge Machining

ELI – Extra Low Interstitial

FDM – Fused Deposition Modelling

HIP – Hot Isostatic Pressing

HT – Heat Treatment

ISO – International Organization for Standardization

LSFF – Laser Solid Freeform Fabrication

MTC – Manufacturing Technology Centre

NC – Numerical Control

NDT – Non-Destructive Testing

NIST – National Institute of Standards and Technology

PBF – Powder Bed Fusion

PSD – Powder Size Distribution

SDL – Selective Deposition Lamination

SEM – Scanning Electron Microscope

SLA – Sterolithography

SLM – Selective Laser Melting

SLS – Selective Laser Sintering

SPC – Statistical Process Control

SS – Stainless Steel

SSS – Sold State Sintered

STL – Standard Template Library

Ra – Roughness Average

RP – Rapid Prototyping

UTS – Ultimate Tensile Strength

WLI – White Light Interferometry

XPS – X-ray Photoelectron Spectroscopy

XRD – X-ray Diffraction

Yb-Fibre – Ytterbium Coated Fibre

YM – Young's Modulus

YS – Yield Stress

Nomenclature

E_d = Energy Input

P_{laser} = Laser Power

T_{melt} = Melt Temperature

Chapter 1 Introduction

1.1 Background

Additive Layer Manufacturing (ALM) is seen by many as a new manufacturing methodology, but without us consciously calling it like that, it is a technology that has been around for a long time in many different guises, a classic method of Additive Manufacturing (AM) is house building; this is an additive process as the house is built layer by layer. In the last twenty years, AM has started to be used to create highly intricate new engineering products. AM is a method that is used to produce parts by adding layers rather than subtracting material as is done in conventional manufacturing.

Stereolithography (SLA) was the first AM method to be established. This was the starting point for all future AM methods. It works by having a vat of liquid polymer and using a laser to cure the photosensitive resin to the required shape for each layer [1]. The first machine was built in 1986. The first patent for an AM machine was requested in 1986 by Charles W Hull for a US patent for an SLA machine [2]. But the first machine to be used was 3D Corporations' SLA – 250 in 1988 [2]. As can be seen AM has been around for many years.

Since its beginning, the process of AM has improved dramatically. There are now more than 10 different Rapid Prototyping (RP) methods in use including SLA, Selective Laser Sintering (SLS), Selective Laser Melting (SLM), Direct Metal Laser Sintering (DMLS), Electron Beam Melting (EBM) and Fused Deposition Modelling (FDM).

After the SLA machine was patented, there were numerous patents in quick succession for different methods. The patents filed were for varying machines, with no single machine having all of the solutions to what is required. The history of AM machines after SLA moved to RP, which is now over two decades old and is the first process of this type. In 1986 the first RP machine was sold [3]. EOS, Electro Optical Systems [4] was the first company to produce an AM machine that works with metals, it was a Direct Metal Laser Sintering (DMLS) machine. They were founded in 1989 and the commercial release of their first machine the M250 was in 1994 with the first delivery in 1995 [5]. DMLS started with a CO_2 laser but it was later replaced with a fibre laser as it has better properties than a CO_2 laser [5]. Since 2002 Fused Deposition Modelling (FDM) has been one of the top choices for RP because of its ease of use and flexibility of manufacturing plastic prototypes [6]. For metal processing the technology trend has

moved toward SLS and Selective Laser Melting (SLM). AM is a quickly evolving technology gaining attention in the public eye and drawing from across the research community and from industry.

AM works through a process of building parts up layer by layer. This can be either in a powder bed or by laying layers or lines of extruded polymers or metals. As mentioned previously there are a number of AM process.

AM is a layer up manufacturing process, more details in section 2.3. Objects are designed using Computer-Aided Design (CAD) software, and the geometry is exported as a Standard Template Library (STL) file. These files are processed using the relevant 3D printing machines software. The software processes the STL's to generate the slices (build layers). This data is then transferred to the build system and the build process begins. This typically happens within a powder bed or by the application of extruded material to a base plate but can be cured in a vat system. Both polymer and metal systems can operate using powder beds or extruded material. Ceramic type components can also be build using powder bed systems, but these require further firing to cure the parts after manufacture.

Polymer systems are usually FDM machines where the material is extruded in the desired pattern on to a base plate, layer by layer to build up the part. This method of producing parts varies by system but does not always require support material to be laid down during the process. These parts are removed from the build plate after they are finished, usually by hand before having the support removed and being ready for use.

A powder bed system is typically an SLS or SLM system, these are designed to melt the powder in the desired shape and usually require supports to be applied which are built using the same material for metal parts. For a polymer material no support is required. The first layer of powder is laid down and melted and this continues layer by layer until the part is completed. Subsequently the part attached to the base plate is removed from the machine, including any excess powder surrounding the build. The part may then require heat treatment, if manufactured in metal, to relax any residual stresses before it is removed from the base plate. The removal is usually done using a band saw or wired erosion. Once the part has been removed from the base plate the supports are removed. Parts produced this way can often have a dimpled surface and so may need to be finished using traditional finishing techniques. In addition, parts produced by this method are not 100% dense because of the manufacturing process.

Finishing processes are used that include Hot Isostatic Pressing (HIP), which can make the parts 100% dense. During manufacture, parts can develop build related defects; including cracks, warpage and shrinkage, which in extreme cases can render the part unusable.

The machines used for the experimental part of this work is a Renishaw AM250 AM machine or an AM400 [8] which both operate using SLM. This method is often confused with SLS. The difference lies in the fact that the SLM completely melts the powder to form the metal parts, whereas SLS only sinters the powder so it fuses on a molecular level [8]. The SLM process works by scanning the pre-defined pattern over the powder layer using a ytterbium fibre laser [7] to fuse the powder into a metal part with no binder required. The build process happens within the confined build chamber of the machine under an inert atmosphere.

Also SLM parts could be used with no finishing processes [9]. To achieve a smooth surface finish, finishing processes are often employed. This new technology has significant potential for many industrial applications. Therefore, it is being studied in detail by an increasing number of researchers around the world investigating a number of different areas, such as the materials used or the process parameters employed, to see where improvements can be made.

The build area and laser set up typical for a machine like the Renishaw AM250 is illustrated in Figure 1:1. This shows a schematic of how the system operates. As can be seen here the powder is spread over the build area forming a thin layer approximately 50µm thick, which is melted by the laser and then the build platform is lowered and powder is spread over the already built part surrounded by the powder bed, and the process repeats itself. This has been explained in further detail in the Literature Review Chapter 2.

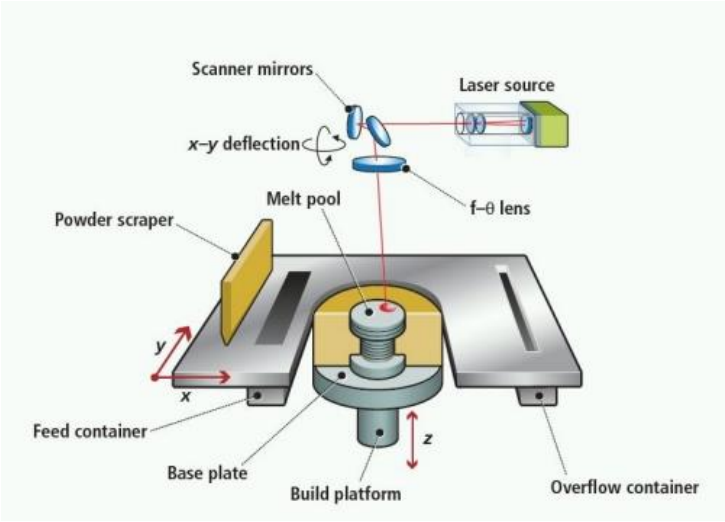

Figure 1:1: SLM Build Area [10]

There is a variety of materials available to use with machines of this type, including different Stainless Steels (SS), Titanium and Aluminium, with new materials with specific material properties and/or better suitability for this manufacturing process being developed.

AM is increasingly being used due to the inherent ability to build highly complex parts that require little or no further processing but also because the AM process has less wastage of material due to its net shape manufacturing feature [11]. The increasing maturity level of ALM manufactured parts and therefore increased industrial uptake can be seen for instance in the aerospace industry where ALM cooling ducts used in F-18 jet fighter have been manufacture using ALM for over 13 years, Other examples include air ducts and other non-critical parts on the 787 Dreamliner [6]. Despite the uptake in industry, there are still knowledge gaps in the AM processing of metals. The work here aims to research some specific areas to enhance the knowledge base in the field. Specifically, the work concentrates on the use of the in-house machine Renishaw AM250 and explores aspects of the SLM technology and its impact on material properties for the widely used stainless steel 316L when comparing with traditionally manufactured SS316L components.

1.2 Summary of Literature Reviews

1.2.1 Initial Research

During the review of the literature, it was realised that although there is information available about the build processes that have been developed in the AM field, the following issues were found:

- Limited information is available looking at using different laser patterns; meander or stripe, to build up the parts.
- Little to no information is available on the microstructure of SS316L AM produced parts.
- Limited work has been performed studying aged powders and the effect of heat treatments or HIPping on parts' properties.

For this reason, the work in this thesis has been designed to allow for a full examination of using different build parameters; laser power, laser pattern, exposure time and layer rotation, to manufacture components that can be studied to establish how these affect the build properties. Along with this work, an investigation into the effect of aged powder and heat treatment on AM parts and AM SS316L parts' properties has been carried out.

The results produced will help define how the build parameters affect the properties of AM parts. This will help fill a gap in the AM research about the most suitable parameters required to get the best properties. Thereby helping others to further develop the knowledge base and understanding of using AM processes to build parts that can be routinely used in industry.

Therefore, the key aim of this work is through numerous, systematic builds and extensive testing using available in-house equipment and the widely used SS 316L material to study the build parameters' effects on AM parts' properties. This is done by specifically focusing on the changes seen in imaging of fracture surfaces and microstructures thereby drawing valuable conclusions to enhance the AM knowledge base.

1.2.2 Subsequent Research

Due to the time passing between the initial literature review being undertaken in 2010 and the subsequent submission in 2023 it was decided to carry out an additional literature review to see how the AM industry and research has progressed and ensure the work is still relevant. The knowledge base has progressed, with publications on AM and mechanical properties increasing each year, approximately 1250 were released in 2020 [208]. When specifically looking at microstructure variations and failure modes this area is still being investigated. Key findings of the subsequent literature review found:

- Limited information is available defining how build parameters, microstructure and failure mode are linked.

The key aim of this work is as before to define a test protocol and test programme for the evaluation and characterisation of the performance of new machines and powders. This work is continued as the knowledge gap still exists. Looking at build parameters' effects on AM parts' properties, by specifically focusing on the changes seen in imaging of fractures and microstructures thereby drawing valuable conclusions to enhance the AM knowledge base further. This information also helps continuing developing the information needed to help define a closed loop system to produce high quality parts, monitor the development of defects and compensate for these during the build process. The results have shown that changes to the processing parameters effects the microstructure which in turns affects the quality of the component produced. Defects present within the part and microstructure lead to reduced mechanical properties and these defects have been reduced in quantity by using the optimum processing parameters.

This knowledge gap still exists as it is a complex area to study; manufacturing, materials properties, failure modes etc, requiring multiple disciplines and this is often not seen in one team unless there is the eco system around the team to develop all of the required knowledge.

1.3 Objectives

The key aim leads to the following objectives of the work within this PhD, which are to:

- Conduct optical and microstructural characterisation of SS316L AM components.
- Perform comparative mechanical testing to compare AM and conventionally manufactured component properties.
- Systematically investigate the effects of laser input energy, scan strategies and build parameters on mechanical properties and microstructure.
- Evaluate the impact of heat treatment on mechanical performance and microstructure.

1.4 Layout of Thesis

First AM samples are studied to investigate their properties. Then the meso/micro structures of the samples will be investigated to see how these compare to conventional metal properties. Sample parts made by AM will be studied to see if defects occur.
This work has been spread over the entire course of this PhD and includes three build programmes within the different sections that have been tied together to produce this thesis.
The thesis has the following chapters:

- Chapter 2 is the literature review looking into what is already known about AM and what kind of parts are produced by these methods.
- Chapter 3 presents the development of the method for the experimental work that has been used to establish the best build parameters for SS316L AM parts.
- Chapter 4 is the analysis of the experimental results and study of what has been found from the experimental work. This includes building a series of tensile samples that were machined and tested in various conditions including standard tensile testing, stress annealed, and heat treated.
- Chapter 5 contains the discussion of the experimental results and how findings relate to previous research.
- Chapter 6 presents the conclusions and future work.

Chapter 2 Literature Review

2.1 Introduction

The purpose of this review is (i) to investigate the Additive Manufacturing (AM) methods that are available, (ii) to understand the current knowledge base for the AM industry and (iii) understand what properties can currently be achieved and the gaps that need to be filled. Furthermore, the properties of AM parts and how these compare to conventional parts due to changes to the manufacturing parameters and powder are investigated. This research has also studied the history of AM and its potential future since AM is a rapidly developing technology for current and for future manufacturing methods used for instance in the aerospace industry to reduce parts count, aircraft weight and emissions and many other industries.

Additionally, the review is looking to establish where AM knowledge currently stands and what work needs to be carried out to help improve and develop this knowledge.

In 2013 the AM industry was believed to be worth approximately US$3000 million and is still growing [13], this is the reason why investigations into AM to help the industry develop and researchers and customers to better understand AM and the parts it produces are necessary. According to Wohler's by 2022 the revenue of the AM market was more than $15.2 billion [208].

This review has found that research into AM is an ever-growing area. As research has progressed it has moved from looking at which parameters to use to make the highest density parts with the best mechanical properties into how to monitor the components during the build and qualification of AM parts. To enable these areas to grow standards are being developed, monitoring systems incorporated into university based systems and now OEMs are adding then to machines as they are manufactured. All of this is generating large datasets that need to be stored, updated and analysed to support qualification activities.

It was noted during this review that defects occurring during the build process are being investigated more than was previously seen. Research is looking at how these are caused, what parameters effect these defects and if they can be seen during the build process. Once more is known it is hoped that methods can be created to help reduce and/or eliminate these.

The previous work on this began generating a closed loop system investigating the effect processing parameters have by generating builds of components manufactured

using varying processing parameters. Building the samples and mechanically testing them, studying the fracture surface and microstructure under the microscope to begin finding patterns and links between processing parameters and failure mechanisms. The work uses data analysis to get a set of parameters giving the best possible quality outcome to allow developers to shorten time to set up machines and give high quality finished components. There was no time during the work to close the feedback loop, but this is an area of future work that is recommended to be progressed.

This work is a supplemental literature review to investigate how the Additive Manufacturing (AM) industry's research has progressed since the initial PhD work was carried out between 2010 and 2015. It will look at the following areas:

- Standards and AM qualification
- Powder including:
    - Powder reuse
    - Powder ageing
- Processes including:
    - Scanning strategies
    - Build parameters
- Component defects including:
    - Deformation, cracking, and warpage
    - Porosity, voids, and lack of fusion
    - Keyhole
- Heat treatment
- Mechanical testing
- In-Situ monitoring
- Modelling
- Simulation and digital twins
- Closing with conclusions and limitations

Since work began in 2010 the AM industry has progressed rapidly. Focus has shifted from manufacturing optimisation to qualification strategies.

There are parts in service on aircraft including the Boeing 787, which is one of the aircrafts that contains AM parts; these are 3D printed fuel nozzles made of titanium [156]. Other areas are beginning to use them for in-service components, but these are currently all non-critical components. To fully understand and qualify AM component

performance further research needs to be carried out to understand the effect of processing parameters on failure modes and their causes.

When looking outside the AM industry microstructure and failure modes have been linked in numerous research papers however this is still not the case for AM. This PhD has developed a methodology to investigate process parameters, the microstructures they generate and how the failures modes are affected by these changes.

Understanding this will allow for optimisation of the build parameters to develop components with the microstructure and failure mode understood to predict how the component will perform and how to avoid failure.

The aim of numerous R&D groups investigations into AM are to help develop high quality components and eventually mitigate against the unexpected failures seen in service of AM components that are not fully understood. There are many causes of failure including: lack of fusion, deformation and warpage, delamination of layers, cracking, keyholes, pores and residual stresses. These failure causes are roadblocks to overcome for AM process acceptance and qualification. These are areas current research is trying to understand so that AM component qualification can be achieved [157].

This review has seen that the AM industry has developed over the last 10 years, research has started to investigate a wider variety of materials along with looking into more specific research cases. All of this is alongside improved modelling and predictive capabilities for the process and outcomes.

2.2 Manufacturing Classification

Manufacturing is a large industry that can be split into many sections as shown in Figure 2:1 and Figure 2:2. There are two main sections. There are the near net shape and the non-net shape technologies. Near net shape means that when the part is manufactured the piece is close to its finished shape and might require some or little surface finishing, whereas non-net shape means that the part requires extensive finishing to achieve the desired final shape. Both of these areas can then be broken down further to look into the different manufacturing techniques that produce parts of this type. Near net shape manufacturing techniques include for instance casting and injection moulding. As mentioned, these parts require little surface finishing and so reduced lead times can be achieved if the required moulds are already available as well as reduced costs. However, moulds can be expensive and complicated to produce. Non-net shape techniques include milling and turning. These methods leave parts that

require extensive material removal followed by finishing. As a consequence, these methods can often take longer unless you need to manufacture, for instance a mould for injection moulding. These manufacturing types can then be broken down further to reveal techniques that use different materials and how they fit into the manufacturing classification. Figure 2:1 and Figure 2:2 show the manufacturing processes, depicting methods like AM and RP that are the same manufacturing technique but work using different substrates and have been categorised under RP for this breakdown. Using different substrates can affect the manufacturing process and the results produced. RP produces parts with poorer surface quality due to its manufacturing speed and process and also these parts do not have the same mechanical properties as AM parts and so cannot be used in the same situations. AM parts are in the near net shape section of the diagram below as they are produced to a standard where the finishing requirements are low.

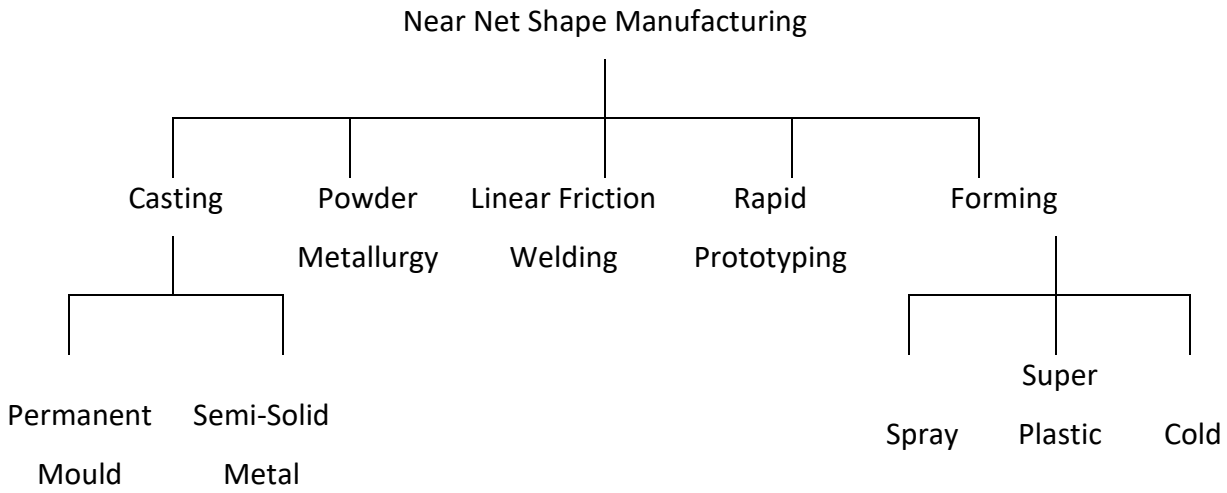

Figure 2:1: Near Net Shape Manufacturing Breakdown

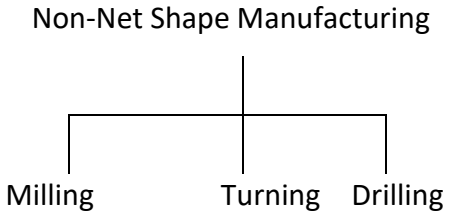

Figure 2:2: Non-Net Shape Manufacturing Breakdown

The different types of AM methods can be broken down into the type of material used or the type of technology used. This can be seen from Figure 2:3, RP produces a

prototype design of a part that can be studied before many are built whereas AM is a process to build parts for use in industry.

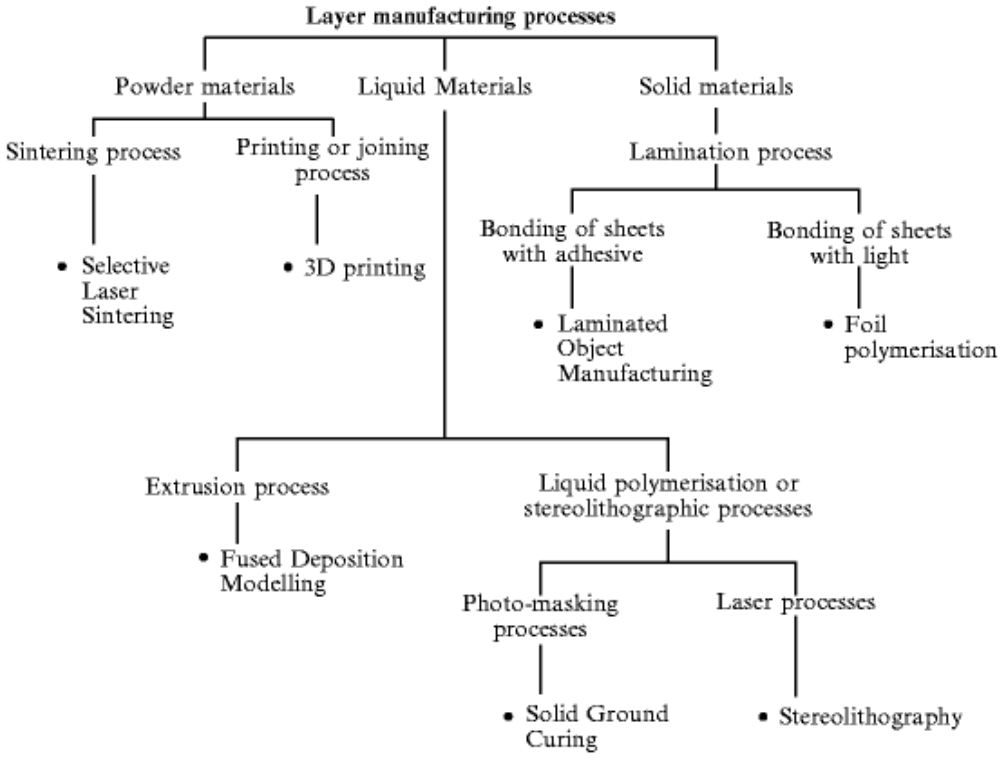

Figure 2:3: Layer Manufacturing Processes [14]

2.3 Additive Manufacturing (AM)

AM is a manufacturing process that has evolved and makes contributions to further manufacturing. It is a process by which parts are generated by building up layers of the part. It is a modern, fast process that requires less tooling than current techniques. It is a fast process in the sense that from designing the part to the finished piece is quicker than conventional techniques due to the machine being able to manufacture the part without the need for specialist tooling [11]. This tooling can be something like the mould, which the molten metal is set in to create the shape of the part. AM techniques are also faster than conventional techniques as near net shape parts come straight out of the machine with less surface finishing needed and also no need to remove less excess material as the part is built with less of this material. It is a process that can currently only be used for smaller parts built within machines as the build chambers in the machines are still quite small, but there are examples coming through of 3D printed larger structures including a bridge in Madrid [15]. Nevertheless, as the technology improves, and more is known about the techniques used it can be improved and developed to allow larger and larger parts to be produced.

AM as the name implies, is an additive process. This means that parts are created by adding material to what is already there. This is unlike current manufacturing techniques like milling which are subtractive. This is where material is removed from a billet to produce a part. Subtractive manufacturing requires material to be removed to manufacture the part and therefore waste material is an issue increasing the cost of the finished component. Changing the manufacturing technique to AM can allow for the removal of excess material in the design stage and so reduce both the cost and weight of the part [16].

AM is a good method for creating medical implants, aerospace and mechanical parts [16]. When the parts are created, they are very close to 100% dense and with a minimal amount of finishing they can become 100% dense. One of the problems with parts made using this method is that the parts are made using a powder and as the parts are sintered, they are sitting in the excess powder. This means that the surface texture of the final part is pitted. In some cases, including when medical implants are being created, pitting on one side can be good as it helps to promote bone growth to the implant. However, in aerospace parts, this is not desirable, and so surface polishing is often required after the part has been formed.

All of the different methods build the parts up within the housing of the machine, but the machines work in different ways with the basic principles of the processes the same. Firstly, they all work with powder, filament, or liquid within the machine. There are different types of material available, and they can only be used in certain machines. Some machines work with plastics while others work with metals. For making high-cost industry parts metal is required but within this review, processes that make plastic parts will also be looked at as these can be used for prototyping parts before they are made out of expensive metals.

Prototyping is carried out because it can be used to see if the CAD designs, that have been created, are able to be fully manufactured and have no mistakes or conflicting parts. They can also be used to produce parts that can be looked at and visually inspected by staff to see if the design is what they are after and then prototypes can be given to customers, managers and other stakeholders to look at and touch a new product before they are manufactured in bulk. However, the main reason that aerospace companies would produce prototypes is that they need to ensure that the parts they have created, in models, are appropriate for the jobs that they are required for.

As stated, AM is a technology implemented in a number of processes; some of which are detailed below. CAD designs – created in a traditional manner for AM parts - are transferred as an *.STL* file onto a computer attached to the AM machine. This computer contains software, which is designed to slice the design into small layers. For example:

- Renishaw – QuantAM [17],
- Stratasys – GrabCAD [18],
- EOS – EOSINT [19].

These are the layers that will be created within the machine; they have a typical thickness of approximately 20 - 100 µm for powders and liquids, between 100 – 350 µm for filament to create a finished part. The production machine is then programmed to create the part, it processes individual slices, and the part is formed by melting or adding material forming the cross-section of a slice using the different AM methods. This is controlled by the machine's computer, which operates the laser or extrusion head, to follow a set course. This process continues with the part moving down after each layer is formed until the whole part has been manufactured. These different methods will be explained in more details shortly as all of the methods vary slightly.

2.3.1 AM Processes

As mentioned in section 1.1 there are a number of AM process which vary the production method of parts.

RP is a process that typically uses plastics to produce freeform models or parts quickly. The process works by creating a part using a 3D CAD design, as with all types of AM. As with other AM processes the model of the part is cut up into slices of a width of 0.005 inches (≈ 0.127 mm) [20].

SLS is a process that is undertaken using a CO_2 laser to melt and fuse the powder particles together to form a part [21]. In the SLS process the laser is not directly applied to the powder but is reflected onto it using a system of galvano mirrors [22]. It is typical that SLS can make parts with tolerances between 0.002 to 0.01 inches (0.0508 to 0.254 mm) [21]. This process uses nearly 100% of the material and so little wastage occurs making this process more economical and sustainable than creating for instance milled parts.

SLS can create parts that are nearly 100% dense and with the addition of HIPping this will make parts 100% dense [23], [24]. It has also been found that parts created using SLS/HIP do not need a container for HIPping, have reduced pre-processing time and

less post-processing steps [24], [25], which leads to easier and quicker to manufacture parts.

There are two types of SLS. The first type is Direct SLS and the other is Indirect SLS. Indirect SLS uses a binder to coat the metallic powder and it is the binder and not the metal powder that is melted. This melted binder then holds the powder together, but the problem with using indirect SLS is that parts made this way are porous and still include the binder so must be debinded and sintered to make the parts hard. Going through these extra processes loses time and means that dimensional accuracy is affected because of shrinkage [26]. The other method, Direct SLS, is thought to be better as it offers higher accuracy parts as no binder is used, but parts created this way are not 100% dense. Parts can only be made to around 70% dense and so further finishing like HIPping is needed to create 100% dense parts that can be used [26], but it is not always necessary to carry out post-processing [27]. So direct SLS produces more accurate parts but does not reduce the time to create them [26].

DMLS is different from SLS as it applies a low scan speed, inert gas atmosphere and high power laser. This is done to ensure full melting of each layer and to try to remove the balling phenomena [28]. The layers are typically 0.02 mm thick [29]. This method uses powder, the most commonly used powder for EOS machines is Ti6AL4V, which is standard Ti6Al4V metal which is a fine powder [30]. This powder can be sintered without being coated in a binder or plastic, which would have a low melting temperature when used in other methods [31]. A typical laser type used could be the 200W Yb-fibre laser (ytterbium coated fibre) [29] to fuse the metal powder together in the shape of the part. In the EOSINT M250 the laser has a wavelength of 10.6 μm and a spot size of 0.3 mm, but this can be adjusted in later machines [32]. Excess material is removed from the parts using compressed air and paint brushes to ensure that the part is not damaged [32].

DMLS has benefits that include the fact that it is faster than traditional methods but also the fact that this method needs no special tooling as the part comes out in the desired shape. It has been seen by the company Du-Puy that lead times have been reduced by as much as 50% [33]. Another thing about DMLS that is a positive is that it requires no pre-heating unit and no inert gas atmosphere needs to be used when working with bronze based powders [32].

It has been seen that DMLS and SLM machines can in fact be used to produce some of the parts required to manufacture these machines [11], this showcases what these

machines are capable of and how machines making machines will develop as these machine mature.

EBM is a process that is designed by the company Arcam [34]. This process is that it is a solid freeform fabrication process which is used to produce fully dense parts [35]. As with the other methods, a layer of powder is laid down which is melted by an electron beam gun [36] using the layers created from the CAD design.

EBM parts are formed in a hot bed process. This means that the environment in which the parts are formed is heated, to between 700°C and 1000°C, as this can stop problems occurring that are due to the rapid heating and cooling of parts during formation. One of the problems removed is the formation of residual stresses that no longer occur [5]. EBM forms parts that are 100% dense, therefore removing the need for post processing [5]. This is all possible because this method brings the powder much closer to its melting point.

Also the cost of building parts using EBM has been found to be less than SLS, DMLS or other additive methods [36] and the high temperature in the machine and material also helps to decrease build times [5].

A paper by Zah and Lutzmann [37] looks at modelling the EBM process and then validating the results using experimental work. This work found that depending on the scan speed and bean power it was possible to predict if there would be melting, delamination or balling formed, see Figure 2:4.

Figure 2:4 shows that with too high a scan speed delamination occurs and with too little beam power, no melting occurs.

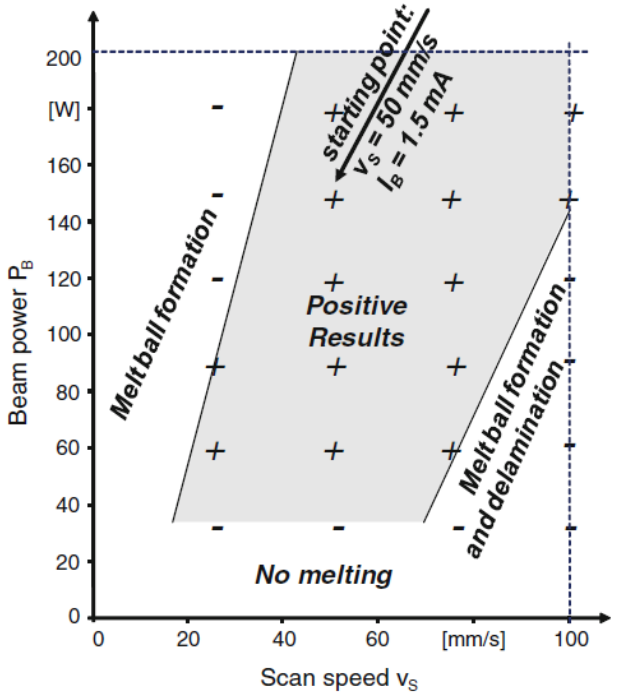

Figure 2:4: Process Parameter Window SS [37]

It was established that FDM can only be used for making plastic parts and so it has not been studied in great detail, it is a good method for producing prototypes or durable single piece parts [38]. However, this method like RP could be used to manufacturer prototypes before metal parts are created, but this method is slower than RP so that may be chosen over FDM.

FDM uses a thermoplastic filament which is heated and moved using a Numerical Control (NC) machine, which then creates the part [39]. Once the material is exposed, it hardens forming the part. It is an additive method, because it still works on the process of laying down layers, which solidifies to form the part. This method is different from the others looked at because instead of melting powder or liquid in the required areas for FDM the material comes through the nozzle and is laid out in the pattern required.

2.3.2 Selective Laser Melting (SLM)

All the above-mentioned processes can be used to manufacture AM parts. This investigation has focused on looking into SLM. This is because Swansea University owns an AM250 Renishaw system which operates using SLM. SLM is a modern metal AM build process that will be investigated further during this work. Although many AM processes are very similar, they have been given different names depending on the company who invented them and what the process does. SLM is very similar to

SLS in that they both use the same method to build the parts the only difference is that SLM goes a step further in that it completely melts the particles [8], producing a solid homogenous mass, whereas SLS heats the powder so that it only fuses the powder together. The laser in SLM is used to completely melt the powder producing a homogeneous part [8]. SLM produces parts that contain fewer voids and therefore are stronger.

The SLM process that was described earlier in Chapter 1 Introduction, is able to produce parts that are 99.8% dense [40]. The process is used by several machine manufacturers including Renishaw and SLM Solutions. SLM processes work using atomised powder. There is a growing variety of different metal powders available.

The use of SLM has more rapidly expanded as a method for producing AM parts due to it fully melting powder particles leading to improved properties when compared to SLS manufactured parts [41]. This method also produces close to fully dense parts with reduced residual stresses due to pre heating [41]. Researchers investigating SLM are now starting to investigate how the build parameters can be changed to help improve the mechanical properties to allow for improvement to SLM parts so that they are comparable to EBM and conventional parts.

SLM has grown as a method for producing AM parts due to it fully melting powder particles, this has led to improved properties when compared to SLS parts. There are other major machine manufacturers who use different processes and one of these is Arcam who use EBM. This method also produces close to fully dense parts with reduced residual stresses due to pre heating [41]. Those investigating SLM are now starting to investigate how the build parameters can be changed to help improve the mechanical properties to allow for improvement to SLM parts, so they are comparable to EBM and conventional parts. Sintering of parts leads to blistering, distortion and shrinkage [42] this is the reason SLM is chosen over SLS.

SLM and other AM processes have increased in popularity as the processes have been shown to decrease the number of parts required, by consolidating parts when designing, as well as helping to overcome conventional manufacturing's limitations [43]. For this reason teams of researchers including Kruth, have been investigating AM processes for a number of years, they have noted that AM parts are effected by the basic laser-material interaction [44] and for this reason numerous studies now need to be carried out to further understand the effects and how this affects the parts properties.

2.3.3 Properties

Testing on SS316L AM parts has found that parts with a UTS of 565MPa [45] can be achieved through SLM and a hardness of 222HV [46] has been achieved by SLM but detailed information on how they might change with the parameter of the manufacturing process employed is not available. Both of these values exceed the minimum required by ASTM [47] and are in excess of those found in conventionally manufactured material. Further investigations into these properties can be found in Chapter 4, Results.

2.3.4 Reasons for AM

AM's potential is increasing as it has the opportunity to reduce part count, manufacturer complex designs, reduce capital costs and reduce time to market [48]. The ability of modification of the microstructure within AM manufactured part by modifying the local build parameters makes it possible to grade the material properties during the build process.

Another reason for using AM is that parts can be designed so that they weigh less than conventionally formed parts because the shape of the part can be optimised and built to a greater degree. This means that material only needs to be placed where it is required. As the part contains less material than a machined part due to machining being unable to remove small intricate shapes of material. Therefore, in the long run, losing a small amount of excess material per part could mean a major weight reduction for an entire component where many small parts are used. It has been seen that AM parts can greatly reduce fuel consumed and CO_2 emissions in particular industries [49]. It is thought that AM uses a tenth of the amount of material when compared to traditional manufacturing for an equivalent part [49].

There are seen to be lots of different efficiencies in the use of AM, many of which have been written about by Yeng et al [50]. They focus on Airbus (formally EADS) and what the company is currently doing. Along with specifying some of the efficiencies, these include:

- AM being 26 times more efficient at using raw material.
- Decrease in processing times to as little as ¼ of the original time.
- Up to a 93% reduction in energy usage.
- It is possible to combine the production of up to 30 parts into a single part.

- That there is a great reduction in the amount of material that is required to be kept in stock for manufacture.
- There is less waste as excess material can be reused.
- It is still possible that when the part comes to the end of its useful life it can be broken down into powder again and made into a new part, so making these parts recyclable.

It's not just Airbus, a number of large manufacturing companies are getting into the AM industry. GE has brought Arcam to begin its foray into AM and has used it successfully to manufacture an engine part, fuel nozzle, that previously need brazing and welding and was impossible to cast. They now make it in one part and it flies on the Leap Engine [51]. GE believe AM and 3D printing will change manufacturing and this is why they are willing to buy into the industry.

Foster [52] states that 95% of material is discarded after conventional machining whereas after an AM process only 5% of the material used is wasted. Basically the entire life cycle is seen to be more efficient for AM parts [52].

Along with the findings of Airbus, and according to Foster [52], other companies have found the benefit of reduced number of parts which include Hettich, a German Based company, who manufactures centrifuges. They have found that 32 parts can be reduced to 3 parts, 2 of which are sintered and require no tooling after manufacture [53].

One of the key advantages of AM is that it can save weight. This can be done by optimising the shape using CAE software to only apply material where stress is seen, and to reduce it in other areas. This kind of work can lead to a 65% weight reduction without compromising the strength of the part [50].

AM parts as mentioned previously are built from CAD design. Editing the design after the first part is created is easier to do with a process that manufactures directly from CAD without the need of tooling then when needing to make new moulds from scratch. This is because all that needs to be done is to make the changes to the CAD design and then transfer this back to the AM machine and build the new part. This is done by many companies and researchers including Miles Pekala who revised a design 10 times in 3 months by printing new pieces in his lab [54].

Along with being able to revise design to improve them, another benefit of making AM pieces is that one can produce customised parts in a series [53]. Therefore, a number of similar designs or parts that are basically the same but can be slightly

modified and then created as individuals without extra work. In addition, it is possible to create one off parts without the cost of creating new tooling for each part for example concept designs.

Porous titanium parts for medical use can be produced by rapid prototyping [55]. This work recommends that further study of processing parameters effect on the quality of SLM parts needs a detailed investigation.

2.3.5 Problems

Parts that are created using SLS are formed in a cold environment. This means that the powder is cold while it waits to be sintered. Then as the laser goes over the powder, it is rapidly heated up to melt it before solidifying when the laser has passed. This can lead to manufacturing problems during the process, which leaves major defects after the part is finished which can mean that the part is no longer suitable for use.

The problems that can occur because of the heating and cooling are warpage and shrinkage of the layers and slippage between the layers. These defects can all be seen once the part is finished. These defects are believed to create parts with structural properties that are lower than for parts with no defects. This is believed to be because the layers are not fully connected to each other so less force will be required to break these layers apart.

In addition, the melt pool that is formed during the SLS process is highly dynamic and has high surface tension; it is made of a low viscosity metal liquid. This means that stochastic tracks can be formed in the surface layer, these lead to a corrugated appearance on the surface and so when a new layer of powder is applied, there can be a thickness across the top which can result in a process defect [56].

Another issue, not directly related to the AM process, can occur when attaching AM pieces to composite sections. Airbus has come up with a design solution, as shown in [57]. They have managed to create parts that have metal pins with arrows that the composite can be layered up around so that once the composite has cured the arrow heads are firmly embedded into it and firmly connect the two materials together and thus reliably transfer the load between them, Figure 2:5.

Figure 2:5: Metal pins to attach AM parts to compisites [57]

One of the major problems with additive manufactured parts is that the parts can undergo dimensional changes due to sintering. Sintering is "the welding together of small particles of metal by applying heat below the melting point" [58]. This is caused when the particles are diffused together the density of the part increases and with it the part size decreases [42]. This kind of defect needs to be avoided, and therefore it is necessary to control the conditions that cause it. This can be done by minimising the dimensional changes by intelligent manufacturing processes, but these dimension changes should also be accounted for in the design. Also it is anticipated with time that the powder composition and sintering pattern can be adjusted to eliminate the problem [42].

Although the porosity is an issue in most cases there are certain sectors that require porous or cellular structures including aerospace and therefore AM parts could answer that need. Wang et al [59] looked into this along with finding out more about the heat affected zone around the melt track and its effect on the surface of cellular lattices. This work also looked at the effect of residual stress on overhangs, as has been found previously residual stress will affect overhangs and the inclined angle of 35° does not work when designing lattice structures and therefore should be avoided to reduce residual stress and overhand defects. Wang et al [59] commented that powder adhesion to the surface is one of the most difficult problems to solve, this is an area that requires further investigation.

Finally, another problem is that balling can occur during sintering. Balling occurs when particles or balls of powder stick to the surface. It is a problem that effects single component sintering; it is obstructing the successful manufacture of these parts and so needs to be avoided, this can be done by using rather strict conditions on the SLS

parameters to prevent complete melting of the particles [9]. Balling is the formation of melt droplets and is not observed when the temperature increase is slow or when "the melt appears inside the sintered powder which resists the surface tension of the melt" [7].

It has been noted in [60] that balling produces pores that are irregular shaped within the builds. This would help to explain some of the pores within the parts built within this work.

Remelting due to the heating of an above layer occurs but Alrbaey et al [61] decided to remelt each layer to see how this affected the surface roughness and it has been found that this has the potential to improve surface roughness as well as eliminated the defects like balling and cavities.

As has been noted from the research there are a number of problems that can occur during AM processes and so it is necessary to learn and understand the process controls required to prevent these and understand the physics of the method to allow minimisation of problems due to mistakes by the operator. The mentioned evidence is the reason why this PhD is being undertaken to help minimise problems during manufacture.

2.3.6 Component Defects

There are numerous causes of failure and defects in AM components. These include warpage and deformation, residual stresses and porosity. As these defects have been better characterised and understood the causes and effects of them are known. As well as the process causing defects as discussed below there are other issues caused like melt balling, exposure to oxygen and humidity causing changes to the composition or lower melt temperature alloys potentially evaporating again changing the composition [178].

Deformation, Cracking and Warpage

Deformation and cracking due to process delays or overbuilding as well as unmelted powder areas within the part.

Warpage occurs in AM components because of the build-up of residual stress within components, generally due to insufficient support to remove heat and fix the component in place during the build or thick sections with high temperature gradients.

Residual Stress

Residual stresses are *"stresses that remain in a solid material after the original cause of the stresses has been removed. Residual stress may be desirable or undesirable".* Residual stresses can be desirable where fatigue life is required as they '*minimise fatigue crack initiation and propagation and increase wear and corrosion* resistance' [179]. Residual stress is formed in AM components by the cyclic heating and cooling "*caused by the unique thermal cycle in AM. This is the critical issue for the fabricated metal parts since the steep residual stress gradients generate part distortion which dramatically deteriorate functionality of the end-use parts"* [180].

The AM process produces large, anisotropic residual stresses which in turn leads to geometric deformations. Residual stresses are anisotropic due to the heating and cooling mainly being in an upward direction during the build process. Heating and cooling also occurs across a layer during each build stage. Also, for most metal AM as the β-grains are anisotropic [181], growing as columnar grains due to the heating and cooling, this leads to the mechanical properties also being anisotropic. Residual stress generation could depend on a number of processing parameters including scanning strategies and dwell time. The effect the heating-cooling thermal cycle has on lattice generation is what affects the residual stresses. As the heating travels through the layers this leads to the anisotropic stress development. Residual stresses are hard to predict, and it is not known how processing parameters affect them. Modelling software and codes look at this and this will be discussed further in section 0. This is a feature that has hindered the widespread adoption of AM [157]. Residual stresses in AM components are normally found to be compressive near the centre of the component and tensile near the surfaces [182][183]. If '*residual stresses exceed the interlayer bonding strength delamination between the layers will take place*' [184]. This is one of the reasons why minimising residual stress build up within components both during and after the build is important.

There are many methods that can be used to measure residual stress experimentally. Robinson et al [185] compared these different methods and found that the agreement between them could be used to draw conclusions on the effect of scanning strategies. The work showed that chequerboard has little effect but XY alternating gives a uniform distribution of stress that was the lowest measured. Hole drilling, to determine residual stress, has an international standard which makes it a good method to use. If

the stress is lower than 60% yield, there are simple calculations which makes it easy to quickly assess the residual stress of a component.

It has been seen by Wu et al [182] that reduced vector length decreases the residual stresses and increases the number of pores seen. Also, that tensile residual stresses often increase near the top surface of a part which leads to the warpage often seen. As the energy per unit length is increased, warpage on sectioning is reduced. These parameters alter the temperature of the sub-layer and the size of the heat affected zone, increasing both results in an increase of the residual stress [182].

Simulation is discussed further later in this chapter, but it is a developing area of the AM industry. Codes are being developed by several research groups to evaluate the AM process. It is beginning to be used to predict the residual stress that is likely to occur in AM components.

Work by Parry et al [186] looked at the arrangement of scan vectors and the effect on the thermal history of a component, which in turn affects the residual stresses formed. The work suggested that the scan vector length has the biggest influence on the component's properties until the critical scan length of 3mm, improving properties the shorter the vector scan length. It was also seen that longitudinal and transverse stresses stabilise towards a constant value when using a 'strip' scan pattern. As the magnitude of heating is increased the residual stresses also increase [186].

Another research area by Cheng et al [170] looking at simulating the process and its effects on residual stress and deformation has been successful in what it aimed to achieve being able to model scan strategies and the effect. This showed that rotation between the layers helps to decrease the deflection when compared to island and line. Lowering the vector length and reducing the heat concentration by adjusting the scan strategy, a reduction in the deformation of 42% might be achievable as predicted using simulation [172]. Being able to predict the effect of scan strategies will help to understand how components will vary but what effect these scan strategies have on mechanical properties is another hurdle that needs to be overcome. Work by Ali et al [169] on Ti6Al4V has shown that varying the vector length or rotation does not show considerable effect on the yield stress and that no correlations between % elongation and % of porosity exists and this in turn suggests that there is no clear relationship between scanning strategy and mechanical properties. Work by Wan et al on Inconel 718 [171] drew the conclusion that scanning strategy plays a significant role in influencing the microstructure and resulting mechanical properties of Inconel 718. The

refinement of the grain size is responsible for the higher tensile strength and fatigue strength.

Ti6Al4V undergoes a heat treatment, after it has been built, to help relieve any residual stress remaining within the components. This is to relieve the stress concentrations and to "*transform the martensitic α' to α phase*" [181]. The heat treatment effects the grains within Ti6Al4V components as longer time at temperature leads to larger grain sizes [187] unlike the small grains seen in general in AM materials. The grain size has an effect on the mechanical properties "*hardness, yield strength, tensile strength, fatigue strength and impact strength all increase with decreasing grain size*" [189]. As the grains in Ti6Al4V are already consistent due to the heat treatment this is likely the reason why limited changes in mechanical properties are seen when changing the scanning strategy.

Kudzal et al investigated 17-4SS [168], they looked into the quantity of austenite within the samples, changing the length of the scan vectors from short (25%) to longer (50%) and saw that a change in a direction within the scan line path resulted in increased delamination porosity along the melt pool boundary. This delamination porosity has been shown by fractography to be an initiation point for cracks and they propagated along these boundaries. This work has also shown that the uni- or bi-directionality of the scan factor did not affect the yield strength. However, it might be critical in determining the ultimate tensile strength and elongation. The author states that where similar microstructures are seen similar mechanical properties are achieved and the failure is likely dominated by the voids seen. All samples tested here were seen to fail through a quasi-cleavage failure through weld line overlap, melt pool boundary and cleavage of ferrite. Pores are crack initiation sites and were aligned perpendicular to the tensile load they are more prone to crack initiation. Mechanical properties are decreased where crack propagation along the melt pool boundaries and overlaps occurs, this is controlled by the laser scan strategy and hatch spacing. Further investigations into the thermal gradients caused by the AM process need to be carried out.

Work by Arisoy et al [190] looked at the effect of energy density as well as layer rotation. Increasing energy density results in larger grains and when using a 67° layer rotation there is less effect on the growth direction and smaller grains can be produced. Combining medium-high scan velocity and medium hatch distance provides ideal

growth of grains aligned to build direction and results in an isotropic build performance.

Porosity

Porosity and voids within AM components can be caused by a number of issues including trapped gas bubbles from the powder production process, insufficient powder per layer, spatter, shrinkage or insufficient laser intensity to completely melt the powder. Porosity in components leads to reduced density and less desirable mechanical properties. These pores can be stress raisers, lead to cracks and fatigue and become failure initiation points [178].

Hot Isostatic Pressing can be used to reduce the pores present within parts, but this carries a cost and time penalty that reduces the benefits of AM.

Lack of Fusion

Pores within AM components can be caused by a lack of fusion. This occurs where the laser power has been insufficient to melt the powder particles. Also, in any metal processed using AM and especially when using refractory metals as they require a higher energy density to melt the powder or if the laser speed is so fast that the energy density reaching the powder particles is reduced and ultimately insufficient.

Microstructural pores are formed unintentionally during the build process and need to be avoided as they affect the components mechanical properties [184]. Using in-situ monitoring to study the formation of these pores during the build process as discussed by Sola and Nouri [184] can be a part of the feedback loop that this work has been looking to establish. If the formation can be detected this can then lead to modifications to the build parameters during the process to improve the void.

Lack of fusion pores reduce the density of the component and lead to localised stress concentrations. These in turn increase the risk of failure at a lower stress value [211].

Keyhole

During the AM process under normal conditions melting of the powder occurs and it remains in place but "*under certain conditions, the mechanism of melting can change from conduction to so-called "keyhole-mode" laser melting. In this mode, the depth of the molten pool is controlled by evaporation of the metal*" [191].

Martin et al [192] have also investigated the formation of keyholes. When keyholes form, they effect the properties of the final component as they are areas of trapped gas within the solidified final structure. Keyholes have been seen to form due to changes

in the speed of the laser travelling across the surface. The scan strategy used effects the laser speed, if a meander pattern is used the laser must speed up and slow down as it travels around the loop at the end of each scan line, if stripe is used this laser acceleration and deceleration does not occur and keyholes are less likely to be produced. It is possible to use mitigation strategies to avoid these penetrating laser voids and this helps improve mechanical properties.

The scan speed and strategy used, and the dwell time influences the properties due to the formation of keyholes as the laser turns a corner or if full solidification occurs before the next laser pass. The longer the time before the laser returns to the same point means that the porosity is increased [183], increased porosity has been seen to lead to reduced mechanical properties and time to failure [193]. Double melting, rescanning the same layer twice or where scan paths overlap, has been seen to cause keyhole effects [168].

Keyhole mode can also be described as evaporation controlled where the metal is vaporised [184] leaving holes in the melt track.

Gas Entrapment

Gas entrapment can occur for a number of reasons including gas trapped within the powder during atomisation, the shielding gas used during the build process and alloy vapours created during the build.

Gas porosity can significantly degrade the tensile and fatigue properties of parts [212]. This is because porosity can be a site for the initiation of cracks and can increase the plastic strain seen during tensile testing.

Powder Properties

The powder used during the process can lead to pores within components. This can be due to poor PSD leading to poor packing in the layer and reducing uniform melting, Also smaller particles melt quicker than larger articles leading to incomplete fusion and lack of fusion defects.

Spherical powders increase flowability and packing density leading to fewer defects and improved density.

When powder is reused, it degrades, this can increase the oxygen and nitrogen present reducing ductility, changes the PSD and can accumulate spatter. This affects the repeatability across builds and can cause defects within the parts.

2.3.7 Materials

The materials that can be used in these processes varies from plastics; photopolymers, thermoplastics and adhesives [62] to metals; stainless steel, titanium, aluminium and Cobalt Chromium (CoCr) alloy. The machines can work either with plastics or with metals but cannot work with both, therefore the companies that make rapid prototyping machines usually will not make machines for selective laser sintering.

Stainless Steel

Along with Titanium, there are a number of other materials that can be used with SLS machines, one of these is stainless steel. It can be used for anything from cutlery to outside furniture. SS is good for making fittings, fasteners, gears and turbine blades.
Stainless steel is steel with around 11% Chromium. It is not in fact stain resistant but does not corrode as easily as normal steel. As well as Chromium other elements like Nickel, Titanium and Copper can be added to give different properties and Carbon or Nitrogen, which are non-metals, can also be added to adjust the materials properties [63].
The British Stainless Steel Association states that "the main requirement is that they, SS's, should be corrosion resistant for the specific application or environment" [63]. The addition of other alloying elements is carried out to help find the required properties and performance from that grade of Stainless Steel.
Stainless steel is 100% recyclable and has a melting point of 1510°C.

The stainless steel used in the EOS machine has a maximum operating temperature of 550°C; this is SS17-4, which is optimised for DMLS. When used in DMLS machines it has a suggested layer thickness of 20 µm and a minimum wall thickness of 0.3-0.4 mm, these requirements can make parts with accuracy of up to 20 - 50 µm.

The parts created using this material have a relative density of 100% of forged parts, which is 8.03 g/cm^3. There also is 17-4 stainless steel made by Vasco which is precipitation hardened steel. It has a density of 7.78 g/cm^3. The properties of this type of stainless steel have been compared to EOS's 17-4 DMLS powder. The ultimate tensile strength of parts made from this powder is 1050±50 MPa, [64], which compares to 1172 MPa conventionally seen, [65], or 89.6 % of forged stainless steel and the yield strength of parts made using the AM process from powder is 540±50 MPa which compares to 1069 MPa, [65], which is only 50 % of yield strength of the forged stainless steel [64].

There are four main families of SS, ferritic, martensitic and precipitation hardening, duplex (ferritic-austenitic) and austenitic. SS316L is usually austenitic with twinning present.

Stainless Steel 316L is often used to manufacture pipes, which fail by cracks forming in the surface, or nuts and bolts where fatigue and surface wear is an issue. Other applications for SS316L include: marine, pharmaceuticals, food preparation, medical implants and fasteners.

Titanium

A light weight, strong metal with high temperature (~500°C) properties is Titanium, Ti-6Al-4V. Titanium is a transition metal found in the fourth column of the periodic table with the atomic number 22. Its abbreviation is Ti and its relative atomic mass is 47.867. Titanium is used to replace aluminium and stainless steel because it has a lower density than steel while exhibiting good mechanical properties, which allows parts created with Titanium to weigh less. Titanium also has a higher melting point than both stainless steel, approximately 204°C higher, and aluminium. Titanium is a non-magnetic metal that has a density of 4,507 kg/m^3. [66] Titanium has a low density due to the way the crystal structure is laid up in hexagonal close packing[66]. From looking at the EOS data sheet for Ti6Al4V it can be seen that the relative density of parts made using AM is approximately 100% with a density of 4,430 kg/m^3 [67]. Although the density is seen to be close to the value of a solid, variations between the Ultimate Tensile strength and the Yield strength can be observed. The Ultimate Tensile strength is 950 MPa [68] for Ti6AL4V and 1150 ± 60 MPa [67] for AM manufactured parts and the yield strength is normally 880 MPa [68] but for AM parts in some instances it has been found to be higher than average at 1030 ± 70 MPa [67]. The material data sheet also gives the parameters for the manufacture of such parts. They are a minimum layer thickness of 30 µm, a minimum wall thickness of 0.3 – 0.4 mm and a build speed of 3 mm^3/s, these are used to create parts with full density. It states that the finished surface roughness will be between 9 – 12 µm Ra [67].

One of the main reasons that titanium is used is that it can retain useful strength at temperatures much higher than aluminium. It is also resistant to attack by a number of natural and chemical environments and has extremely high resistances to pitting and stress corrosion cracking. It is particularly corrosion resistant to chlorides, it is much better in comparison to stainless steels [69].

It was said in the 1960's that the reason why the use of titanium has grown so much is that titanium has a high strength, low density and excellent corrosion resistance [69].

Aluminium

Another material that can be used and has been looked at here is Aluminium. This can be used for food packaging but also its high strength to weight ratio means that it has a particular use in aircraft as well.

Aluminium is the 13th element in the periodic table and has the symbol Al. Its relative atomic mass is 26.982. It is not found as an element in the earth's crust but is instead found combined as ore with other elements. It is a metal with a very low density and like stainless steel it has good resistance to corrosion [70].

Aluminium has a density of 2.7 g/cm^3; this compares to a density of 2.68 g/cm^3 for the EOS aluminium alloy AlSi10Mg powder for DMLS, after processing into solid components. These parts are comparable with the powder only 0.7 % less dense than sheet aluminium. Aluminium has a melting point of 660°C. The aluminium powder used by EOS is Aluminium AlSi10Mg; this is an alloy that was especially created for casting, and it has good properties for this. It is now also used as a material for DMLS. For this reason, the properties of parts made from this powder will be compared to Aluminium 6061. This type of aluminium alloy is between 95.8 – 98.6 % aluminium [71].

Sheet aluminium 6061 has a tensile strength of 310 MPa and a yield strength of 276 MPa, [71], while aluminium AlSi10Mg powder has a tensile strength of 445 ± 20 MPa and a yield strength of 275 ± 20 MPa [72]. It can be seen that although the tensile strength varies greatly the yield strength are in fact almost identical.

For parts created using the EOS Aluminium powder the minimum wall thickness should be 0.3 – 0.4 mm, as with stainless steel and titanium. Using this powder in an EOSINT machine a surface roughness of 15 – 19 µm Ra can be achieved. Parts built in the EOSINT M270 machine with aluminium powder can be used as built or they can be heat treated to improve the characteristics. To heat treat the aluminium it needs to annealed for 2 hours at 300°C [72].

Other Materials

Along with being able to print the aforementioned metals, a number of other materials have also been developed so that they can be used to print items these include Cobalt, ceramics, paper, foods, wax, polymers and clothes.

Companies like Mcor Technologies have developed a 3D printer that work with other materials to benefit the systems they work with. Mcor prints paper using a method called Selective Deposition Lamination (SDL). This works like most previous methods in that the parts are built up layer by layer, but instead of metal, paper is used as the build material. This is claimed to make cheaper parts that are essentially reconstituted wood [73].

Not only can AM be carried out for metals and plastics but as mentioned other materials can be printed. ALM has been tried by the University of Exeter researchers using chocolate [74]. This is a 3D printer, so the method is to extrude the material from a nozzle, rather than melt the material from a powder. This method works on the same principles as AM where a layer is laid out in the required shape and then this layer solidifies, and a new layer is formed on top. A method like this could reduce the manufacture times of specialist chocolate treats and even allow for an individual's design to be made [74]. 3D printed food is becoming a reality for showing the skills of 3D printing machines, although in 2014 this was not yet available for home use. An article [75] has been written talking about the current developments in 3D printed food and how at the recent shows companies have been showing their machines and what can now be done. Mondelez International have 3D printed Oreos at a recent show and what has been seen is that food can be printed that tastes as it should although some structural issues were found with these Oreos.

As has been seen, new materials are being trialled for 3D printing. Wax is currently being trialled by Shapeway as a material to use to build 3D parts [76]. Shapeway's have found that wax can be used but as it is incredibly fragile consideration needs to be given when designing a part.

3D printed clothes are starting to become more prevalent as the 3D printing of materials is becoming easier. An article on Business Insider talks of how an Australian based XYZ Workshop are creating designs that can be 3D printed [77].

2.3.8 Design for Manufacture

Manufacturing parts can be done by many methods, and it is important to ensure that the best process is used to achieve the best results. In addition, to ensure what is designed is also the best shape for the job.

New manufacturing techniques require new design processes to ensure that they are used to their full potential to create new designs and parts.

AM is not suitable for every part and should not be used to just manufacture parts that were previously conventionally manufactured without an initial investigation into whether the part is suitable, or a redesign is required. If a part is desired to be produced using AM, then this should be an initial requirement before the design process starts. The parts' final role and requirements should be researched before design begins to ensure that what is produced minimises the use of supports during the build, is suitable for AM and is likely to build correctly. Input for AM designers during the initial stages of a project will help to achieve the desired outcome. AM of parts designed for conventional manufacture can end up costing more than if they were produced conventionally wasting more material, supporting the part or through failed builds.

2.3.9 Subtractive vs Additive

Common, everyday manufacturing techniques use a subtractive method to build parts. This is where the part required is cut out of larger volume of metal to obtain the desired shape. On contrast, the new AM manufacturing technique builds the parts up layer by layer, using only the material needed for the actual part, and for some supports.

Subtractive manufacturing can lead to a high amount of waste material and therefore increase the cost of parts. Additive manufacturing allows for all left over material to be reused and so there is very little wastage therefore reducing the material costs of this manufacturing method.
Renishaw has found that powder can be reused for up to 20 builds and still achieve parts with comparable properties [40].

2.3.10 Optimisation

Optimisation is "to make the best or most effective use of a situation or resource" according to the Oxford Dictionary [78]. The shape optimisation of a part is the process to find the optimum design of that part. This can be done by optimising the thickness of the part, by placing material only where it is required for structural support, by adjusting the shape to the use and by adjusting the part material.
Ensuring the part is fit for the job is essential. Parts can be built that fit the specification but with new manufacturing techniques, these designs can be further optimised so they perform the task using as little material as possible. This has been shown by Tomlin and Meyer [16] where a bracket has been optimised which reduces weight while still performing its required tasks.

Along with modelling of the process of selective laser sintering, modelling has also been carried out that is used to optimise the design of SLS parts. Some modelling has been carried out for instance by Airbus [16], such as the optimisation of a nacelle hinge from the A320. The original part was made from HC101 Steel and weighed 918 grams whereas after optimisation using Altair Hyperworks – Optistruct for subsequent AM the 2nd design iteration of the part weighed just 326 grams and was made out of Titanium. Looking at Figure 2:6 and Figure 2:7, the change in design has been dramatic with the removal of a large amount of the excess material. The material is only placed where it is required for the structure to perform its function.

Figure 2:6: Original A320 Nacelle Hinge Bracket [16]

Figure 2:7: Optimised A320 Nacelle Hinge Bracket [16]

This weight saving will help reduce cost of flying the part but it was found that the weight saving that can be gained by optimising a small piece, like above, is small in comparison to the amount of work spent on the optimisation and design process [16]. This is because the optimisation process takes a long time and so to start with it is mainly being used to look at larger parts for weight savings. But it has been suggested in [16] that using groups of parts that are similar and optimising them could help to spread the time and cost of optimisation over a selection of parts and so make optimisation for small parts more effective in the long run.

2.3.11 Topology

Topology is “the study of geometrical properties and spatial relations which remain unaffected by smooth changes in shape or size of figures” or “the way in which constituent parts are interrelated or arranged” according to the Oxford Dictionary [78]. The topology or shape of a piece have an effect on its ability to perform and its weight. The topology can be changed and designed to suit but it is not always possible to build all designs with common manufacturing techniques. Whereas when building parts using AM it is possible to build more complex geometric shapes as it is not about taking away but adding material and therefore highly intricate designs can be achieved.

2.3.12 Future Development

The development of AM processes will continue towards capabilities to build much larger parts at much higher speeds with increased repeatability. Airbus aim to be able to create the first AM machine that can make parts with a length of 5 meters and then scale this up further to make parts including wing spars [79].

It is said that AM should be fully developed for first use within two years of the start of this PhD [52]. Although parts made by AM are already in use in Formula 1 Motorsport; in the Force India car and on the Bloodhound SSC, [52] it needs a larger market uptake to help develop the process before it will be fully commercial and in high demand. This is like all new processes and the products manufactured using it, it needs to be tested and fully working before it can be used in such a highly safety conscious environment with demanding requirements on weight reduction and therefore small safety factors, like it is the case for aircraft.

A further article presents in more details about the plans that Airbus have to improve AM technologies [80]. Airbus plans to continue working on AM technologies which will enable them to reduce the weight of aircrafts, and so will enable a reduction in the amount of fuel used per aircraft per year. A 1kg reduction in weight will mean a saving of $3000 over the lifespan of the aircraft and this in turn will mean a reduction in greenhouse gas emissions helping all companies and countries to reach their climate change goals. To do this Airbus will continue looking at AM technologies with the aim to allow them to take a 35 meter long gantry already in use in-house for layering up composite wings, and instead use it to print titanium parts straight on to the wings.

The article [80] also talks about how other companies are trying to improve AM technologies to see if it is possible for these methods to be used in mass production.

Currently AM is not cost effective when compared to conventional methods of mass manufacture.

The future of Additive Manufacturing is that it will speed up the time it takes for companies to be able to manufacture and produce parts. Some believe this will be reduced by between 50 and 80 % [80] but it can also mean that it is easier for companies to copy each other's ideas and so it will be a race to see who can get to market quicker [80].

The article [80] also talks about how other companies are trying to improve AM technologies to see if it is possible for these methods to be used in mass produced products. Currently it is too expensive to mass produce products compared to the price of mass production using traditional styles of manufacturing.

The future of Additive Manufacturing is that it will reduce the time it takes for companies to be able to manufacture and produce parts. Some also believe part numbers will be reduced by between 50 and 80 % [80]. It can also mean that it is easier for companies to copy each other's ideas and so it will be a race to see who can get to market quicker [80].

As part of their ongoing work Airbus aim to work towards large scale platforms to create bigger parts and to develop a mature system to be able to produce parts that are functionally graded [50].

In further research Airbus has managed to develop the technology to such a state that it can now manipulate metals, nylons and carbon reinforced plastics at the molecular level. This means that these materials can be applied to high stress, safety critical areas like aviation materials safely [49]. This shows that AM technology is constantly being updated and changing due to extensive research in this field [81]. This will result in continuous improvements for the foreseeable future.

GKN are teaming up with Airbus to create a research centre with the aim of working towards establishing Additive Manufacturing in the industry. Their head of manufacturing engineering Mark Himpson says that GKN hope to be using AM "in the next three to four years to create components that are certified for use by airlines" [82].

Another area of future development is free space deposition. This has been investigated by a research team at the University of Cambridge [83]. Free space deposition uses a moving support structure to support layering material like writing on paper. This is currently being tested and is done by heating material and feeding it

on to the surface rather than melting powder that is already laid out on that surface. The aim of the research is to develop a moving support structure to allow for free space deposition and as things stand this is possible experimentally. Further research is required so that it can be used commercially [83]. To carry out these experiments a machine was built to perform the tasks and this cost £5,000 (not including the Computer Numerical Control, (CNC) machine) which means this could also be a cost effective process [83].

One of the final points noted about AM came from a recent article in Professional Engineering, [84]. The interesting point made is that in the future every home has its own 3D printer, and these can be used to buy the design for a toy or product, direct from the designer and then print it at home. This will greatly affect the manufacturing chain, cutting out the company that currently buys the design and manufactures the product and the transportation to the shops. This will be true for plastic printing but is unlikely to happen with metal processes.

What becomes apparent when researching AM and its future is that it is believed by many that 3D printing will revolutionise the way we live [85]. The materials that can already be used to print parts is very wide ranging from plastics to metal to food products like chocolate and as research in this area continues the variety of AM ready materials will increase. In addition, the size of 3D printing machines is getting smaller and the cost of them is decreasing as they become more widespread within industry. This is allowing people to start purchasing 3D printing machines for their homes. The capabilities of these machines including mixing different materials and making complex patterns are encouraging their increasing use by more and more companies in different industries. According to Lipson [85], the final part of the 3D trail will occur when machines can control the behaviour of the materials. When this happens, it is believed by Lipson, that it will be virtually possible to print anything.

2.3.13 Finishing Processes

When parts come out the of AM machines, they are not always 100% dense which in turn typically means a reduction in desired properties. For this reason, companies will require finishing processes to be carried out on the parts to make them 100% dense. There are a number of different processes that can be undertaken, and these will yield different results and different increases in the parts density. Some of these are mentioned below.

Baking

When DMLS parts are finished, they are often taken from the build area on the build tray and placed in an oven to undergo a stress relief bake for 1 hour. The temperature of this varies according to the material that is used [86]. This is carried out to improve the properties of the part.

It has been shown by Yadollahi et al. [87] that heat treating after build has an effect on the microstructure and properties of SLM 17-4PH SS parts. The microstructure has been shown to form a fully recrystallized structure after heat treatment.

Heat Treatment

Heat treatment is known to relieve residual stresses, but it is something that needs careful consideration to avoid microstructural changes as these have been seen to affect the mechanical properties [194]. There are many methods used to measure residual stress and to predict it through simulations. Some links between mechanical properties and residual stress have been noted in [157] where there is seen weak correlation between increased tensile strength and yield stress and increased residual stress. Numerous papers show that increased residual stress is linked to only one processing parameter, this provides general knowledge but needs developing to look at more complex effects.

Works by Brandl and Greitemeier [88], and Vrancken et al. [89] have looked at the effect of heat treatment on Ti6Al4V samples and its microstructures and mechanical properties.

Brandl and Greitemeier found that heat treatment had an effect on the microstructure and that certain heating cycles can produce a homogeneous grain structure but reduces the hardness. Further work in this area is required to increase the hardness and thus the yield/tensile strength [88].

Vrancken et al. found that applying heat treatments below the β transus for different periods had little effect on the microstructure but changing the cooling rate did. Low cooling rates allow grains to grow during cooling. This work found that as the maximum temperature was increased there was an increase in fracture strain and a decrease in yield stress [89].

Hot Isostatic Pressing

Hot Isostatic Pressing (HIP) is a finishing process that can be applied to Additive Manufactured parts to produce 100% dense parts with no porosity [90]. HIPping was

first invented in 1955 and as time has passed it has improved and can be used for a greater selection of processes including AM parts [91].

HIP is a process that is carried out using metal powder in a steel can [90]. The process occurs at high temperatures with pressure applied to all sides of the object. Within the housing where the process occurs, argon gas is pumped in to start the process this helps to increase the pressure, which in turn helps the process occur.

For HIPping of Titanium following Electron Beam Melting it is recommended that the parameters followed are a temperature of 920°C and a pressure of 110 MPa for 120 minutes [92]. These parameters would be the same if a Titanium alloy was used [93]. HIPping has an effect on the microstructure of parts as well, [94] shows how the microstructure varies due to HIPping changing martensitic microstructure to alpha and beta.

Cold Isostatic Pressing

Like HIPping, Cold Isostatic Pressing (CIP) is a finishing process that can be applied to Additive Manufactured parts to produce 100% dense parts.

CIP occurs at room temperature but with high pressure. This can be used before HIP or on its own.

When CIP is carried out on its own, the powder is placed in an elastomeric container of the desired shape. The container is placed under high pressure by a liquid. The liquid is surrounding the entire vessel with powder resulting in even pressure around the surface giving the process its name of Isostatic. The pressure used varies from 20,000 to 60,000 psi (137.9 to 413.7 MPa) [95]. While the pressure is being applied the metal powder fuses together to create the part. When this is used in conjunction with AM methods, the aim is to push the solidified powder to fill any pores within the part in the formed shape closer together to create a 100% dense part. It has to be remembered that this can cause shrinkage of parts – which has to be accounted for when the part is designed.

Epoxy Infiltration

Along with HIP and CIP, parts created through DMLS can be finished by the process of epoxy infiltration. This is a process that has two steps. The first is the epoxy infiltration and followed by a curing step for the epoxy. The part and the epoxy need to be pre-heated to 60°C. The epoxy is infiltrated from the bottom to the top by capillary action or the parts can be soaked in an epoxy bath. Once the parts are fully infiltrated they need to be cured in an oven for 2 hours at 160°C [32].

2.3.14 Surface Finishing

When the part has been finished and it is at its final density, in a further step the surface roughness is improved. When the part comes out of the AM machine there is surface roughness and pitting, Figure 2:8, and more often than not a smooth surface is required for the structural or functional performance of the part. For this reason, parts are usually finished after manufacture. This can be done by a number of different ways from hand polishing through to sand blasting. These different methods are explained in more detail below. Surface finish can be critical further down the manufacturing route, and naturally also when using the parts. It is therefore important to look into the surface finish of parts. When comparing to conventionally manufactured parts the surface finish of AM parts is usually not desired. For conventionally manufactured SS316L standards allow the worst surface roughness to not exceed 7.5µm [96]. Using this value for AM would not be acceptable. However, in some instances the pitting mentioned above can be helpful or even desired, such as when producing medical implants; a pitted surface can help encourage bone growth to the implant. This pitting is caused due to the sintered parts remaining in the powder bed surrounded by excess powder. This excess powder then stops the edges of the part from being smooth by attaching itself to the sintered powder.

When a smooth surface finish is required after AM manufacture surfacing finishing is required, through for instance surface polishing. Polishing can be done by hand, but there are also methods like laser polishing, tumbling, shot penning, and electroplating that can clean up the surface.

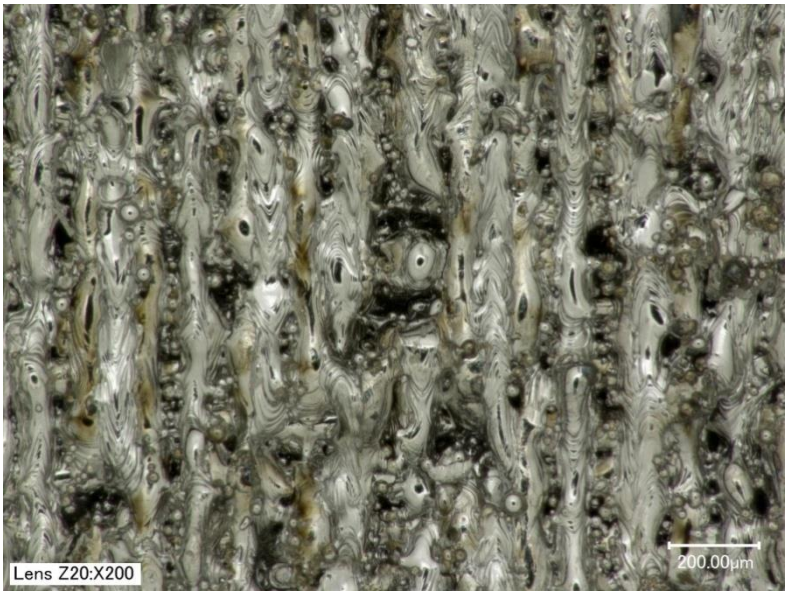

Figure 2:8: Surface of an AM cube

One of the main processes used to surface finish SLS parts is using hand tools, grinders and polishing wheels. These are used to remove any support structures and to bring the surface quality to between 180 – 320 Ra [86]. After this, it is possible to improve the surface quality by continued polishing. This polishing can improve the surface quality to reduces the roughness to 32 Ra [86].

Another widely used method for polishing parts surfaces is sand blasting, which is also applied to remove excess material and to smooth out the surface [32]. Sand blasting is the process of blasting a stream of sand, usually propelled by air, at the part to remove the excess material. Normally sand is used but abrasive blasting can be carried out using a number of other materials. Sand is the most commonly used but can break up into fine dust, which can cause silicosis in the user.

Parts can be removed from the surface plate using a band saw or Wire Electrical Discharge Machining (EDM). EDM is also a finishing technique that can greatly improve the surface of AM parts, this has the advantage that a flat clean surface finish can be obtained. Wire EDM is a process that uses brass wire and creates an electrical discharge between the wire and part. What happens is that as the spark travels, material is removed from both the wire and the part. This helps to smooth out the surface of the part [97].

Along with smoothing out the surface of parts, it is also possible to plate the parts with other material. This can improve the properties of the part, protect the surface, seal the outer skin of the part and it ensures the surface is incredibly smooth as a polished metal can be used. Plating can be done by physical vapour deposition, where the particles are deposited using a vacuum coating machine.

2.4 Experimental Work

One of the major aims of this thesis is to carry out experimental work. Therefore, previous experimental work has also been thoroughly investigated. Experimental work can include mechanical testing, non-destructive testing, microscopy and metallurgy. Destructive testing including tensile testing was mentioned briefly in Section 2.3 and is one of the main methods used to determine mechanical properties of AM parts. Along with destructive testing there are options to perform non-destructive testing including Computer Tomography (CT) scanning and x-ray. CT scanning has been used to study cellular lattices built by SLM methods [98]. This work using this

examination method demonstrated that it is possible to build AM parts that show no defects.

2.4.1 Powder

As investigations into mechanical properties of AM components have developed it has been realised that what goes into the system, along with processing parameters used affect the quality and properties of these components.
Powder and its properties are one of the keys for the success of AM. Therefore, the condition of the powder in its 'virgin' state is attracting interest. The method of production through gas, water or plasma atomisation defines the quality of the powder and this in turn is likely to have an effect on the quality of the parts produced.

Along with the original production method, the geometry - spherical or irregular - and the particle size are important to the finished parts' condition.

Powder quality can be measured in many ways, Particle Size Distribution (PSD), particle shape, flow, packing density, age, frequency of reuse and chemical composition for instance. These properties can be defined but ASTM are yet to generate a standard that defines an appropriate quality powder for AM or a definition of inadequate quality.
If the Powder Size Distribution (PSD) is too wide, smaller particles will sit between larger ones, inhibiting flow. If it is too narrow there could be inefficient packing and pores could remain after melting [40].

SS316L powder is manufactured by a number of suppliers and has a chemical composition similar to that shown in Figure 2:9. Powder used in AM process normally has a size distribution varying between 10 and 45µm.

It is believed there are approximately 900 suppliers of powdered material [13] but these do not only supply the AM market which makes up 0.0047% [13] of their customer base.

CHEMICAL ANALYSIS						
		Units	Min	Max	Result	Approved
C	Carbon	weight %	-	0.03	0.02	Y
Cr	Chromium	weight %	17.5	18.0	17.8	Y
Cu	Copper	weight %	-	0.10	0.08	Y
Fe	Iron	weight %	-	Bal	Bal	Y
Mn	Manganese	weight %	1.00	1.45	1.05	Y
Mo	Molybdenum	weight %	2.30	2.40	2.35	Y
N	Nitrogen	weight %	-	0.10	0.09	Y
Ni	Nickel	weight %	12.5	13.0	12.6	Y
O	Oxygen	weight %	-	0.05	0.03	Y
P	Phosphorus	weight %	-	0.025	0.015	Y
S	Sulfur	weight %	-	0.01	<0.01	Y
Si	Silicon	weight %	0.55	0.75	0.63	Y

Figure 2:9: Chemical Composition of SS316L Powder

SS316L powder, as with all AM powders, is supplied by a number of manufacturers, there is currently a drive to standardise production processes and material to allow for better comparison between final products and to work towards faster introduction to current process chains [99]. For this to be successful it is also necessary to understand what affect powder has on finished parts.

Powder quality and initial details including chemical composition and particle size are provided by the supplier on purchasing the powder. This is normally verified by companies purchasing the powder as part of their routine quality control. Powder is generated using a number of methods including; gas or plasma atomisation and plasma spheroidisation. The manufacturing process effects the quality of the powder produced. Companies including LPW [100] are working to improve the powder feedstock which is used for AM builds. In a recent investigation LPW looked at determining the best processing parameters to generate what they believe to be the best quality powder feedstock for improved flowability and packaging [101]. Ensuring the powder that goes into the AM process is highly spherical and of a constant acceptable quality will help towards the qualification process for AM parts.

Powder is mixed and tracked in lots. Knowledge of the powder's origin is necessary to be able to qualify AM metal components and understand what has gone into the part produced. When powder initially enters the AM process and system it is classified as 'virgin'. After each build and pass through an AM system, the addition of 'virgin' powder and the mixing of lots the powders history is changed to reflect this. Companies like LPW are designing software to trace this and this software tracks details to help qualification of powders and with it of AM parts.

AM processes reuse metal powders within the process for numerous builds. How much used powder and 'virgin' powder to use within builds is currently being investigated to establish how this affects both part quality and build system performance. Along with the mixture of used and 'virgin' powder it is necessary to establish how many times powder can be reused before it is so degraded that it is no longer useful to guarantee the quality of manufactured AM parts. To this end powder recycling has been studied in detail by companies including the National Institute of Standards and Technology (NIST) in the US [102] and Renishaw [40] and is discussed further below.

Powder characterisation is being investigated more as AM processes are developing. Companies are starting to question if the powder quality has an effect on the finished part and the quality needs to be established. This is from the initial manufacture method, particle size distribution, to the chemical composition. Powder characterisation can provide large amounts of data: it is important to understand which properties are important, requiring control, and which do not impact part quality and so can be ignored.

NIST [102] investigated a number of powder characterisation techniques alongside characterising mechanical properties of AM parts through a long term NIST-led inter-laboratory study to determine design allowable mechanical properties for AM parts [103]. The powder characterisation involved investigating particle density, particles size x-ray CT and diffraction, SEM analysis and chemical composition. This investigation showed that initial powder batch spread from numerous containers showed consistency across the lot which as an initial finding allow confidence across a batch. Investigations of processed powder showed that there was an increase in larger, greater than 60µm, particles suggesting that the powder recoater pushes these over the build plate and they are not incorporated into the build. The work has also shown that although the majority of particles are roughly spherical in 'virgin' powder not all are. It is not specified how this powder was produced, and this may have led to powder quality problems. A number of articles have been written on this area by NIST including an article comparing powder recycling's effect on powder and material properties [104], this continuing work shows how teams are researching more and more into specific areas that they feel have a significant effect on AM parts and how important it is to get standards for these materials. The work within this article [104] ran 11 identical builds and found that the mechanical and material properties were similar for all builds. This work led NIST to suggest a new tracking method for powder

looking at total exposure time rather than number of builds. This would need working on as powder in systems like the RenAM500M where powder is recycled and reused within the machine it would not be possible to monitor which powder had been within the build and exposed.

NIST [102] began researching powder characterisation in 2014, in 2016 Missouri University [105] continued work into powder characterisation, this is as the ability to reliably produce parts of acceptable quality is sought after. This work has led to an initial leading argument that particle morphology, chemistry and microstructure should be studied for powder samples and now work should continue to establish what effect changes to these properties have on final part properties.

These initial investigations have given work for others to continue to fully understand powder characteristics.

It is believed that the powder market will be worth $1.1bn by 2024 [106]. This interest in the powder market means that the quantity within powder batches produced by manufacturers will increase and the quality of the powder produced will improve. This will help to improve the quality and final performance of all AM parts. The demand for AM powders is increasing with increased investment in AM equipment, research and development and technology improvements. Demand will increase as AM is further accepted as a suitable alternative to current manufacturing methods.

Powder Reuse

AM powders are costly for certain materials where demand is minimal and base material is expensive, therefore reusing the powder is necessary. Powder reuse can be within the AM machine like the RenAM500M where it is sieved and recycled internally with virgin powder added at intervals to keep material levels sufficient for building. The powder can also be taken out of the AM machine and sieved using a separate sieving station and then put back into the machine. Both of these methods are called powder reuse in this thesis. There is another type of powder recycling where the powder can be re-spheroidsed and any over or undersize powder removed. This is a costly process but for certain situations this may be necessary.

The issues arise where the powder is changed during the process, sieving removes any oversize particles, but the chemical composition may change, and this is not as easy to spot or sort out.

Chemical compositions for known materials are provided and powder for AM should be brought to this specification but as the powder is reused the chemical composition changes; it is not fully understood how this varies [160]. Repeated exposure to air affects the nitrogen and oxygen content due to the large surface area exposed to the atmosphere thus, increasing Oxides and Nitrides [161]. The powders' shape and size also change as they are heated and cooled during the process. Around the edges of the melt pool partial solidification is likely to occur and these particles will not adhere to the part surface and will be recycled and appear in future builds. Investigations into the characteristics of virgin and recycled powder are emerging; Gorji et al [162] have used X-ray Photoelectron Spectroscopy (XPS), X-ray Diffraction (XRD) and Scanning Electron Microscope's (SEM) to study both virgin and recycled SS316L powder. They have seen that the changes are not significant in size. However, there is a mix of irregularly shaped, bonded spatter and satellite particles present in the reused powder along with an increase in surface oxides. For powder made of refractory metals, oxygen has a degrading effect on part performance therefore this increase needs to be understood and reduced if possible [160], [163]. Increases in Oxygen during powder processing increases the Yield and UTS but the ductility is decreased, and this will affect component performance [164] [165].

Powder Ageing

There are a number of reports talking about the effect of powder reuse on Ti6Al4V powder. Seyda et al found that the particles coarsen and the flowability increases with uses and there are significant effects on laser melted components [107].

Work by Renishaw has found that although there is an increase in oxygen and nitrogen levels during powder reuse this has stayed within spec and not seen to have a detrimental effect on the parts produced. They also found that sieving the powder has kept the PSD consistent and improved the flow rate. There was no evidence found to suggest powder disposal was necessary and that topping up with 'virgin' powder when levels drop within the system should help with the oxygen and nitrogen levels [40].

Both of these studies have found similar results and believe there is little effect on the quality of produced parts from recycling of powder.

When this research began it was believed that powder ageing could potentially cause an issue when manufacturing AM components. Work on this has been progressing, the Manufacturing Technology Centre (MTC) in Coventry have used a Core Research Project (CRP) to investigate storage conditions effect on powder quality. From this

work it appears that ageing does not influence the powder as much as storage conditions do and therefore if powder is kept in a sealed container until use this area no longer needs focus [160].

2.4.2 AM Properties

As discussed, AM is a new process that builds parts up additively, layer by layer, rather than cutting them out of sheet material or cast ingots. It is growing in popularity and for this reason, investigations into how AM parts perform and compare to conventional parts properties are increasing. Previous work and investigations are being studied here and the thesis will build on these findings.

This background experimental work is still limited in certain areas; therefore, this thesis is going to expand on previous experimental work working towards achieving a full picture of how they compare. Researchers including Kruth [8], [29], [77], [94]–[102], King [117], [118] and Hague [119], [120], lead the industry in investigating AM machines, materials, parts and properties and working to share this knowledge with others. This work is helping to lead other researchers down the path required to develop a significant knowledge base around AM.

Experimental work has begun investigating a number of areas already including showing that hydrogen has been found to affect SS304 AM parts deteriorating the mechanical properties [121]. Along with how variability and anisotropy effects the mechanical properties of austenitic stainless steel [103]. This work helps us to understand how further investigation is required to fully understand and qualify AM parts.

Along with establishing the properties it is necessary to compare these to ASTM or BSI standards. It may be that although properties are different from what we would expect of conventionally manufactured parts, the properties still meet required standards and so the next objective would be to optimise these properties but not to completely disregard AM parts as they have potential and for lower risk parts could be successfully employed already.

Tensile Strength

Mechanical property including tensile strength has been carried out by Cherry et al [122], on the same SLM machine used in the PhD, looking at how the exposure time and point distance affect the build properties. The work has been continued during this

PhD to see how changing the laser pattern during the build will affect the properties on top of exposure time and laser power changes.

The previous work has shown that changing these two basic parameters has affected the builds and showed the best conditions were with a laser power of 104.52 J/mm^3, using the Renishaw AM250 at Swansea. It has also been seen that this is slightly lower than the Renishaw recommended parameters, which give a laser power of 125 J/mm^3 [122].

Tensile testing has also been carried out on nanocrystalline 316L austenitic stainless steel and this has shown that in this case the yield stress can by 6 times higher than when compared to a coarse grain part [123].

Experimentation by Spierings et al [124] has found that a Ultimate Tensile Stress (UTS) of 588MPa is achievable with a yield strength of 259MPa. This shows that properties that are comparable to conventionally manufactured parts can be achieved.

Fatigue Strength

Fatigue is a typical failure mode in aerospace parts including brackets, which are likely to be manufactured out of stainless steel as is being studied in this work. AM parts can be designed and optimised to reduce weight and provide cost savings to aerospace companies [16].

Fatigue testing of SS316L carried out in [125] shows that the sub surface defects seen in AM parts lead to approximately 40% reduction in fatigue strength when compared to conventionally manufactured parts.

Residual Stress

It is not fully understood how parts made by a heating and cooling process will be effected and what kind of residual stresses will be formed, initial investigations have shown that a low scanning rate leads to a high cooling rate which will in turn cause larger residual stresses [126]. Larger residual stresses are likely to increase part deformation and warpage, which is a downside of AM parts.

Further evaluation [126] of residual stress found in SLM SS316L parts has shown that normal residual stress is higher along the scan direction than perpendicular to it and that in some areas residual stresses were found to exceed the yield strength of wrought.

Failure Modes and Analysis

Fracture is the separation of a body into two or more pieces due to an applied stress. Parts can fail in a number of different ways including ductile or brittle fracture.

Ductile materials have extensive plastic deformation, and the failure is a relatively slow process. Ductile failures when imaged are seen to contain spherical 'dimples' and forms a 'cup' and 'cone' at the break. Whereas brittle failures occur rapidly and show minimal plastic deformation.

Brittle materials are considered to have a fracture strain of less than 5% in most cases and this is a rapid failure with little preceding warning.

Ductile failures are preferred over brittle due to plastic deformation giving warning of the failure, and higher strain energy required for ductile failures means that the material is generally stronger [127].

Table 2:1 [128] details the typical fracture surface characteristics found for different modes of fracture.

Mode of Fracture	**Typical fracture surface Characteristics**
Ductile	Cup and Cone Dimples Dull Surface Inclusion at the bottom of the dimple
Brittle Intergranular	Shiny Grain Boundary cracking
Brittle Transgranular	Shiny Cleavage fractures Flat
Fatigue	Beachmarks Striations (SEM) Initiation sites Propagation area Zone of final fracture

Table 2:1: Typical fracture surface characteristics related to mode of fracture [128]

AM parts have been seen to fail due to incomplete fusion or initiation points at internal defects [125] these issues are specific to AM parts because of insufficient laser power

or energy to fully melt the powder during the build. Work needs to be carried out to establish if properties can be changed to minimise and remove unmelted powder found within parts.

A dislocation is a crystal defect; these can occur in all microstructures and affect material properties of those parts. Dislocations are halted by grain boundaries and therefore smaller grain sizes will in turn improve failures rates.

Pore Stress Raisers

Stress raisers are flaws that have an ability to amplify stress in that location, they lead to failure and have more of an affect in brittle than ductile failures [127].

Work by Speirs et al looked into the effect of pore geometry on parts mechanical properties [113]. This showed that it was possible to achieve comparable human bone mechanical properties in AM parts.

Another project by Ziółkowski [129] has used x-ray CT to measure the discontinuity and porosity within SLM SS316L parts. The x-ray CT was used to study the porosity of parts this has been compared to microscope evaluation of the same surface and has shown that CT cannot pick up all of the smaller defects and pores. This study has also shown that building the in x and y direction leads to the highest number of pores when compared to building in the z direction where very few pores are seen.

In [130] it has been observed that un-molten powder particles, shrinkage cavities and gas porosity are due to rapid solidification rates (higher scanning speed), gas entrapment and remelting associated with the process.

Microstructures

The microstructure of additively manufactured parts made of SS316L has shown columnar growth up thin walled samples and there has been seen to be a difference in the microstructure of the final two layers when compared to the main body of the sample [131].

Yasa and Kruth [109] studied laser remelting to see how it improved the microstructure of AM parts. It is widely understood [130] that microstructure of AM parts is uncontrollable and although it has been characterised the effect of changing parameters is not fully understood.

Remelting a layer although it greatly increases the manufacturing times this has been proven [109] to reduce the porosity by allowing pores between melt pools to disappear

and it refines the microstructure. Brandl et al [132] have found that the microstructure can be homogenised by peak hardening which in turn improves the parts properties.

Niendorf et al comparing different laser powers have investigated the microstructure of SS316L. This work has found that using a stronger 1000W laser power generates a coarse, strongly textured microstructure which affects the mechanical properties. The 1000W grains are highly elongated and can grow to sizes of more than 1mm. For the 400W laser power the microstructure was found to be weakly textured fine grained, that is often seen in literature about AM parts [133].

2.4.3 Parameter Effects

The first paper looked at on experimental work, is the paper by Khaing et al [32]. The paper looks at parts made using the EOSINT M250 machine DMLS system with nickel, bronze and copper-phosphide powder. The parts were created within the machine with layers of up to 50 μm then epoxy infiltrated, as mentioned in Cold Isostatic Pressing. It was seen that delamination occurs between the base plate and the part and that there are dimensional discrepancies between the CAD design and the final model, these ranged from 0.003 to 0.082 mm [32]. But it was also found that the epoxy infiltration of the parts improved the surface roughness from between 12 – 16 μm to 4 – 7 μm Ra, and with hand polishing it is possible to improve the surface roughness to less than 1 μm [32]. It has also been found that the surface density of the parts before infiltration was 6264 kg/mm^3. However, one of the main problems that has been found relating to DMLS parts is the scan lines within the part are visible and that there are also unmelted sections, which will increase the porosity of the part. It is seen that for DMLS to be successful at creating 100% dense parts optimisation of process parameters needs to be undertaken [32].

Another paper that looks at the effect of parameters is written by Senthilkumaran et al [134] which looks at different building strategies and their effect on the accuracy of a part. It is necessary to remove the shrinkage inaccuracies by compensating for them in the design [134]. Nevertheless, this would mean part shrinkage would need to be known during the process. Therefore the paper, [134], looks at how to make the compensations efficient enough to improve accuracy of the parts, because currently not enough is known and so parts are not always accurate.

So it has been found in [134] that there is an effect on the shrinkage of parts due to their build direction and also because of the scan lengths. It is noticed that lower scan

lengths create higher shrinkage, and that shrinkage is non-uniform in the Y-direction relative to the X-direction when the strip length matches scan length. A final point noted is that shrinkage is lower following the scan direction and highly non-uniform compared to shrinkage across the scanning field [134]. What has been found here needs to be noted for any further work so that the effects can be studied and then minimised in any parts created. Many companies including EOS have investigated this to reduce shrinkage of parts for customers.

A paper by Fischer et al [135] is to do with the sintering of commercially pure titanium. It investigates the parameter effects on the process maps as well as on the surface roughness. What has been found gives further information on how the laser parameters affect SLS. It can be seen that to minimise surface roughness lower values of peak power, gives a smooth surface and lower power gives insufficient energy or too long liquid lifetime, both of which can lead to balling and distortion in the layer [135].

Previous work [136] has explored how changing the laser power, scanning velocity and layer thickness effects single layer tracks. This work also studies the microstructure of these tracks, it has found that there are mainly austenitic grains, and these show the scan pattern. Tensile tests were carried out on parts built here and a number of the tests showed comparable UTS and Young's modulus. The fracture mechanism was briefly studied, and this has found that these are mainly brittle with some defects or stress raisers lowing the UTS of certain test samples.

Work by Mahamood et al [137] has shown that increasing the laser power saw an improvement in the surface finish of parts.

Antony et al [138] have investigated both experimentally and numerically single track SS316L work to obtain the optimal build settings of 150W laser power, 2.4m/min scan speed and a spot diameter of 400µm. These properties were found to affect the smoothness; distortion and balling but mechanical properties effects were not investigated.

Kruth et al [108] investigated scanning strategy and laser remelting strategies. The work found that an island scanning technique reduces residual stress found within parts and that laser remelting helps to reduce the grain size.

Further work by Brandl et al [132] looked into the fatigue testing of AM parts. This work is important in high-cost industries as load bearing parts in automotive and aerospace industry are often exposed to cyclic loads beyond 10^7 cycles. This work mainly investigated high cycle fatigue using between 5 and 15 specimens. The work

used common round un-notched specimens (Kt = 1.0) according to ASTM E466-07 with tangentially blending fillets between the test section and the ends for this fatigue analysis. A uniaxial test setup with a stress-ratio of R = 0 (pulsating tension) and N = 10^7 cycles as the maximum number of cycles was selected. The test frequency was varied between 70 Hz and 140 Hz depending on the applied load.

As well as investigating the effect on fatigue properties, in a separate study Guan et al, investigated the effect on tensile properties [139]. It was found that tensile properties are independent of slice thickness and overlap rate but increase slowly with increasing interval number of deposited layers before the original layer angle is reached again. It was found that slice thickness affects the surface roughness but that the microstructure is similar and there is no noticeable effect on the tensile properties.

Fatigue crack growth has been investigated in SS316L for both with and without HIP treatment. High Cycle Fatigue and crack growth are not affected by process induced imperfections and therefore there is no significant difference between HIPped and unHIPped. Also that austenitic SS316L shows good fatigue properties as built [45].

Anisotropy of microstructure and properties has been observed in some cases due to build direction. Anisotropy of mechanical properties has been found for AM parts at ambient temperatures and further investigation looking at the properties at high temperatures has been undertaken [140]. This anisotropy is still seen at high temperatures and the microstructure is affected by the build orientation.

Keyhole-mode occurs when the method of melting changes from conduction. In keyhole-mode, the depth of the melt pool is controlled by evaporation of the metal. The threshold for moving into keyhole-mode is dependent on the layer depth and powder distribution and can be used to provide the optimum power, speed and beam size to avoid this phenomenon. King et al have investigated this and found the keyhole threshold to be $\Delta H/hs \approx (30 \pm 4)$ [118].

Work by Antony et al has investigated wettability and its effect on scan tracks and balling. The work found that optimum conditions can lead to continuous track and the main factors effecting this are laser power and scan speed [141].

Scanning Strategies

AM machines come with a set of standard parameters that can often be modified including the scanning strategy. This is the path the laser follows while melting the powder. A selection of potential scan patterns are shown in Figure 2:10.

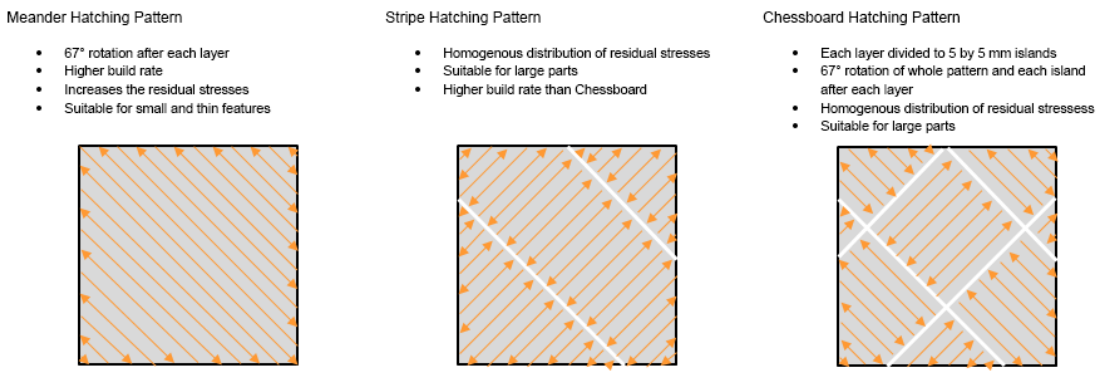

Figure 2:10: Laser Scan Patterns [167]

There are numerous SLM processes, machine suppliers and scan patterns. This work focused on Renishaw as that was the machine available and the stripe and meander scan strategies as these are similar, but one is continuous, and one has breaks in the scan pattern. This was to allow for investigation into what effect these changes had. Stripe scanning is unidirectional going from the front of the build plate to the back with the laser on, returns to the front with the laser off and starts again, whereas the meander pattern is bidirectional and follows a continual trail with the laser turned on. These laser patterns were chosen as there is an effect on the part solidification when using bidirectional when compared to unidirectional. From work by Jhabvala et al [166] scanning the entire area with a single pass had a detrimental effect on the properties and should be avoided. For this reason, hatches were used to avoid consolidation problems. Hatches are smaller areas of the build surface that are scanned by the laser completely before it moves to the next area to scan.

The scan strategy strongly influences thermal history, defect formation, microstructure and final part performance. Two of the most widely used patterns are meander and stripe [213]. These laser patterns create different thermal cycles influencing the microstructure, porosity distribution and mechanical behaviour. Meander improves uniformity, is simple, leads to low distortion and improved surface roughness [214]. Whereas stripe leads to improved porosity control, better thermal management and improved fatigue [215]. Different geometries and cross-section sizes require different heat-flow patterns. The availability of both strategies allows manufacturers to adapt printing to complex or thermally challenging designs [213]. It was found during the literature review that the effect of varying the process parameters and scan strategy had not been fully investigated and understood. As the AM industry has developed, more research into these effects has been carried out. This involves looking at the

effect on microstructure, mechanical properties, residual stress, deformation and warping. Work has looked at the effect of the length of the scan line [168], [169], the scan layer rotation [169][170][171] as well as using simulation to help develop novel scanning techniques [172]. These research projects have established that the scan strategy does have an effect, and changes can help adjust the microstructure and mechanical properties, this is discussed further.

Build Parameters

It has been seen [173] that there are variations across the build plate that can affect the components' density and mechanical properties. Initial studies have established that the gas flow over the powder bed effects the properties, due to '*inefficient removal of by-products*' which effect the melting of subsequent layers. What needs to be understood is how these effects vary the properties and ensure these changes are separate from those that come from adjusting the build parameters. The changes across the build plate have been attributed to both the gas flow and also when the laser power isn't as expected. The laser power could be affected due to the laser window having dirt marks or scratches, which diffuse the beam, or the laser being misaligned.

Along with the build plate location the support structures can also affect the properties as they can change the heating and cooling speeds and microstructure of the components. Cloots et al [174] have looked at minimising the support structures needed for SLM components. Changing the support structure used, affects the heat dissipation and the final density of the component, this is due to dwell time on the layer and the heat build-up within the component [175]. Reduced density has been seen to reduce the tensile strength [176] of the component and the failure mode. The support structure adjustments also affect the surface roughness, an increase in surface pitting can create initiation points which affect the failure mechanism seen. Although these are negatives of support structures, they also offer a benefit where they can be designed to help with thermal management and heat dissipation from the component as it is built.

Gong et al [177] have looked at the effect of changing the build parameters to change the energy density supplied and how this affects the generation of defects. Too high or too low energy density affects the parts quality. Too high causes over-melting and vaporisation leading to keyholes and pores formed within the solidified material. Too low energy densities mean that there is reduced melting and the layers may not adhere

to the lower and/or adjacent layer. Both changes will have created different failures modes for the components, but these have not been studied within this work.

Build Orientation

What little is known about AM parts currently leads us to believe that AM parts will have anisotropic properties. Due to this, work is being carried out to investigate how build orientation affects the parts properties.

Brandl [132] also looked at whether there was an effect due to the build angle. This work found that there are differences in fatigue life due to build orientation, but these differences can be minimised by heating during the build at 300°C. This has also been investigated by Tolosa et al [46] to see the effect of changing the build orientation and comparing it to wrought properties. The samples tested all had densities exceeding 99.9%. It was found that the parts had tensile strengths exceeding rolled conditions in all directions. Guan et al [139] also looked at the effect of build orientation and their results didn't match those previously reported as they found that all directions produced UTS in excess of wrought 304 with the vertical samples showing an optimised combination of strength and ductility.

Heat Treatment

It is known that parts built using SLM are likely to have residual stresses when they are built. One of the known current methods to combat residual stress is heat treatment. Work is now starting in the AM field to investigate the effect of heat treatment on SS316L parts manufactured using SLM.

Work by Montero Sistiaga et al [142] investigated the effect heat treatment has had. It has shown that heat treatment can help to dissolve the cellular dendritic structure, lowering the hardness, yield and ultimate tensile stress along with increasing the impact energy absorbed by the parts. This work has also noted that inclusions reduce the elongation values of SS316L parts.

2.4.4 Binding Effects

As well as papers looking at how parameters can affect parts, papers have been written on the different types of binding mechanisms, including the paper by Kruth et al [22]. The paper [22] looks at the method of selective laser sintering, powder used in this method can be Sold State Sintered, (SSS) which occurs between $T_{melt}/2$ and T_{melt}. This uses diffusion to bond the particles and has the advantage that many materials can be processed this way. In addition, there is liquid phase sintering, which is partial melting,

the binder is melted, and the powder remains solid, with the binder being used to hold the powder together. However, if debinding is not carried out after sintering then the parts that are created are hybrid polymer/metal parts and not 100% dense metal parts. The final method that could be used is full melting. This is used to produce 100% dense parts that have good properties when compared to bulk material. This is the method that is currently being explored the most as it is seen to be where the future lies [22].

2.4.5 Effect of Temperature

Another of the papers explores temperature measurements during SLS of titanium powder [143]. The paper draws comparisons between continuous wave sintering and pulsed sintering temperatures at the skin and averages. It was found using these experiments that in fact the average power to achieve consolidation with pulsed laser is 30% lower than for continuous laser, but the consolidation is better with continuous laser due to liquid phase sintering efficiency and so yields stronger connections between the particles. It is also seen that for continuous wave there is no difference between skin and average temperature but in pulsed laser interaction the average temperature was lower, but the sintering was stronger, it is believed that this occurs because a higher skin temperature rise must exist. Finally, it is noted that the measurements of temperature predict the advantages of pulsed laser sintering. This is because lower average power and thus lower average temperature yields stronger consolidation due to the much higher peak skin temperature. What has been found means that complete melting does not take place therefore less shrinkage occurs, so higher lateral precisions and less residual thermal stresses occur in the finished piece. Zhang et al [136] have shown that preheating the part leads to an increase in stress and strain but that it also increases the deformation rate affecting the dimensional accuracy.

2.4.6 Measuring Temperature

To be able to see the effect of temperature in the process it is necessary to measure the temperature. The paper by Gao et al [144] looks at using infrared thermograph non-contact testing to monitor the temperature in the material and the chamber. The proposed temperature method is compared to simulations to see how the new method compares. It was found that the results from the experiment and simulation are a close match, 310°C simulated and 314°C tested [144]. The method works by using a

thermograph to film the powder bed and the video signal is transferred to a computer so it can be analysed by the team.

Using a temperature measuring device has shown that there are three temperature stages during the AM process for each layer. The first is the preheat stage where the temperature is constant, the second is the transient sintering stage where the temperature gradually rises to the melting temperature and the third and final is the heat diffusion stage where the heat leaves the sintered area, and this area turns to solid. Unfortunately there is another heat peak shown in the experiments [144], where the laser returns to the starting position for the next run it heats the area around the powder as it goes over because although it is off it is still hot. This can be a problem for the powder as it does not like the constant heating and cooling of layers and this is believed to be what causes bending and curvature of the layers leading to warping and delamination. Therefore, this needs to be accounted for within modelling and a method to remove this problem should be further investigated.

The results that have been found from measuring the transient temperature in the SLS process show that the temperature at the sintering point rises when the scanning speed decreases and the laser power increases. This is believed to mean that as the laser power increases more heat is absorbed by the powder and at a slower sintering speed there is a longer sintering period [144].

2.4.7 Material Composition Effects

There are also papers that have been written including by Nakamoto et al [145], which look at how the carbon content of steel powder affects its properties. Although for aerospace parts Titanium will be used, it is good to study which parameters can be changed to improve the properties of SLS parts. It has been seen that generally as the carbon content is increased then the micro hardness and yield stress also increase. But also it has been seen in the experiments carried out that these factors also increase when a part is produced using a lower energy input [145]. This point can be taken on board and may be of help in the production of aerospace parts. The powder composition has also been seen to have an effect due to the formation of impurities in the final parts [131] and leading to weak bonding points between layers.

Along with looking at the composition of the powder, the effect of powder size has also been investigated. Boisselier and Sankare [131] found that a wider spectrum of

powder distribution and a higher quantity of finer particles <50µm lead to smaller grain size and an effect of the powder flowability resulting in issues.

2.4.8 Build Chamber Effects

Matthews et al [117] have investigated denudation of powder due to the gas flow and look to see what kind of effect this has on the melt path. This work found that particles are drawn into the melt pools behind the laser, and this directly affects the surface roughness. Before this work was carried out, limited information was known about this effect but having further investigated it during this work, it has now been included in finite element models helping to further understand the process. Figure 2:11 from the work shows the effect of the Bernoulli on the build process. Showing how the particles are moving during the scan process and melt with a fraction of them colliding with the melt pool and being incorporated into the melt and the remaining fraction being swept away from the melt pool in a rearward direction relative to the laser scan direction.

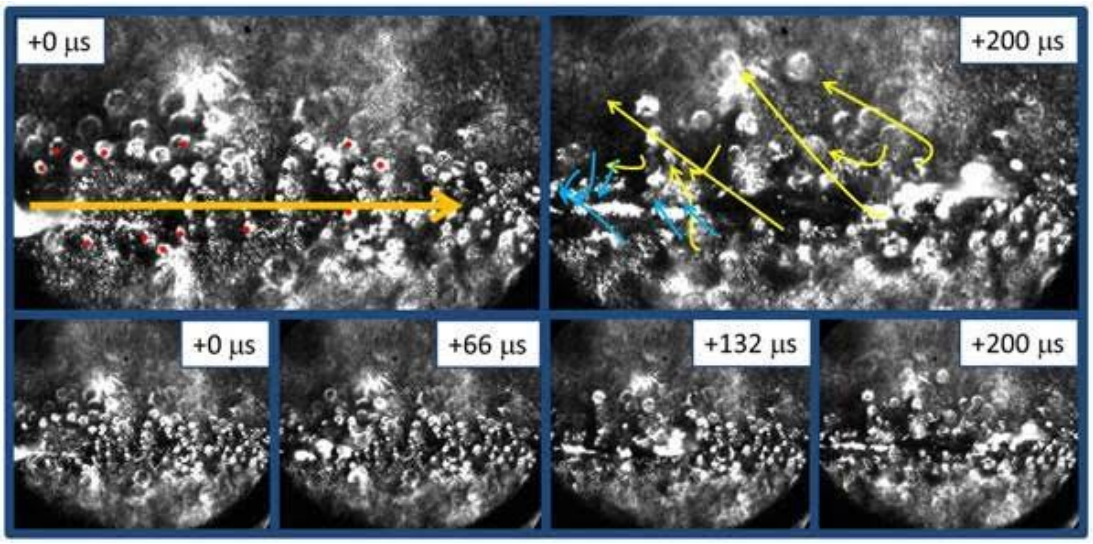

Figure 2:11: High-speed imaging of melt track progression and powder movement under the influence of the hot vapour Bernoulli effect. . [117]

2.4.9 Mechanical Testing

To fully characterise AM components, mechanical testing needs to be carried out. Varying processing parameters or scan patterns and carrying out testing to see what effect this has on the properties has been investigated [195] but this testing has mainly been on a limited number of samples.

As ASTM standards are developed for AM materials the testing procedures and the samples to test will be defined. Until then there will be variations between different

research groups so read across between studies should be carefully considered. For this work standard testing of density, porosity, tensile strength and hardness were carried out.

When looking to qualify components, large numbers of data sets and points are needed to show the spread. For this reason, the University of Mexico has started to look at high-throughput tensile testing [193]. The study looks to compare tensile samples first vendor to vendor, then within a build and finally build to build. It showed that this testing method on micro tensile bars has been seen to produce comparable results and revealed that rare defects are in fact seen in only ~2% of the population. Residual porosity is seen to be a cause of failures. The work also looked to see how hardness can be compared to strengths from tensile testing. It was seen that hardness can be used as an estimate for tensile properties.

NDT methods that are used on components manufactured conventionally are now starting to be transferred over and used on AM components [209]. These include tests like hardness testing which is suggested as a method to help determine the strength properties. This work can be developed still to add automation and comparison to other data sets. These comparisons will help to further understand and characterise the failure mechanisms and causes. Using AM is helping to ensure the quality of components manufactured and checking for presence of defects or porosity [209].

Harris and McShane, [196] have studied the anisotropy of AM materials and how this affects the fracture surface in compression. This work looked at developing lattice structures and how changing the density affected the properties. It was found that the components ended up with relative densities that were similar also had similar mechanical properties. The work saw that the development of pores in the fracture surface affected the mechanical properties. Internal pores that are caused by trapped gas or changes in thermal history have flat uninterrupted surfaces whereas where the powder had fully solidified to the surrounding melted powder the surface shows the dimpled effect of a ductile fracture.

When looking at SS316L, Bartolomeu et al [197] found that the finer microstructure found in AM components means that the mechanical properties are increased when compared to hot pressing or conventional casting. From this it is possible to see that there is a link between the manufacturing route and the microstructure and mechanical properties obtained. Another research project [198] has described this in more detail looking at how the composition of grains is known to affect the failure mechanisms of

components. SLM is a good process to increase abrasion resistance of components, but this work hasn't looked at how these changes in microstructure affects the failure modes of these components [198]. Barba et al [181] showed that changing between contouring and hatching strategies influences the component's microstructure.

2.4.10 Modelling

Modelling of AM processes needs to be carried out because as it stands not enough is known. Therefore, to find the optimal solution it is often required that operators of the machines follow the method of trial and error. As this rarely produces the required result on the first go, this type of method can be very costly and time consuming. Therefore, to improve efficiency, computer simulations are being created that can work through the process and produce the required outcome on the first go of machining.

Modelling will be very important and can be used before building begins to help develop the build process and eliminate parameters that are shown by modelling to produce 'bad' samples [146].

In the past, there has been lots of work done on looking at different types of modelling for SLS and other AM processes. Modelling has been carried out on a variety of different scales. Also modelling has been carried out that is a simplification of what occurs in the real world. There are a number of papers written where the model is based on a homogeneous material; this is where there are effective properties applied to the whole layer and not applied to each individual particle. Also modelling can be more realistic by applying the properties to sub divided layers of the simulation. However, none of these are as good as applying the properties to each individual particle though these simplified models require less computation resource to resolve. The paper by Kormer [56] looks at simulation on a mesoscopic level and this allows the properties to be applied to an individual particle. This paper explains both the dominant mechanism (bolded titles in Figure 2:12) [56] and simplifies the secondary mechanism to simplify the process to be able to computationally model it.

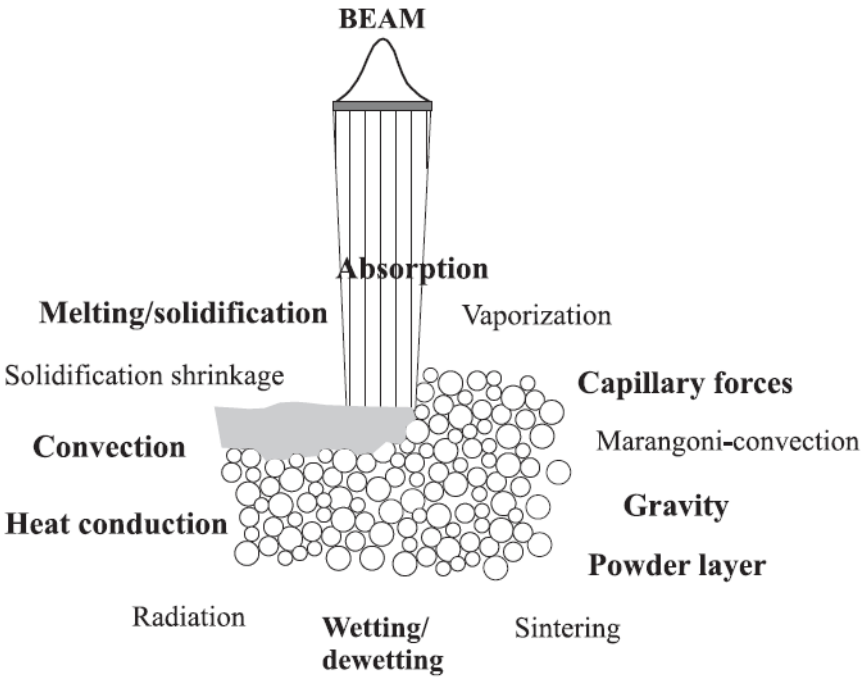

Figure 2:12: Reactions during SLM [56]

One of the problems with the SLS process is that it is very complex and so requires a lot of information to be input into the simulation to ensure that a truly accurate result is produced. Also, when modelling the homogenous process, it is necessary to model powder shrinkage. This can be up to 50% and occurs during the solid – liquid phase transition. This can be challenging and requires a number of extra equations to be input.

Modelling of the parts and of the build process is developing. This allows prediction of what the finished part will be like. To continue to progress this what now needs to be investigated is to see how the results from the simulations compare to the results shown in the in-process monitoring data sets and the parts produced. The problem here is that the simulation software (currently available) doesn't predict what the melt pool emissions or material temperatures will be. The layers are added to the simulation at the melt temperature; therefore, we don't have any information about how power deposited onto the surface heats the material and creates visible emissions.

2.5 Simulation and Digital Twins

Process modelling is developing as a tool to simulate the build process, to establish deformation and residual stresses likely to occur during the AM process and to help create a digital twin to be kept, adding to the component qualification dataset. This

requires several stages looking at micro, meso and macro scale simulation of Selective Laser Melting (SLM) builds [203]. The first stage of this simulation looks at the micro scale effects of the build process including the melt pool. This then feeds into further stages of simulation looking on the macro scale at part wide effects including warpage and distortion. A digital twin *"is a virtual model of a process, product or service. This pairing of the virtual and physical worlds allows analysis of data and monitoring of systems to head off problems before they even occur, prevent downtime, develop new opportunities and even plan for the future by using simulations."* [204].

Simulating the build process to generate whole parts and predict part properties will help engineers understand how parts should perform but simulations need to be compared to and validated by experimentation [203]. This can be done using in-situ process monitoring information and through mechanical testing.

Although complex models of the AM process are being developed and are still not accurate enough to fully validate a component build history a simplified model of the additive process used by Letenneur et al [205] has been created to predict the density of components produced using different build parameters. Being able to predict the density means that the pre work through parameter optimisation builds on the machine can be reduced. The design of experiments is set up using previously established parameter sets. Work is then undertaken to define the best parameter set needed to generate high density components with comparable mechanical properties. The work within this thesis was started before Letenneur et al [205] and would have been helped by it due to reduced initial parameter sets to test. This would help with developing high quality parts quicker as well as to validate and qualify these components for service environments.

2.6 In-Situ Monitoring

In-situ monitoring can take many forms, machine vendors are starting to put conventional, high speed and thermal cameras, thermocouples, photodiodes, pyrometers and sensors into systems. What can be seen currently does not provide enough data in real time and work on developing these systems further is required. There is no agreement between vendors or consumers on what data is needed as not enough information is currently known. There is also a data storage issue with many of these methods as the amount of information produced requires large storage areas which is currently expensive to purchase and maintain. The longer-term aim of in-situ monitoring is to be able to feedback the results of what is seen during the layer building

to generate an adaptive control programme that can adjust the process as the build is running to mitigate against defect formation. This would help to close the feedback loop this research has begun establishing. Data analytics and artificial intelligence would help with this as it would provide the examination of the data received and the detection of issues and the necessary corrections to mitigate these [210].

This is also an area that is widely investigated by several universities and publications in this area are increasing. Paul Hooper and his team Imperial College London [199] are using in-situ monitoring to investigate the melt pool, its temperature and cooling rates and the effect these have on component properties. Using in-situ monitoring combined with variations in parameters and scan path could allow for a new tool to be developed to identify the formation of defects and their causes along with working out how to control the microstructure of AM components. Virginia Tech, Iowa State and Johns Hopkins are a few more universities looking at in-situ monitoring for various AM processes.

Previous work, including this PhD, has seen that the microstructure of AM components varies from conventionally machined material. The microstructure has been seen to grow through the layers as the parts are built up. It has also been seen that the microstructure of SS316L within a layer is made up of many smaller grains, but heat treatment has been seen to effect this [183].

Spears and Gold [200] make the point that currently the results from changing parameter settings are currently only qualitive and more needs to be done to understand these results. Statistical Process Control (SPC) is a method of measuring and controlling quality by monitoring the manufacturing process and drive continuous improvement [201]. To be able to develop SPC for AM more needs to be done to improve the process models being used and feed in the required materials data and in-process information to validate the models. Once these models are improved it is possible that they will be able to predict the microstructure that will be achieved and the likely defects within the component and failure mechanism which in turn can be linked back to work carried out for this thesis.

In-situ monitoring as it is established will become the control mechanism to check how the build is progressing and feedback into the control loop to obtain the desired optimised component.

Work by Strum et al [202] looked at using in situ monitoring on material jetting to detect defects. This method shows that defects in excess of 2.28% of the part volume

can be detected. Adding this to the feedback loop this PhD has started to develop would allow for defects to be detected during the build process and actions undertaken to minimise or remove these defects.

2.7 Qualification of AM Components

The future for AM components use is increasing but for this to happen part qualification needs to be established. Part qualification will not be an easy route to take due to the differences in part quality when produced during AM processes. SLM components have been seen to contain defects within this literature review and these defects will have effects on parts performance and properties. Understanding these defects and why they form is an area where little research has been carried out and is an area where further investigation should occur. Once researchers can predict why these defects are formed it may be possible to modify AM build processes to minimise these defects and produce perfect parts.

To begin the qualification process first the parts must be designed for AM. Once components have been designed a build plan needs to be designed. This will include the parameters that are used to build the part.

Modelling can be used to investigate which parameters are believed to provide parts with the best properties and these can be used to reduce the number of parts manufactured. This would allow for a reduced set of test parameters to provide the best results for part properties.

Chandrika Kamath at Lawrence Livermore National Laboratory has tested this theory using software to predict which build parameters should be used to manufacture single scan path tracks.

To understand the properties of AM parts, standard test parts can be produced and tested but to understand how each individual part would react this method may not give you all of the information required. Some companies including GE lock down a specific machine and operator to a certain part, but this is not a cost effective method when your company produces one offs or small production runs. In this case when building the individual part, it would be possible to build a traveller part which can be investigated after the build. A traveller part would be of a similar design of the part, showcasing its distinctive features. This would allow the designer to be able to understand how the parts design affects the parts properties a part must be built using the process that can be investigated. GKN use traveller parts to characterise their parts.

It is not always possible to do but when it is reasonable building an exact replica of the part or a traveller including the parts distinctive features, allows for the design dependant properties to be investigated and the material characterised to qualify that machine to build that part. The part will be cut up to produce tensile bars and similar for testing. Along with mechanical testing, Non-Destructive Testing (NDT) and microstructure evaluation can be carried out.

The monitoring of in-situ process data during the build is increasing but the issues with this lies with the amount of data that is produced and how to store and process this data in real time.

All of the future work towards qualification that has begun and is mentioned in this section will help to produce fully formed standards that will help qualify parts for use but first the full extent of what data we can achieve and what information this data provides needs to be explored.

2.7.1 Standards

As AM technologies have developed, international standards have also been progressing, including: 'AM Stainless Steel Alloy (UNS S31603) with Powder Bed Fusion (PBF)' [158] and 'AM Titanium-6 Aluminium-4 Vanadium ELI (Extra Low Interstitial) with PBF' [159]. These standards detail the AM of components using the specific material and a PBF process and the acceptance requirements for them.

Standards are also currently being developed to help test and qualify the AM process and components. These standards are being developed by the American Society for Testing and Materials (ASTM) and International Organization for Standardization (ISO) groups alongside leading experts in the AM field. Initial investigations and research projects are being used to help support this and the need for this information has helped to progress AM research which has moved it past just focusing on the main materials (SS316L, Ti6AL4V and Inconel718) and basic mechanical properties to a much broader range of materials, mechanical tests and looking at subsequent in-situ process monitoring to help develop high quality AM components.

These standards have begun developing manufacturing plans and mechanical testing plans which supersede the testing protocol defined in the thesis but compliment it and its aims. These were to define a standard method of testing AM components to ensure the best processing parameters are used to manufacture AM components for service.

2.8 Conclusions

This literature review has twice found that although work has continued to progress during the last 5 years, there are still gaps in the research. Numerous investigations into mechanical strength, density and microstructure along with looking at failure mechanisms have been carried out but the true link between these has not been clearly established yet.

This means that although the original PhD was carried out between 2010 and 2015 the information gained is still relevant. As shown earlier, more of the recent studies have investigated Ti6Al4V carrying out a comprehensive study of what is known. Although that research is on Ti6Al4V and this work looked at SS316L, it can be seen that there is a lack of understanding of the effects of '*net-shape, size effects, microstructural analyses or chemical changes*' on components mechanical properties. The work looks at how the processing effects the microstructure and chemistry and then links to the mechanical properties. This is similar to the work carried out within this thesis and once the mechanical properties can be linked back to the processing parameters once the failure modes are determined the closed feedback loop is created.

The gaps in the published research suggests that being able to feedback what is observed during the build to improve components properties by predicting the output is what is desired by the AM industry. This feedback will also help tailor the microstructures and failure modes and in turn to tailor the components properties. This work has looked at establishing correlations between the process parameters used, the microstructures seen and the effect these have on the failure modes and mechanical properties. The study of images of samples fracture surfaces and microstructures will help develop the dataset needed to be able to understand what is happening within AM components during the build. Add this to the published research and a well understood feedback loop could be developed.

2.9 Limitations

Although this review of the literature has shown that there have been developments there are still areas of research that continue being investigated. Using in-situ monitoring for feedback loops is improving and this work here will help feed into that. This work has not fully developed what it had intended, but it has shown the beginnings of the process and could be developed by other researchers. With time, AM will continue developing and comprehensive in-situ monitoring will become

common place. But until that happens what occurs during the build process will not be fully understood or characterised.

2.10 Future Work

From the research reviewed and the work carried out here to develop this, further work should be carried out looking to close the feedback loop. The introduction of in-situ monitoring to more machines will be essential with this. It is necessary to understand why these parameters cause these failures. This becomes the feedback input.

The methods established during this work can be used to feed into an Artificial Intelligence (AI) engine. This can be trained using images and information gained in similar projects and this AI engine would be able to control the machine, vary parameters as needed to produce the desired outcome.

Simulation of the build process is not at a state yet where the integration with an AI engine would be successful, and this is an area that still needs extensive development.

2.11 Summary

This literature review has looked at the literature that is available currently concerning the AM manufacturing process and what is known on this subject. What has been found is that there is a selection of manufacturing techniques available, and they are just starting to be used to manufacture parts for industry use.

The review has shown that there are many manufacturing techniques and materials that can be used but that more research needs to be carried out to fully develop the methods to receive the best possible parts.

The long-term outlook of the AM industry is that new manufacturing techniques will allow parts to be built where they are needed and to reduce the need for transport. This is due to the ability to remove excess material and so reduce the weight of parts built using this method.

The literature review has found that there are challenges still associated with AM parts manufacture and fully understanding how they develop during the build process and how the final form can vary. It also found that numerous problems have the potential to occur during the manufacturing of AM components. These issues are not currently fully understood, the work here will look to provide an explanation as to why these occur and how process parameters affect them.

The rest of this work will be looking to find out information on the SLM technique mentioned above and looking at seeing if it is possible to predict the failure mode of

AM parts, whilst also testing different build parameters and heat treatments experimentally to see how the parts properties vary due to these changes.

The subsequent review of the literature has looked at more recent papers around AM and how research has developed since this PhD began. What has been found is that there have been improvements to the research and understanding of AM along with its implementation, but work is still continuing to fully understand and optimise the process.

As AM has been adopted more widely and research has continued, it is clear to see that it is growing from strength to strength, and more is understood about the process and properties but there is still more to understand.

This work will continue to investigate the effect parameter and processing conditions have on the failure modes of AM parts alongside how these properties vary during testing and investigation. Additive Manufacturing is still a developing technology with improving implementation and use within industry. Research into the technology continues and components manufactured this way. Qualification of AM components is the current hurdle needing to be overcome by both industry and academia ready for full implementation in manufacturing processes.

This work will investigate the properties of AM test samples and how they vary with changing processing parameters and heat treatments to allow a better understanding and support a system of test artifacts and parameters to allow full characterisation of a system when it is purchased and installed.

Chapter 3 Method

The following chapter defines the experimental work that establishes the properties of SS316L AM built parts and the parameters that are to be varied during the work. The analysis of these experiments is discussed in Chapter 4, Results. The experiments to be undertaken in this work included: sizing, density, porosity, roughness, tensile strength and hardness and these experiments will be discussed and explained here. Along with these experimental tests, microscopic analysis has been carried out and the methods behind this are explained. This work has been carried out as it allows for a thorough examination of AM parts to provide a broad range of figures that can be used to further understand the parts AM processes produce.

The chapter will conclude by summing up the process and parameters that will be used in the manufacture and analysis of the SS316L parts.

This chapter describes the experimental methods from this thesis's work, including:

- the builds generated,
- build parameters used,
- specimen design,
- mechanical testing techniques, and
- optical and scanning electron microscopy.

3.1 Aims

- The aim of this work is to conduct a scientific study of AM components focused on microstructural characterisation including grain morphology and defect distribution,
- fractographic analysis to identify crack initiation sites, fracture features and material defects,
- failure mode identification, and influence of build parameters, and
- mechanical property evaluation including strength, density and variations due to build parameters.

3.2 Manufacturing the Test Pieces

For this work, AM parts were produced on the Renishaw AM250 and AM400 machines, at Swansea University, Figure 3:1 and Figure 3:2, within an air-conditioned room at 21°C and 40-45% humidity. The conditions of the room are as specified by

the machine manufacturer. The AM250 and AM400 work using the method of Selective Laser Melting (SLM) to build up the parts.

Figure 3:1: AM250 AM Machine

Figure 3:2: AM400 AM Machine

The author has had the opportunity to experience using an AM machine during this work, all initial samples were produced by the author. This has given the opportunity to fully understand how the AM process works and the ability to design and manufacture parts using this method.

The AM250 machine operates a maximum 200W laser with a beam diameter of 70µm. The build area is 250 x 250 x 300 mm (X, Y, Z) and the layer height can vary from 20 to 100µm. The AM400 machine operates a maximum 400W laser with a beam diameter of 70µm. The build area is 250 x 250 x 300mm (X, Y, Z) and the layer height can vary from 20 to 100µm.

No changes were made to the machine or parameters during these builds other than those stated below.

Table 3:1: Summary Table of Machine Parameters

Machine	AM250	AM400
Build Programme	1 & 2	3
Supplier	Renishaw	Renishaw
Maximum Laser Power	200W	400W
Laser Power Used	BP1 – Varied BP2 – 200W	200W
Spot Size	70µm	70µm
Laser Type	Continuous	Continuous
Possible Layer Thickness	20 - 100µm	20 - 100µm
Layer Thickness Used	50µm	50µm
Exposure Time	BP1 – Varied BP2 - 80µs	80µs

To manufacture the parts the starting point is to create the 3-D geometry in generic CAD software. These CAD files are then input into AutoFab where the supports are attached and the 50µm slices of the build defined. The file is subsequently saved as an .MTT file. This file is then transferred to the machine to start the build. These slices define the area and the path the laser will melt during each layer of the build. This is also when the build plate is set up which is the carrier for all parts within the build. The support layer is a highly populated, low-density layer built under the parts to allow for easier removal from the build plate.

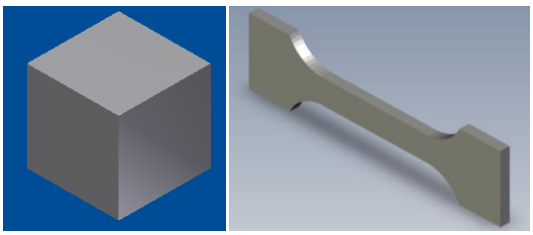

Figure 3:3: CAD Image: (a) 10mm Cube, (b) 30mm Gauge Length Tensile Bar

The 10mm cube and tensile bar's geometry is illustrated in the CAD images in Figure 3:3.

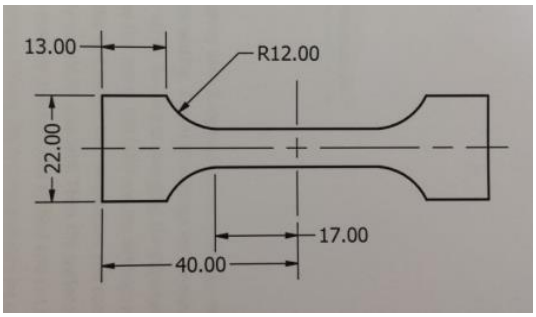

Figure 3:4: Scale drawing of the Tensile bars (mm)

Figure 3:4 shows the dimensions of the tensile bars used, the bars had a thickness of 3mm. The size of the tensile bars were determined using BS EN ISO 6892-1:2009 [147], Metallic Materials – Tensile Testing.

It has been chosen to build these parts to provide the most data to establish the properties of these SS316L AM parts. The tensile bar will provide the Ultimate Tensile Strength (UTS), Young's Modulus (YM) and Yield Stress (YS). The cube can be used to test the density, surface roughness, hardness and to look at the external surface and internal microstructure.

The UTS is calculated from the data produced by the tensile test machine, it is the maximum stress obtained during the tensile test. The YM is defined as the gradient of the linear portion of the curve; this is calculated using a macro to eliminate subjectivity. The YS is defined as the point where linearity of the curve ends. The stress and strain calculated within this work is the nominal stress and stress at the cross-sectional area has not been taken into account during the processing.

3.3 Powder

This work uses two different types of powder. It must be noted that comparisons between the results found from the two separate powders should be avoided as the powder composition and particle size distribution may influence the mechanical

properties of the final components. If it had been possible the same powder would have been used for all of the work, but operational constraints have affected this. Results for samples made using the same powder can be directly compared.

3.3.1 Powder One

For the first set of builds, the powder used was SS316L supplied by LPW produced via gas atomisation under argon. The powder composition specification is shown in Table 3:2. The powder particle sizes were found to vary from 15µm to 45µm [122]. The powder was sieved between uses using a 45µm sieve. The powder can be reused; this reuse is limited by the Oxygen content of the powder to ensure it meets the required standard. LPW [148] found that mixing with 'virgin' powder helps keep the oxygen content low. This process also requires sieving between uses to remove any larger and burnt particles and to keep the PSD comparable.

Table 3:2: Composition of Powder One [7]

Grade 316L		Fe	C	Si	Mn	P	S	Cr	Ni	Mo	N	Cu	O
Wt.%	**Min**	Bal						17.5	12.5	2.25			
	Max		0.03	0.75	2	0.025	0.01	18	13	2.5	0.1	0.5	0.1
	Actual		0.019	0.67	1.45	0.019	0.006	17.9	12.7	2.36	0.06	0.2	0.022

3.3.2 Powder Two

For the later aged powder builds, SS316L from Sandvik-Osprey was used. The powder composition is shown in Table 3:3. The powder PSD fractions are D10 -18.2, D50 – 30.2 and D90 – 50.4. This powder was also sieved between uses using a 45µm sieve.

Table 3:3: Composition of Powder Two

Grade 316L	C	Si	Mn	P	S	Cr	Mo	Ni	N	O	Fe
Wt.%	0.02	0.7	0.7	0.02	0.01	16.8	2.3	12.4			Bal

3.3.3 Ageing

The second powder in this research has been sieved so that it can be recycled and reused within the AM machine. Further investigations would need to be carried out to see how many times the powder can be recycled before it becomes ineffective for

building AM parts resulting in compromised parts when compared with ‘virgin’ powder.

Ageing of powder has been considered both in terms of how long it is kept before it is used within the machine and also the number of times it has been through a build process.

The way this has been checked is that Particle Size Distribution (PSD) has been investigated after each build to see if there has been any effect on the powder size or distribution due to going through the build process. This is to ensure that the powder size remains within spec when compared to ‘virgin’ powder. The powder was not optically inspected between builds.

Powder two was aged powder; the aging process here was defined by the number of times the powder was reused without the addition of ‘virgin’ powder. The powder was reused over a period of 6 months with sieving between builds. The powder was ‘virgin’ when initially used in the machine. Over 6 months it was possible to build more than 30 build using this powder without the addition of ‘virgin’ powder until there was insufficient powder left to generate a build.

3.4 Builds

3.4.1 Purpose of Builds

Build Programme 1

Build Programme 1 (BP1) was the initial work carried out; the purpose of this programme was to investigate the effects of laser power, exposure time, hatch style and layer rotation on mechanical properties and microstructure. These parameters were varied as shown in Table 3:8. There was a total of six builds carried out. These were built on the AM250 at Swansea University (Singleton campus) using new LPW powder. Cubes and tensile bars were built, and these were tested macroscopically and microscopically.

Build Programme 2

The purpose of Build Programme 2 (BP2) was to investigate the effect of aged powder within in the AM build process. These were built on the AM250 at Swansea University using aged Sandvick-Osprey powder. The aged powder in this instance is powder that has been run through the machine for numerous builds until there was not enough powder left for a new build.

Table 3:4: BP2 Build Parameters

Laser Power (W)	200
Exposure Time (μs)	80
Hatch Style	Meander
Angle Increment (°)	67

Table 3:5: BP2 Heat Treatment/HIP Parameters

	Ramp Up (mins)	Hold (mins, °C)	Ramp Down (mins)	Pressure (MPa)
HT1 (BP2)	90	120 @ 450	90	N/A
HT2 (BP2)	360	240 @ 1150	360	N/A
HIP	360	240 @ 1150	360	100

Build Programme 3

Build Programme 3 (BP3) was designed to investigate the impact of heat treatment post build on mechanical performance. These were built on the AM400 at Swansea University using new Sandvick-Osprey powder. BP3 contained one build.

Table 3:6: BP3 Build Parameters

Laser Power (W)	200
Exposure Time (μs)	80
Hatch Style	Meander
Angle Increment (°)	67

Table 3:7: BP3 Heat Treatment Parameters

	Ramp Up (mins)	Hold (mins, °C)	Ramp Down (mins)
HT1 (BP3)	360	240 @ 1150	360
HT2 (BP3)	90	120 @ 450	90
HT3 (BP3)	420	250 @ 1125	240

3.4.2 Build Programme 1 (BP1)

Six runs were built in total, and these are explained below. The first two builds set up the test array of the set parameters, shown in Table 3:8. Two builds were used; they built the same parts using different laser patterns to see if the laser pattern has an effect on the parts properties. It was chosen to vary the parameters as shown to continue a study that was already being performed at ASTUTE, Swansea University [122].

Table 3:8: Test Parameters and Part Position

	Laser Power (W) →		
Exposure Time (µs) ↓	A1 – 80/160	B1 – 80/180	C1 – 80/200
	A2 - 105/160	B2 - 105/180	C2 - 105/200
	A3 - 130/160	B3 - 130/180	C3 - 130/200

Taguchi method could have been used to define the test parameters using an orthogonal array to design the experiments [149]. Taguchi method uses three steps, system design, parameter design and tolerance design to optimise the process [150]. Using Taguchi's method would study the entire parameter space with fewer experiments [151] but to coincide with another AM project [122] it was decided to use the same design of experiments points as that work.

The laser patterns that were chosen were Meander and Stripe, illustrated in Figure 3:5. The difference between these patterns is that stripe is unidirectional going from the bottom to the top with the laser on, returns to the bottom with the laser off and starts again, whereas the meander pattern is bidirectional and follows a continual trail with the laser turned on. These laser patterns were chosen as it is understood that there is an effect on the part solidification when using bidirectional when compared to unidirectional. Work by Wei et al [152] has investigated the melt pool and solidification of parts using these two methods and helped to begin to understand the difference and laser scanning patterns effect. There is other previous work [153] that has investigated simulating different laser patterns to see what effect they have on the parts properties. From this work it can be seen that scanning the entire area with a

single pass had a detrimental effect on the properties and should be avoided. For this reason, in this study hatches were used to avoid consolidation problems.

The pattern is rotated after each layer by a desired amount, 90° for the first set and the recommended rotation of 67° for the final set. This was the same for both patterns. The rotation between layers was varied to ensure that the laser scan paths did not continuously build on top of each other leading to consolidation of melt tracks and pores or unmelted areas or overheated areas within the part [153].

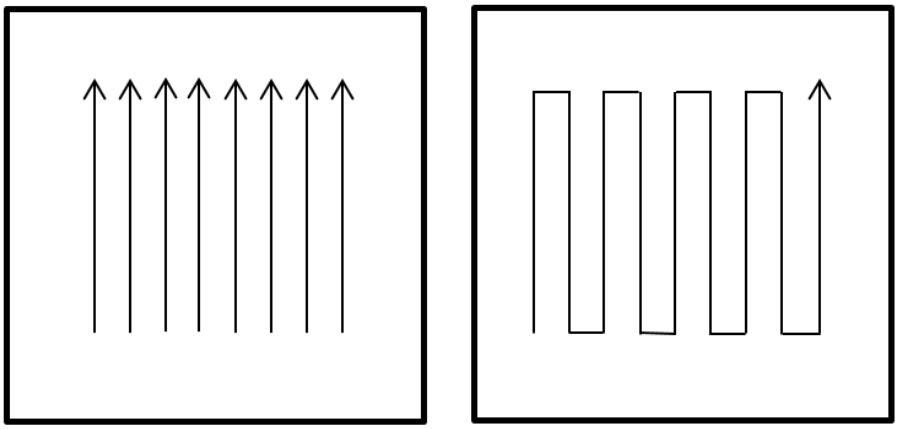

Figure 3:5: (a) Stripe Laser Pattern, (b) Meander Laser Pattern

These two laser patterns were chosen for this work because the meander pattern is the recommended laser pattern and should provide the best results due to the continual laser path and the stripe pattern is the simplest pattern the machine uses. The meander pattern with 67° offset is preferred, as this rotation ensures that all of the powder is melted due to this rotation performing the highest number of layers before covering the original pattern again.

The first build for each laser pattern, manufactured both cubes and tensile bars and for the second build, it manufactured cubes and flat bars. The settings for the two different hatch styles are described here showing the parameters used during this work.

The builds carried out using the Meander hatch style, Figure 3:5(a) had the following fixed build parameters:

- Hatch style – Meander
- Angle Increment – 90°
- Point Distance – 65µm
- Start Angle – 0°
- Hatch Space – 0.124mm

- Layer Depth – 50µm
- Contour Spacing – 0.1mm
- Offset and Border not hatch pattern – approx. 200µm
- Laser speed – 590mm/s

The parameters that are mentioned above show the two parameters; hatch style and angle increment, that are changed with the rest remaining constant. The first, hatch style, is the pattern the laser traces over the powder to build up the part. These patterns are shown in Figure 3:5 and are those used for these builds. The hatch style is one of the few parameters changed as it is thought this may also affect the quality, as parts of the powder may not be melted during the pass. Whereas certain patterns ensure that this powder is melted during the next laser pass due to the angle rotated. It may also affect the quality as the laser pattern will affect the cooling rate of the powder. The angle increment, the rotation of the pattern after each layer, is also changed, as with a smaller rotation angle more of the powder will be melted.

All of the rest of the parameters shown in Run 1, section 3.4.2, are now kept the same for both builds to isolate the parameters which have an effect and to eliminate the effects of changing too many parameters at once. These include;

- point distance, which is the diameter of the laser at the point where it hits the powder,
- start angle, which is the angle of the first layer,
- hatch space, which is the space between the laser lines,
- layer depth, which is how far down the base is moved before a new powder layer is applied,
- contour spacing, which is the distance between the laser lines,
- offset and border size, is the size of the border of each layer and
- laser speed, which is the speed the laser moves.

The values chosen for the hatch spacing, point distance and layer depth are the manufacturer recommended values for when building with SS316L on the AM250.

The second hatch style used was the stripe laser pattern, Figure 3:5(b). All parameters were the same as for the meander hatch style, except those below that do not apply to the meander laser pattern:

- Hatch style – Stripe
- Stripe length – 10mm

- Stripe width – 1mm
- Stripe overlap – 0mm
- Hatch order – left to right

These parameters control the geometric parameters of the laser path. The stripe length is how far the laser moves before it returns to the start axis. The stripe overlap defines an overlap of paths. In this case, this has not been performed but it could be used to increase melting of the powders to ensure all powder is melted. Finally, the hatch order decides which way the laser moves across the build area.

After these two builds were generated, it was decided to build more cubes from both laser patterns with the build parameters of these being the three extremes of exposure time and laser power from the previous series along with some flat bars built to study warpage or distortions during the build. These were Run 3 and 4. Run 3 had the same parameters as Run 1 and Run 4 had the same parameters as Run 2.

The final runs, Run 5 and 6, were the same builds and setting as in Run 1 and 2 but changing the angle increment to 67° in both runs.

Table 3:9: Runs and Parameters Used

Run	Laser Pattern	Rotation (°)	Build Parameters			
				Laser Power (W)		
1	Meander	90	Exposure Time (µs)	80/160	80/180	80/200
2	Stripe	90		105/160	105/180	105/200
				130/160	130/180	130/200
				A	B	C
3	Meander	90	Exposure Time (µs)	80	105	130
4	Stripe	90	Laser Power (W)	160	180	200
				Laser Power (W)		
5	Meander	67	Exposure Time (µs)	80/160	80/180	80/200
6	Stripe	67		105/160	105/180	105/200
				130/160	130/180	130/200

Test Series

The first series was of three cubes and three tensile bars, to ensure repeatability and accuracy for each of the settings, illustrated in Table 3:8. The layup is a 3 by 3 matrix, depicted in Figure 3:6. It was chosen to build the tensile bars standing vertically to

ensure enough samples could be built on the same plate. The layup of the build plate was chosen so that all samples for a particular setting were grouped in line and with enough space between different groups.

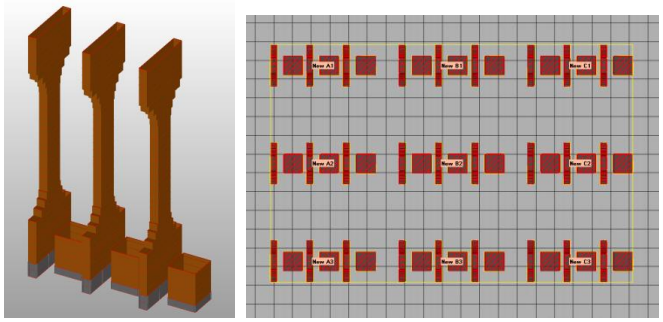

Figure 3:6: (a) Cube and Tensile Bar Set Up, (b) Build Plate Layup

The laser power and exposure time is changed as shown in Table 3:9. The test series includes the Renishaw recommended parameters; 105µs exposure time and 180W laser power to check if these are the best parameters. It has been chosen to vary these parameters to see what affect they have on the properties and microstructure of AM parts.

Laser power has been chosen, as this will affect the quality of the parts because the difference in laser powers may cause a varied amount of melting and re-melting of the powders to different layer heights. The laser power is the optical power output of the beam [154] and this will affect the melting of the powder.

Exposure time has been chosen, as it is believed that this will affect the powder melt quality and therefore the part quality and density. This would be due to there being air gaps or unmelted powder within the finished parts. The exposure time is how long the laser remains on a single point and again this will affect the melting rate.

Both parameters increase the localised power input leading to a larger melt pool and to a larger heat affected zone in the solid parts of the build and the powder around it.

It is necessary to ensure that too low an exposure time or laser power is avoided, as these do not allow for full bonding of the powder meaning parts may not build successfully and therefore their properties cannot be tested.

It is also believed that changing these parameters will affect the density and porosity of the parts because not all of the powder is expected to be melted during the shorter exposure time or lowest laser power. Therefore, this will influence the properties of the parts as lowering the density will likely lower the strength and stiffness of the part due to pores or cavities within the finished part.

Additionally, the surface roughness will be affected. This is likely to occur as the different exposure times will allow for more or less surrounding powder to be melted and drawn into the part. In addition, the time before the powder cools allows for more of the unmelted surface particles to be drawn into the parts surface and these will lead to an uneven and unfinished rough surface.

A second series was built to show if there was any warpage or distortion, or damage that occurred during the build process as an effect of residual stress. Parts were designed with this in mind, with parts built long and flat showing the highest warpage, therefore, it was decided to use these. These parts were built using the optimum settings and the two extremes, shown in Table 3:10.

Table 3:10: 2nd Test Series Parameters

	A	B	C
Exposure Time	80	105	130
Laser Power	160	180	200

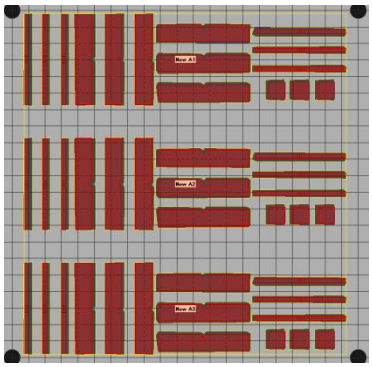

Figure 3:7: Build Plate Layup

The flat samples built were 55 x 10 x 2.5 mm. To determine whether warpage is affected by build direction, the plate was laid up as depicted in Figure 3:7. Six parts were placed vertical to the plane of the plate and six horizontal. Within these, three were built horizontal to the front of the plate and three vertical. The build settings used for these builds are the same settings as Run 1 and 2 previously.

A third test series was designed and built to ensure the results produced included the recommended settings from Renishaw of 67° rotation between the layers believed to give the best results. The difference between rotations should affect the density and porosity because when compared to other rotation angles a 67° rotation gives the maximum number of rotations before the 0° layer is melted again. This should allow

for more of the surface area of the powder to be melted during this process than if a 90° rotation is used and if the layer below is re-melted.
Each build plate was set up like the first series as an array of three 10mm cubes and three 30mm gauge length tensile bars for each set of parameters listed in Table 3:10.

Defining the Rules

The rules for the test series set out the test parameters for each section of the test. For the Volume Area, Volume Border and Volume Offset Hatch along with each row and column within the test series; 80, 105 and 130µs for the exposure time and 160, 180 and 200W for laser power.

3.4.3 Build Programme 2 (BP2)

Build programme 2 (BP2) builds were generated on the same AM250 machine using the Sandvik-Osprey aged powder. Three builds were tested to produce a second set of samples. Both vertical and horizontal flat tensile test bars were produced. These bars were all built using the same laser power, exposure time and laser pattern, due to the fact that during this work it was established that the density and properties could vary across a build plate even if the build parameters remain the same.
These parts have been built using what Swansea University AM team has defined as the optimal parameters for building parts. These parameters have been chosen to allow post-processing options to be studied and see how these affect the properties of AM parts.
If it had been possible the BP2 builds would have been built using the same powder and parameters as the original work but due to operational constraints, the timings of BP2 and the machine build programme this meant it was not possible and changes to powder and parameters had to be accepted. As these builds were part of a larger build programme at Swansea University the build numbers correspond to the series within the ageing study, for this work build 17, 18 and 21 were used.

Defining the Rules

The build parameters used to manufacture these new tensile bars were:

- Hatch style – Meander
- Point Distance – 60µm
- Start Angle – 0°
- Angle Increment – 67°
- Hatch Space – 0.11mm

- Layer Depth – 50µm
- Contour Spacing – 0.04mm
- Offset and Border not hatch pattern – approx. 200µm
- Laser speed – 590mm/s

These were built with an exposure time of 80µs and a laser power of 200W.
A number of samples from each of the three builds were tested, the first set were tested with no further finishing processes applied. Two sets were tested that had been heat treated and the remaining samples from each build were HIPped before testing.
Two heat treatments were used. The first was to stress relieve the material which was achieved through a 90 minute ramp, 120 minutes at 450°C and 90 minute ramp down in the vacuum furnace. The second heat treatment matched the HIP thermal cycle of 6 hours ramp up, 4 hours at 1150°C and 6 hours ramp down.
The HIPping treatment used was at a pressure of 100MPa.

3.4.4 Parts BP1 & BP2

Once the machine had finished building the parts, the excess powder was removed and sieved, and the build plate taken out of the machine. Then the pieces are labelled to identify test series and position within the series.

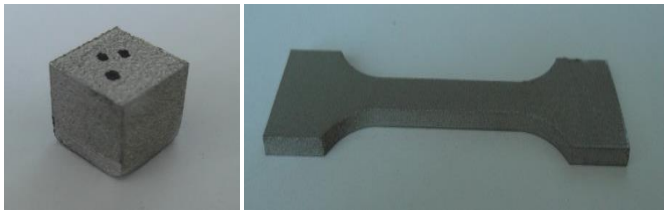

Figure 3:8: AM Built: (a) 10mm Cube, (b) 30mm Gauge Length Tensile Bar

The test pieces are then removed from the base and the supports removed. Typical completed parts are pictured in Figure 3:8. No further finishing tasks have been applied to the cubes or the original flat tensile bars.

3.4.5 Build Programme 3 (BP3)

Build programme 3 (BP3) has been designed as an opportunity to conduct high temperature tensile testing in addition to previous test conditions. Therefore, newly manufactured BP3 samples were tensile tested at 500°C. Along with newly manufactured BP3 samples being tested using previous test conditions from BP2.

Defining the Rules

The samples for build programme 3 were built on a Renishaw AM400 using a parameter set representing the parameter set used on the Renishaw AM250 for BP1 and BP2's samples. This has introduced some variation but the same laser power, beam shape and wavelength have been used and are both continuous lasers. This is as the original machine was no longer available as it had been upgraded to the AM400 used. Due to the time span between build programmes a new powder lot from Sandvick-Osprey was used for these samples. This lot is from the same manufacturer as the previous samples (BP2) as this has provided reasonable consistency across the time frame. Twenty vertical tensile bars were built for tensile testing five samples in each of the following test conditions:

- As built,
- Heat treatment – a 360 min ramp, 240 minutes at 1150°C and a 360 minute cool to room temperature in a vacuum furnace (HT1),
- Stress relieve – a 90-minute ramp, 120 minutes at 450°C and 90-minute ramp down to room temperature in the vacuum furnace (HT2),
- Heat treatment – 7 hours ramp up, 250 minutes at 1125°C and 4 hours ramp down to room temperature in the vacuum furnace (HT3),
- As built with high temperature (500°C) tensile testing – initially it was intended to carry out this high temperature tensile testing to evaluate the effect this has on AM components unfortunately this testing was not possible due to tensile test machine issues only allowing one sample to be successfully tested.

As was established in the previous testing, the density and mechanical properties can vary across the build plate therefore the following build parameters were used to manufacture these tensile bars:

- Exposure time – 80µs
- Laser power – 200W
- Hatch style – Meander
- Point Distance – 60µm
- Start Angle – 0°
- Angle Increment – 67°
- Hatch Space – 0.11mm

- Layer Depth – 50µm
- Contour Spacing – 0.04mm
- Offset and Border (not hatch) pattern – approx. 200µm
- Laser speed – 590mm/s

As discussed, these build parameters were chosen to match those used in BP2's builds on the AM250 and are the proposed optimum build parameters from the previous piece of work.

If it had been possible the subsequent builds would have been built using the same machine, powder, and parameters as the original work. Unfortunately, due to operational constraints, the timings of subsequent build programmes and the machine build plan, it was not possible and changes to powder and machine had to be accepted. Due to these changes, there is the possibility of variability in the results seen. The effects can't be quantified for this work but were necessary to get more data. Longer term the proposed future work should look at the effect across builds from the same machine as well as across different machines.

Parts

For this piece of work only tensile bars were manufactured. These were built on one plate, the powder removed, and the plate taken off the machine to label the parts before they were removed from the base plate using EDM. The tensile bar design was as shown Figure 3:9 and the samples were built to the tensile geometry and not machined from bulk AM materials, therefore the surface effect of the AM build process has also been studied.

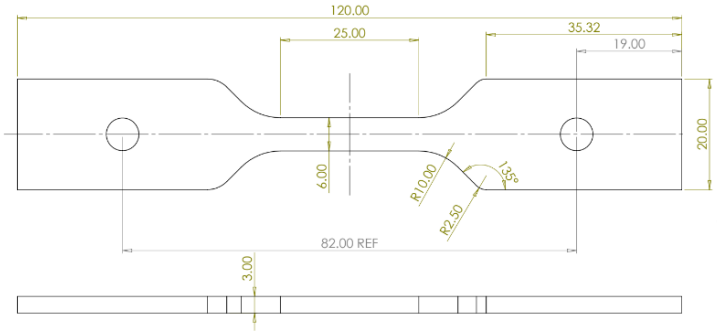

Figure 3:9: ASTM Subsize for BP3

Testing

The parts built during this phase were tensile tested and the roughness evaluated for all samples, along with a study of the fracture surface and microstructure of a selection

of samples. Due to the time constraints and limited samples no further testing was carried out.

3.4.6 Process Energy

Varying the build parameters changes the laser energy density applied during each pulse of the laser. The energy input will affect the melting of the powder and is affected by the exposure time increasing and the laser power used as shown in Equation 3:1.

$$E_d = \frac{P_{laser}\left(\frac{exposure\ time}{hatch\ space\ \times point\ distance}\right)}{layer\ thickness}$$

Equation 3:1: Input Energy [124]

3.5 Testing

The parts that have been built are then tested to establish the properties so that these can be compared to the ASTM standard minimum values that SS316L should achieve. This is to ensure that the properties achieved are comparable to conventionally manufactured parts. The following testing was carried out to give a range of properties:

- Roughness.
- Density.
- Tensile strength.
- Hardness.

One of the claimed benefits of AM parts is that it produces finished parts that need no further processing; this testing will provide information to establish to what extent this statement holds – the tests are selected to compare both mechanical performance and surface finish.

Along with mechanical testing an optical study of the samples was carried out. This included looking at the outer surface, fracture surface and the porosity and microstructure of the parts. Optical analysis has been carried out in some situations, i.e., surface study; this is a non-destructive testing method and so can be used on parts that are manufactured for use to ensure they are fit for purpose.

3.5.1 Sizing

When building parts, it is necessary to understand the accuracy of the parts built by AM, especially when the accuracy of the finished part is important to its end use. For

this reason, the parts were all measured to check accuracy and investigate if the different parameters affect the parts dimensions and accuracy. Design for AM parts is difficult and needs to consider the usual requirement for surface finishing which will affect the final size.

All the parts were measured by hand using calibrated digital callipers to .01mm accuracy.

3.5.2 Roughness

The surface roughness of the cubes is measured to assess how the build process and being surrounded by unmelted powder as the part cools affects it.

Figure 3:10: Wyko WLI Machine

Roughness testing was performed using White Light Interferometry, (WLI). The machine used was the Wyko WLI, Figure 3:10. The machine was set up to take readings using the 5 times magnification lens with 1-time internal magnification and using the parameters of;

- backscatter - 70µm,
- scan length - 100µm and
- modulation threshold - 2%.

These settings gave the best evaluation of the roughness of the parts surfaces. Each cube was tested three times on each side, excluding the bottom due to remains of build supports which would have distorted the results. The surface roughness is related to the peaks and troughs on the surface. The roughness testing was carried out by taking three readings on each side and the top surface of the sample, as shown in Figure 3:11. The bottom surface was not tested, as it is not representative of the build, as it had

already had post processing carried out on it due to the removal from the base plate and of the supports.

The roughness average (Ra) is calculated from the average of a surfaces measured microscopic peaks and troughs. The Ra is what has been used to investigate the roughness in this work. There are other measures that have not been considered and are not discussed in further here.

The reading positions are shown in Figure 3:11, these locations were chosen to look for uniformity along the diagonal of the cube. These positions also allow for the start, middle and end of a laser track to be investigated when studying stripe samples.

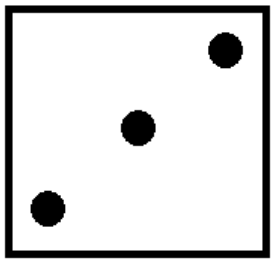

Figure 3:11: Roughness Measurement Positions

3.5.3 Density

Density testing was carried out to see how much changing the parameters would affect the density and to see if it was possible to achieve a fully dense part.

The testing was carried out on the three 10mm cube parts for each set of parameters to ensure the accuracy of the results.

Firstly, the theoretical density of the cubes was found on a scale to 0.01mg accuracy. The weight of a cube of 10mm Stainless Steel 316L should be 8.00g/cm^3 and this was used to calculate the theoretical density. The density testing was carried out on an Attension Machine, shown in Figure 3:12 (a), using Archimedes method [155].

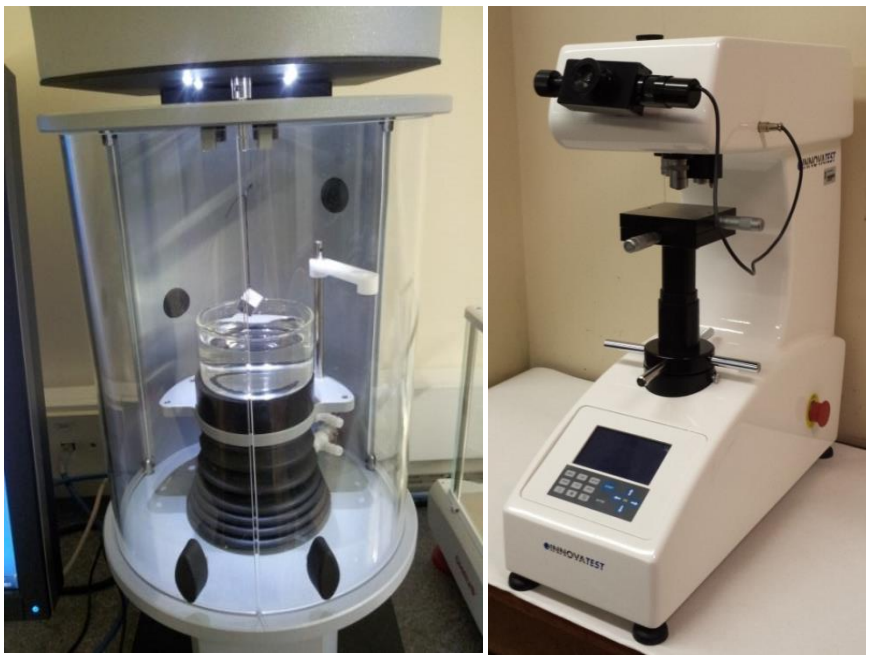

Figure 3:12: (a) Attension Density Test Machine, (b) Hardness Testing Machine

3.5.4 Tensile

The UTS of a material is an important property to understand its strength compared to ASTM A240/A240M [47].

For the first sets of samples, tensile testing was performed on a Hounsfield H25KS tensile test machine using wedge grips, Figure 3:13. The following set up of 25kN load cell, 1mm/min position control rate and a 25mm extensometer was used to measure the strain of the sample.

For the second (BP2) and third (BP3) sets of samples, tensile testing was performed on a Tinius Olsen H25KS tensile test machine again using wedge grips. The set up was a 25kN load cell, 10mm/min position control rate and a 27.5mm extensometer.

For both testing methods, the extensometer was attached directly to the specimens to eliminate the “take up” in the grips. The tensile test bars were marked with a known gauge length so that after the test had finished the parts could be pushed back together and re-measured to calculate the extension. The strain was calculated at each time step using the extension recorded at that point and the original gauge length.

Figure 3:13: Tensile test set up of both the Hounsfield and Tinius Olsen Tensile Test Machines

3.5.5 Hardness

Vickers hardness testing was carried out on the Innovatest Nexus 4303, Figure 3:12 (b), using a 10s dwell and a 1kg weight with nine readings per cube.

Testing was carried out on the top surface and centre of the cubes, the samples where metallography prepared to allow the best results to be achieved.

The position of the hardness readings are shown in Figure 3:14. A spread across the surface of the cube was used to ensure that any effects due to the different parameters used on the 200µm skin do not distort the results.

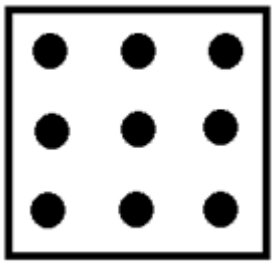

Figure 3:14: Position of Hardness Measurements

3.6 Metallographic Preparation

3.6.1 Polishing

Whilst it is important to understand the physical properties of a sample, it is also important to know how the sample is built up and how the internal structure and microstructure affects the properties. This also helps to establish how the parameters which were changed have affected the internal build structure of the parts.

To study the microstructure and build pattern within the cubes, cubes with the following parameters: 80/160, 105/180, 130/200, for the exposure time and laser power respectively, for each laser pattern, were cut in half, one vertically and one horizontally and mounted in Bakelite.

To be able to study the microstructure of the part it is necessary to get a smooth polished surface that can be etched, and the microstructure brought out. Therefore, the cubes were polished on a Presi machine using the parameters described in Table 3:11.

Table 3:11: Polishing Method

	Step 1	Step 2	Step 3	Step 4	Step 5	Step 6
Base	P320	P800	Top	ADR2	Supra	Supra
Lubricant	Water	Water	9	3	Non Crystalling SPM	Water
Pressure (daN)	2	2	2	2	2	2
Plate Speed (tr/min)	300	300	300	150	150	150
Head Speed (tr/min)	125	125	125	135	135	136
Direction	Same	Same	Same	Same	Opposite	Same
Time (secs)	Till Flat	120	120	240	60	30

During the polishing of the samples, an issue arose. It was found that although the same polishing method was used for all of the samples there was an increase in the number of scratches found on the samples with the highest porosity. This may be because the pores on the sample surface held the polishing particles within them, and then when the next polishing stage was undertaken the particles were dislodged from the pores and scratched the surface. To overcome this problem, more thorough

washing was carried out between stages. Although this reduces the risk of scratches, it did not completely eliminate them. This means that extra time and care needed to be taken to ensure that accurate reliable results and analysis could be achieved.

3.6.2 Porosity

The optical porosity of the cubes is measured to see how the porosity has been affected by the AM build process, to see the effect on the amount, shape and size of pores due to adjusting the build parameters. The cubes cut horizontally and vertically were used to measure the porosity to see if it varied with or across the build direction and to see how it varied due to changes in the parameters.

Polished but un-etched samples were imaged to calculate the porosity, to avoid the etching process exaggerating the pores and distorting the results.

The porosity is measured by taking images of the cube surface using an optical microscope, five times for each sample, and then using ImageJ to calculate the porosity within the part, which can then be compared to the Archimedes density previously calculated.

3.6.3 Etching

Once the samples had been cut, mounted and polished, they are etched for microstructure examination. Etching is a chemical reaction that cuts into the unprotected areas of the surface/microstructure leaving the microstructure visible for study and so the type of grains i.e., austenitic, martensitic or containing carbides can be determined.

Not all etching agents have the same effect on every material and therefore it is necessary to find the best etch for this specific task. As Stainless Steel is difficult to etch a selection of possible etches were tried until the best results were found using V2A and Nital.

For BP1 and BP2 the etch used was the V2A etchant heated to 50°C as this gave the best results and showed both the laser pattern and microstructure. For BP3 the etch used was standard Nital etch, this gave good results again showing both the laser pattern and microstructure depending on the heat treatments applied.

3.7 Microscopy

Imaging of the cubes has been performed to study how not only the external structure and microstructure has been affected by changing the build parameters but what effect this has had on the failure mode of the part during experimental testing.

To begin the study the surfaces and internal structure has been studied to see how the part is built up and how changing the build parameters affects the internal and external structure of AM parts. As well as studying what is seen on the surface, including any defects, the parts were also studied to see if the surface is in anyway affected by changing the exposure time, laser power or laser pattern.

3.7.1 Optical Microscopy

Optical microscopy was carried out using the Keyence and Reichert Microscopes.

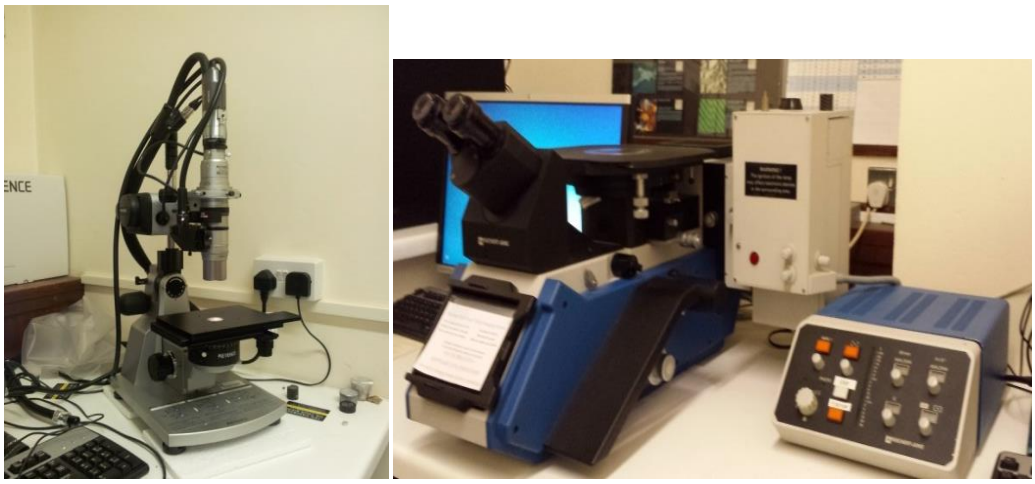

Figure 3:15: (a) Keyence Microscope, (b) Reichert Microscope

The Keyence microscope has interchangeable lenses. The 20 – 200 times magnification lens was used for the overall images. The 100 – 1000 times magnification lens was used to get close-up images of the microstructure and fracture surfaces of the tensile bars to see if there were any defects that may have initiated the failure.

The Keyence microscope, Figure 3:15(a) was used to study the surface of the cubes including: the pattern formed by the laser, seeing if there are any gaps or holes on the surface and how far down the layers these travelled, along with if there were any unmelted particles or defects on the surface.

Optical microscopy using the Keyence was carried out on the fracture surface of a number of tensile bar samples, which were also studied from the side. Some of these

samples were then mounted and polished so the microstructure could be studied using the SEM.

The Reichert Microscope Figure 3:15(b) was used to take images of the cross section of the cubes to study the porosity and microstructure.

The Reichert had advantages over the Keyence in that there was no reflection (glare) of the light on the surface of the AM parts and this allowed the surface to be studied and understood much easier than on the Keyence.

3.7.2 Scanning Electron Microscopy

The Jeol 6100 SEM and EVO LS25 SEM, Figure 3:16 have been used to take surface images at higher magnification looking at individual particles on the surface. In addition, it enabled the author to look at the cross section of the cubes to study the microstructures. This allows investigation of the growth pattern within AM parts to see how this varies due to having a horizontal or vertical orientation in relation to the build direction.

The SEMs have also been used to study the fracture surface of the tensile bars to see if there are any notable defects or initiation causes.

Figure 3:16: Scanning Electron Microscopes Used (a) Jeol6100 SEM, (b) Zeiss EVO LS25 SEM

3.7.3 Microstructure

The microstructure of the cubes was studied to establish how the internal structure has grown during the AM process. The AM microstructure is also compared to that of

rolled SS316L's microstructure to see if they are comparable. The microstructure of a number of samples was studied to see if it was affected by the parameters used and to see if the microstructure affects the properties.

The microstructure of the following parameter cubes; 80/160, 105/180, 130/200, for the exposure time and laser power respectively, were studied. These cubes were mounted and polished before being etched, so the microstructure could be studied on the microscopes, these processes are described in Section 3.6.1 and 3.6.3. The samples were studied on both SEM and optical microscopes; this allowed for both overall and detailed close up images to be obtained. Using a lower magnification allows for a larger area of the microstructure to be studied while higher magnifications give close up views of the individual grains structure and composition.

Along with studying the cube microstructure, the microstructure of tensile samples, were also studied to see if there were any noticeable defects or changes in the microstructure.

3.8 Summary

This chapter sets out the experimental testing that has been undertaken to see how the properties of the SS316L AM parts vary due to changes in the build parameters:

- laser power,
- laser pattern,
- layer rotation, and
- exposure time.

The results of the experiments are analysed in Chapter 4, Results, and discussed in Chapter 5, Discussion.

Chapter 4 Results

The following chapter analyses the experiments discussed in Chapter 3, Method, to establish the properties of SS316L AM built parts and to see how the properties vary when the build parameters are changed, whilst also being able to compare to the minimum required properties to be classed as SS316L.

The experiments undertaken in this work include:

- Sizing.
- Roughness.
- Density.
- Tensile.
- Hardness.
- Porosity testing.

The microstructure of the cubes was also studied and discussed within this chapter. The chapter concludes by stating the parameters found that produce parts which meet the ASTM standard, for use when building SS316L AM parts.

The reader should be aware that there are limitations faced when producing AM parts, these can include build position as has been previously mentioned by Renishaw in conversation and previous research [158] found. This will have a slight effect on the properties seen and the work undertaken here needs to take this into account to minimise its effect on the results produced.

4.1 Conventional Mechanical Properties

The parts built using the AM method have been compared to ASTM A240 [47], as this is how materials have previously been characterised. The minimum values to be classed as SS316L by ASTM Specification A240/A240M – 16 [47] were a hardness of 222HV, a UTS of 485MPa, a yield stress of 170MPa, extension of 40% and from A to Z of Materials a density of 8.00g/cm^3 [159].

Table 4:1: Minimum Properties of SS316L ASTM A240/A240M [47] A to Z of Materials [159] ASTM A480/A480M [96]

	SS316L
Density (g/m^3)	8.00 [159]
UTS (MPa)	485 [47]
Yield Stress (MPa)	170 [47]
Extension (%)	40 [47]
Hardness (HV)	222 [47]
Roughness (µm)	<7.5 [96]

As well as the values given in Table 4:1 to compare the test results to, a piece of conventionally manufactured SS316L was etched to compare the microstructure. This is shown in Figure 4:1.

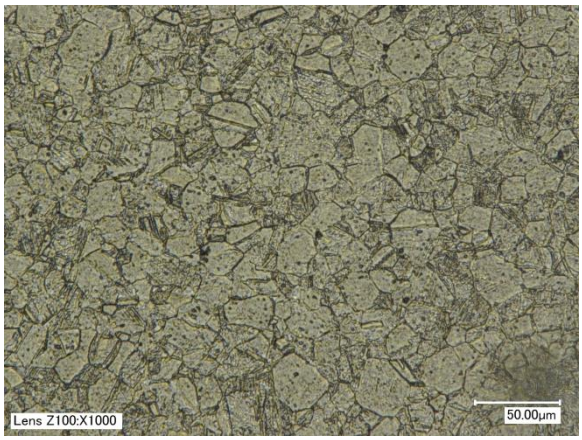

Figure 4:1: 316L SS Microstructure

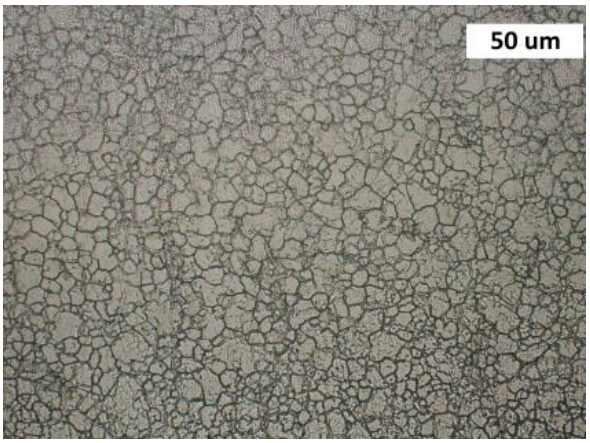

Figure 4:2: As received Surface of Sheet SS316L

Figure 4:1 and Figure 4:2 show the surface of conventional manufactured SS316L. The images show the microstructure, showing grains of similar shapes and sizes. Figure 4:2 shows grain that are slightly smaller than those shown in Figure 4:1 but they both show very consistent sizes between 10 and 20µm on average. The images of these two samples show that there are never grains over 40µm in this conventional SS316L and the average is much smaller.

4.2 Sample Preparation

The BP1 and BP2 parts were built on a Renishaw AM250 Selective Laser Melting (SLM) machine using LPW Ltd.'s or Sandvik-Ospreys SS316L powder on a base plate of stainless steel. The BP3 parts were built on a Renishaw AM400 SLM machine using SS316L powder on a base plate of stainless steel.

The aim of this work is to find out how as built parts properties vary due to changes to four of the build parameters, mentioned in Chapter 3, Method. As has been previously seen these will have an effect on the properties of the finished AM parts, the parameters include;

- Laser pattern - the pattern the laser follows to melt each layer having an effect on the cooling rate of the powder.
- Laser pattern rotation – the rotation of the laser pattern with each layer could affect the amount of powder melted.
- Laser power - will affect the melting of the powder whilst also affecting how quickly the melt pool is formed due to an increase in laser power causing the melt pool to form quicker, therefore drawing a higher amount of the surrounding powder into the melt pool.
- Exposure time - affects the period of time the laser is on each section of powder, therefore the longer the time step the greater an amount of powder that is melted.

The runs and parameters used are shown in Table 3:8 and Table 3:10 for BP1 in the Method Chapter and for BP2 and BP3 one set of parameters was used, 80µs exposure time and 200W laser power.

4.3 Process Energy

The energy density or input energy is used to melt the samples during the build process has been calculated so it can be compared across both sets of builds. For BP1 these are shown in Table 4:2.

Table 4:2: Energy Input (J/mm3) for Build Parameters Investigated BP1

		Exposure Time		
		80	**105**	**130**
Laser Power	**160**	31.76	41.69	51.61
	180	35.73	46.90	58.06
	200	39.70	52.11	64.52

Calculating the process energy means that samples from the two separate build parameters will be able to be compared more effectively, but it must be remembered that comparison across powders should be caveated with the fact the powder differences may have an effect on the final properties.

For the new builds, BP2 and BP3, due to the decrease in point distance and hatch space, the energy input is 48.048J/mm^3.

4.4 Samples

The warpage found during this work has been shown in Figure 4:3. Here it is seen that the front of the bars have pulled from the base plate. The right hand side of this image is the front of the build plate and therefore the front of the build area. It is believed that this is caused by residual stress built up within the part during solidification. There is a highly compressive centre, which causes tension in the outer sections of the bars causing the build-up of residual stresses within that part. This issue only occurred at the front of one plate during one build.

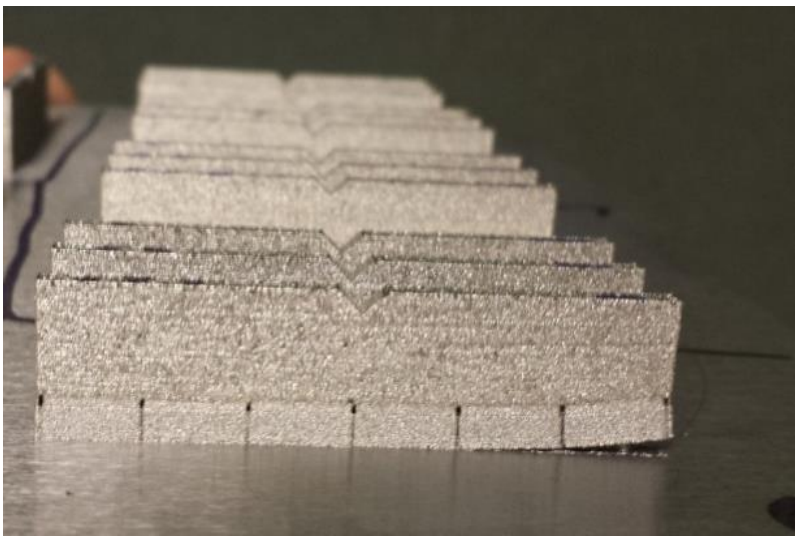

Figure 4:3: Warpage Seen

4.5 Materials Characterisation Imagery

4.5.1 Powders

The LPW SS316L powder was examined in an SEM both before and after the build process, Figure 4:4 and Figure 4:5.

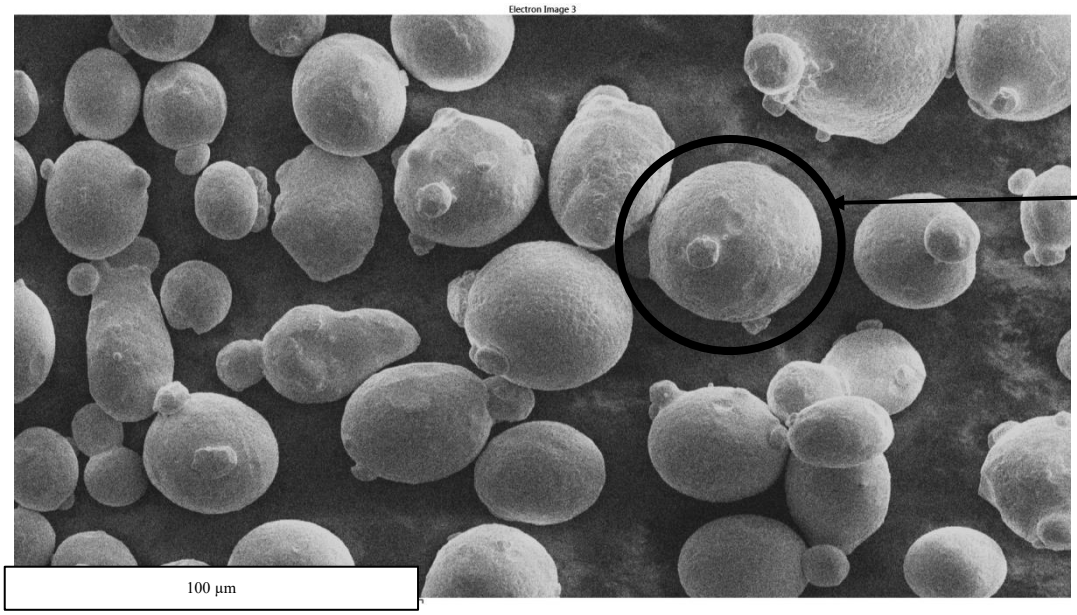

Figure 4:4: 'Virgin' Powder

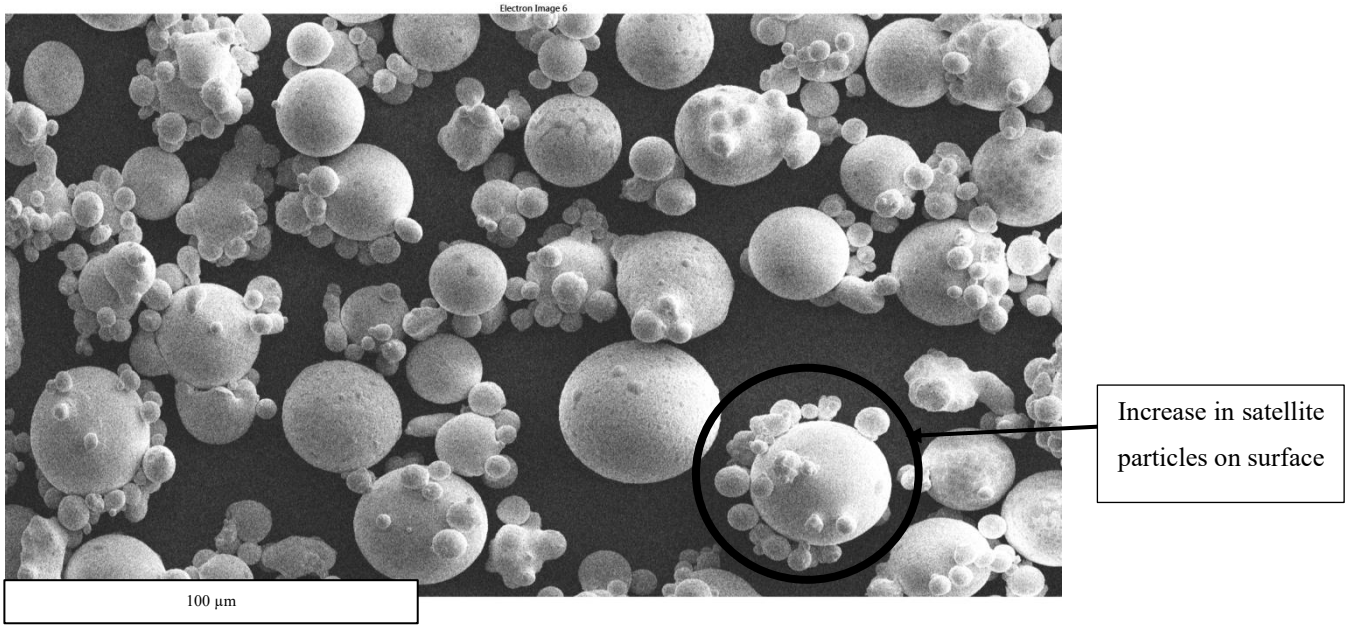

Figure 4:5: Used Powder

From these images, Figure 4:4 and Figure 4:5 it is possible to see that there is a change to the powder after it has been through the build process, smaller particles are visible that have attached themselves to the larger particles. The particles that exceed the sieve size will be removed during the sieving process but any that are smaller will be retained and will go into the next build, it is possible to see that there are numerous powder particles with satellites attached that are below 45µm and will be retain for future builds.

What is seen with these powders is corroborated by what has been seen in other research for what 'virgin' powder looks like straight out of processing compared to how the powder changes [106] because of the AM build process. This previous work has also showed the effect powder has on the properties of AM parts; this is discussed further in section 5.4.4.

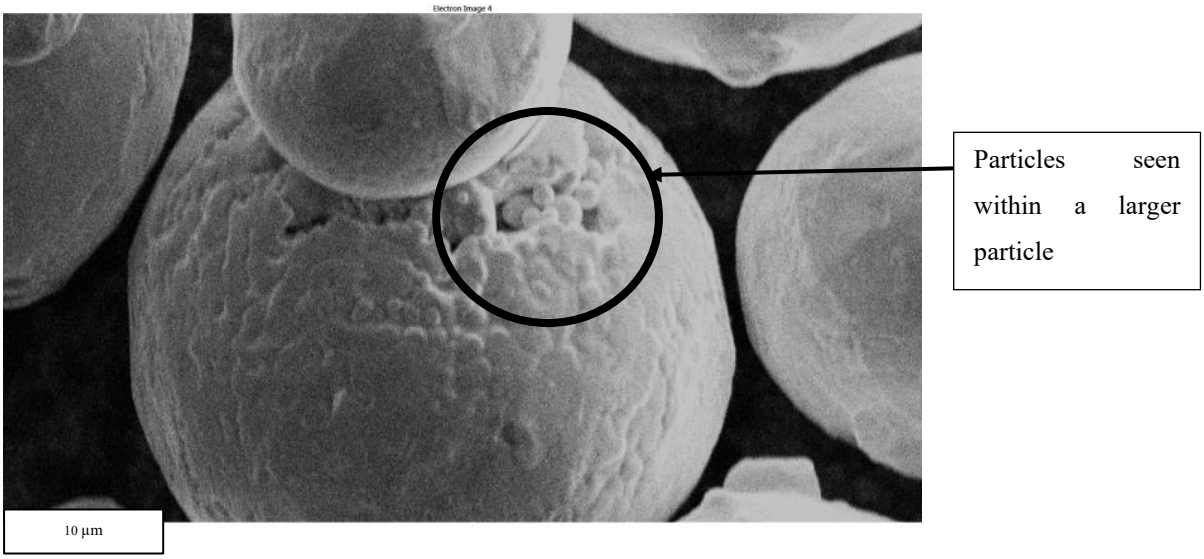

Figure 4:6: 'Virign' SS 316L powder

Figure 4:6 shows 'virgin' SS316L powder before it had been through a build process. This powder shows what appears to be smaller particles between 2 and 5µm, within the surface of a larger particle of approximately 50µm is diameter. The powder production process can create powder of different qualities, and this is an example of poor quality powder but there is no way to remove this from the process.

Powder Size Distribution

As mentioned in Section 3.3, the Powder Size Distribution (PSD) fractions are D10 - 18.2, D50 – 30.2 and D90 – 50.4. The powder was sieved between uses using a 45µm sieve. For the aged powder that was reused for 21 builds, which included the samples tested for this work it was found that the PSD did not vary greatly, remaining within 5% of the original values for the entire series of builds. This shows that sieving can help maintain a good spread of powder to work with that is within specification and produces the desired quality parts.

4.5.2 Surface Structure

Figure 4:7 shows the meander turns visible on the surface of a part, what can also be noted in this image is that the laser path is raised above the layer below and does not merge with its neighbour.

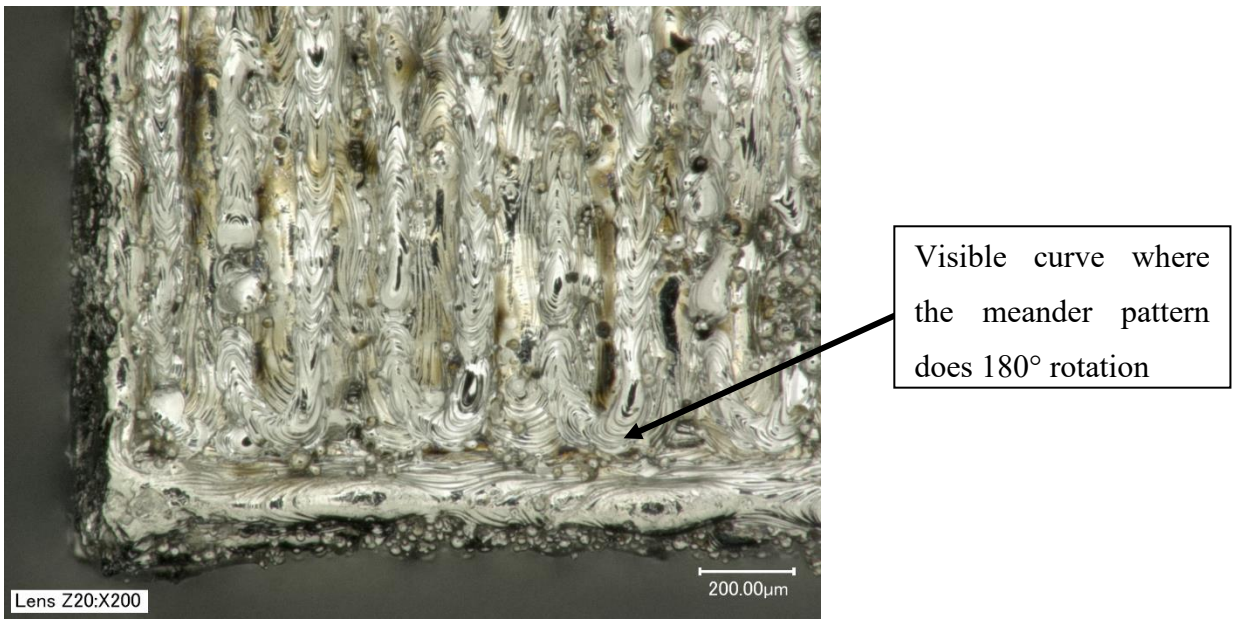

Figure 4:7: Meander turns the surface of a105µs exposure time, 180W laser power, 90° rotation cube

90° Rotation Unaged Powder Samples

Figure 4:8 and Figure 4:13 are of the top surfaces of the cubes that have been taken on an optical microscope. These images show that the surface conditions have changed due to the different build parameters used.

These images show how as the laser power has increased, there is improved cohesion seen between the laser scan paths.

Figure 4:8 shows the surface of the Meander laser pattern cubes; these images show the pattern of the top layer of the sample. This is at 90°s to the edge of the sample, whereas as is shown in Figure 4:13 the Stripe laser pattern samples show a diagonal pattern across the top.

The images also show how the change in parameters affects changes in the surface of the AM cube. As the exposure time has increased, the scan lines are clearer and more pronounced and there is seen to be less unmelted and balled particles on the surface.

		Laser Power (W)
		160
Exposure Time (µs)	80	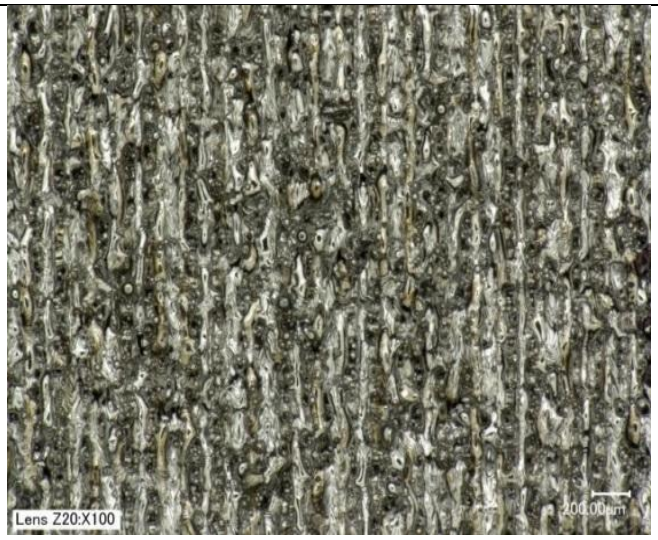
	105	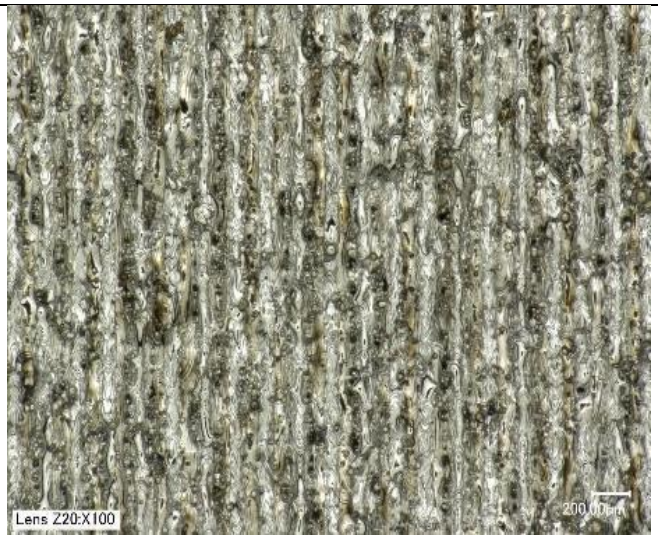
	130	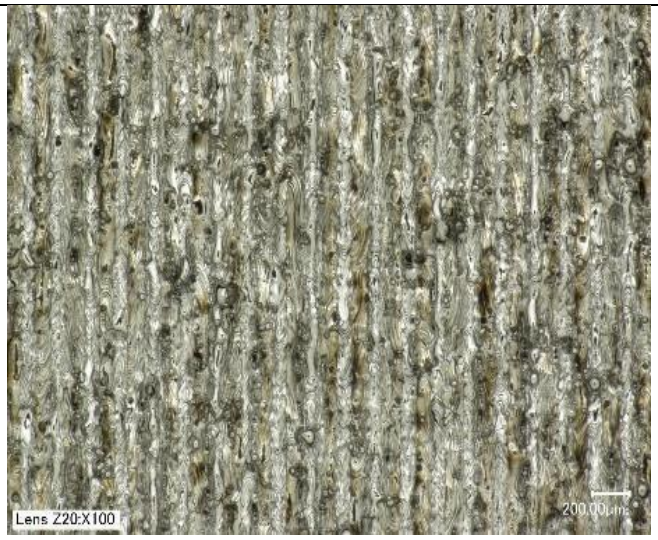

Figure 4:8: Top Surface of 90° Meander Cubes – 160W Laser Power

		Laser Power (W)
		180
Exposure Time (µs)	80	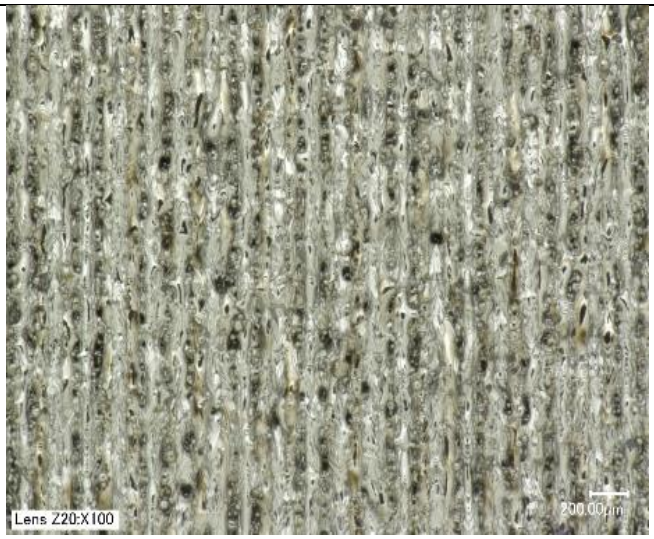
	105	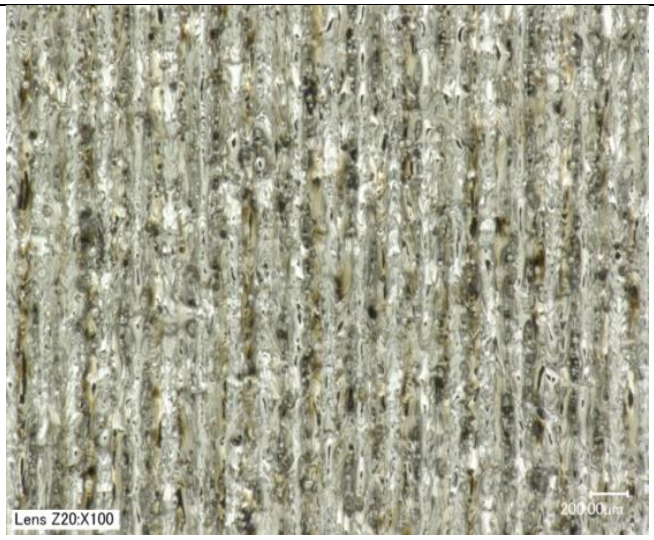
	130	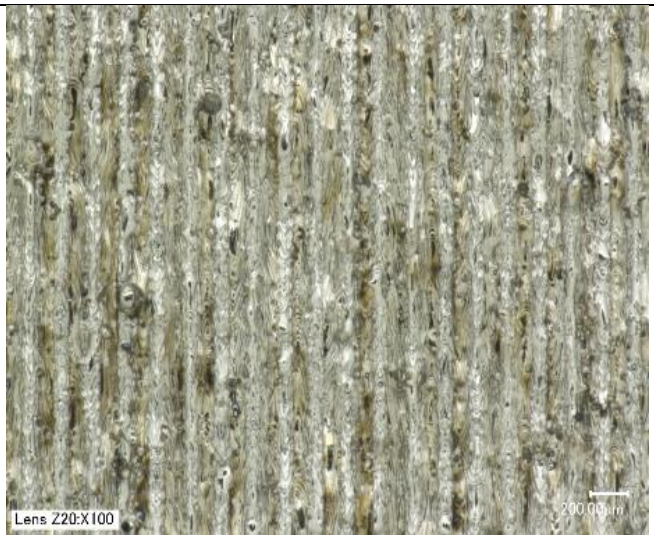

Figure 4:9: Top Surface of 90° Meander Cubes - 180W Laser Power

		Laser Power (W)
		200
Exposure Time (μs)	80	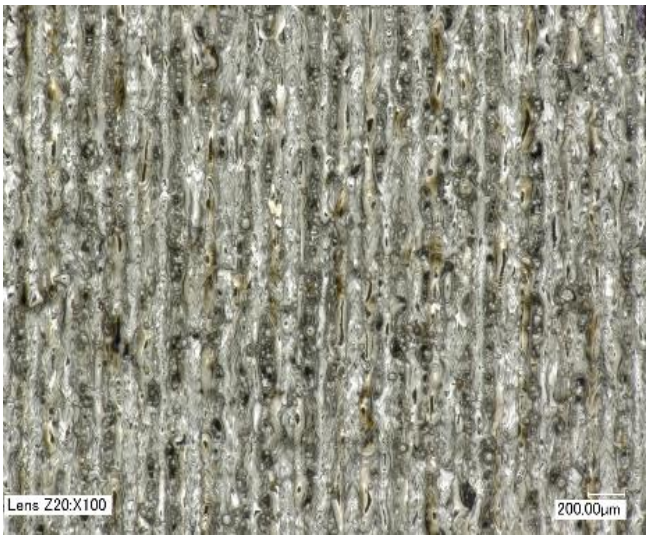
	105	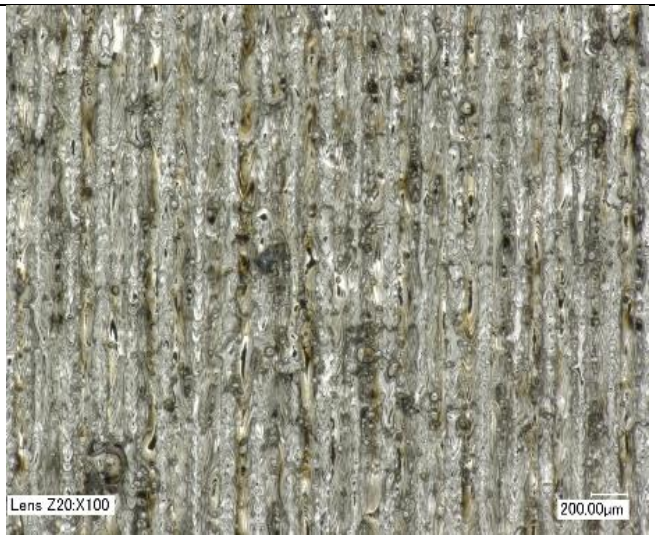
	130	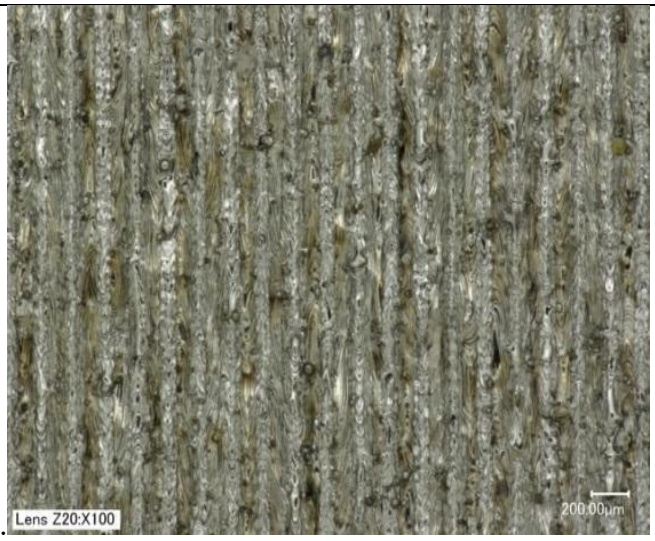

Figure 4:10: Top Surface of 90° Meander Cubes – 200W Laser Power

		Laser Power (W)
		160
Exposure Time (μs)	80	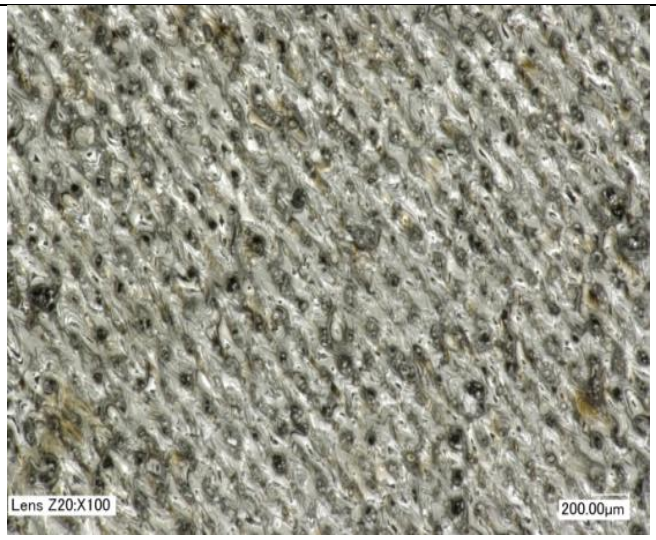
	105	
	130	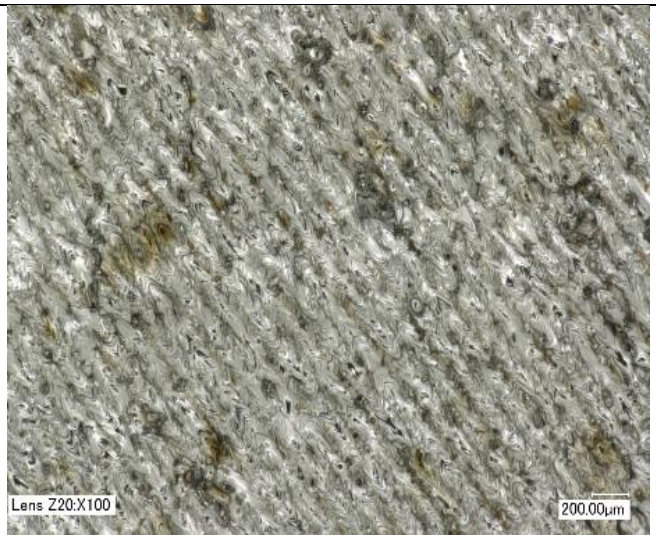

Figure 4:11: Top Surface of 90° Stripe Cubes – 160W Laser Power

		Laser Power (W)
		180
Exposure Time (μs)	80	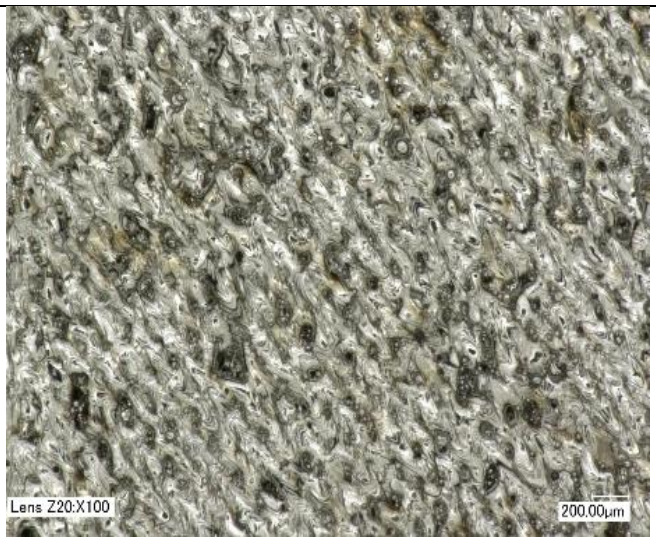
	105	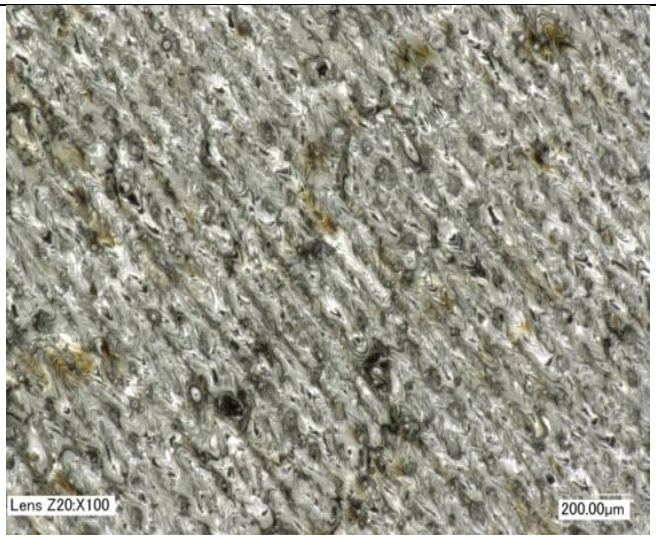
	130	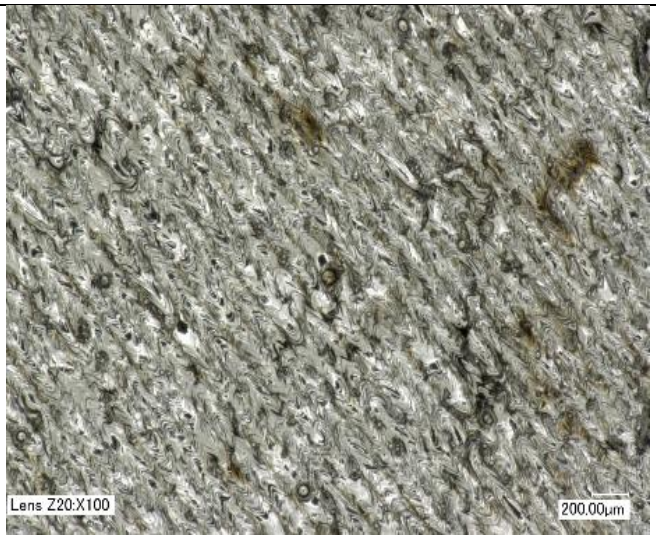

Figure 4:12: Top Surface of 90° Stripe Cubes – 180W Laser Power

		Laser Power (W)
		200
Exposure Time (μs)	80	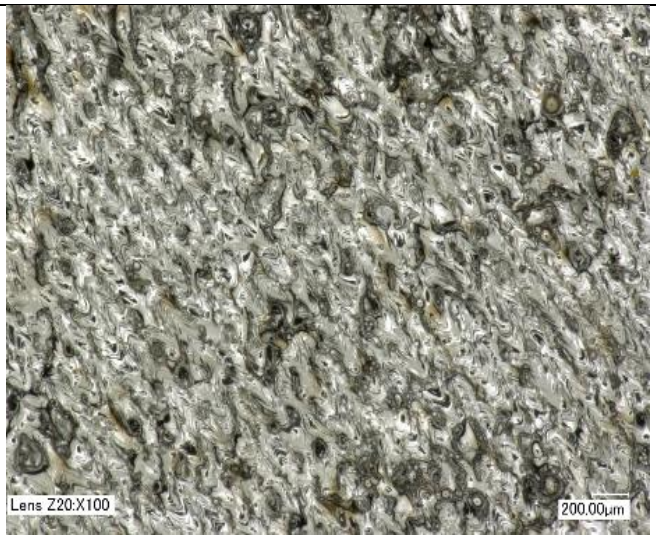
	105	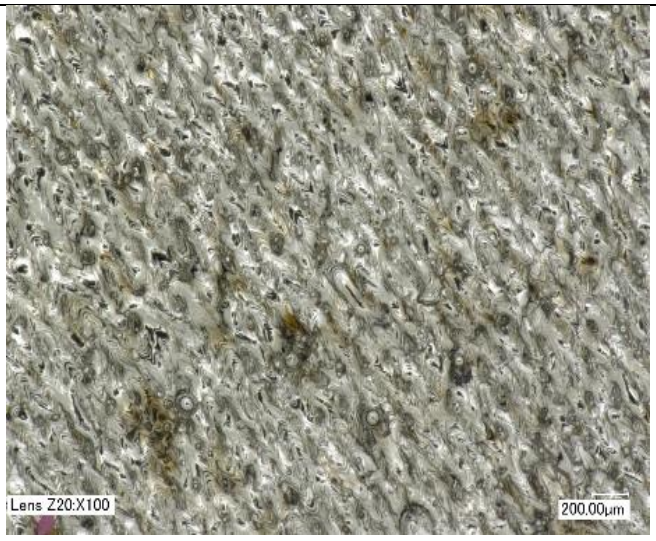
	130	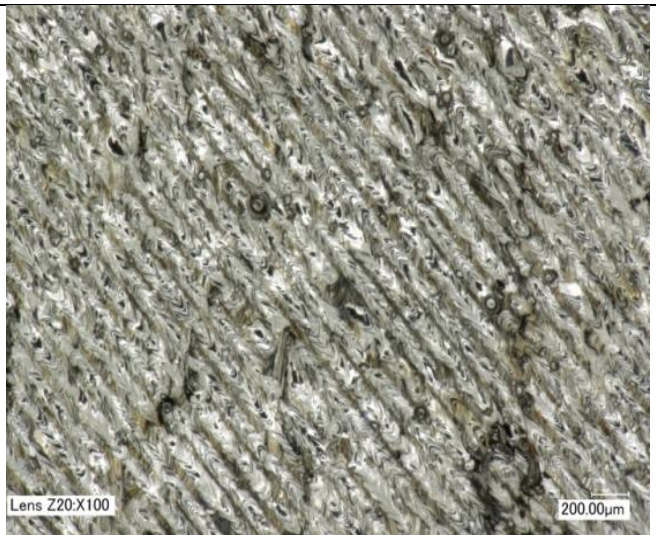

Figure 4:13: Top Surface of 90° Stripe Cubes – 200W Laser Power

Figure 4:8, Figure 4:9, Figure 4:10, Figure 4:11, Figure 4:12 and Figure 4:13 show how the surface of AM cubes varies with changing laser power or exposure time. From these images it is possible to see that the higher the exposure time the neater the laser path with less unmelted powder particles attached to the laser path. This is the case for both the stripe and meander laser pattern. Increasing the laser power seems to have little effect on the surface composition but it does appear to increase the height of the laser track which would lead to increased surface roughness for higher laser power samples as seen in the results. Lower laser power gives a cleaner looking surface matching the reduced surface roughness seen for these samples.

A SEM has been used to image the surface of the AM cubes. These images again clearly show the laser path that has been travelled. Along with how the powder has been melted and solidified along the laser path. Figure 4:14 is an example of this. This SEM image also show how there are powder particles attached to the surface of the part and pores created between laser tracks that penetrate to the layer below.

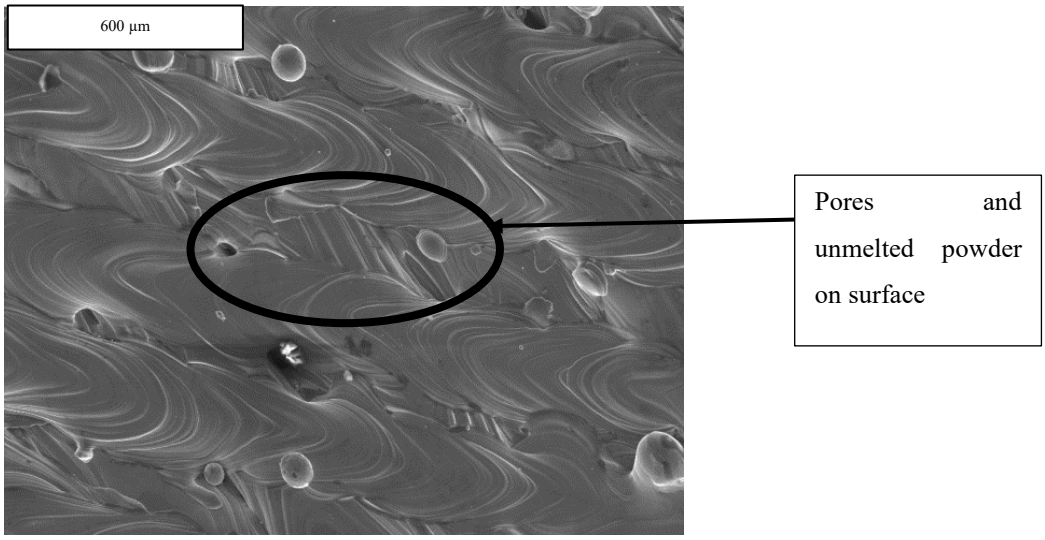

Figure 4:14: Exposure Time 105, Laser Power 180W, Stripe Laser Path, x200 mag

The optical microscope images, Figure 4:8 and Figure 4:13, also show how the laser pattern on the top layer of the cube is a meander pattern for both laser patterns, due the ‘skin’ being manufactured using the best build settings. As well as showing the laser patterns on the top surface, these images, Figure 4:8 and Figure 4:13, show the effect that the lowest exposure time and laser power has on the build parameters, producing parts with numerous pores on the surface which are likely replicated throughout the part.

67° Rotation Unaged Powder Samples

Once again it is clear from the images, Figure 4:15 and Figure 4:16, is that increasing the laser power used to melt the particles has led to better defined scan tracks on the surface of the cubes. Figure 4:15(a) shows the lowest laser power and it is noticed that the scan pattern is barely defined, also shown in Figure 4:16(a). Figure 4:15(c) and Figure 4:16(c) demonstrate how as the laser power increases the laser patterns show clearer definition suggesting that increasing the laser power leads to increased melting and cooling of the particles to ensure consistency within the parts and a lower concentration of pores.

The optical microscope images show that there is an effect caused by changing the build parameters, laser pattern and laser rotation and this has affected the surface of the cubes built.

Figure 4:15: Top Surface of 67° Meander Cubes (a) 80µs exposure time and 160W laser power, (b) 105µs exposure time and 180W laser power, (c) 130µs exposure time and 200W laser power

Figure 4:15 shows that using the meander laser pattern to build up the cubes has led to higher coverage of the top surface and more defined stochastic tracks.

What can be clearly seen from Figure 4:15 and Figure 4:16 is that using the 67° rotation of the laser pattern with each new layer and higher laser power has reduced to none the number of pores or sections with no powder seen on the surface of the cubes when compared to the 90° samples. It is also possible to see that the offset to the

rotations has led to there being no opportunity for pores to travel down through the layers; this is because the layers are no longer built directly on top of each other.

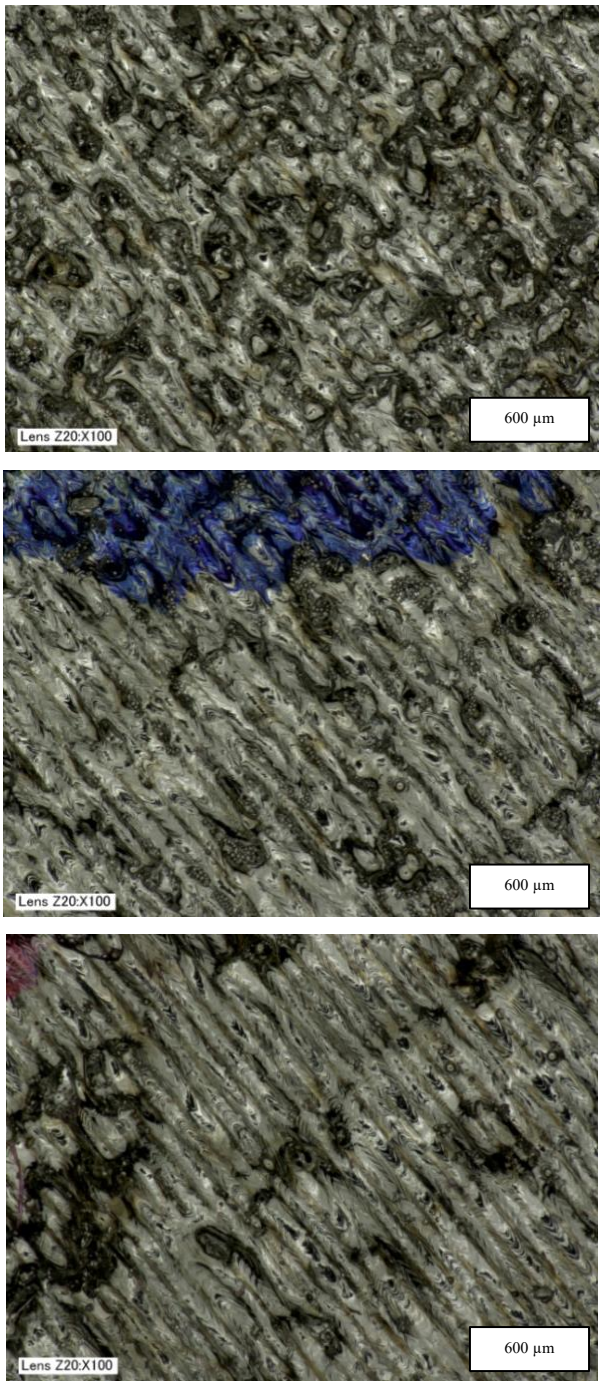

Figure 4:16: Top Surface of 67° Stripe Cubes (a) 80µs exposure time and 160W laser power, (b) 105µs exposure time and 180W laser power, (c) 130µs exposure time and 200W laser power

Figure 4:17 and Figure 4:18 show the surface of the cubes taken using the SEM. Here it is possible to see that again the top laser track is visible as is the layer below. It is also possible to see how the rotation has affected the path of the laser with the top layer being vertical to the side of the image whilst the layer below crosses the image

at an angle. What can also be studied at this higher magnification is that there are particles adhering to the laser track in all of the images, but the size of these particles varies. Figure 4:17(c) shows some larger particles attached to the top surface of the cube.

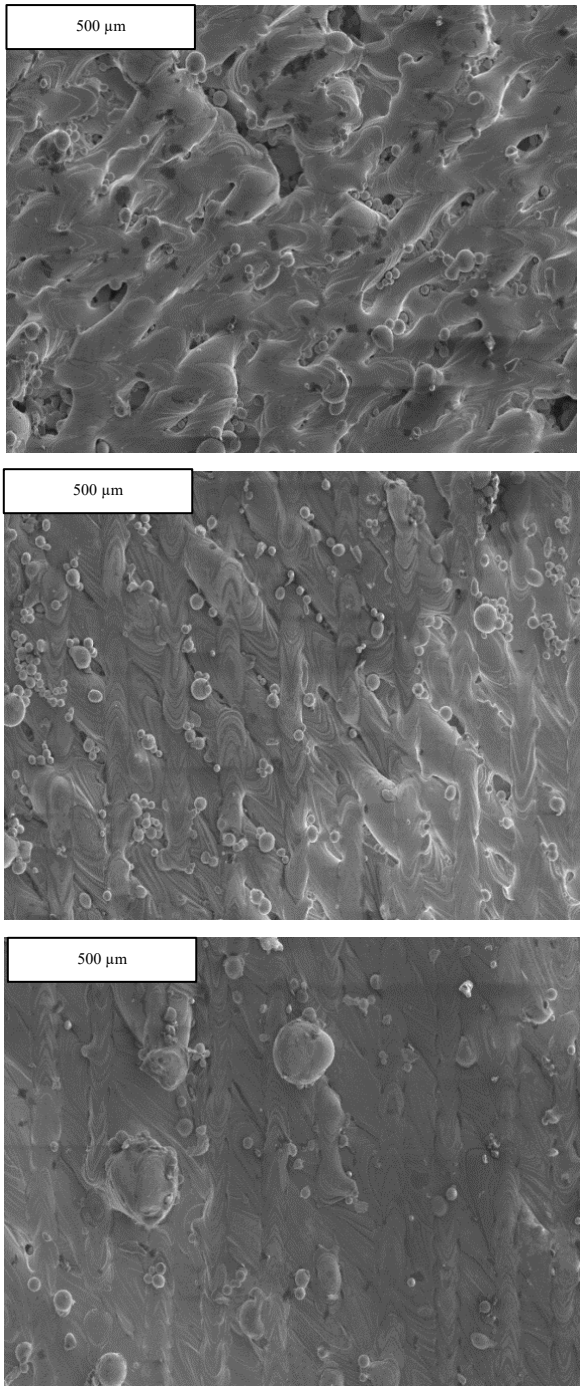

Figure 4:17: Top Surface of 67° Meander Cubes (a) 80µs exposure time and 160W laser power, (b) 105µs exposure time and 180W laser power, (c) 130µs exposure time and 200W laser power

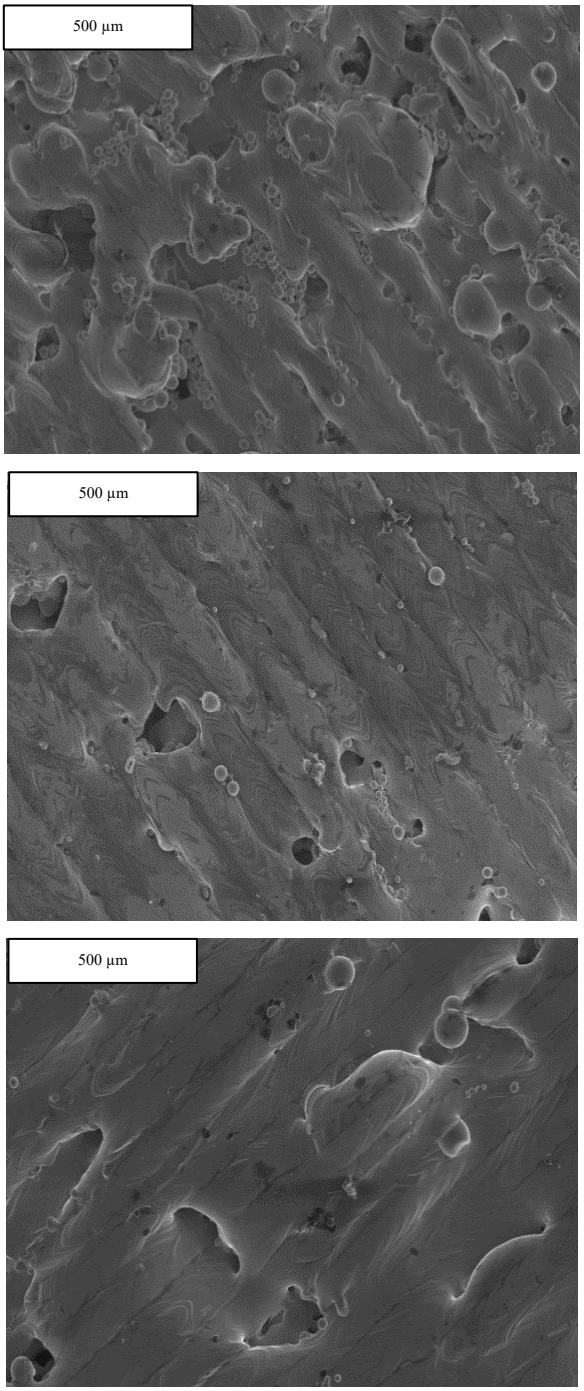

Figure 4:18: Top Surface of 67° Stripe Cubes (a) 80µs exposure time and 160W laser power, (b) 105µs exposure time and 180W laser power, (c) 130µs exposure time and 200W laser power

The images, Figure 4:17 and Figure 4:18 correspond with the surface roughness measurements taken using the WLI. The images in Figure 4:17 show decreasing roughness as you move from (a) to (c), this matches what is seen where the laser tracks are clearer defined and rise from the surface higher than seen in (c). In Figure 4:18 the

tracks are less defined with lower pits and rises than in Figure 4:17 corresponding to the lower surface roughness seen here on average. Figure 4:18(a) not only has clearly defined laser tracks it is also possible to see that there are powder particles stuck to the surface above the laser tracks and this will be adding to the surface roughness seen, which is the highest for this set of images.

A study of the cubes sides was performed to see if there are any differences in the number of unmelted particles that are drawn into the side of the cubes. This is thought to be resulting from the changes in build parameters leading to different amounts of unmelted powder being drawn in. This in turn will lead to changes to the roughness of the sides of the cubes as shown in Figure 4:19, Figure 4:20, Figure 4:21 and Figure 4:22.

When comparing images of the top of samples to the images of the sides of samples it is possible to see that the results found through the roughness testing are corroborated and the side surfaces have a higher number of particles attached increasing the roughness seen. It is also possible to see that on average the meander images show more particles present again leading to an increased surface roughness.

For the 90° rotation samples the images of the sides, Figure 4:19 and Figure 4:20, when compared to Figure 4:8 and Figure 4:13, show that there is a higher number of particles attached to the sides of the cubes than are found on the top. This could be due to material being drawn into the melt pools at the side of the builds. It can also be seen that these particles are all around the same size at approximately 50µm. Suggesting that there is little variation in the powder particles size before the build or that smaller particles are completely engulfed, whereas larger particles aren't as more input energy is required to melt those particles. It can only really be seen in Figure 4:20(b) that the particles vary greatly in size suggesting that the laser power or exposure time in this case has had an effect on the particle size remaining.

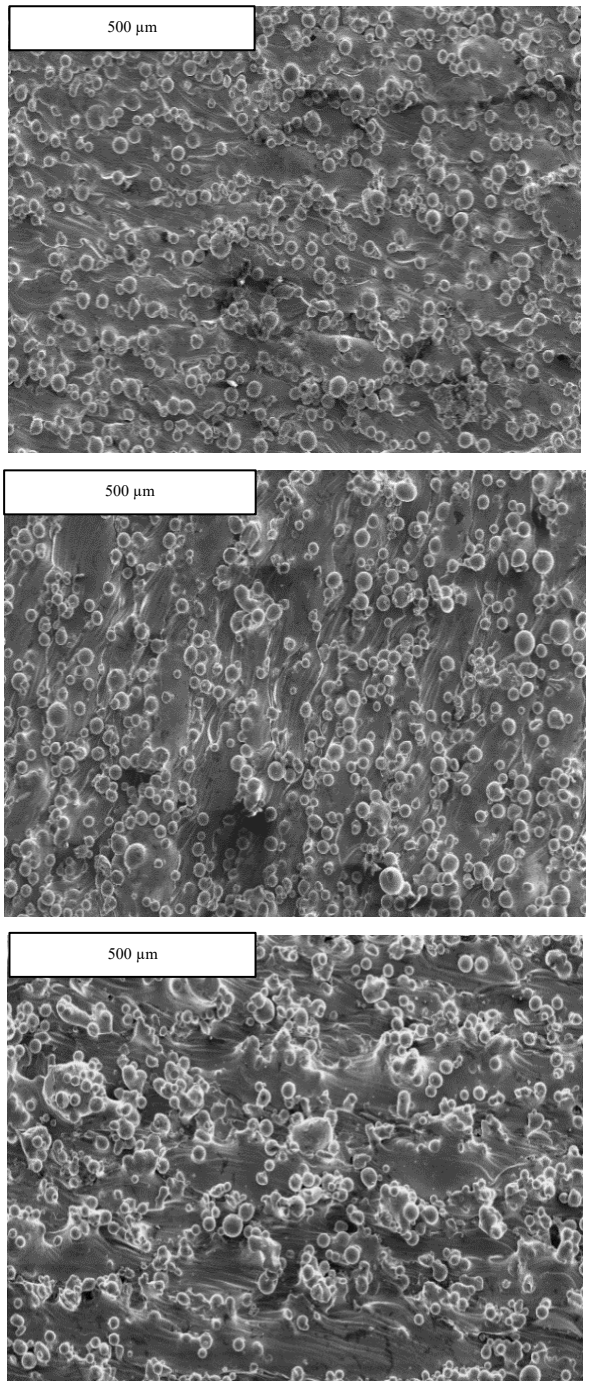

Figure 4:19: Particles on the side of the 90° rotation Meander pattern cubes (a) Exposure Time 80µs, Laser Power 160W, (b) Exposure Time 105µs, Laser Power 180W, (c) Exposure Time 130µs, Laser Power 200W

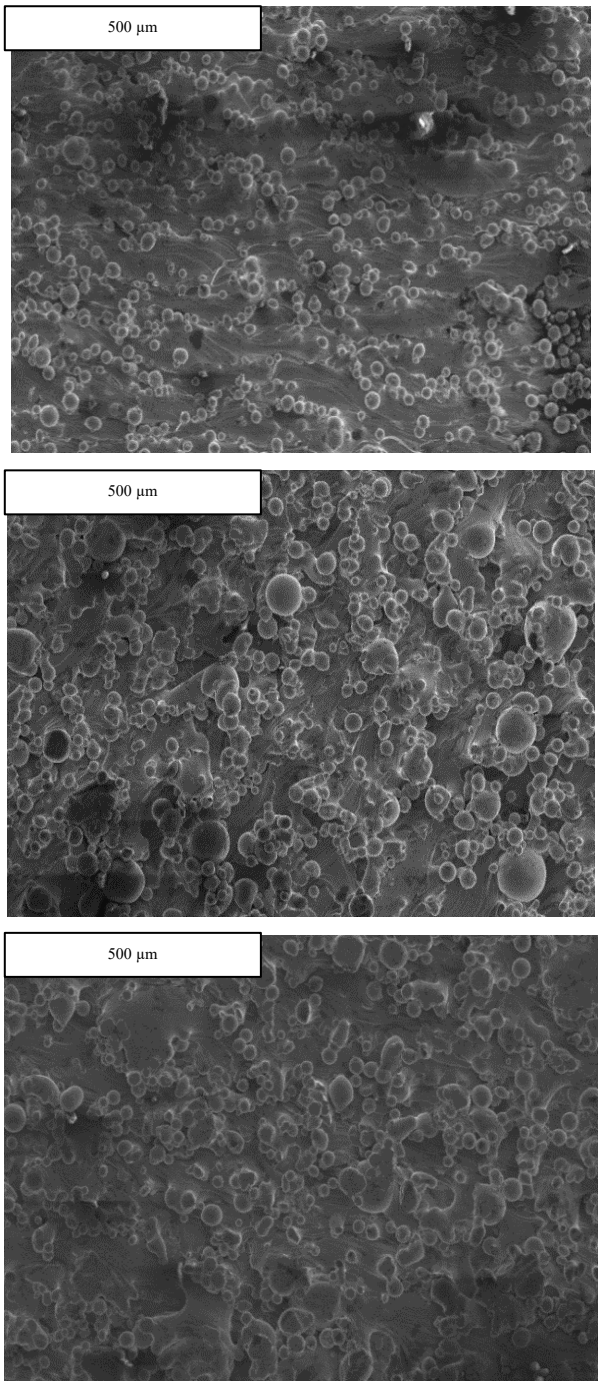

Figure 4:20: Particles on the side of the 90° rotation Stripe pattern cubes (a) Exposure Time 80µs, Laser Power 160W, (b) Exposure Time 105µs, Laser Power 180W, (c) Exposure Time 130µs, Laser Power 200W

From the images of the 67° rotation samples, Figure 4:21 and Figure 4:22, it is again possible to see that the layers built up during the build process cannot be viewed on the sides of the cubes. It is also possible to see how powder particles have been drawn into the sides of the cubes as with the 90° rotation cubes. Again, these particles are all approximately the same size with the amount seen remaining constant between the different parameters used to build up the cubes.

Figure 4:21 and Figure 4:22 show the particles that are sitting on the sides of the cubes, and this is likely to be the reason why the roughness on the cubes varies with exposure time. As the exposure time increases the images of the sides of the cubes show varying sizes of particles drawn in, but also that the surface under the particles is not as smooth. Where the layers are built up roughness is seen in the outcropping material. This increase in exposure time allows a greater number of particles to be drawn into the surface whilst also allowing for higher melting of the powder leading to the melted powder extending further before solidifying.

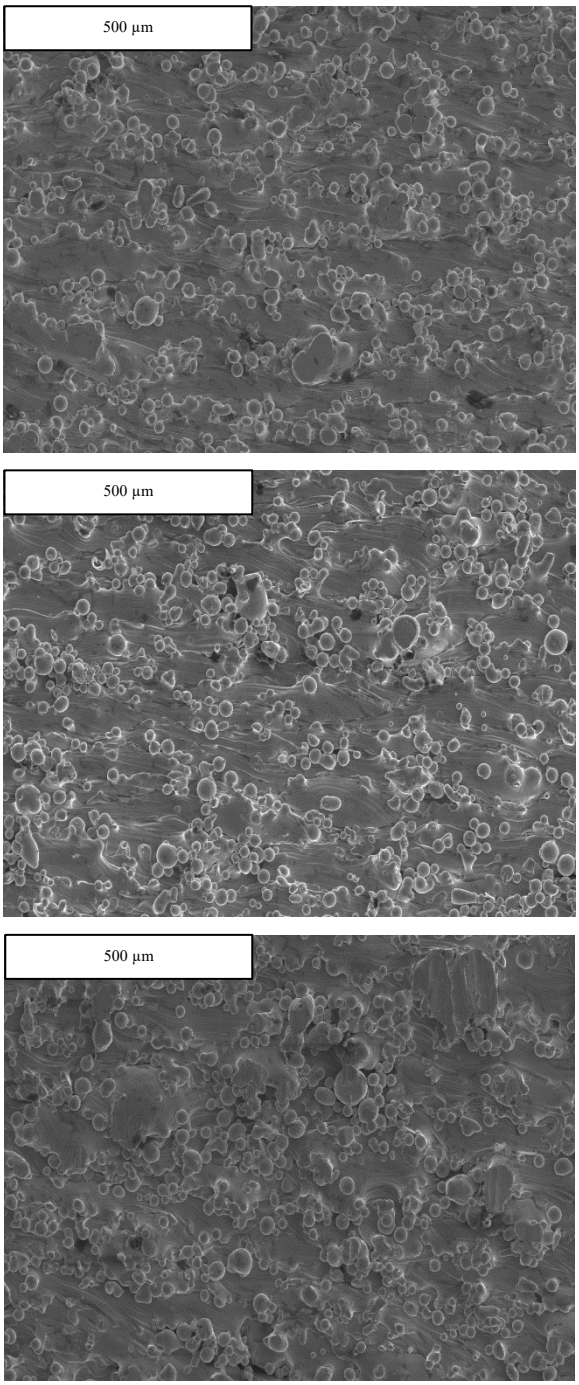

Figure 4:21: Particles on the side of the 67° rotation Meander laser pattern cubes (a) Exposure Time 80µs, Laser Power 160W, (b) Exposure Time 105µs, Laser Power 180W, (c) Exposure Time 130µs, Laser Power 200W

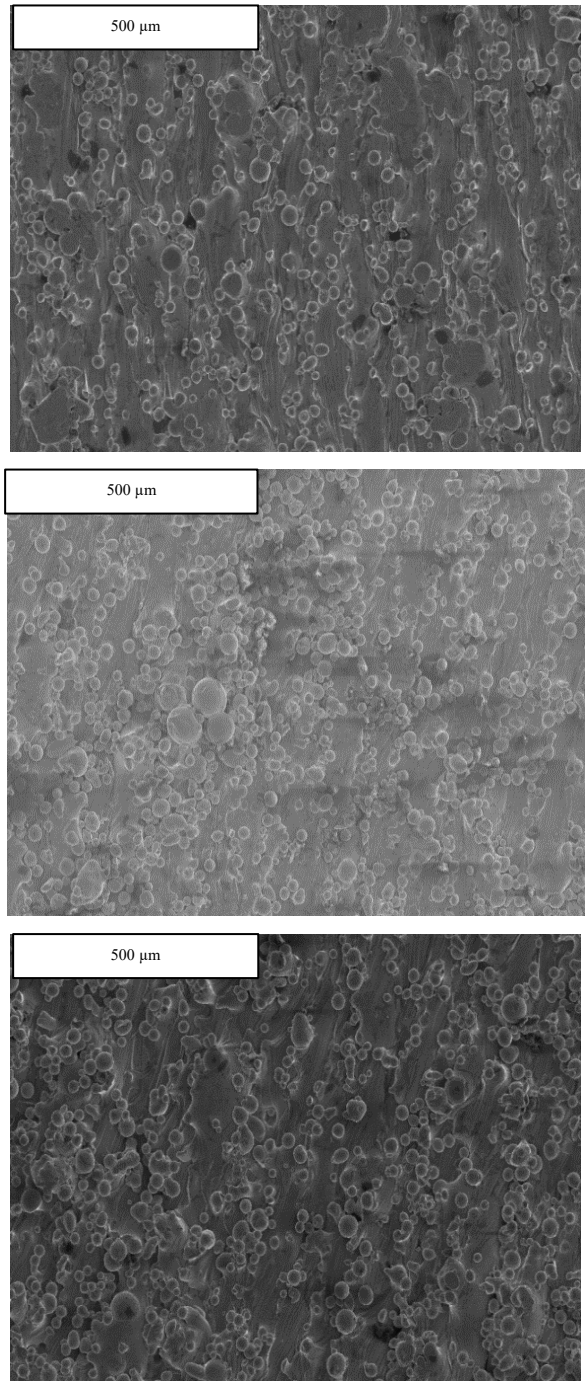

Figure 4:22: Particles on the side of the 67° rotation Stripe laser pattern cubes (a) Exposure Time 80µs, Laser Power 160W, (b) Exposure Time 105µs, Laser Power 180W, (c) Exposure Time 130µs, Laser Power 200W

Looking at the images in Figure 4:19, Figure 4:20, Figure 4:21 and Figure 4:22 it is possible to see that the powder attached to the sides of the samples shows a spread of powder sizes, this powder shows no satellites attached to it and at this magnification looks to be consistent with 'virgin' powder as studied in Figure 4:6. These powder

particles are all below 50µm suggesting the build process has had no effect on making the surrounding powder change due to having been through an AM cycle.

Surface Roughness Unaged Powder Samples

Figure 4:23 and Figure 4:24 show the changes noted between the top surfaces of a meander cube, Figure 4:23 and a stripe cube, Figure 4:24. This shows how the surface of a meander cube has less pores and that the scan tracks are clearly defined unlike the stripe scan pattern where it appears to be a messier surface finish. These cubes were further investigated to define experimentally the differences seen as surface roughness values.

When comparing Figure 4:17 and Figure 4:18 to Figure 4:21 and Figure 4:22 it is possible to see how the surface roughness varies between the sides and tops of samples. The sides show numerous powder particles drawn into them, but these particles are small in comparison to the laser tracks which cover the entire surface and the particles are partially drawn into the surface decreasing their effect on the surface roughness seen. As there are so many particles they create a covering of the sample side, evening out the surface roughness seen, unlike the laser tracks where there are numerous pits and rises across the surface due to the spaced out nature of laser tracks and the addition of pores into the surface and larger powder particles attached to the tracks.

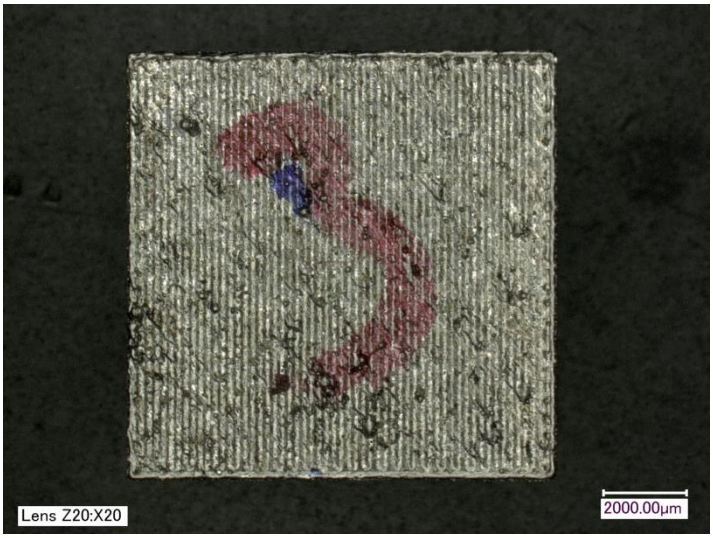

Figure 4:23: Top of Exposure Time 130µs, Laser Power 200W, Meander Laser Pattern, x20 mag

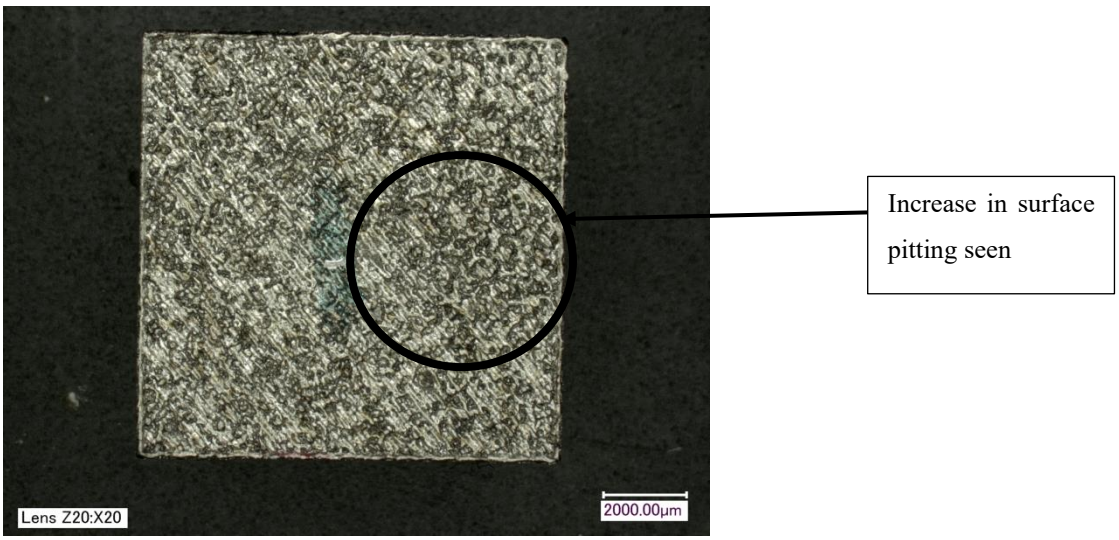

Figure 4:24: Top of Exposure Time 80µs, Laser Power 160W, Stripe Laser Pattern, x20 mag

White Light Interferometry (WLI) was used to study the surface roughness of the parts. The variations shown by studying the parts under the optical microscope and SEM can clearly be seen in the roughness variations. Surface roughness needs to be understood to see how parts will interact with other parts along with the fact that surface roughness affects parts characteristics [160].

The surface roughness readings were averaged to give the results for the top surface and then the average of the sides and these are shown in Figure 4:25 and Figure 4:26. The results show that roughness is affected by a change in parameters. The roughness on the sides of the 90° rotation samples are shown to increase as the laser power increases for both the meander and stripe laser pattern. Whereas the roughness on the top surface appears to decrease with exposure time and remain approximately the same across the laser powers.

The following parameters of 130µs exposure time and 180W laser power have the lowest top surface roughness in both the meander and stripe laser pattern. However, for the average roughness of the sides, 130µs exposure time and 160W laser power for meander laser pattern has the lowest roughness whereas the stripe laser pattern, 105µs exposure time and 160W laser power has the lowest roughness.

The results from the roughness testing on the 67° rotation samples showed that the lowest roughness on the top surface of the cubes was found to occur for the parameters of 130µs exposure time and 180W laser power with a meander laser pattern. The highest top surface roughness occurred for the parameters of 130µs exposure time and 200W laser power with the stripe laser pattern. Whilst the lowest average surface

roughness of the sides occurred for both laser patterns at 80μs exposure time and 160W laser power, with stripe being the lowest overall. The highest surface roughness occurred for 130μs exposure time and 200W laser power for the stripe sample.

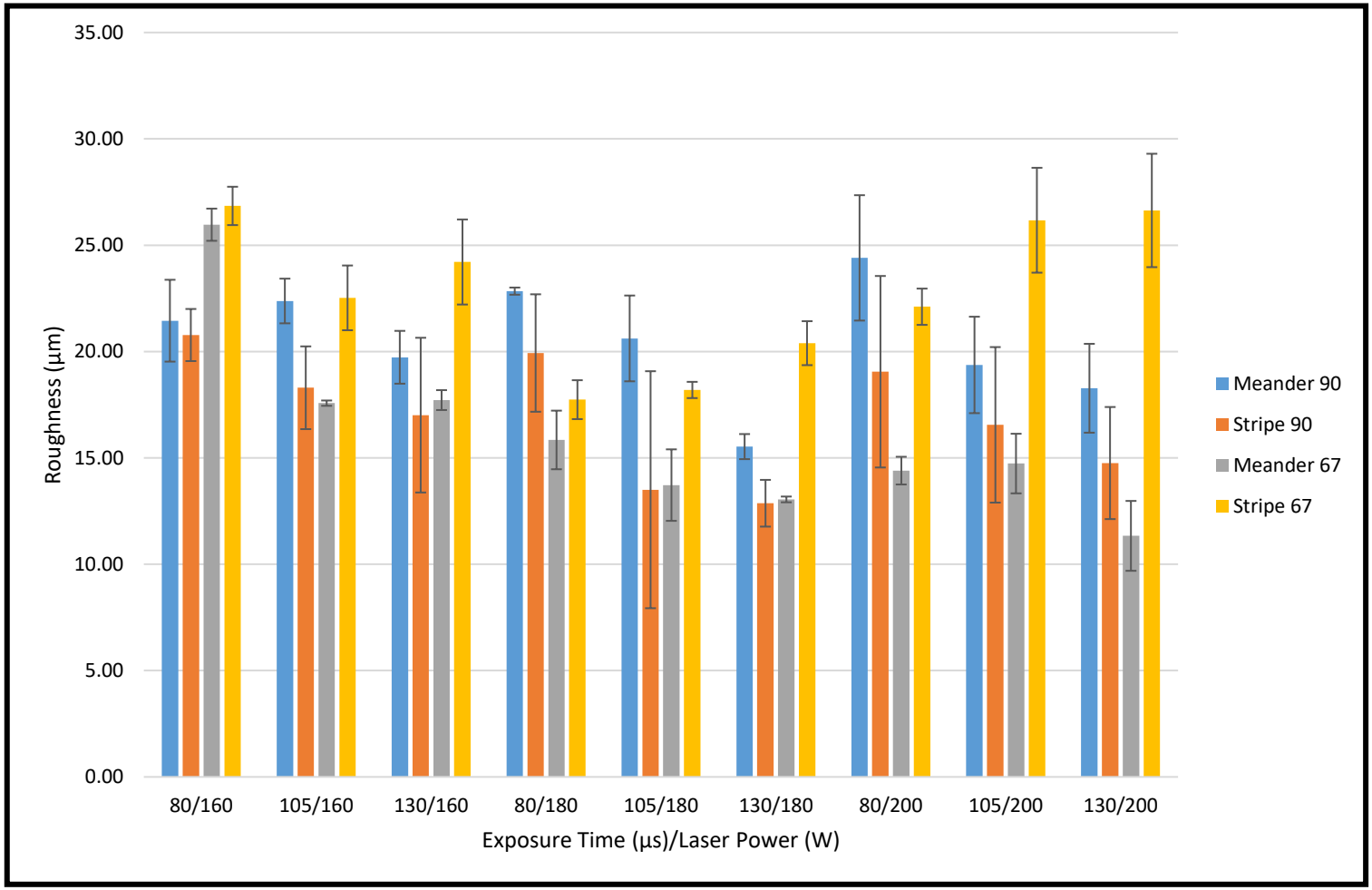

Figure 4:25: Roughness Top

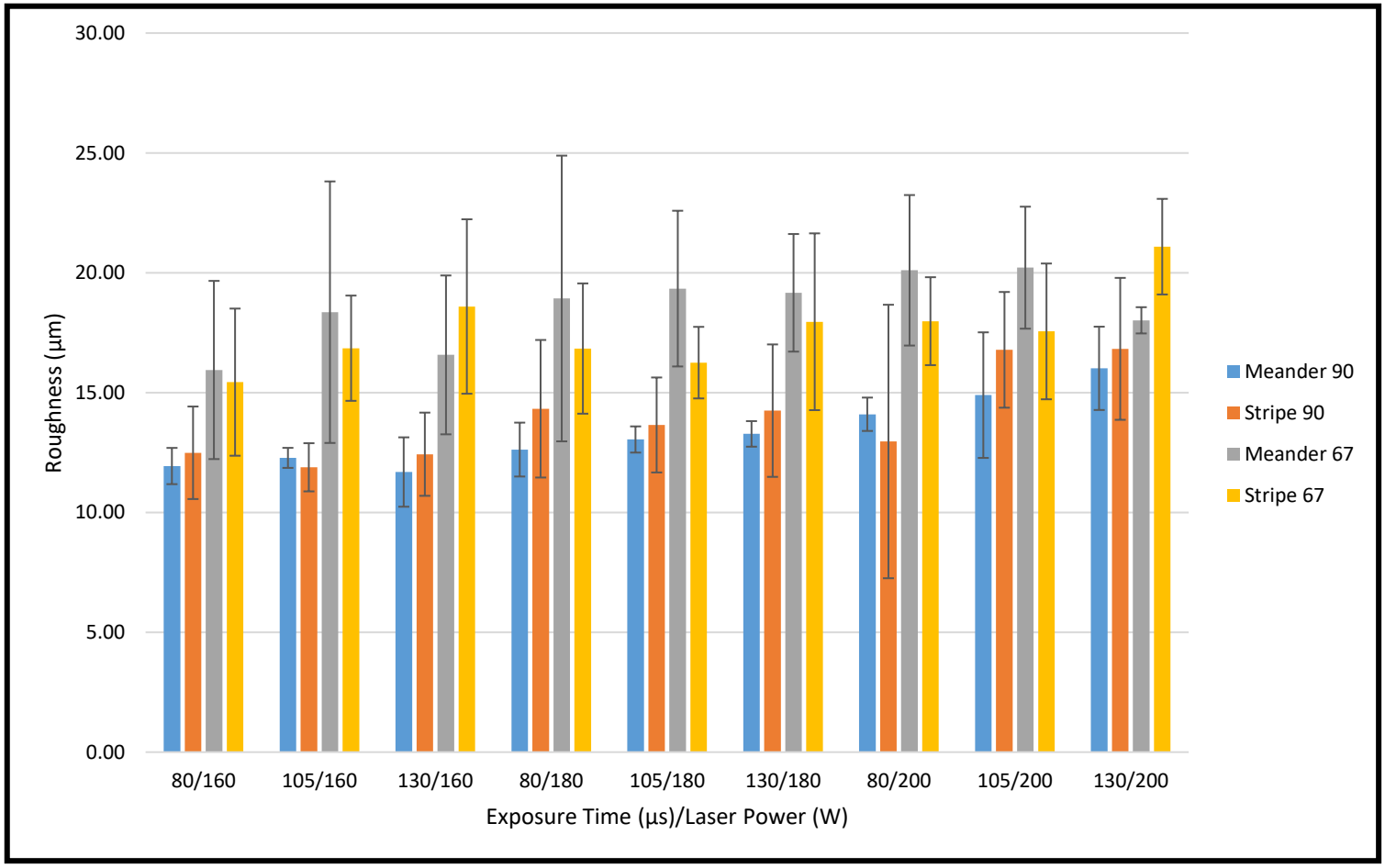

Figure 4:26: Roughness Sides

Figure 4:26 show the roughness values (Ra) of the sides and for the 90° samples the side surface roughness gets progressively larger, whereas the 67° samples are more consistent across the board. The lowest value seen is for the lowest exposure time and laser power. This could be because powder is adhering to the surface and lightly solidifying to the part but then falls off during post processing.

Figure 4:25 shows the surface roughness of the top of the samples show no clear trend across the spread but does show that a laser power of 180W produces the lowest surface roughness. This could suggest this power is enough to melt all particles on the surface but not to generate a balling effect which affects the roughness value. This is seen from the images, Figure 4:8 and Figure 4:13, where there are less powder particles on the top surface of 180W samples.

The standard deviation of the roughness results shows for the higher roughness seen for the 67° rotation samples that the variation is bigger. Whereas for the 90° the roughness is lower, but the standard deviation is lower indicating there is more predictability and repeatability of these results. Higher standard deviation shows that the process used is not as statistically robust and consequently not be suitable for use and potentially design. The surface roughness values are not just the sole source of evidence but are further supported by the results seen in the images.

When comparing the standard deviation for the sides roughness to the top roughness, Figure 4:26 to Figure 4:25 it is possible to see that the top has much smaller standard deviation meaning more consistent results for the top surface. Where the side standard deviation is larger and thus roughness would be less predictable and repeatable and once again prove to be harder to design for.

Summary

The roughness testing has found that the surface roughness is higher for most build settings when using the 67° rotation laser pattern and stripe laser pattern to build the samples. Whereas for the meander laser pattern there is no consistency, as to which rotation provides the lowest overall surface roughness.

Correlation between the roughness measurements taken and the images studied in this section provides quantitative data to show that the roughness between the sides and top varies along with showing how this varies when compared to build parameters used. Also, that it is possible to use WLI and optical microscopy to study the samples of AM parts and both methods will allow you to compare between samples to achieve correlation and trends.

Aged Powder Samples

Figure 4:27, Figure 4:28 and Figure 4:29 show the surface of three samples taken within an SEM. Figure 4:27 shows an as built sample with no heat treatment or finishing processes applied. This image shows particles adhering to the sides of the surface that vary in size from approximately 50µm to 150µm. Figure 4:28 shows a sample from the same build that has been heat-treated for 120 minutes at 450°C. This image shows much smaller particles adhering to the surface of the sample. Figure 4:29 shows another sample from the same build but in this case a heat treatment of 4 hours at 1200°C was applied. This image shows particles approximately the same as for heat treatment 1 with a couple of larger particles also present but none as large as those in Figure 4:27.

These images show the effect heat treatment has on the surface of AM parts by increasing the temperature and allowing further powder particles to be melted into the part, solidifying to create a smoother surface. The effect of heat treatment on an AM components surface leads to reduced surface residual stress, changes to the microstructure and improve fatigue performance due to improved initiation resistance, improving the parts performance.

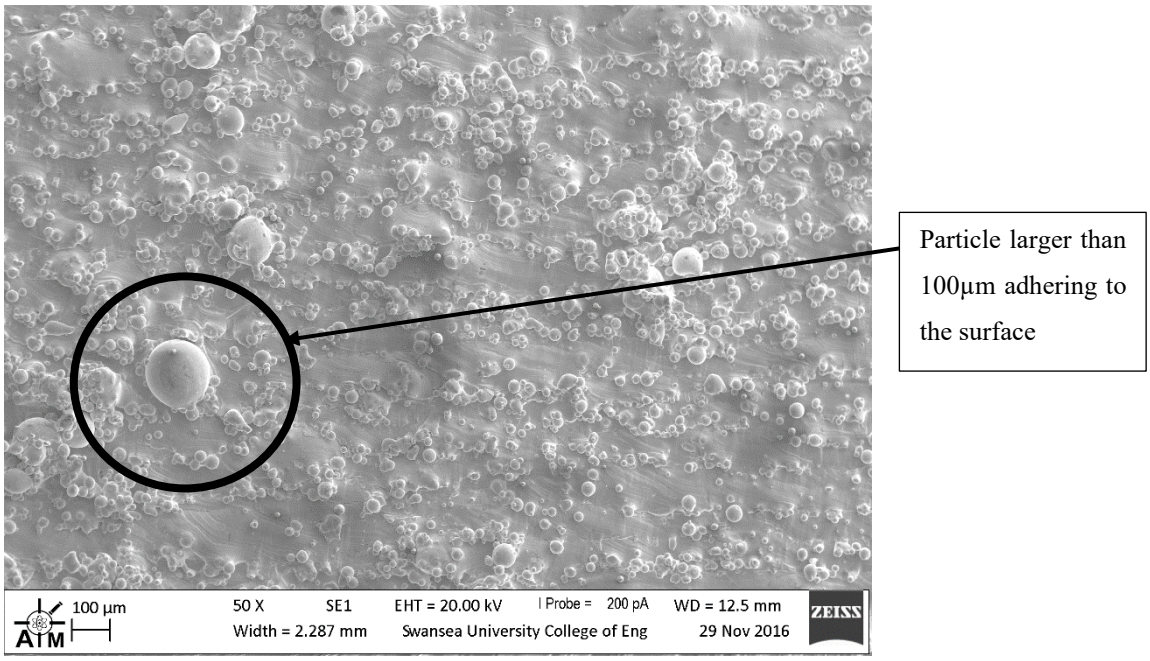

Figure 4:27: Build 21 Vertical, Meander Laser Path, Exposure Time 80µs, Laser Power 200W, As Built

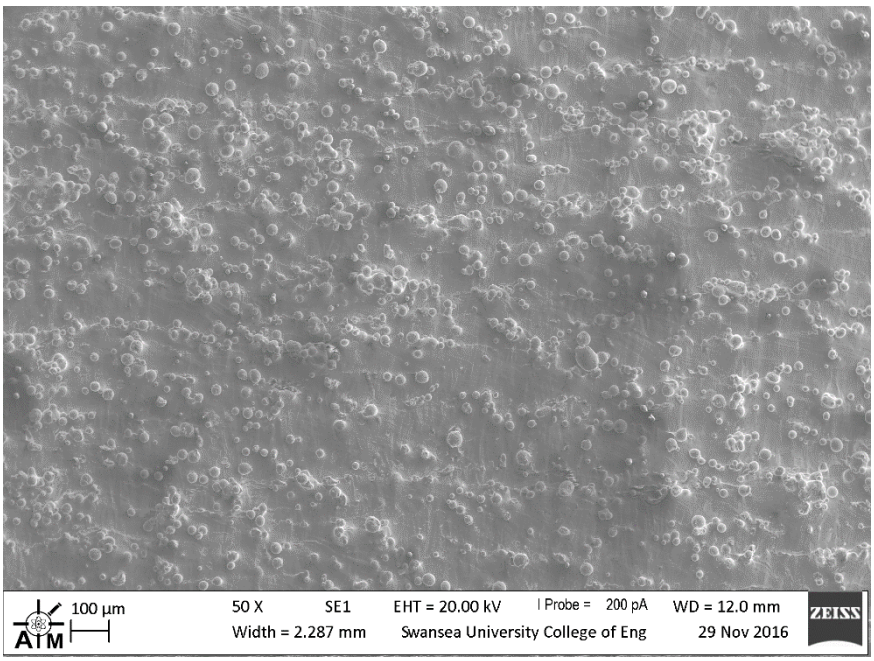

Figure 4:28: Build 21 Vertical, Meander Laser Path, Exposure Time 80µs, Laser Power 200W, Heat Treatment 1 Applied

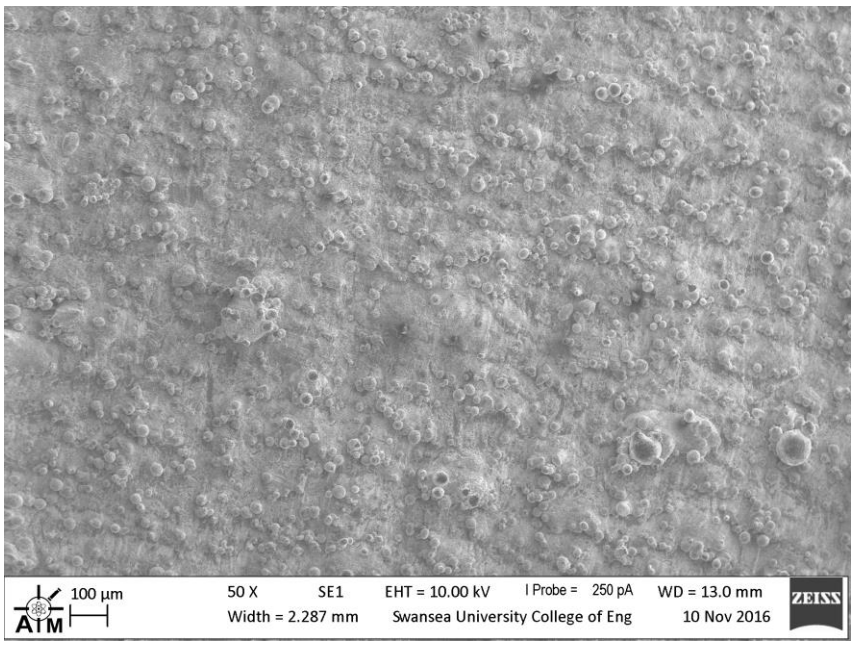

Figure 4:29: Build 21 Vertical, Meander Laser Path, Exposure Time 80µs, Laser Power 200W, Heat Treatment 2 Applied

Surface Particles

Figure 4:30, Figure 4:31, Figure 4:32 and Figure 4:33 show particles on the surface of as built parts. These images show the variation in quality of parts and how they are affected by the heating during the build process.

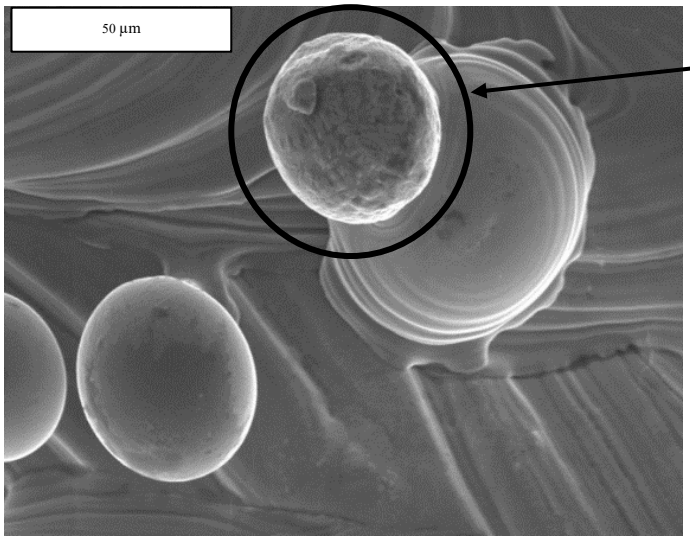

Figure 4:30: Exposure Time 105, Laser Power 180W, Stripe Laser Pattern, x1000 mag

Figure 4:30 as shows how particles can be partially melted during the process and adhere to the surface after manufacture. This indicates that the laser power may be too low and doesn't provide sufficient energy to melt all of the powder drawn into the laser track. Figure 4:31 and Figure 4:32 show how the surface of powder that has been through the process is affected. It is possible to see that these powder particles no longer have the smooth surface of freshly manufactured powder.

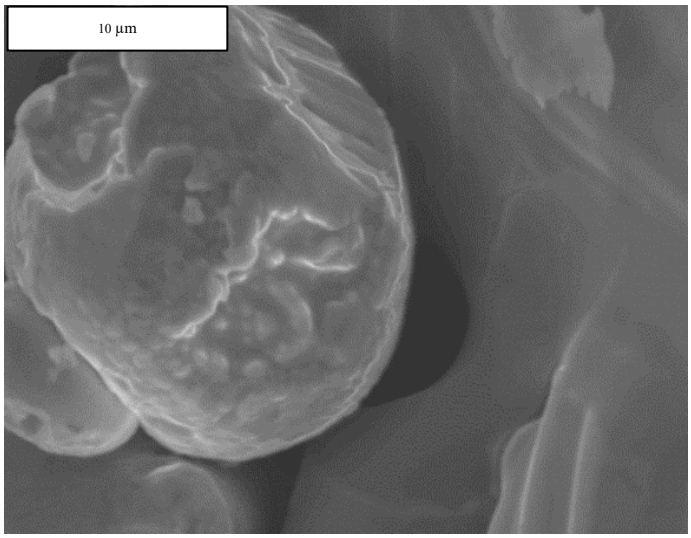

Figure 4:31: Exposure Time 130, Laser Power 200W, Stripe Laser Pattern, x3000 mag

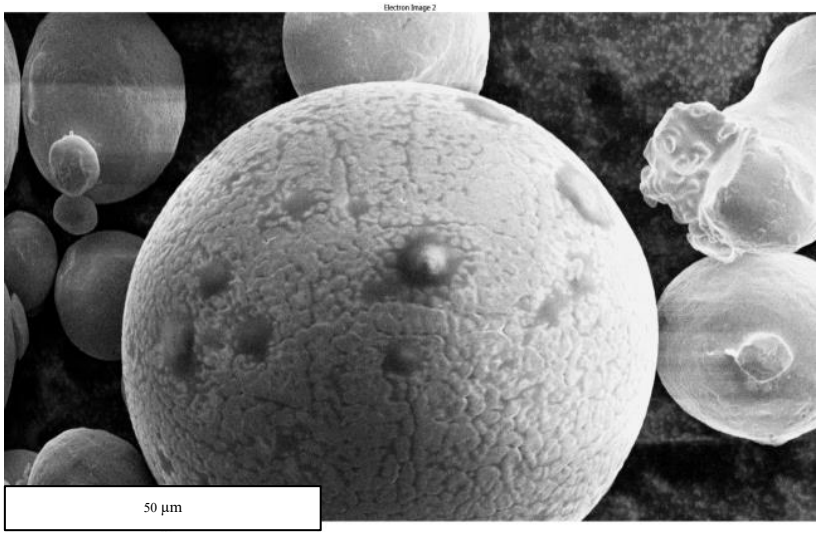

Figure 4:32: Particle of SS316L Powder after the AM process

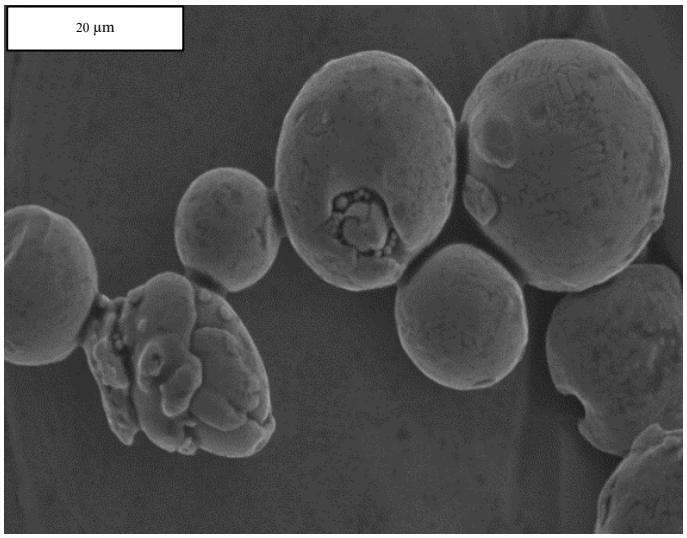

Figure 4:33: Particles on the surface of a 105µs exposure time, 180W laser power, 67° rotation meander pattern cube

Figure 4:33 once again shows how there can be smaller particles within larger particles as well as the effect of poor powder production leading to powder that resembles an egg with a layered surface.

What can be seen from Figure 4:30, Figure 4:31, Figure 4:32 and Figure 4:33, is that the powder is changed from 'virgin' powder due to the AM process, Figure 4:4. But the images also show particles of approximately the same size as seen in 'virgin' powder, but the surface has been affected by the AM process and this has likely changed the powders composition.

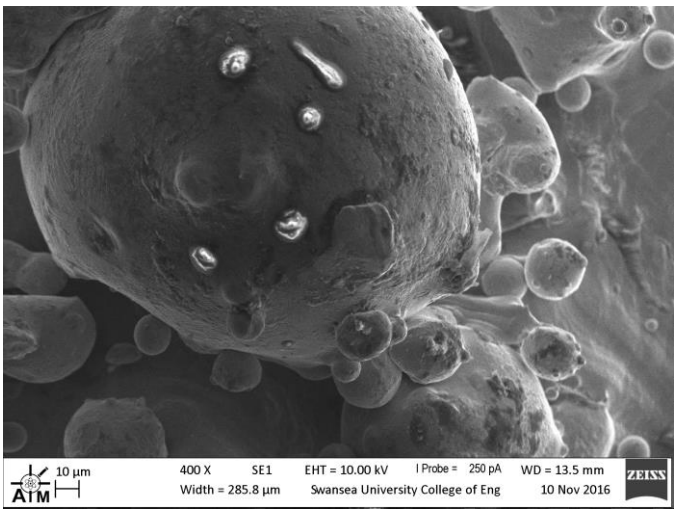

Figure 4:34: Build 21 Vertical, Meander Laser Path, Exposure Time 80µs, Laser Power 200W, As Built

Figure 4:34, Figure 4:35 and Figure 4:36 show higher magnification images of the powder particles adhering to the samples surface. These images show unmelted or partially melted powder adhering to the surface of the parts. From Figure 4:34 it is possible to see that there are larger particles approximately 300µm in size with smaller satellite particles of 40µm surrounding it and being drawn into the larger particle. Figure 4:35 shows the surface of a sample that has undergone heat treatment 1, here it is noticed that there are only smaller particles approximately 40µm in size and the surfaces of these start to show distortion from the smoother surfaces seen on the particles in Figure 4:34. Figure 4:36 shows the surface of a sample that has undergone heat treatment 2, here there are particles ranging in size from 15µm to 40µm. The surface of these particles shows distortions and what appear to be droplets of metal covering them. Particle distortions are expected when a component undergoes phase change during heat treatment. It shows that the heat treatment has had an effect on the component, likely reducing residual stress and changing the microstructure. This change can effect the mechanical properties of the component as microstructure influences strength, ductility, creep, and fatigue.

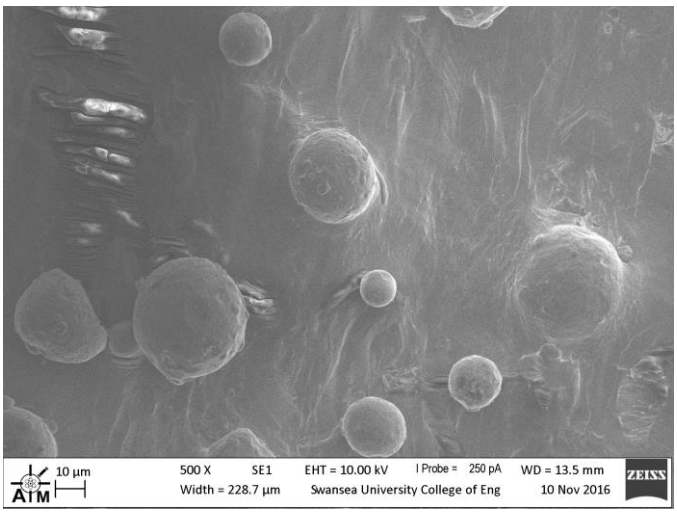

Figure 4:35: Build 21 Vertical, Meander Laser Path, Exposure Time 80µs, Laser Power 200W, Heat Treatment 1 Applied

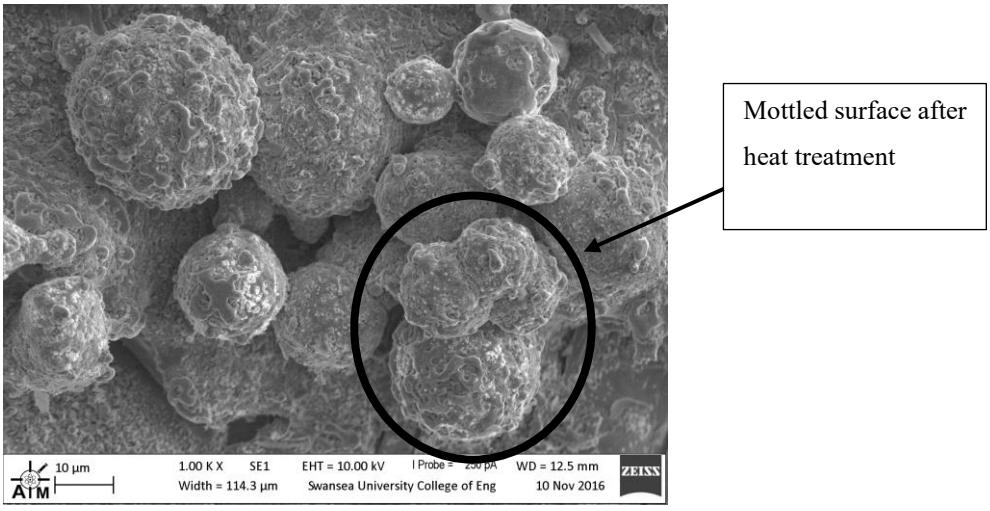

Figure 4:36: Build 21 Vertical, Meander Laser Path, Exposure Time 80µs, Laser Power 200W, Heat Treatment 2 Applied

Comparing the images in Figure 4:37 it is possible to see how the heat treatment applied has affected the surface of unmelted particles. Figure 4:37(a) has had heat treatment 1 applied whereas Figure 4:37(b) had heat treatment 2 applied. Heat treatment 2 has an effect on the particles surface but still is not enough heat to completely melt the surface particles and draw them into the part.

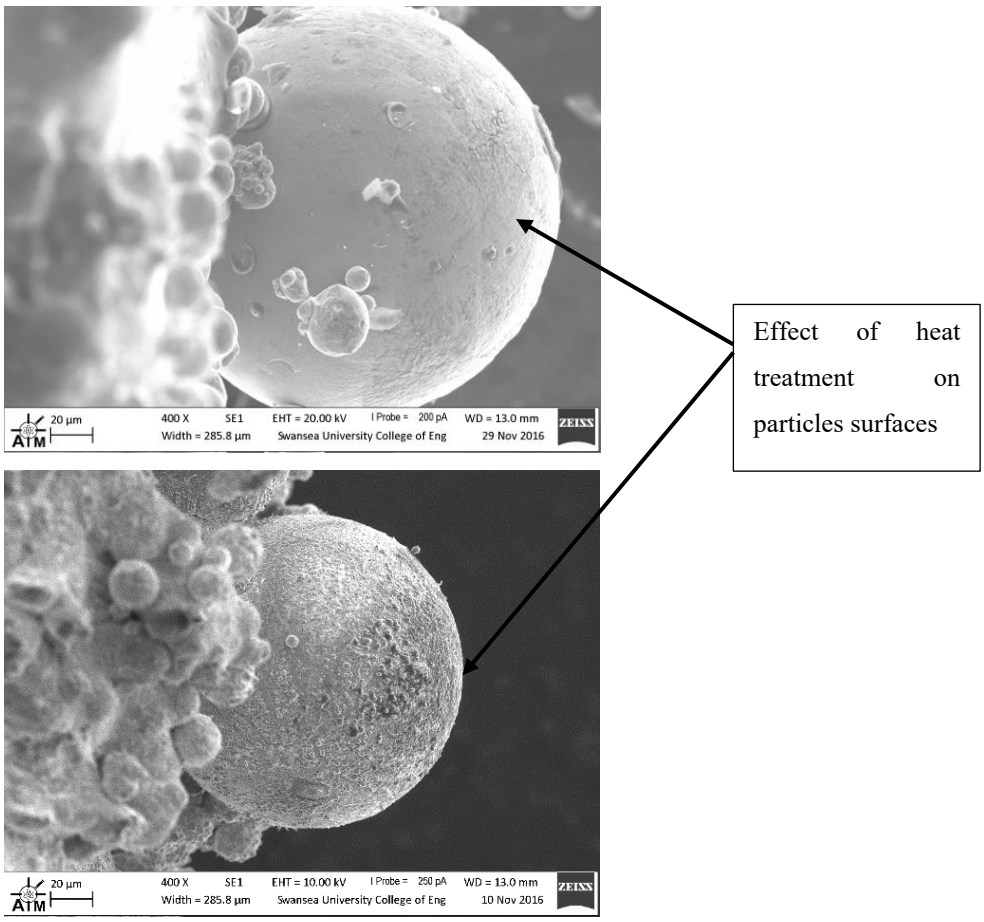

Figure 4:37: Build 21 Vertical, Meander Laser Path, Exposure Time 80µs, Laser Power 200W, (a) Heat Treatment 1 Applied, (b) Heat Treatment 2 Applied

4.5.3 Porosity and Density

The porosity found should compare to the density as this shows the empty pockets within the cubes. The porosity is measured using images of a layer of the cube; it is a 2D measure of the black pores on the white surface.

The porosity was shown to vary across the surface of the cube with the centre area appearing to have a higher porosity value and the edges appearing to have lower values.

This variation in porosity is seen in Figure 4:38, which shows the edge and centre respectively, of the cube built using the meander laser pattern with an exposure time of 80µs and 160W laser power. Figure 4:38 shows a porosity of 0.78% for (a) the edge while (b) the centre shows a porosity of 6.94%. This shows how the porosity varies within the part in this case by 6.17%. The areas chosen to take the porosity images had to be carefully selected and a high number of readings taken to ensure statistical accuracy as the porosity varied so much across the sample.

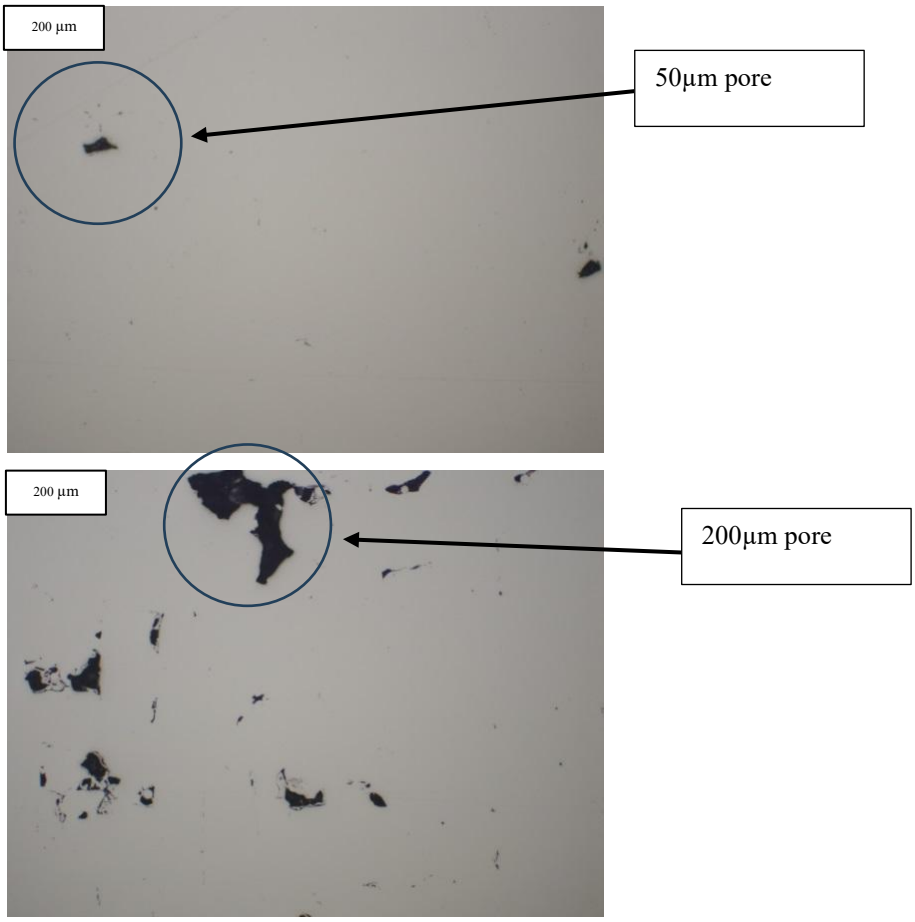

Figure 4:38: Porosity comparison on 80µs exposure time and 160W laser power cube (a) Edge, (b) Centre

Porosity is a major factor affecting the density of AM parts. Figure 4:39 is a macro image showing an example of where the porosity is arising from, and these areas have been highlighted by the circles shown.

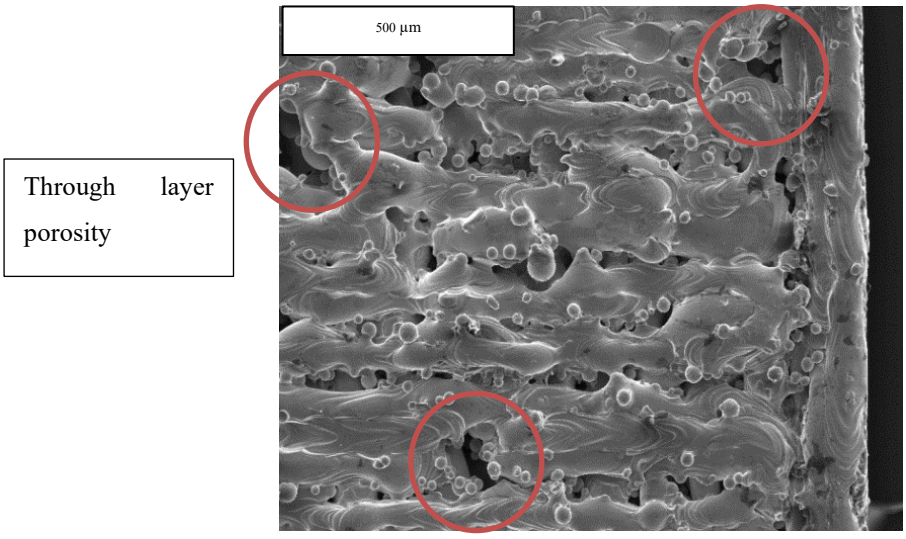

Figure 4:39: Top of Exposure Time 80, Laser Power 160, Meander Laser Pattern, 90° rotation, x75 mag

Figure 4:40 shows more of these pores between scan tracks on the surface of parts. From these images it is possible to see through the layers to the lower layers but also to understand why the density is reduced. This sample has a porosity of 11.09% and a density of 6.76g/cm^3, this high porosity and lower density (reduced by 1.24g/cm^3) can be confirmed by what is seen in the image where there are large areas with no material present on the top and subsequent layers.

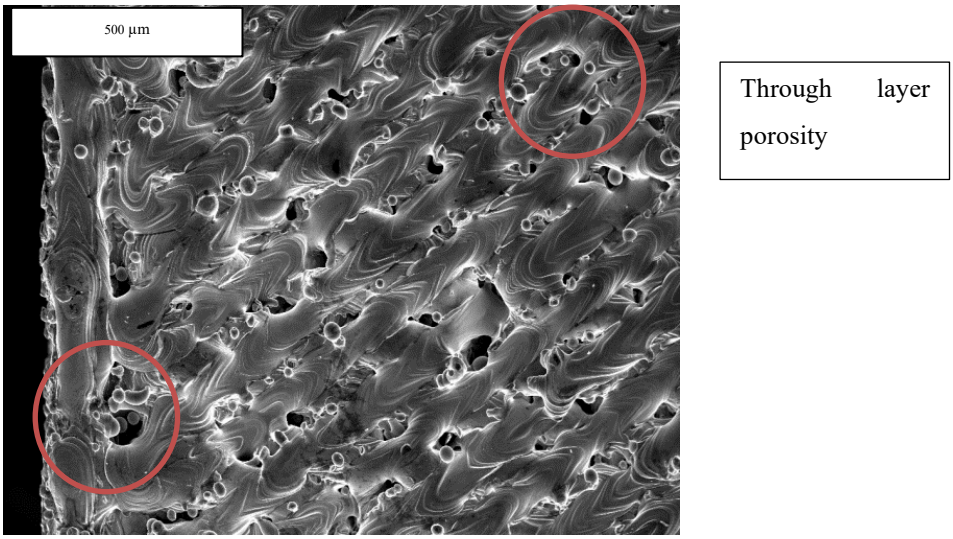

Figure 4:40: Top of Exposure Time 80, Laser Power 160, Stripe Laser Pattern, 67° rotation, x75 mag

Figure 4:41 shows that these pores and gaps between the laser tracks are not just present on the top surface but can also be seen in lower layers where there are also unmelted powder particles sitting within gas pockets.

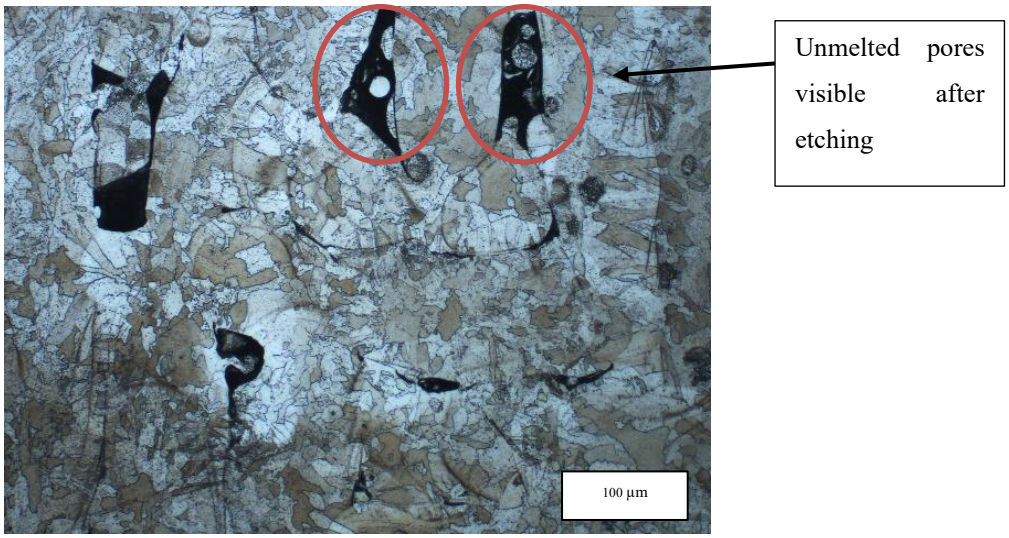

Figure 4:41: Unmelted particles within pores after etching

Table 5:1and Table 5:2 show the porosity found across a layer and through the layers of both rotations used.

The porosity calculations for the 90° rotation samples show that there is a difference between the two test directions. The results also show that the porosity does not always correspond to the density found earlier in the testing.

The porosity of the 67° rotation samples has found that the porosities are not a close match to the densities found using Archimedes method.

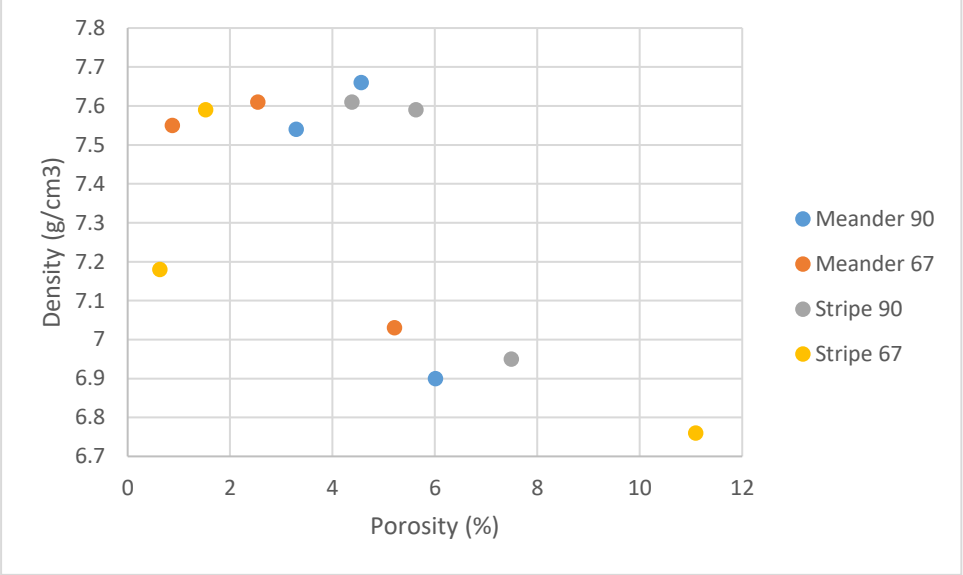

Figure 4:42: Plot to show Porosity vs Density

From the results found within this work shown in Figure 4:42 it is not possible to state if there is a trend between porosity and density.

The porosity is not believed to be representative of the sample due to it only being taken on one layer. To mitigate this effect, it would be an idea to perform CT evaluation of the entire cube particularly looking at the centre of the cube to see how the porosity varied across the part and the effect of different laser patterns on the internal pores.

4.5.4 Tensile Test Samples BP1 & BP2

Comparisons have been made looking at the tensile test results and these samples have been investigated further to see what changes appear in the composition and microstructure of the samples.

The purpose of the tensile testing was to investigate the effects of laser power, exposure time, hatch style and layer rotation on UTS, yield strength and fracture

surface. Build Programme 1 (BP1) was the initial work carried out varying the parameters as shown in Table 4:3.

Table 4:3: Test Parameters and Part Position

	Laser Power (W) →		
Exposure Time (µs) ↓	A1 – 80/160	B1 – 80/180	C1 – 80/200
	A2 - 105/160	B2 - 105/180	C2 - 105/200
	A3 - 130/160	B3 - 130/180	C3 - 130/200

Tensile testing for Build Programme 2 (BP2) was to investigate the effect of aged powder within in the AM build process on the UTS, yield strength and fracture surface. The build parameters used are shown in Table 4:4 and the heat treatment parameters are shown in Table 4:5.

Table 4:4: BP2 Build Parameters

Laser Power (W)	200
Exposure Time (µs)	80
Hatch Style	Meander
Angle Increment (°)	67

Table 4:5: BP2 Heat Treatment Parameters

	Ramp Up (mins)	Hold (mins, °C)	Ramp Down (mins)	Pressure (MPa)
HT1 (BP2)	90	120 @ 450	90	N/A
HT2 (BP2)	360	240 @ 1150	360	N/A
HIP	360	240 @ 1150	360	100

Ultimate Tensile Strength (UTS)

The UTS's found in this work are shown in Table 5:1, Table 5:2, Table 5:3, Table 5:4, Table 5:5 and Table 5:6. These are the results for all the conditions and powder investigated. These results compare favourably [45] to results found during the

literature review in the aged powder studies but the previous mixed powder studies many of the results were lower than those found in previous work.

The time interval, cross head displacement, extensometer displacement and force are recorded for each time step during the test. The data from this is used to calculate the stress and Young's Modulus for each sample. The peak load recorded during the testing is used to calculate the UTS of that sample.

These tables show that the highest 90° rotation UTS occurs for the 130μs exposure time and 200W laser power with the meander laser pattern and 130μs exposure time and 180W laser power for the stripe laser pattern.
These tables show that the highest UTS for the 67° rotation is 556MPa and this occurs when there is an exposure time of 130μs and laser power of 200W with the meander laser pattern and of 459 MPa for the stripe laser pattern with an exposure time of 105μs and 200W laser power. Again overall, the meander laser pattern test samples give better results than the stripe pattern.
Tensile testing performed on the samples has shown that there is a large variation in the UTS found across AM samples. Table 5:1, Table 5:2, Table 5:3, Table 5:4, Table 5:5 and Table 5:6 show the UTS, Yield Strength and Young's Modulus for all of the samples tested.

For the samples manufactured using aged powder it is possible to see that for the as built samples all of the UTS's are above 600MPa, bar one of the horizontal samples for the as built tests. The effect of heat treatment 1 can be seen for the vertical samples, they show that the UTS has increased slightly, but there is no consistency in how the Young's modulus and yield stress have changed due to the treatment being applied. The extension has been seen to be approximately consistent. When heat treatment 2 was applied, it was found that the UTS, yield and extension were all reduced. With the majority of samples with UTS's below 600MPa. Again, as with heat treatment 1, there has been a reduction in the extension of the samples.

The highest UTS found was 650MPa and this was for build 18 vertical sample, the corresponding yield stress was 184MPa and the Young's modulus 2.8GPa. The highest UTS is not found to correspond to the highest yield stress found of 353MPa or the highest Young's modulus of 7.5GPa which were found for different samples.

The strain to failure was shown to be consistent between as built and heat treatment 1 within an improvement by approximately 50% between heat treatment 1 and heat

treatment 2. The maximum strain to failure seen was 18.103% for a heat treatment 2 sample from build 17, which was the first build in this test series.

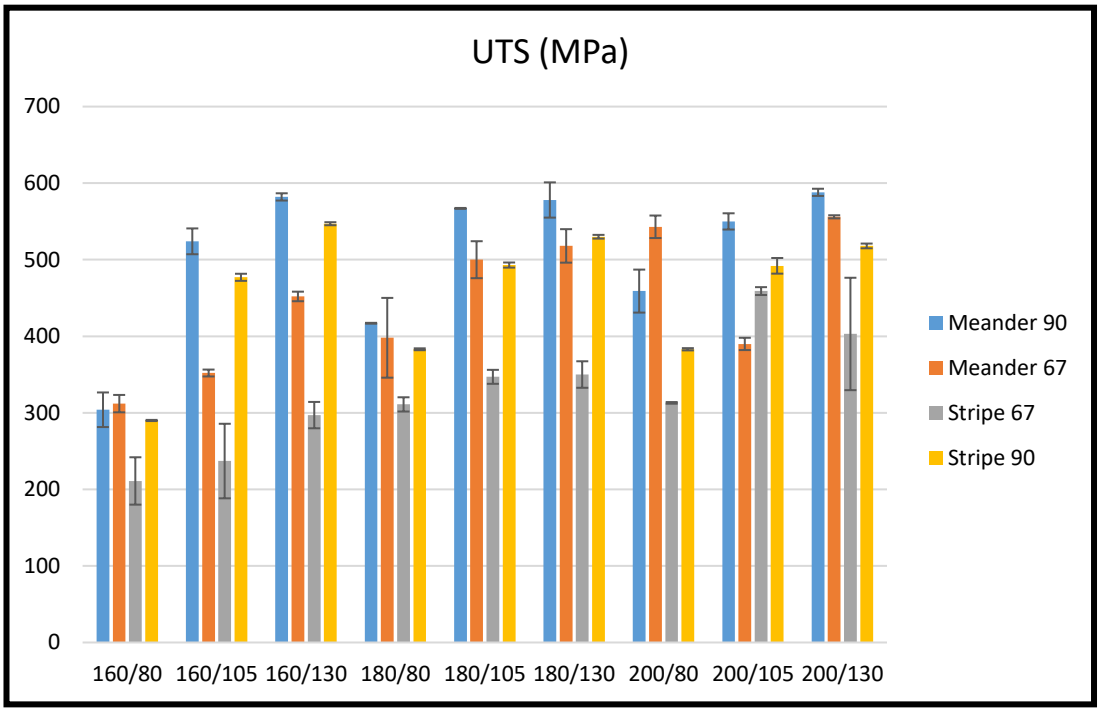

Figure 4:43: UTS of Initial Samples

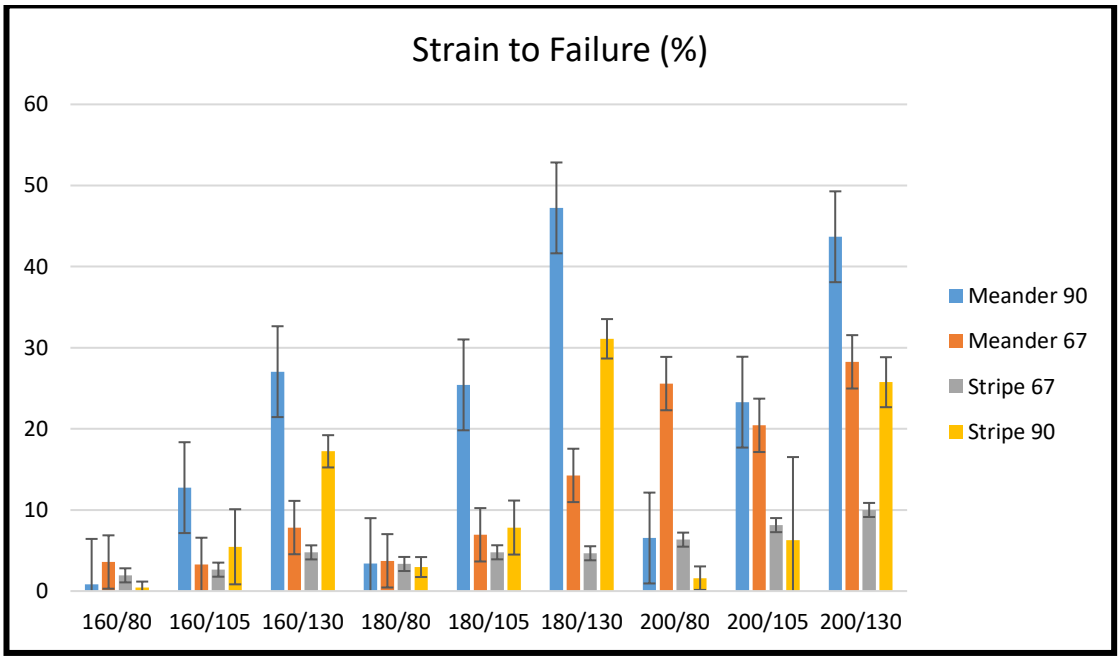

Figure 4:44: Strain to Failure of Initial Samples

When looking at Figure 4:43 it is possible to see that the UTS is consistently much lower overall for the stripe, 67° rotation samples. If you exclude the lowest laser power and exposure time sample (160W, 80µs) the average UTS's are similar and comparable with a few exceptions for all three of the other settings.

Figure 4:44 shows the strain to failure of the original samples, this figure shows that in most cases the strain to failure is very low with only a handful of cases where it exceeds 20%. What can be seen also is that only the meander, 90° laser pattern gives consistently good results and only for the higher laser power (200W) do we see improved results across all build parameters.

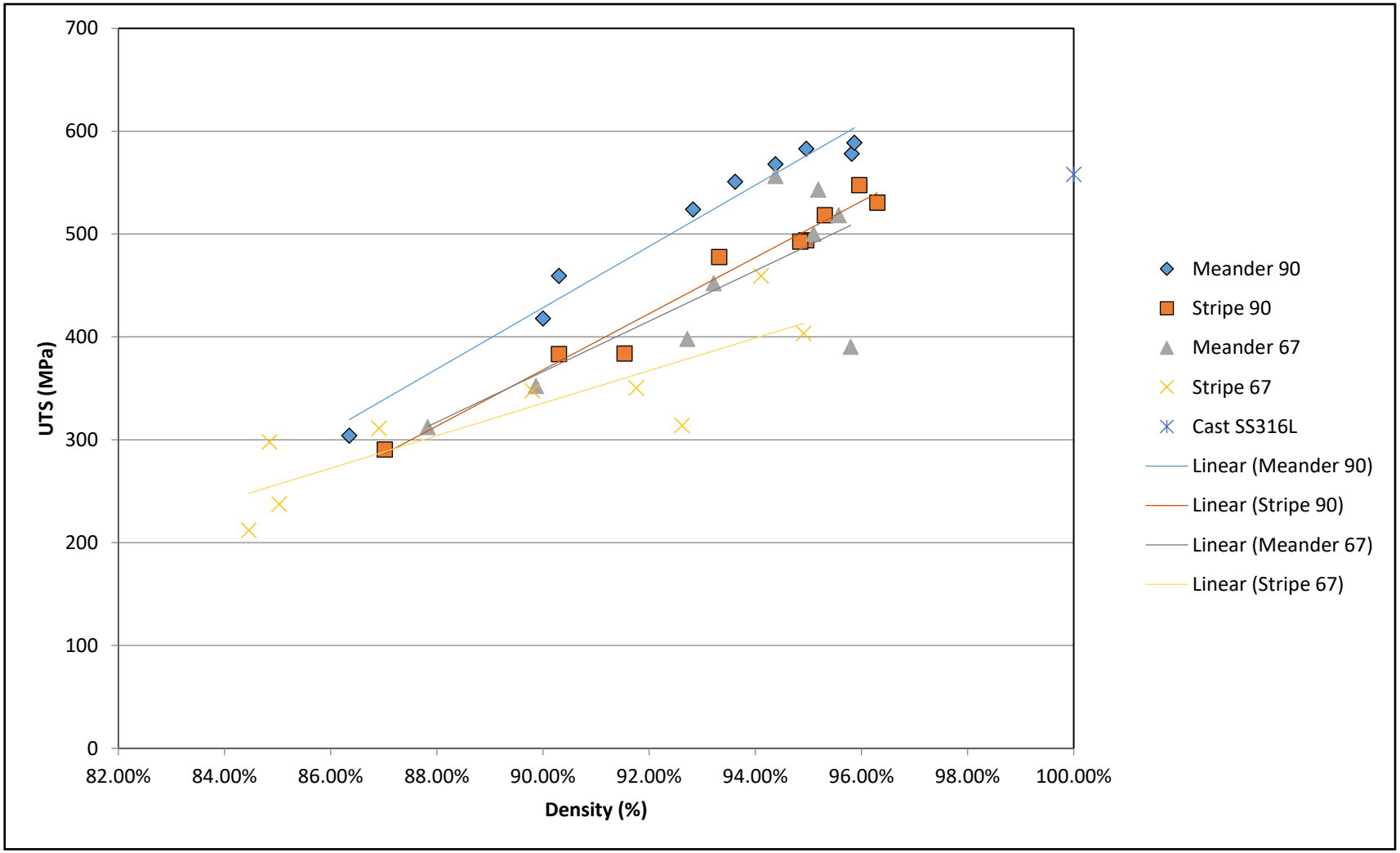

Figure 4:45: A graph showing the trends in densities for the four sets of unaged powder build parameters

The graph shown in Figure 4:45, shows the UTS plotted against the density. From this graph, it is seen that for the 90° layer rotations the trend is linear, as the density increases the UTS increases, whereas for the 67° layer rotations this trend is harder to see. This suggested that 90° layer rotation has more consistent build properties across the range tested here.

When looking at the microstructure of a selection of samples taken from across the range of Densities and UTS's it is possible to see as the density increases the visible pores reduce but also that as the UTS increases these pores are also reduced and that the microstructure shows larger average grain sizes.

Figure 4:46 shows a typically produced Stress Strain graph for use in calculating the UTS, Yield Stress and Young's modulus. This graph shows the Stress Strain curve for three samples manufactured using the same build settings on the same build plate, next to each other. From this graph, it is possible to see how there can be significant variations in stress vs strain for parts built using the same parameters and powder. These variations give an average standard deviation of 13.87. This graph also shows how the Yield Stress changes within parts, with the same build parameters but that the Young's Modulus is likely to be consistent due to the elastic region following the same trend.

As it is known that the laser power and exposure time were the same for all of these parts, something else must be affecting the parts mechanical properties for such a change in strain to failure to be seen between the three samples. This could be that there was something fundamentally wrong with the testing or data or more likely it is due to a defect present within that sample that caused it to fail prematurely and earlier than the rest.

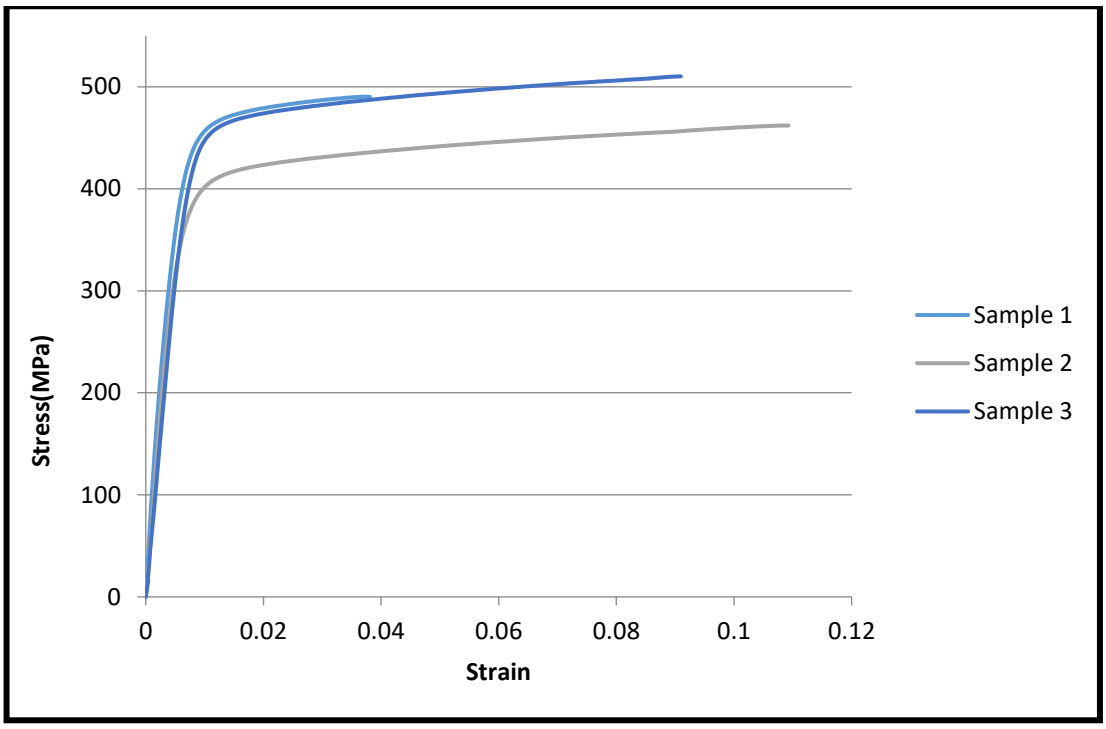

Figure 4:46: Stress Strain Graph for 105µs exposure time, 180W laser power, 67° layer rotation and meander laser pattern tensile (all three built samples tested)

Strain to Failure

The average extension and strain to failure for each set of parameters are shown in Table 5:1, Table 5:2, Table 5:3, Table 5:4, Table 5:5 and Table 5:6, the average is based on three samples tested for each set of parameters that have been used for this work.

The results of the extensions of the tensile bars gauge length show that; the lowest strain to failure occurred in the samples with an 80µs exposure time and a 160W laser power. These were lower for stripe than for the meander laser pattern.

The highest strain to failure occurred at 130µs exposure time and 180W laser power, with an average extension of 14.22mm for the meander pattern and 9.36mm for the stripe pattern.

These extension results show that the meander is the better of the two laser patterns in terms of strain to failure, samples with a meander laser pattern are more ductile and their tensile strength is lower as seen from the results.

The results of the 67° rotation samples show that again the meander samples have the highest strain to failure and that the 130µs exposure time and 200W laser power, meander laser pattern has the highest strain to failure of 25.75%.

Summary

The strain to failure of the tensile bars was shown to be at its maximum for the meander laser pattern using a 90° rotation of the pattern each layer and 130µs exposure time with 180W laser power. This was seen to be an increase of 46% on the 67° rotation samples using both a meander laser pattern and 130µs exposure time as before but a laser power of 200W.

Young's Modulus

The Young's modulus has been calculated for all the tensile bars that were tested. Measurement of the Young's modulus is subject to the interpreter's opinion concerning the point of yield. These results are shown in Table 5:1, Table 5:2, Table 5:3, Table 5:4, Table 5:5 and Table 5:6.

From these results, it has been found that the highest Young's modulus does not occur with the highest UTS or yield stress. The results show that the Young's modulus appears to decrease with powder reuse but shows no consistency in value when compared to the yield stress or UTS found.

As Built Unaged Powder Tensile Samples

When testing the samples on one occasion a sample failed to fracture fully. This sample has been imaged using both optical and SEM to see if there are any obvious reasons for this to occur.

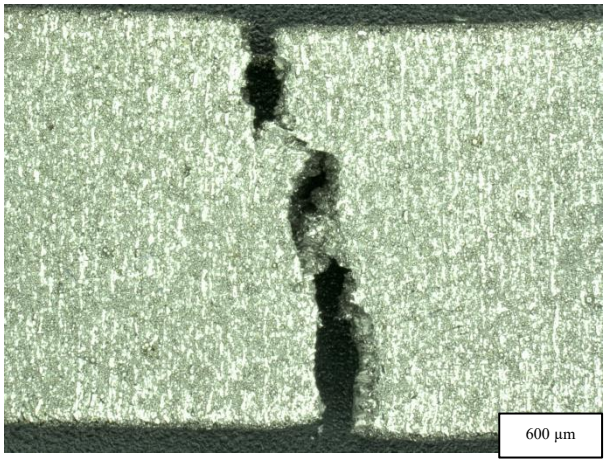

Figure 4:47: Fracture of 67° rotation and stripe laser patter, 80µs exposure time and 180W laser power sample, UTS 311 MPa

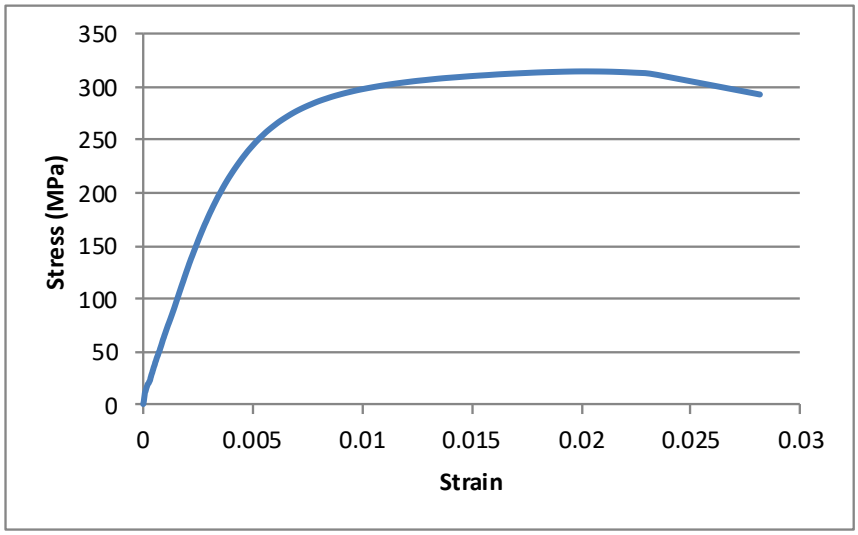

Figure 4:48: Stress vs Strain Graph for Fracture of 67° rotation and stripe laser patter, 80µs exposure time and 180W laser power sample, UTS 311 MPa

Figure 4:47 shows a tensile bar that although it has begun to split the bar did not totally fail. The results of stress vs strain, Figure 4:48, show how the sample has a reduced strain below 0.03 and the curve is not smooth. Another sample from this parameter set shows that the maximum stress found was 330MPa, shown in Figure 4:49. This graph also shows a strain to failure rate of 0.045. This result is comparable to the other results for tests using these same build parameters.

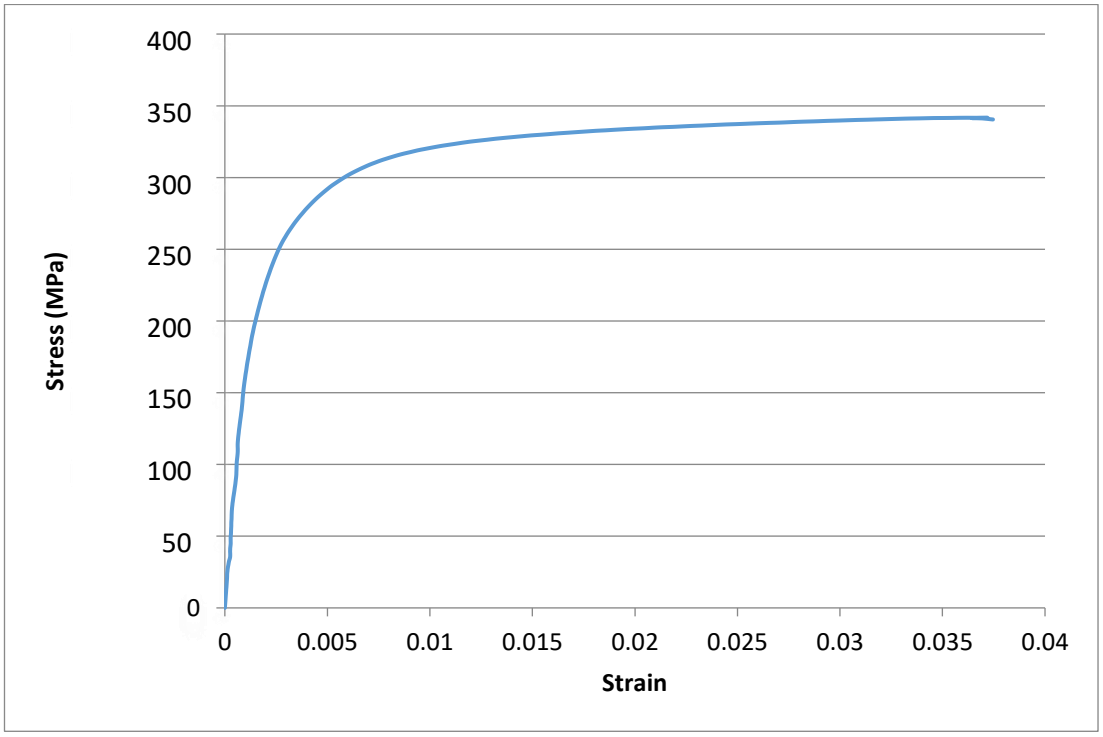

Figure 4:49: Stress vs Strain graph of 67° rotation and stripe laser patter, 80µs exposure time and 180W laser power sample, UTS 330 MPa

The 90° rotation, meander laser patter, 130µs exposure time and 180W laser power samples were shown when compared to others to have a larger than average extension. The average strain to failure of the B3 samples was 16.5% and the extension of the samples was 14.22mm. The sample shown in Figure 4:50 has an extension of 15.3mm, which was the largest extension, found in these samples.

Figure 4:50: Extension of 90° rotation and meander laser patter, 130µs exposure time and 180W laser power sample, UTS 578 MPa

Figure 4:51 shows the stress vs strain graph for the sample shown in Figure 4:50. This sample had a UTS of 552MPa which was the one of the 'highest' found within these

tests and is explained by the large extension but perhaps not by the reduced strain to failure when compared to the other samples.

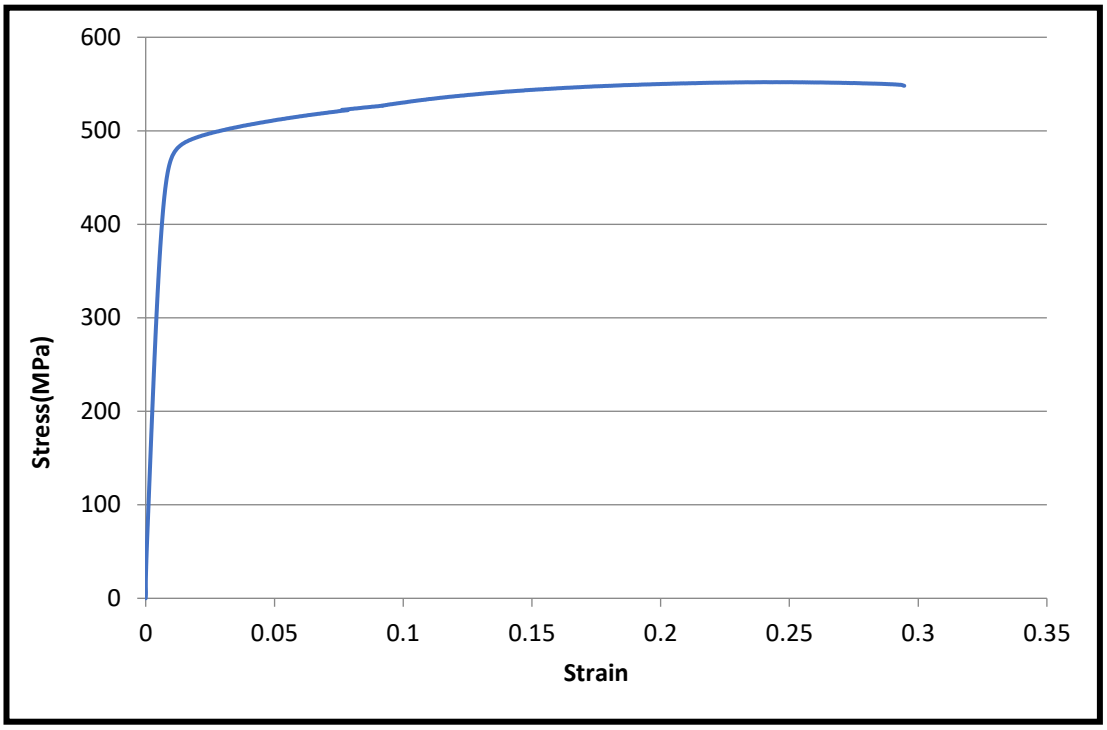

Figure 4:51: Stress vs Strain Graph of 90° rotation and meander laser patter, 130µs exposure time and 180W laser power sample, UTS 578 MPa

Not only have some of the samples fractured across one layer there have been cases shown in Figure 4:52, where there have been weak points on a number of layers and each of these layers has fractured and these fractures have joined together through a number of layers to break the bar. These samples had an average UTS of 398 MPa. Figure 4:53 shows the stress vs strain graph which is as expected and shows a strain to failure of 0.037.

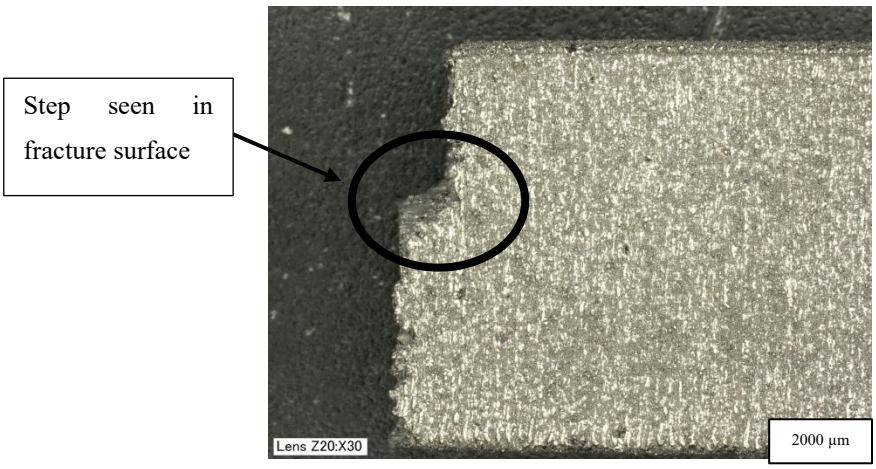

Figure 4:52: 67° rotation and meander laser pattern, 80µs exposure time and 180W laser power, UTS 339 MPa

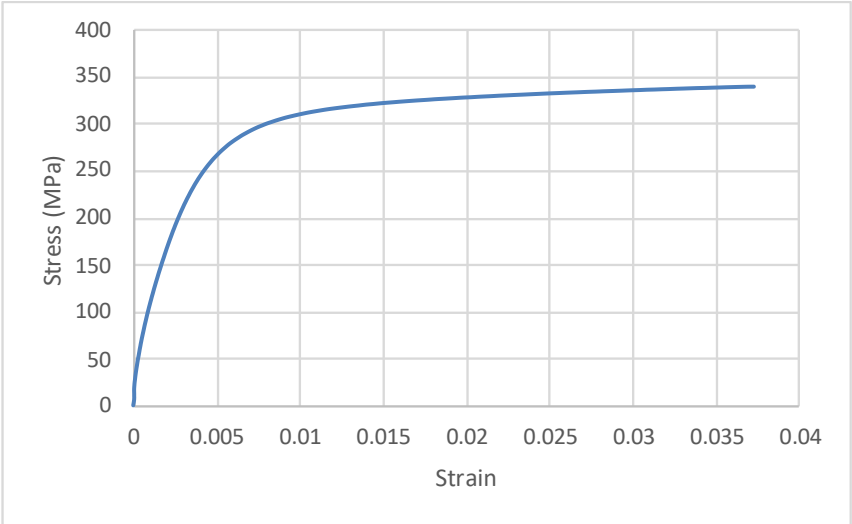

Figure 4:53: Stress vs Strain Graph for 67° rotation and meander laser pattern, 80µs exposure time and 180W laser power, UTS 339 MPa

Figure 4:54 is an image of a sample with a UTS of 556 MPa, from this it is possible to see areas where the layers are starting to pull away from each other. What is also noticeable is that even though the layers are pulling away from each other in areas there are still the bonds between the layers that has meant that the sample was able to extend by 8.48 mm and have a UTS comparable to cast. The stress vs strain graph for this sample shown in Figure 4:55 has an increased strain to failure when compared to move of the other samples seen, this is likely due to the necking and plastic deformation seen in Figure 4:54.

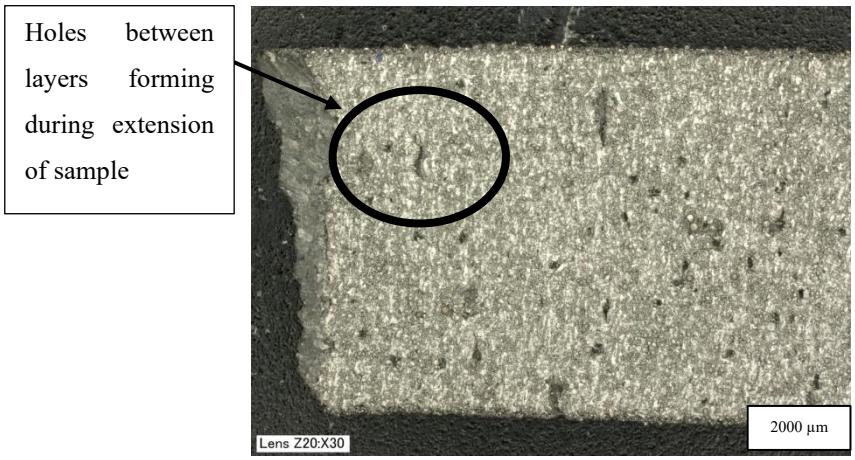

Figure 4:54: 67° rotation and meander laser pattern, 130µs exposure time and 200W laser power, UTS 556 MPa

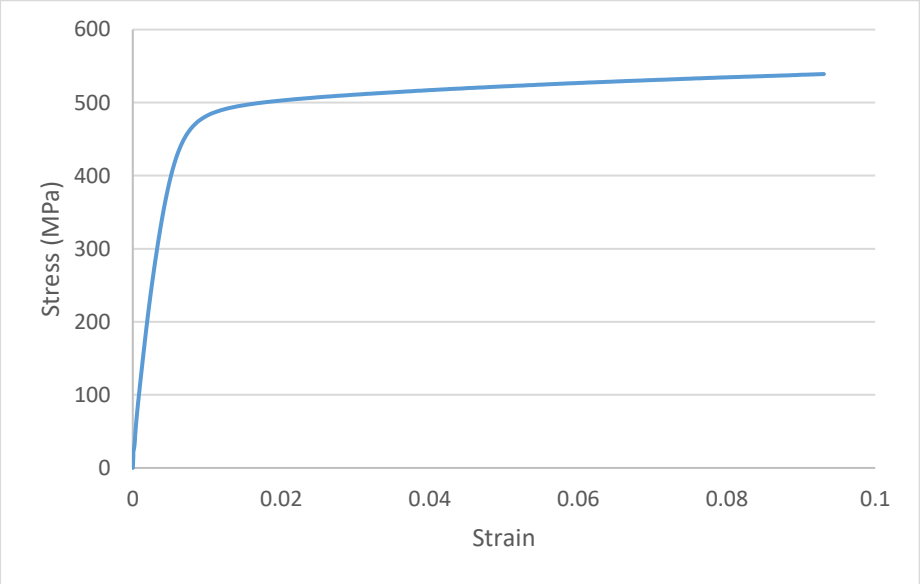

Figure 4:55: Stress vs Strain Graph for 67° rotation and meander laser pattern, 130µs exposure time and 200W laser power, UTS 556 MPa

Figure 4:56 and Figure 4:58 show SEM images of the same phenomenon shown in Figure 4:54. Here it is possible to see how the cracking between layers has occurred. Figure 4:58 looks inside the sample where it is possible to see there is likely to have been a pore with unmelted powder at this location.

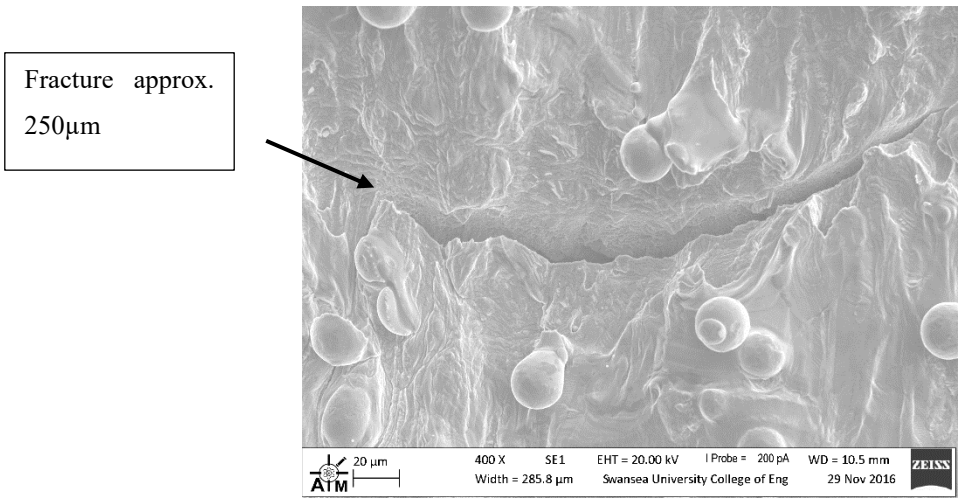

Figure 4:56: 90° rotation and meander laser pattern, 130µs exposure time and 180W laser power, UTS 587 MPa

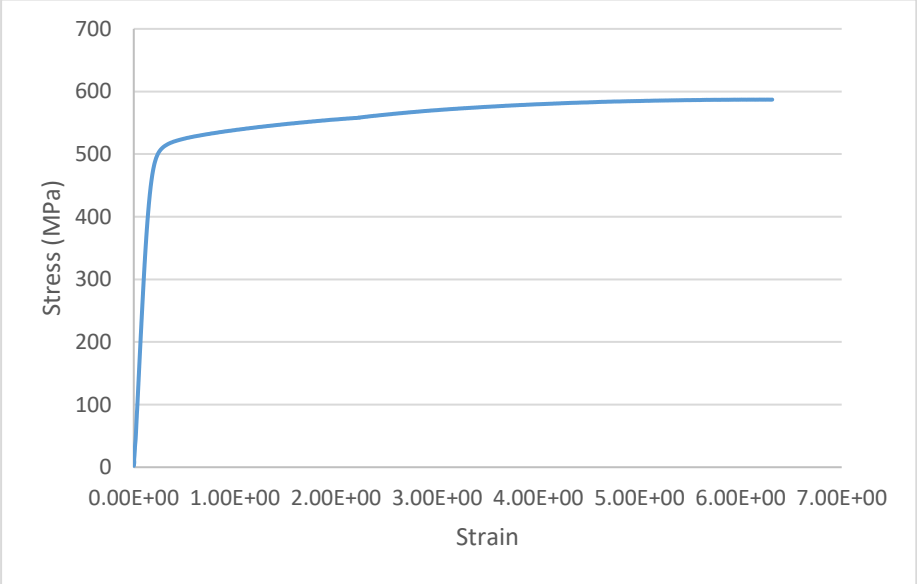

Figure 4:57: Stress vs Strain Graph for 90° rotation and meander laser pattern, 130µs exposure time and 180W laser power, UTS 587 MPa

Figure 4:57 and Figure 4:59 showing the stress strain graphs for Figure 4:56 and Figure 4:58, show increased strain to failure with a smooth curve and both UTS above 500 MPa showing these defects don't always lead to reduced mechanical properties.

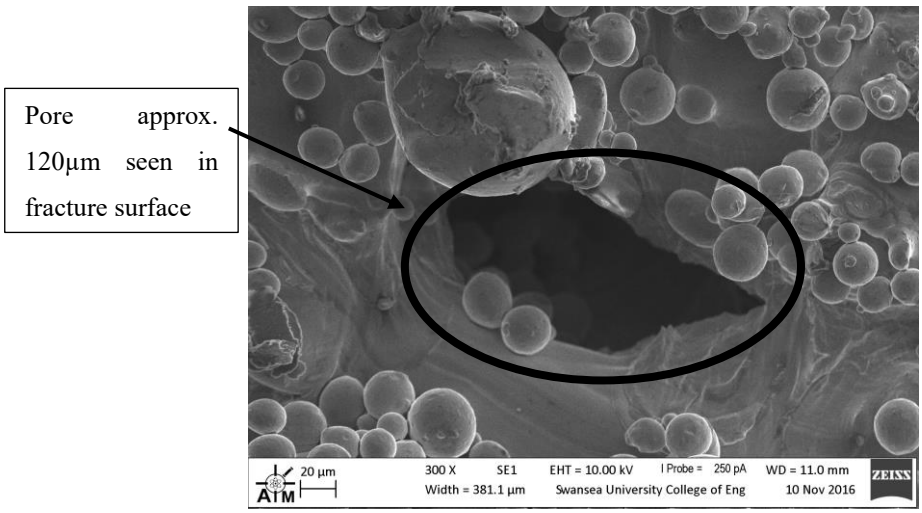

Figure 4:58: 67° rotation and meander laser pattern, 130µs exposure time and 180W laser power, UTS 526 MPa

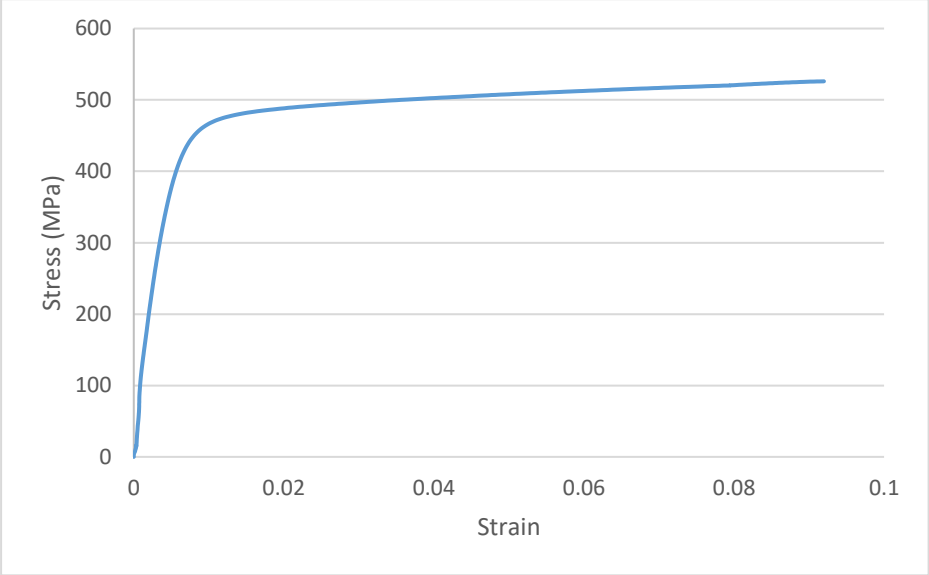

Figure 4:59:Stress vs Stain Graph for 67° rotation and meander laser pattern, 130µs exposure time and 180W laser power, UTS 526 MPa

Aged Powder Tensile Samples

Both an optical microscope and an SEM. have been used to study samples from the aged powder testing. These images have been taken to study the fracture to see how AM parts compare to conventionally manufacture test pieces.

Figure 4:60 and Figure 4:61 show two samples from the same build, the first is as built and the second has had heat treatment 1, 90 minute ramp up, 120 minutes at 450°C and 90 minute ramp down, applied. It is possible to see that for both samples, there has been some necking suggesting they are both ductile. However, for the non-heat-

treated sample, Figure 4:60, the fracture shows significant difference, the fracture has cracked horizontal to the direction of the tensile load possibly across a build layer. Whereas the heat-treated sample shows the sample fracturing in a more traditional manner. This would suggest that the heat treatment helps solidify the layers and make the sample similar to cast material. Similar results are seen in the images that follow, Figure 4:63, Figure 4:64 and Figure 4:65 relating to build 21 and the effect heat treatment has had on the surface. These images again show how the fracture goes across layers in the as built sample, but heat treatment helps to solidify the layers producing conventional fracture methods.

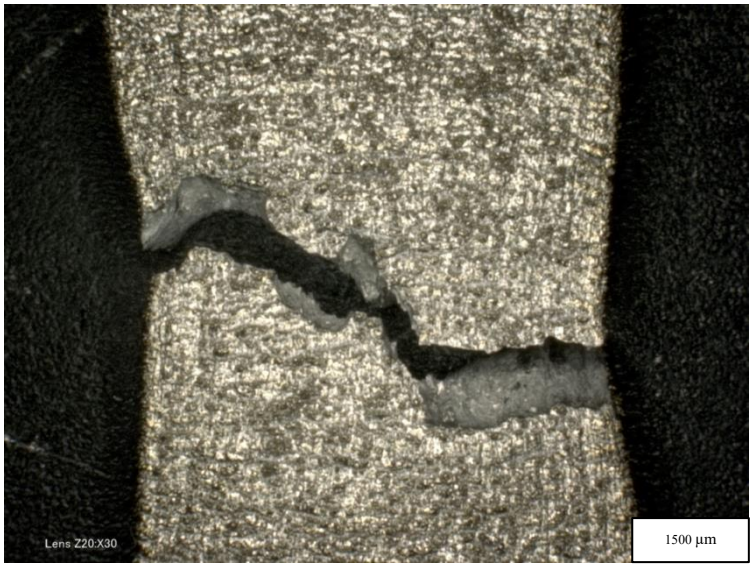

Figure 4:60: Build 17 Vertical, Meander Laser Path, Exposure Time 80µs, Laser Power 200W, As Built, UTS 615 MPa

Figure 4:61: Build 17 Vertical, Meander Laser Path, Exposure Time 80µs, Laser Power 200W, Heat Treatment 1 Applied, UTS 645 MPa

Figure 4:62 shows a Keyence image of a vertical tensile bar that was tested as built. From the image, it is possible to see that the fracture has gone through the layers at a 45° angle and has not travelled along any layer in particular. This sample had a high UTS, 620 MPa, and show slight necking along with a ductile fracture surface.

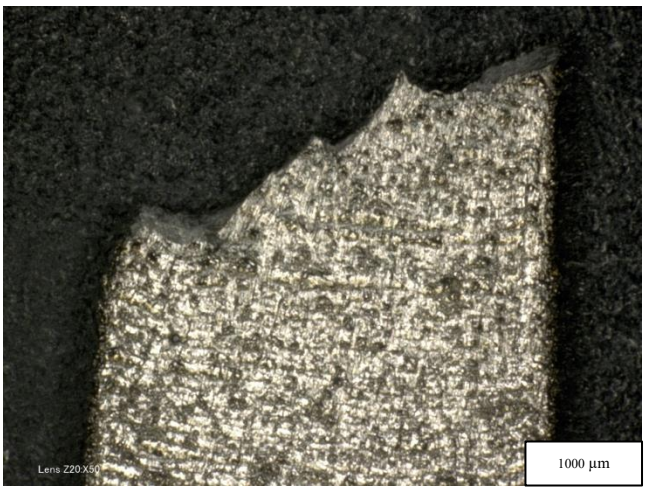

Figure 4:62: Build 21 Vertical, Meander Laser Path, Exposure Time 80µs, Laser Power 200W, As Built, UTS 620 MPa

Figure 4:63 shows another sample from the same build as Figure 4:62 but in this example taken on the SEM it is possible to see that the fracture although still going through the layers it has taken a much shallower angle.

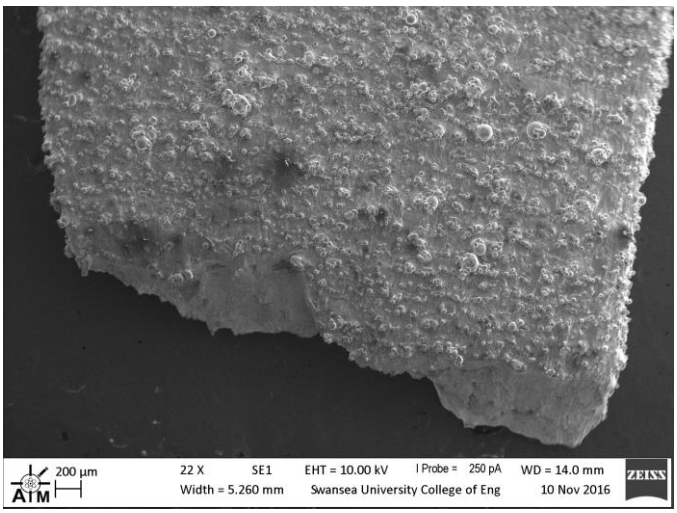

Figure 4:63: Build 21 Vertical, Meander Laser Path, Exposure Time 80µs, Laser Power 200W, As Built, UTS 634 MPa

Figure 4:64 shows a sample from the same build as Figure 4:62 and Figure 4:63 but this sample has had heat treatment 1 applied. From these images, it is possible to see that necking has taken place and, in this case, rather than fracturing at 45° across the sample, this fracture has travelled along one layer perpendicular to the side of the sample.

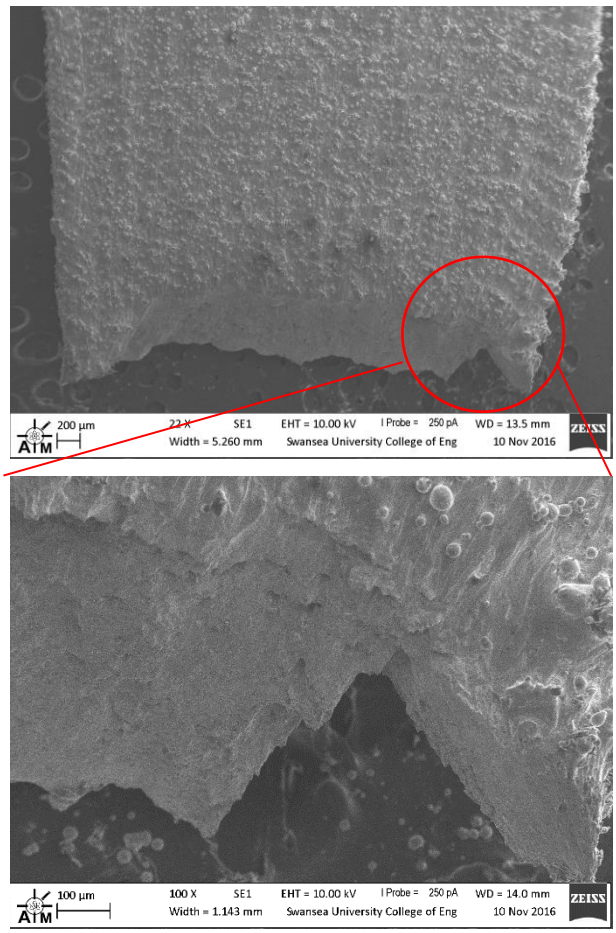

Figure 4:64: Build 21 Vertical, Meander Laser Path, Exposure Time 80µs, Laser Power 200W, Heat Treatment 1 Applied, UTS 582 MPa

Figure 4:65 is another sample from the same build as Figure 4:64 but has undergone heat treatment 2, 360 minutes ramp up, 240 minutes at 1150°C and 260 minute ramp down. In this image, it is possible to see that the fracture is at 45° through the layers in the same position as seen for the heat treatment 1, Figure 4:64, both samples appear to have cracked from a shear plane as expected from conventional samples.

Both Figure 4:64 and Figure 4:65 show small necking of the sample and a reduction in cross section. This shows that there is reasonable plastic deformation and therefore the sample is ductile. The jagged 45° fracture surface could suggest that where the failure occurs on the surface would be transgranular in nature and suggesting the laser path is not having an effect on the failure. It could be suggested that the microstructure is dominating the failure and not the laser path when the sample has been heat treated. The fracture surface of both failures shows no powder particles present. This means that there is no unmelted powder present within the final AM parts, especially after heat treatment. The images show that there are also no pores present on the samples

fracture surface which would have initiated failure if there had been pores and have led to the increased UTS found within these samples.

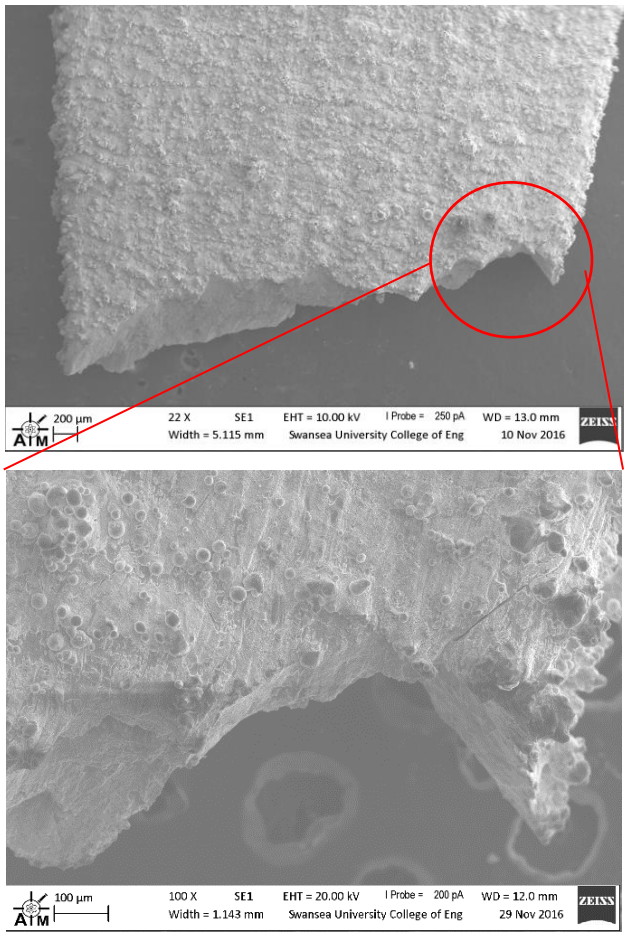

Figure 4:65: Build 21 Vertical, Meander Laser Path, Exposure Time 80µs, Laser Power 200W, Heat Treatment 2 Applied, UTS 592 MPa

4.5.5 Tensile Test Samples BP3

As with the previous build programmes comparisons have been made looking at the tensile test results and these samples have been investigated further to see what changes appear in the composition and microstructure of the samples.

Tensile testing was carried out on the BP3 samples to see how heat treatment effected the UTS, yield strength and fracture surface. This is particularly relevant due to the new AM400 machine used for this programme of builds.

Three different heat treatments, Table 4:6, were used in the third build programme which showed that all samples displayed necking and fractured within the gauge length.

Table 4:6: Heat Treatments for Build Programme 3

	Ramp Up (mins)	Hold (mins, °C)	Ramp Down (mins)
HT1	360	240 @ 1150	360
HT2	90	120 @ 450	90
HT3	420	250 @ 1125	240

Ultimate Tensile Strength (UTS)

The UTS's found in BP3 are shown in Table 5:6. These results are comparable to the results found earlier in this work but also to those found in [45].

The results show that the highest UTS is found for the as built samples, 623MPa, and the lowest is when the sample has been subject to HT1, 571MPa. The results show that applying a heat treatment reduces the UTS but increased the strain to failure if the right treatment is used.

The strain to failure was calculated from the extension and it is possible to see that this is consistent around 50% for all samples. HT1 has reduced the strain to failure to its lowest at 47.3% and HT3 increased it slightly from as built to its highest at 53.1%. This is an improvement on the results from BP1 where there were no results exceeding 50%.

Young's Modulus

The Young's modulus has been calculated for all the tensile bars that were tested in BP3. These results are shown in Table 5:6.

From these results, it has been found that the highest Young's modulus does not occur with the highest UTS or yield stress. This is due to stiffness and strength not being directly linked and therefore unable to predict one from the other. The results show that the Young's modulus is highest for HT1 and HT3 and lowest for HT2, this is the opposite of UTS and yield stress. Showing the changes to the microstructure improving the UTS are not affecting the stiffness.

4.5.6 Fracture Surface

As Built Unaged Powder Tensile Samples

This study has been performed to see if there is a link between the fracture modes seen within the images to the properties of the AM parts. If a link is found it is hoped that

these changes in failure mode will link to changes to certain parameters and this can all be explained by examining the images.

Figure 4:66: 90° rotation and meander laser patter, 130µs exposure time and 200W laser power, UTS 588 MPa (sample 1)

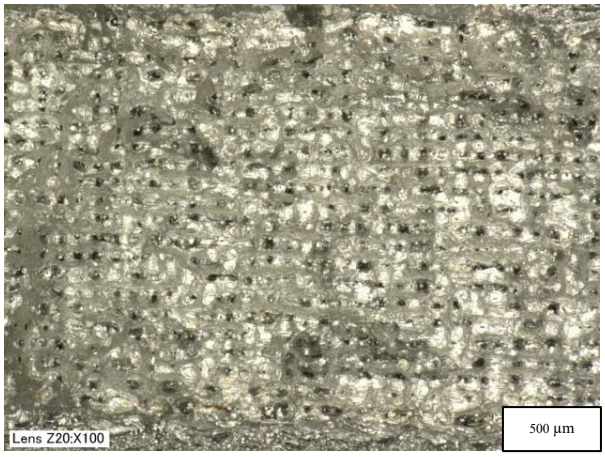

Figure 4:67: 90° rotation and meander laser patter, 105µs exposure time and 160W laser power, UTS 524 MPa (sample 2)

Figure 4:66 shows that for 130µs exposure time and 200W laser power, 90° rotation and meander laser pattern, the powder has been fully melted and there has been sufficient cohesion between the powders particles for the fracture to be similar to what would be expected in cast SS316L. This sample has a UTS comparable to cast at 588 MPa.

Whereas Figure 4:67 shows that for a lower exposure time and laser power it can be seen that the laser path tracks have been formed, however they do not appear to solidify vertically with the direction of the build. It is clear to see from the image that for this reason that the sample has fractured along a build layer.

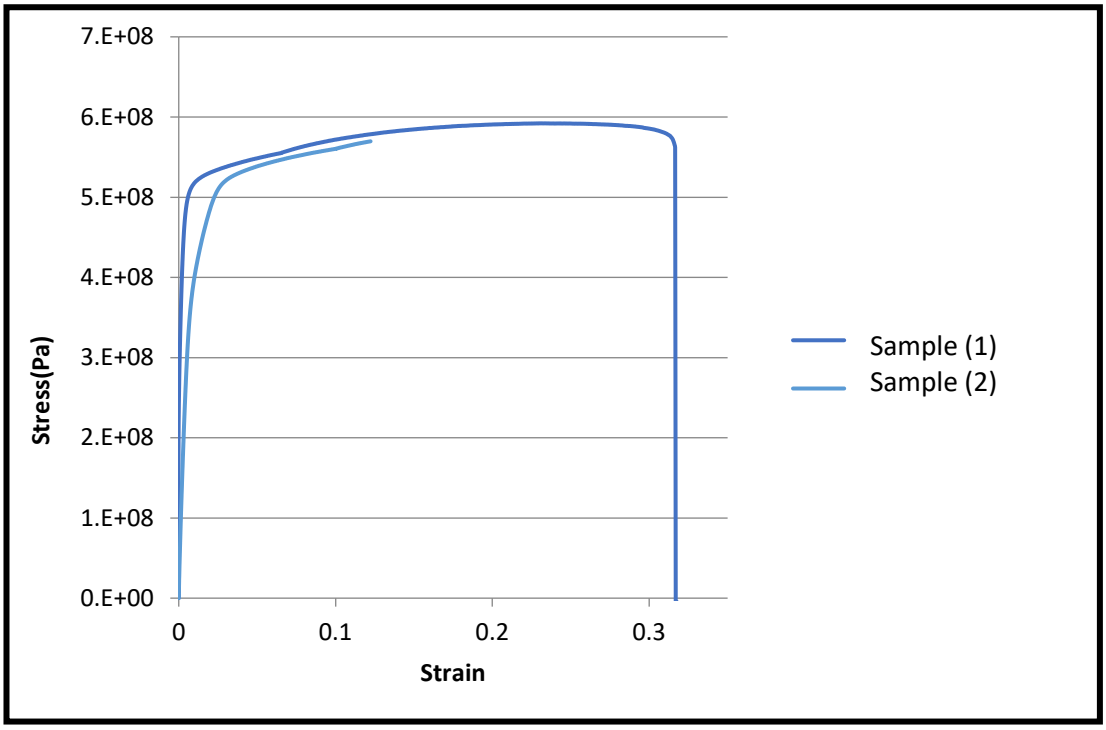

Figure 4:68: Graph of Stress vs Strain for the tensile bars shown in Figure 4:66 and Figure 4:67

When analysis of the stress vs strain graph Figure 4:56, when compared to Figure 4:66 and Figure 4:67 , was carried out it has shown that along with slight changes in the UTS, it is also possible to see a 60% reduction in strain to failure. Sample 2 did not reach the expected strain to failure similar to cast material and fractured earlier reducing its strain to failure. This suggests that the UTS found of these parts is dependent on the strength between the layers, showing the importance of layer cohesion. This is shown by Figure 4:54 showing a smooth fracture surface where it is possible to see the ductile fracture surface whereas Figure 4:67 shows a brittle fracture between two layers.

From Figure 4:68 it is possible to see that although the UTS's of sample 1 and sample 2 are comparable the strain to failure is much lower for sample 2 due to the premature failure.

For the fracture shown in Figure 4:67, the reduced cohesion between layers and the scan pattern is visible. For these parts it is also noted that the fracture has cut through a layer and this sample break would explain why there was much lower UTS than expected for certain samples. This shows that the UTS of tensile specimen in this case is dependent on the bond between the layers.

Along with being able to see layer breaks a number of other samples show pits or voids that appear to have contained no powder and therefore have led to voids within a layer. These pits would be local stress raisers and could potentially become an initiation point for fracture, further study would be needed to clarify if these voids are the source of the cracking and thus failure.

Figure 4:69, shows how a pore or void in the corner of a tensile bar that is likely to have helped to initiate the fracture in this sample. This sample has one of the lower UTS's found at just 272 MPa and a low strain to failure as seen in Figure 4:70.

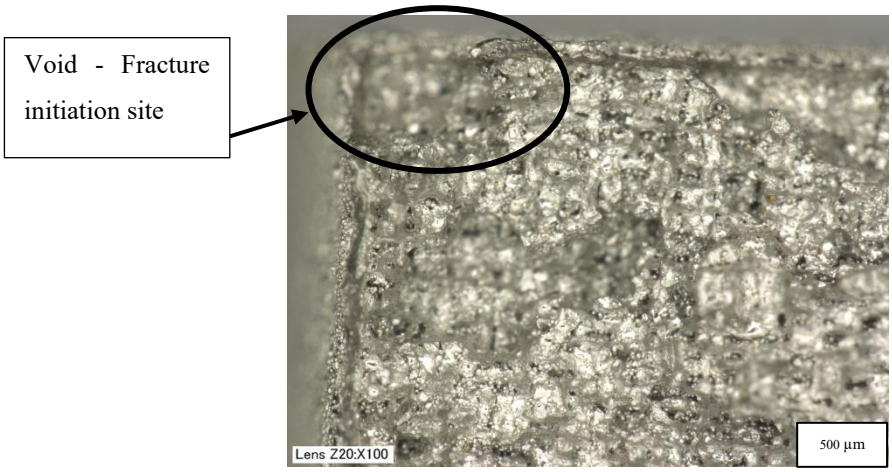

Figure 4:69: 90° rotation and stripe laser pattern, 80µs exposure time and 160W laser power, UTS 272 MPa

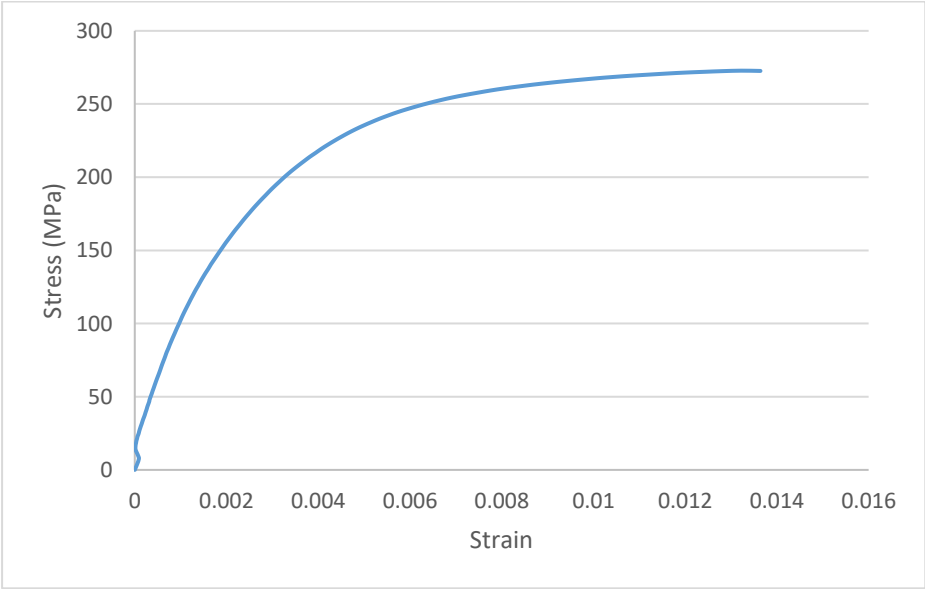

Figure 4:70: Stress vs Strain Graph for 90° rotation and stripe laser pattern, 80µs exposure time and 160W laser power, UTS 272 MPa

From Figure 4:71, shows it is possible to see how there are no defined scan tracks within this layer, this sample has a UTS of 304 MPa and so it is possible to see that there is more cohesion between these layers than for samples with lower UTS's but still this sample has fractured quickly and with a reduced UTS especially in comparison to the first sample studied which has a UTS of 588 MPa where the cohesion between the bonds can be clearly seen due to the slipping on the fracture surface, this is reflected in Figure 4:73.

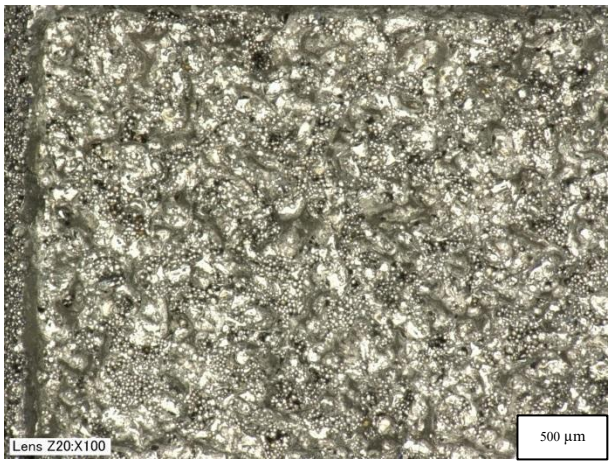

Figure 4:71: 67° rotation and meander laser pattern, 80µs exposure time and 160W laser power, UTS 304 MPa

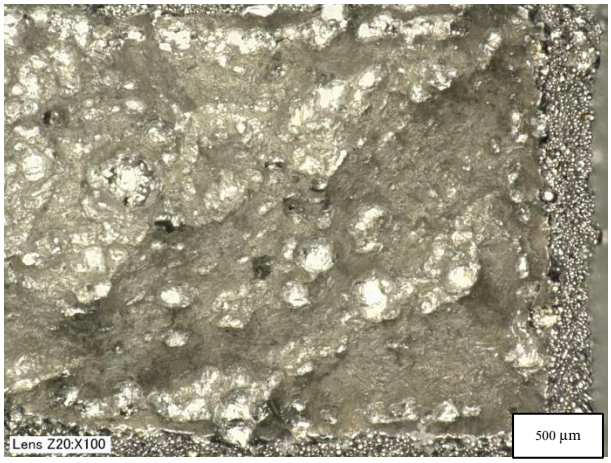

Figure 4:72: 67° rotation and meander laser pattern, 80µs exposure time and 160W laser power, UTS 304 MPa

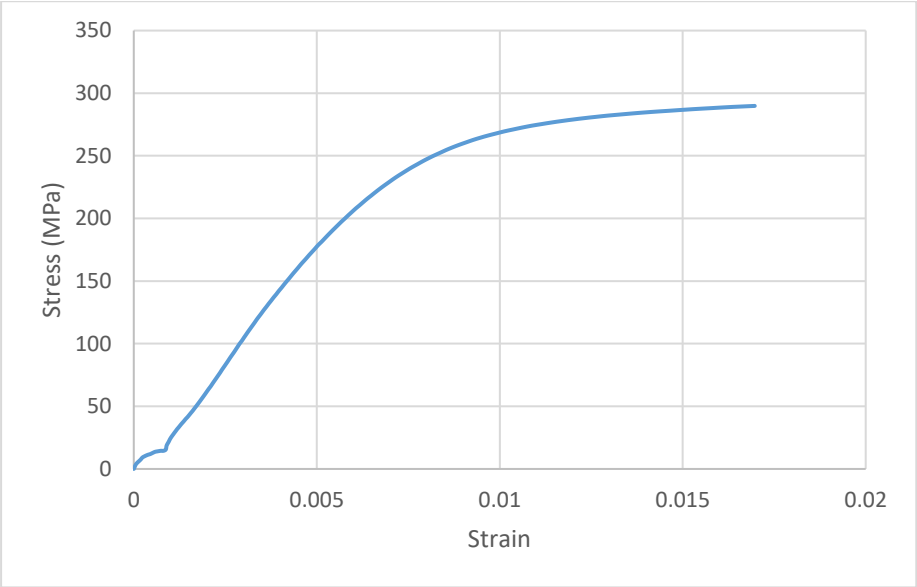

Figure 4:73: Stress vs Strain Graph for 67° rotation and meander laser pattern, 80µs exposure time and 160W laser power

When comparing the UTS found in the 67° rotation and meander laser pattern, 130µs exposure time and 200W laser power sample, to that of the 90° rotation and meander laser pattern, 130µs exposure time and 200W laser power sample, which has a UTS of 588 MPa, it is possible to see that both fracture surfaces are similar looking.

Figure 4:74 and Figure 4:75 show samples that have had no processing applied to them after the build process. From these images, it is possible to see that there has been cohesion between the particles and the tensile fracture is ductile. Figure 4:74 shows what appears to be pores within the samples fracture surface.

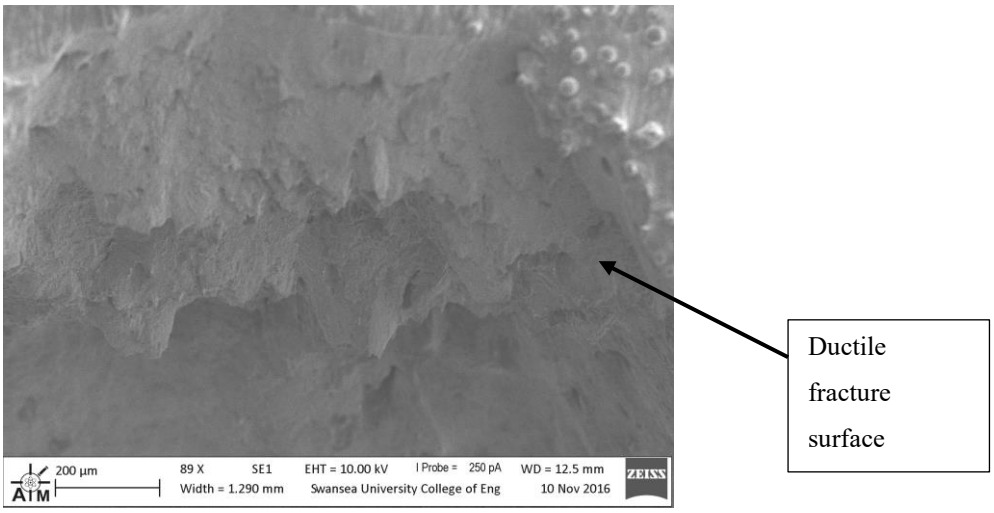

Figure 4:74: 90° rotation and meander laser pattern, 130µs exposure time and 180W laser power, UTS 511 MPa (sample 1)

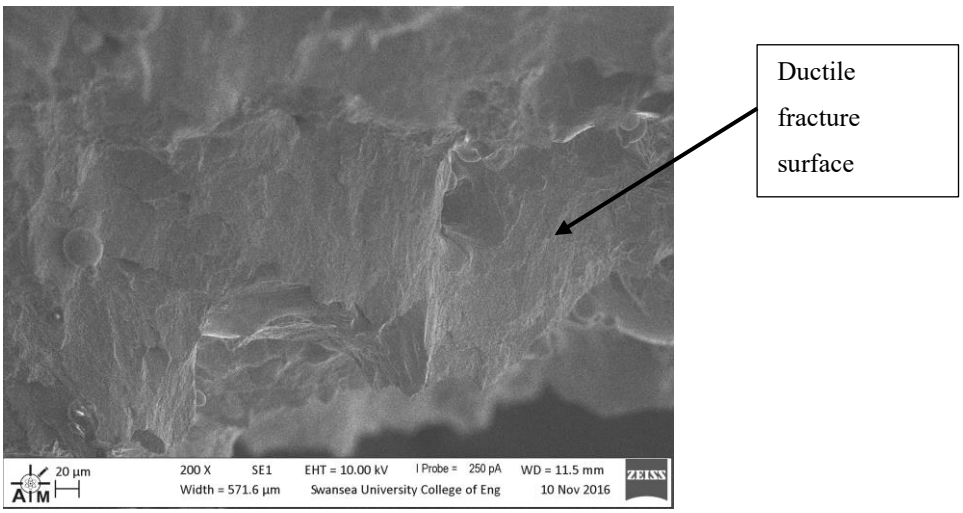

Figure 4:75: 67° rotation and meander laser pattern, 130µs exposure time and 180W laser power, UTS 526 MPa (sample 2)

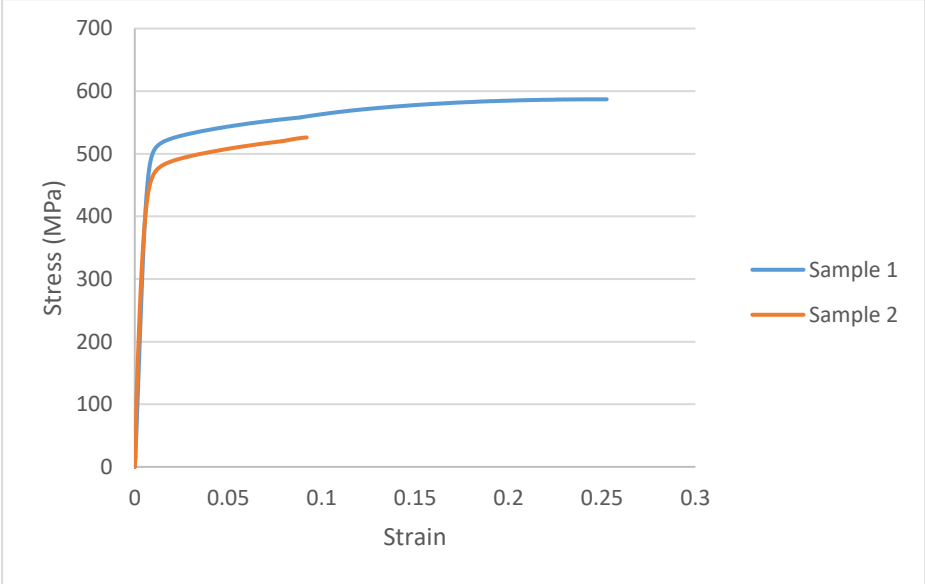

Figure 4:76: Stress vs Strain Graph for Sample 1 and 2

Figure 4:76 shows the stress strain graphs for the two samples shown in Figure 4:74 and Figure 4:75. From the images it is possible to see that both samples have ductile fracture surface, but the graph shows the stain to failure was much lower for Figure 4:75 showing this sample had much lower plasticity. This could be due to inclusions, defects that cause premature failure or the change in layer rotation causing changes to the microstructure that affected the failure [223].

Aged Powder Tensile Samples

Samples from the aged powder builds were imaged under both the optical microscope and SEM to look at the samples fracture surface. Figure 4:77 shows the fracture

surface of an as built sample. These images show the initiation corner and the fracture travelling across two layers along with the unmelted particles within the fracture layer and pores surrounding these pores.

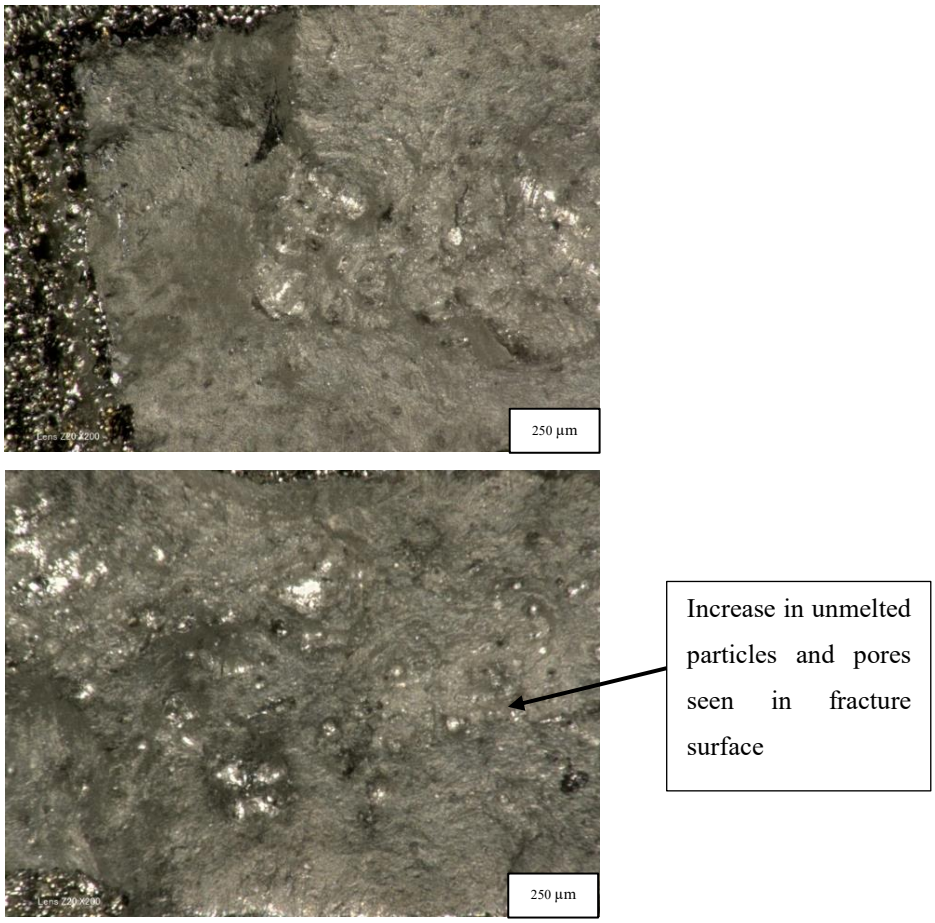

Figure 4:77: Tensile Fracture Surface Build 17 Vertical, Meander Laser Path, Exposure Time 80µs, Laser Power 200W, As Built

Round Tensile Samples

A couple of round tensile bars were tested but it was found that their failure point was much more scattered and not consistent with failures through the centre of the gauge length. It was thought this could be due to the machining of the samples and so these results have not been included. The samples were microscopically studied to see if there were any obvious defects or causes of the failures. Figures Figure 4:78 and Figure 4:79, show the fracture surface of a round tensile bar. From these images, it is possible to see how the fracture started in the bottom half of the image and has shifted across three crack planes.

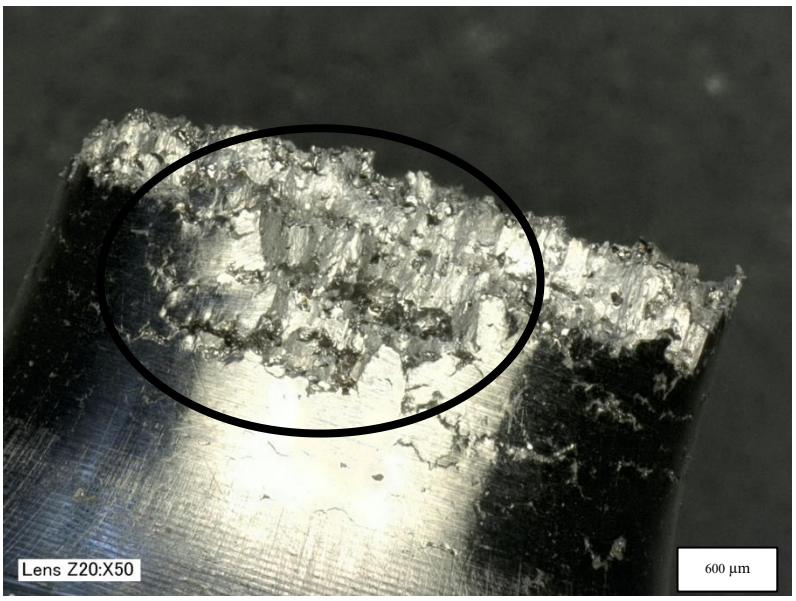

Figure 4:78: Build 25 Vertical, Meander Laser Path, Exposure Time 80µs, Laser Power 200W, Machined from Round Bars

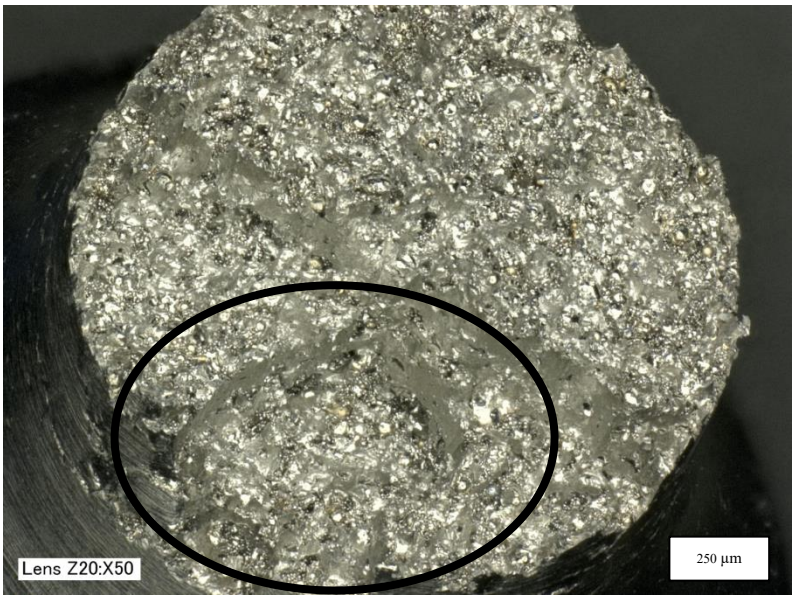

Figure 4:79: Build 25 Vertical, Meander Laser Path, Exposure Time 80µs, Laser Power 200W, Machined from Round Bars

This fracture surface was further investigated in the SEM. Figure 4:80 and Figure 4:81 show the crack initiation site in more detail. From these images, it is possible to see that the fracture area is very porous and there is a high concentration of unmelted powder particles in this area.

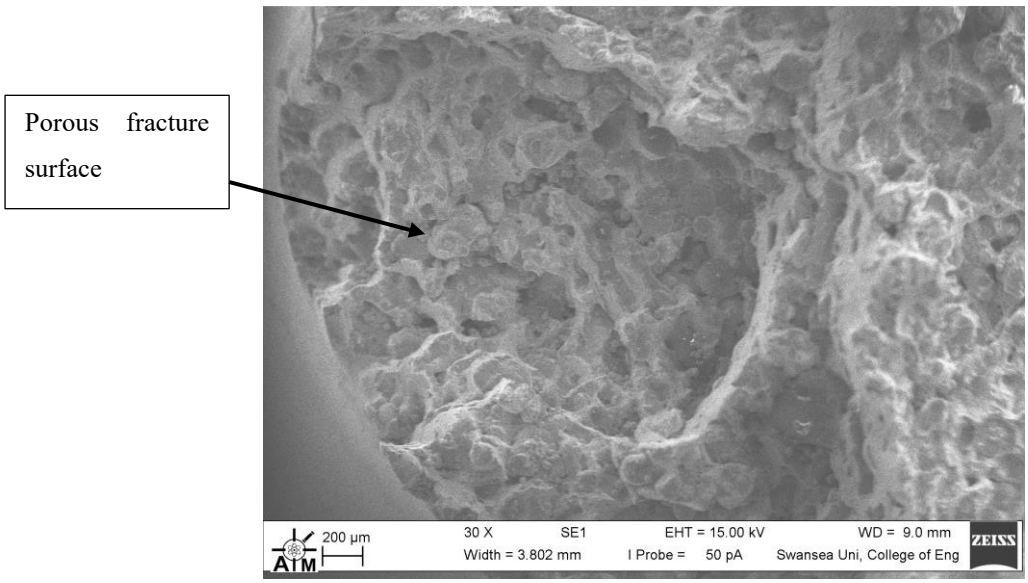

Figure 4:80: Build 25 Vertical, Meander Laser Path, Exposure Time 80µs, Laser Power 200W, Machined from Round Bars

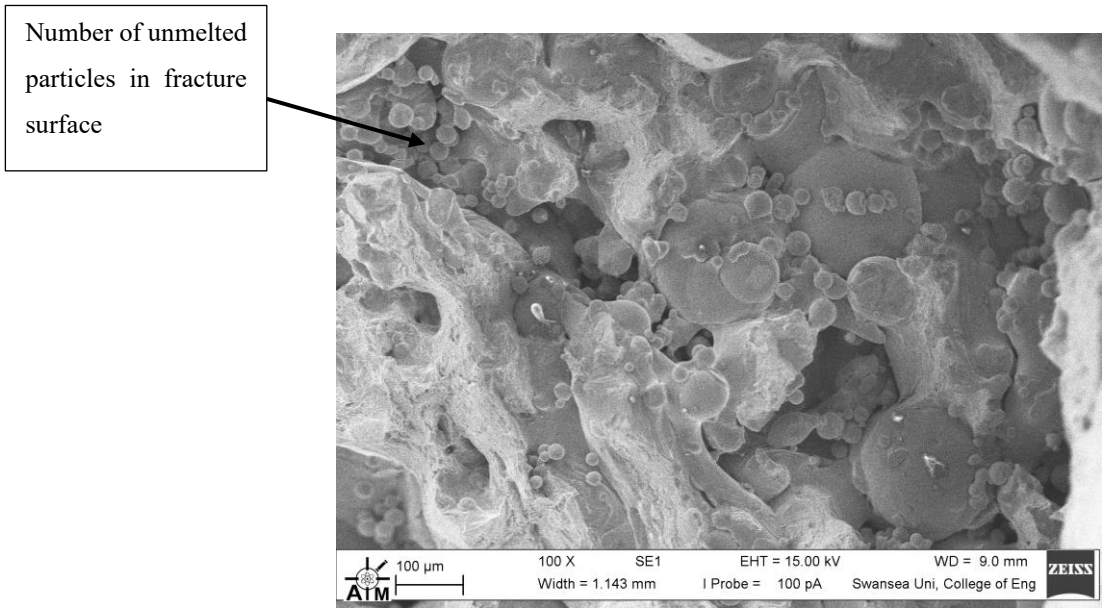

Figure 4:81: Build 25 Vertical, Meander Laser Path, Exposure Time 80µs, Laser Power 200W, Machined from Round Bars

Figure 4:81 and Figure 4:82 shows how within these individual samples there are areas that are melted completely to form cohesive joins between the powder particles and there are areas that are made up of a majority of unmetled particles. It is also possible to see in this image an area where it appears there was never any melted powder. This is likely due to trapped gas during the build process. The unmelted powder present within this sample shows that there has not been enough input energy to melt the

powder but also that further heat treatment is necessary to ensure all powder within final parts is melted to solidify the part and create a stronger more homogeneous part.

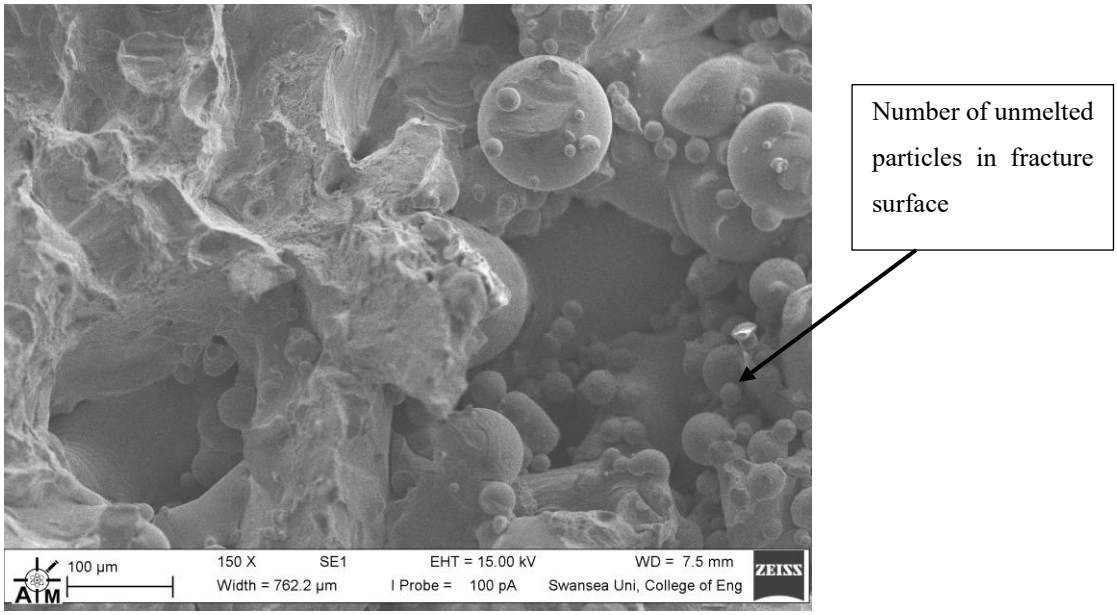

Figure 4:82: Build 25 Vertical, Meander Laser Path, Exposure Time 80µs, Laser Power 200W, Machined from Round Bars

Figure 4:83 shows a close up of the surface of a solidified melt pool; from this it is possible to see powder sticking to the side of the solidified melt pool, which was not drawn into the melt pool while it was molten. It is also possible to see what appears to be a fracture surface where two a joining solidified melt pools have been separated.

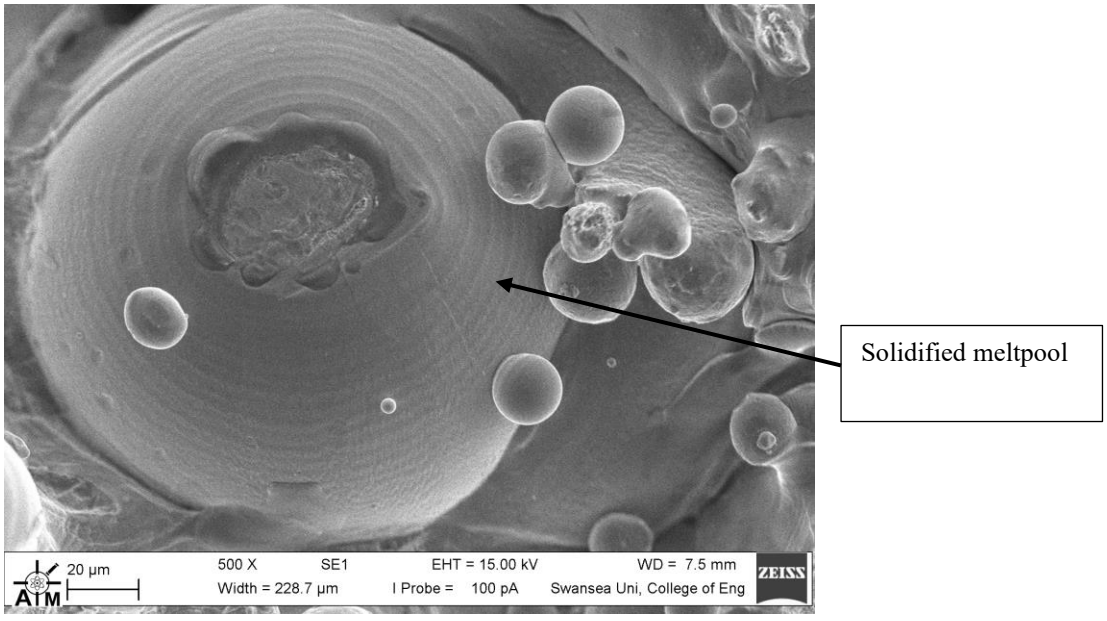

Figure 4:83: Build 25 Vertical, Meander Laser Path, Exposure Time 80µs, Laser Power 200W, Machined from Round Bars

Heat Treated Tensile Samples

The samples tested during BP3 were manufactured during the same build on an AM400. When looking at samples produced on the newer AM400 Table 5:6 it is possible to see how porosity within the parts has reduced, to be as low as 0.5% compared to the 1-2% found when using the AM250. It is clear to see that the porosity now forms a border of pores near the surface of the sample.

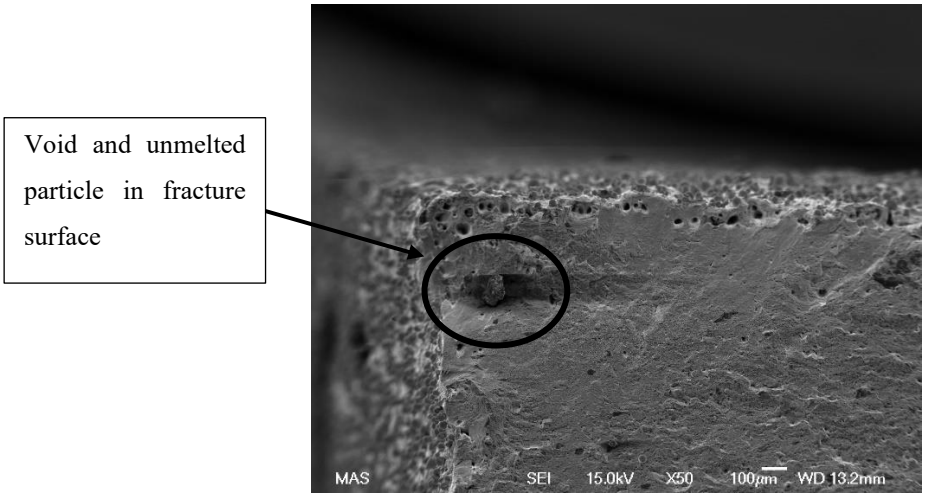

Figure 4:84 B1 fracture surface

Figure 4:85 and Figure 4:86 show the fracture surface of a tensile sample that has undergone HT1. Here it is clear to see how the fracture initiated in the bottom right-hand corner most likely at a defect and spread quickly across the majority of the bar leading to the decreased UTS. The fracture corner shows a brittle fracture. Whereas Figure 4:88 shows an as built sample, with a mostly smooth fracture surface where it is possible to see how the fractures have broken through a number of layers. What can be seen from the graphs, Figure 4:87 and Figure 4:89, is that although these have different fracture surfaces the graphs look similar with no reduction in UTS or strain to failure seen.

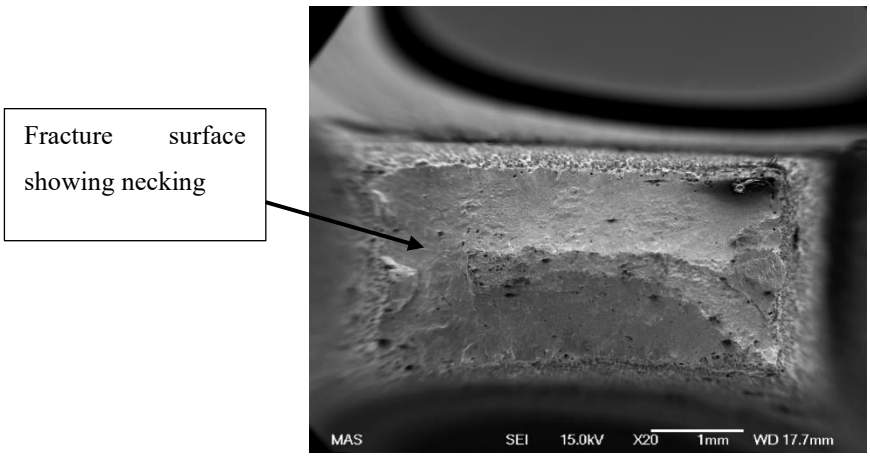

Figure 4:85 B10 HT1 x20 Fracture Surface

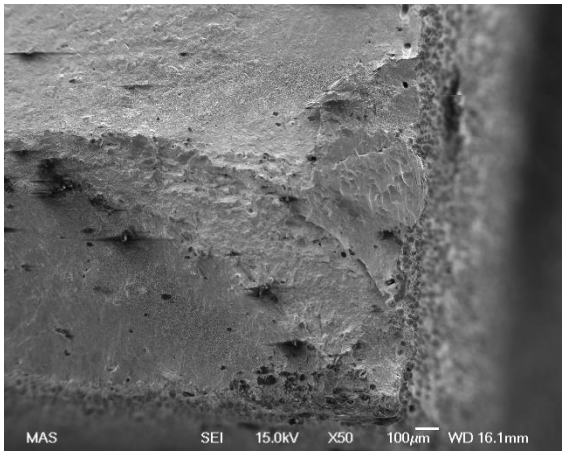

Figure 4:86 B10 HT1 x50 Fracture Surface, UTS 593 MPa

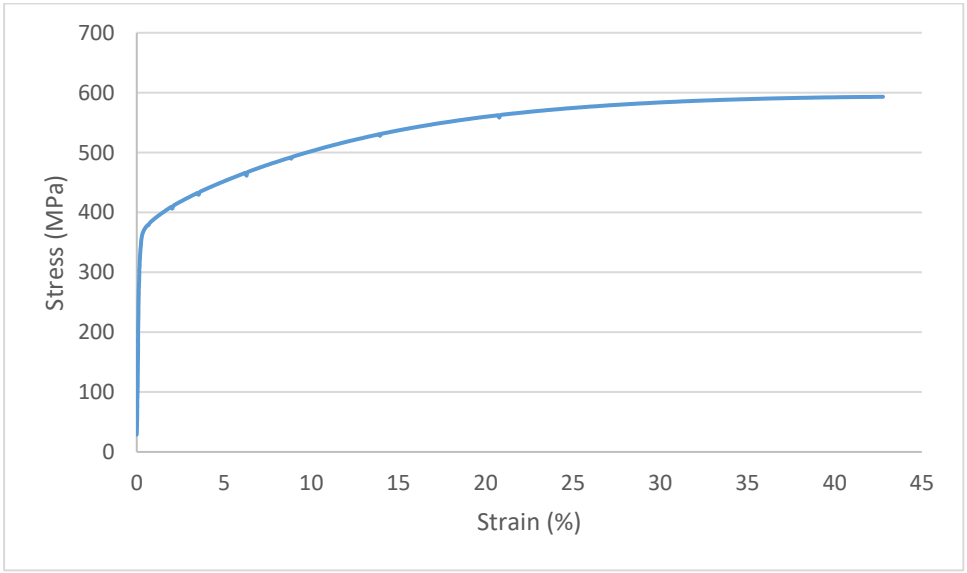

Figure 4:87: B10 HT1 Stress vs Strain Graph, UTS 593 MPa

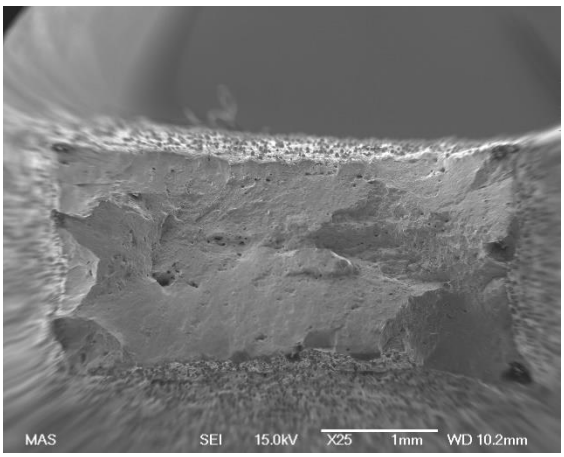

Figure 4:88 B3 As Built x25 Fracture Surface, UTS 615 MPa

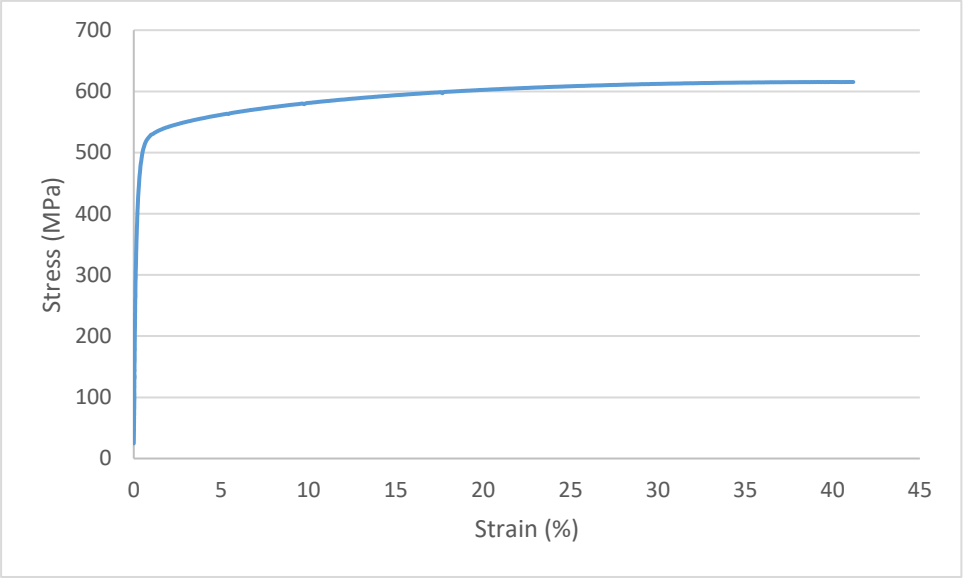

Figure 4:89: B3 As Built Stress vs Strain Graph, UTS 615 MPa

The lowest UTS was seen in HT2 where the fracture surface shows an increase in defects and a very brittle finish, Figure 4:90. There was 10MPa difference in UTS to Figure 4:92 which shows a similar fracture surface with brittle failures and a number of surface inclusions which could be initiation points. Again the stress strain graphs for these samples are similar, Figure 4:91 and Figure 4:93.

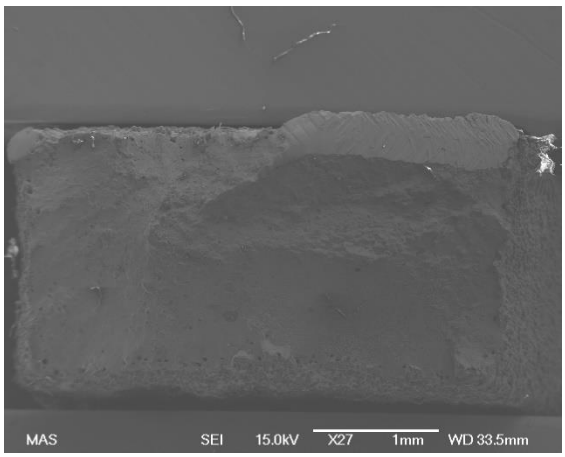

Figure 4:90 B8 HT1 x27 Fracture Surface, UTS 576 MPa

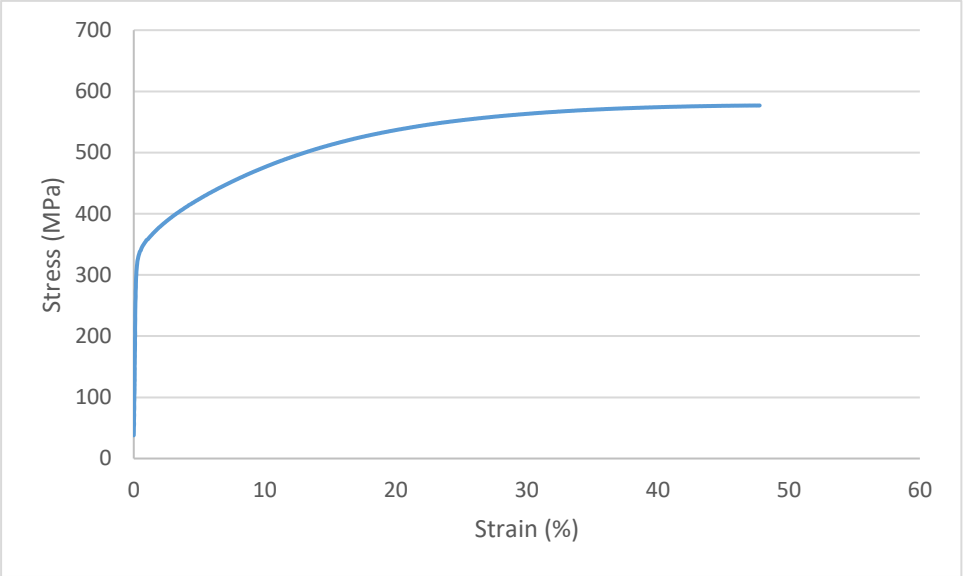

Figure 4:91: B8 HT1 Stress vs Strain Graph, UTS 576 MPa

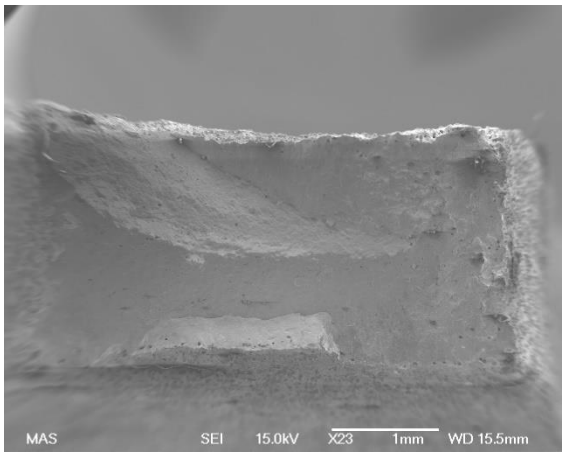

Figure 4:92 B16 HT3 x23 Fracture Surface, UTS 588 MPa

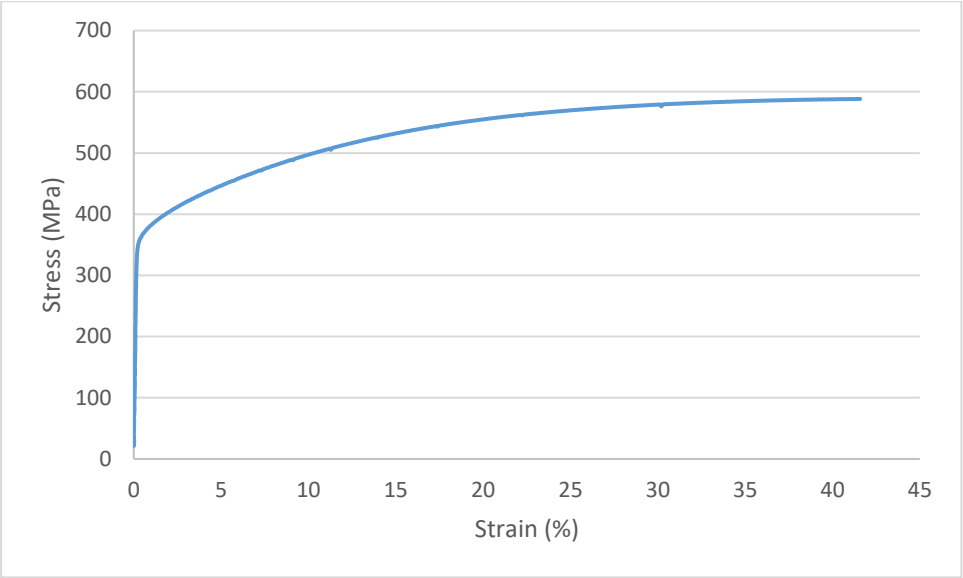

Figure 4:93: B16 HT3 Stress vs Strain Graph, UTS 588 MPa

Figure 4:94 the as built sample also shows an unmelted particle sitting near the surface likely an initiation site for the failure.

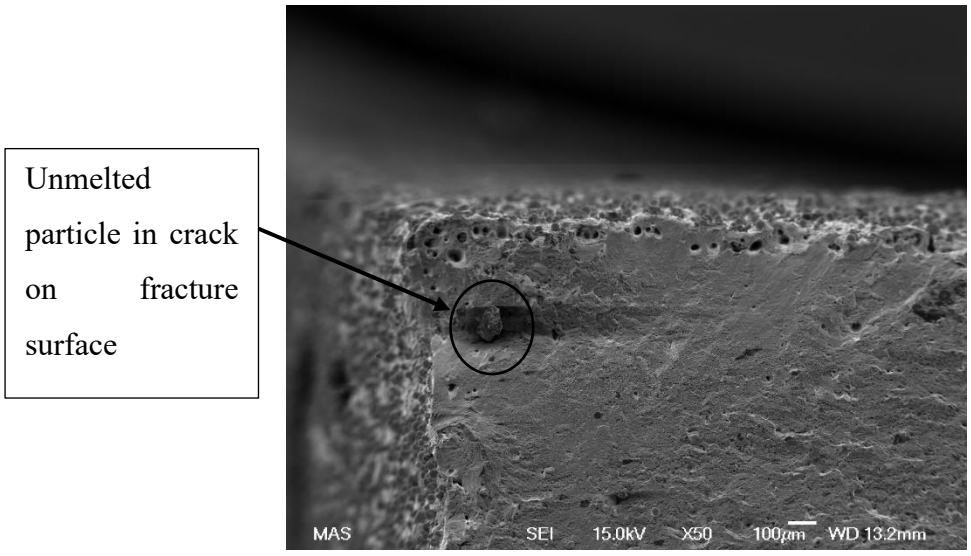

Figure 4:94: BP3 As Built Fracture Surface

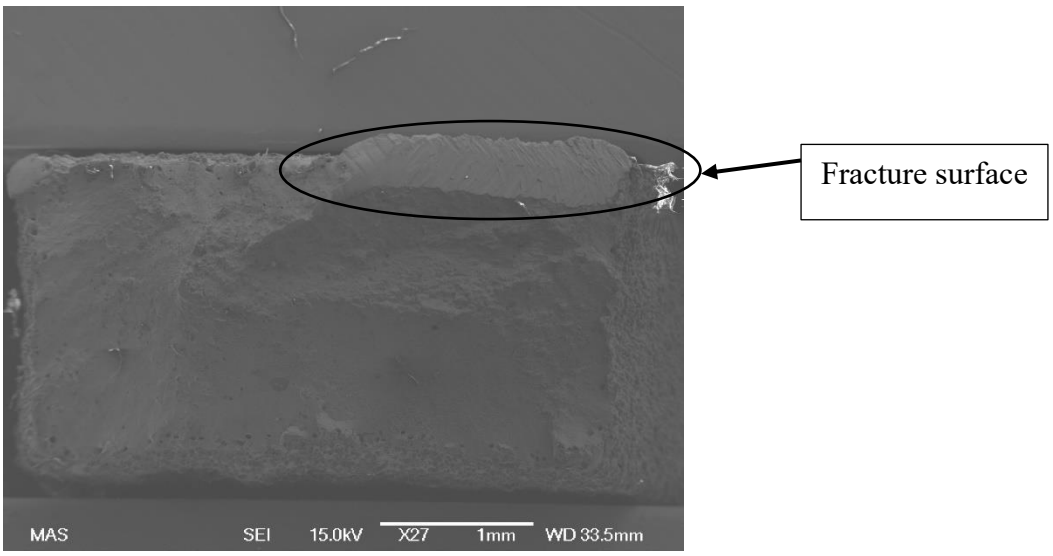

Figure 4:95: BP3 HT1 Fracture Surface x27

When looking at Figure 4:95 and Figure 4:98, it is clear to see where the failure has travelled across the fracture surface. Figure 4:95, shows what appears to be a brittle fracture in the top right corner but closer examination of the surface, Figure 4:96, shows a ductile failure as expected.

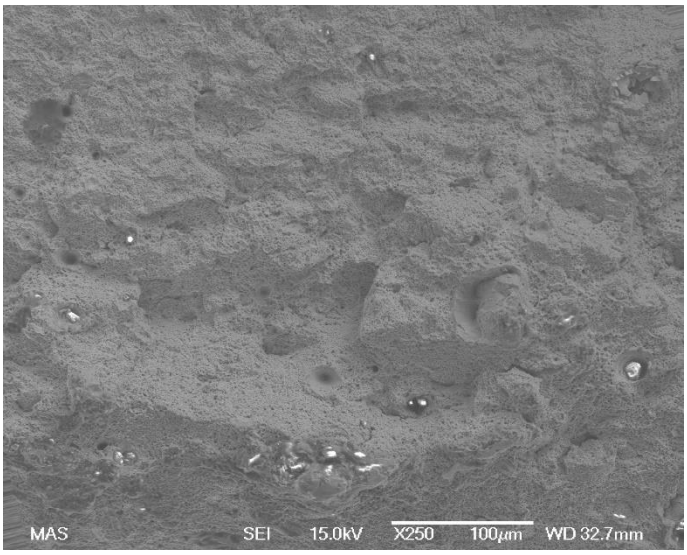

Figure 4:96: BP3 HT1 Fracture Surface x250

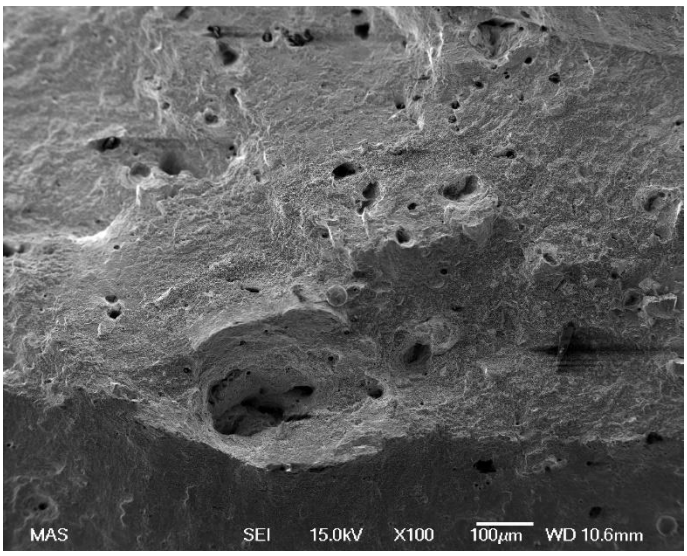

Figure 4:97: BP3 HT2 Fracture Surface

Figure 4:97 shows a standard ductile fracture surface with a rough surface travelling between the pores and voids commonly seen within AM parts.

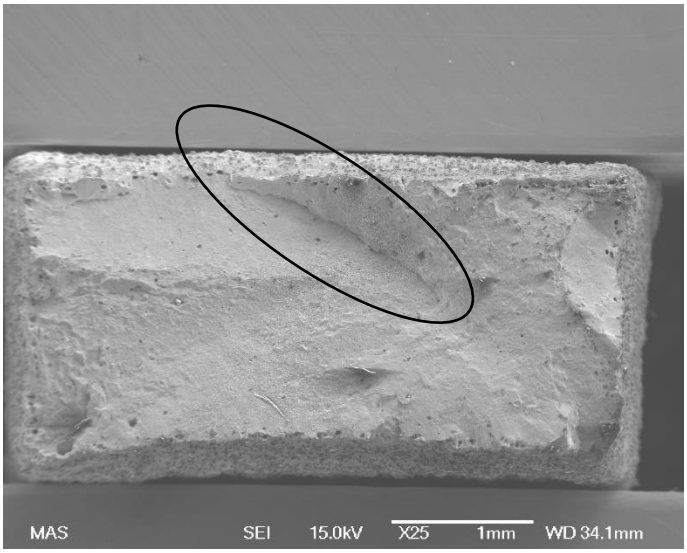

Figure 4:98: BP3 HT3 Fracture Surface

HIP Tensile Samples

Although not all of the data has been evaluated for the HIP samples looking at the fracture surface it is possible to see the effect HIPping has on AM samples. Figure 4:99 shows the surface of a HIPped sample, it can be seen that there are clear fracture paths through the material and no pores. Figure 4:100 is an as built sample with numerous pores and no fissures.

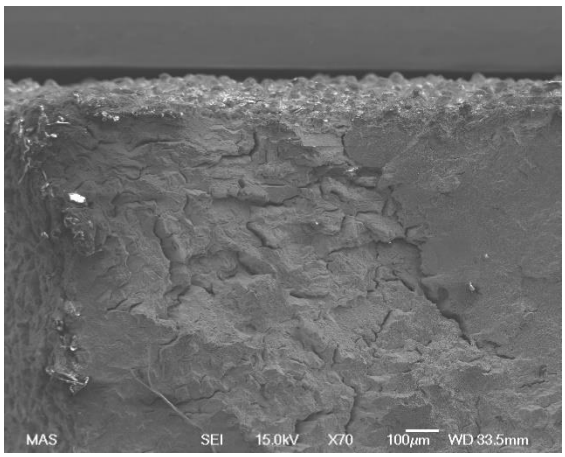

Figure 4:99 B28 HIPped x70 Fracture Surface

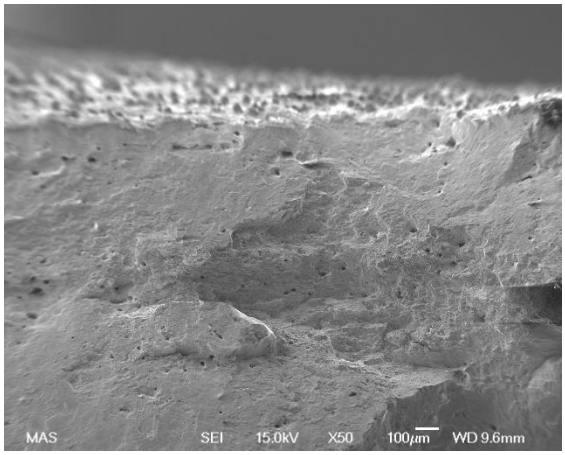

Figure 4:100 B3 As Built x50 Fracture Surface. UTS 615 MPa

4.5.7 Microstructures

The microstructure was studied after the mounted cubes had been etched. It was found that approximately 2 minutes was the optimum time for the etching to give the best results, shown in the images below. The final etch used was the V2A etchant. This was used as it gave the optimum results showing both the grain structure and the laser path.

Across a Layer

The microstructures that are shown in Figure 4:101 and Figure 4:102 show how the microstructure is built up across the layer within the cubes. These images are of the cross section and show how the microstructure grows within the layer, as well as being able to study the grain structure and see how this structure is affected by the laser tracks.

The cooling rate will vary across the melt pool due to the heating coming from surrounding powder, the time before the next laser path and the position within the layer. These changes in cooling rate will affect the microstructure seen within each melt pool as can be seen in the microstructure images within this work.

Figure 4:101(b) show what are possibly unmelted particles sitting on the surface of the scan track seen in this microstructure.

Figure 4:101 and Figure 4:102 show the microstructure across a layer of 90° rotation meander and stripe cubes. It is possible to see from these images how increasing the laser power leads to more defined melt pools. The images also show how increasing the input energy has reduce the number and size of sections with no microstructure. The increase in laser power and input energy effects the microstructure and this in turn has improved the UTS and density of the parts produced.

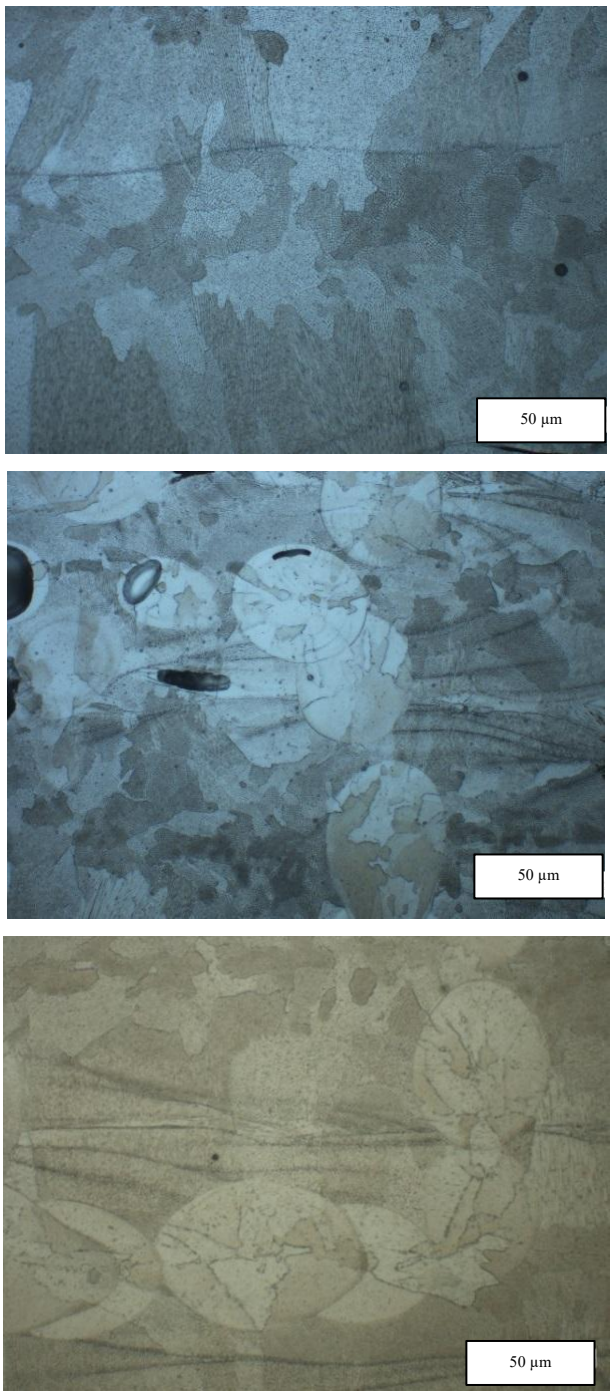

Figure 4:101: Microstructures of the 90° Meander Cubes, within a layer (a) 80µs exposure time and 160W laser power, (b) 105µs exposure time and 180W laser power, (c) 130µs exposure time and 200W laser power

Figure 4:102: Microstructures of the 90° Stripe Cubes, within a layer (a) 80µs exposure time and 160W laser power, (b) 105µs exposure time and 180W laser power, (c) 130µs exposure time and 200W laser power

Figure 4:101 and Figure 4:102 show the grains seen within a layer if you compare the grain size to the parameters used it is possible to see that as the laser power and exposure time increase the grain size increases. Apart from Figure 4:101(a) where the largest grain sizes are seen, 80µm, in a columnar shape rather than the randomly

distributed from melt pools as seen in the other images. The rest of the images show grain sizes varying between 30 and 50µm. Both of the 130µs exposure time and 200W laser power samples show larger grain sizes, approximately 50µm, than the 105µs exposure time and 180W laser power samples at approximately 30µm.

Figure 4:103 clearly shows the laser tracks. This is the centre of a 130µs exposure time, 200W laser power meander cube cut horizontally; the laser pattern within this cube is seen to be moving across the sample.

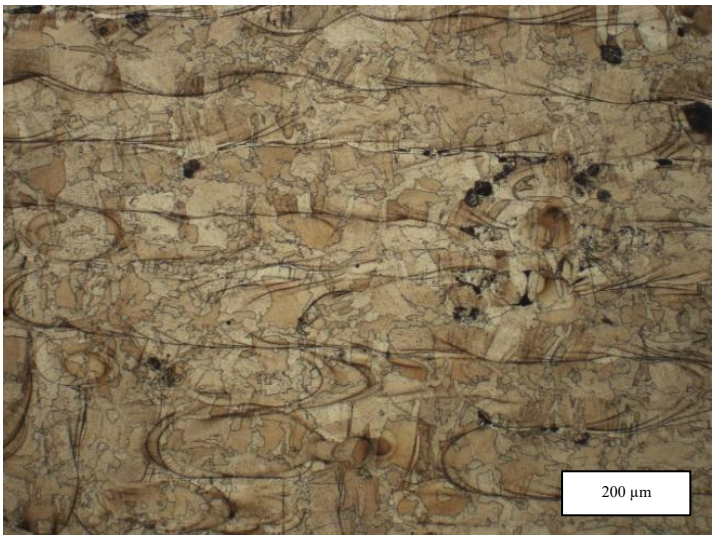

Figure 4:103: Scan Pattern within a 90° Meander Pattern Cube, 130µs exposure time and 200W laser power

Through the Layers

Along with cutting the samples and etching them so that the microstructure within the layer could be studied, another cube was cut in half from top to bottom to study how the microstructure grew through the layers as the part was built up.

Figure 4:104 and Figure 4:105 show how the microstructure has been built up through the layers. These images show that there are grains that grow from the bottom of the image up through the layers to the top of the image suggesting that when the next layer is built the previous layer is still solidifying and the grains can continue growing through the layers. As well it is noted that these grains do change direction but still maintain a growth pattern up the part as it is built. The grains are seen to grow up the layers in all of the images but are clearest in Figure 4:104(c) where on the right side of the image there is a grain that grows up the layers.

Figure 4:104 and Figure 4:105 show that grains growing through the layers can grow in size to a length longer than the image height which means these grains can exceed

500µm, much larger than those seen growing across a layer from Figure 4:101 and Figure 4:102. As mentioned previously these grains are also columnar unlike those grown in a layer which a circular. This columnar growth is due to the heating and subsequent reheating of the same area as the layers build, which allows the grain to continue growing rather than solidifying and no longer propagating.

Columnar grain growth is generated by the strong thermal gradients built up during the process and provides the benefit of high strength in the build direction. This though generates anisotropy within the component where it is weaker and more ductile perpendicular to the growth.

Cutting the samples in any direction is not a true representation of what is within the part as this is a 2D cross section of the samples rather than a true view of how the microstructure and grains run through the entire part.

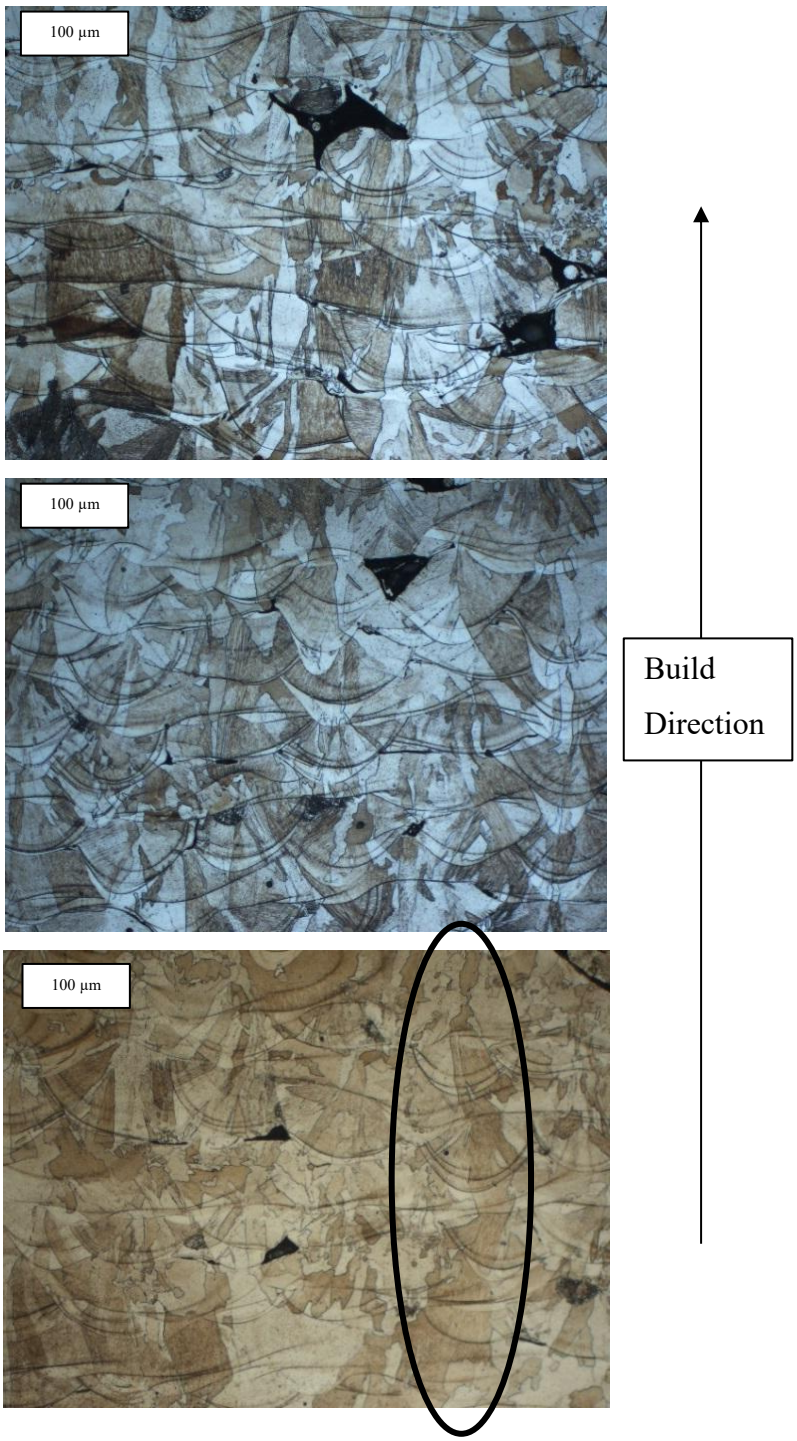

Figure 4:104: Microstructures of the 90° Meander Cubes, through the layers (a) 80µs exposure time and 160W laser power, (b) 105µs exposure time and 180W laser power, (c) 130µs exposure time and 200W laser power

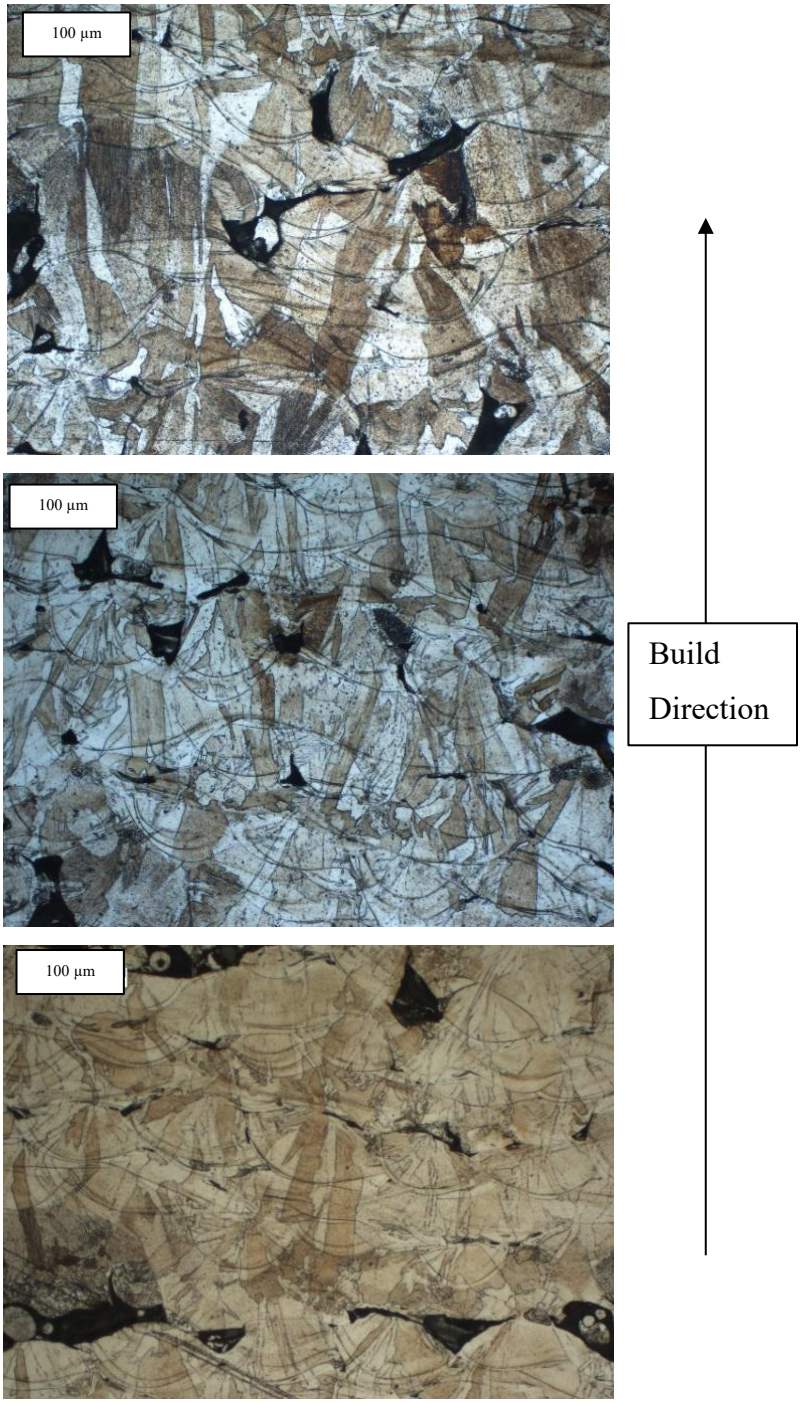

Figure 4:105: Microstructure of the 90° Stripe Cubes, through the layers (a) 80µs exposure time and 160W laser power, (b) 105µs exposure time and 180W laser power, (c) 130µs exposure time and 200W laser power

Comparison

Figure 4:106 shows the difference between the two laser patterns. The first image, Figure 4:106(a), shows the meander laser pattern and how the scan tracks loop, as indicated by the arrow, around at the top of the path and returns. Whereas in the second

image, Figure 4:106(b), which shows the stripe laser pattern, where there is no loop back down at the end of a path and this is because in this laser pattern the laser is off for the return to the start axis and builds the new path next to the previously melted path. With the laser being continuously on for meander this leads to long uninterrupted scan vectors increasing residual stress [216] and heat accumulation zones but more uniform coverage of the layer. Whereas stripe has shorter scan vectors and therefore produce better thermal management to improve the microstructure homogeneity and reduce distortion. But the start stop nature of stripe leads to increased defects around these points [217]. Therefore, careful consideration is needed as to which scan strategy is used thinking of the part to be built, the time and if increased density or reduced residual stress is most important.

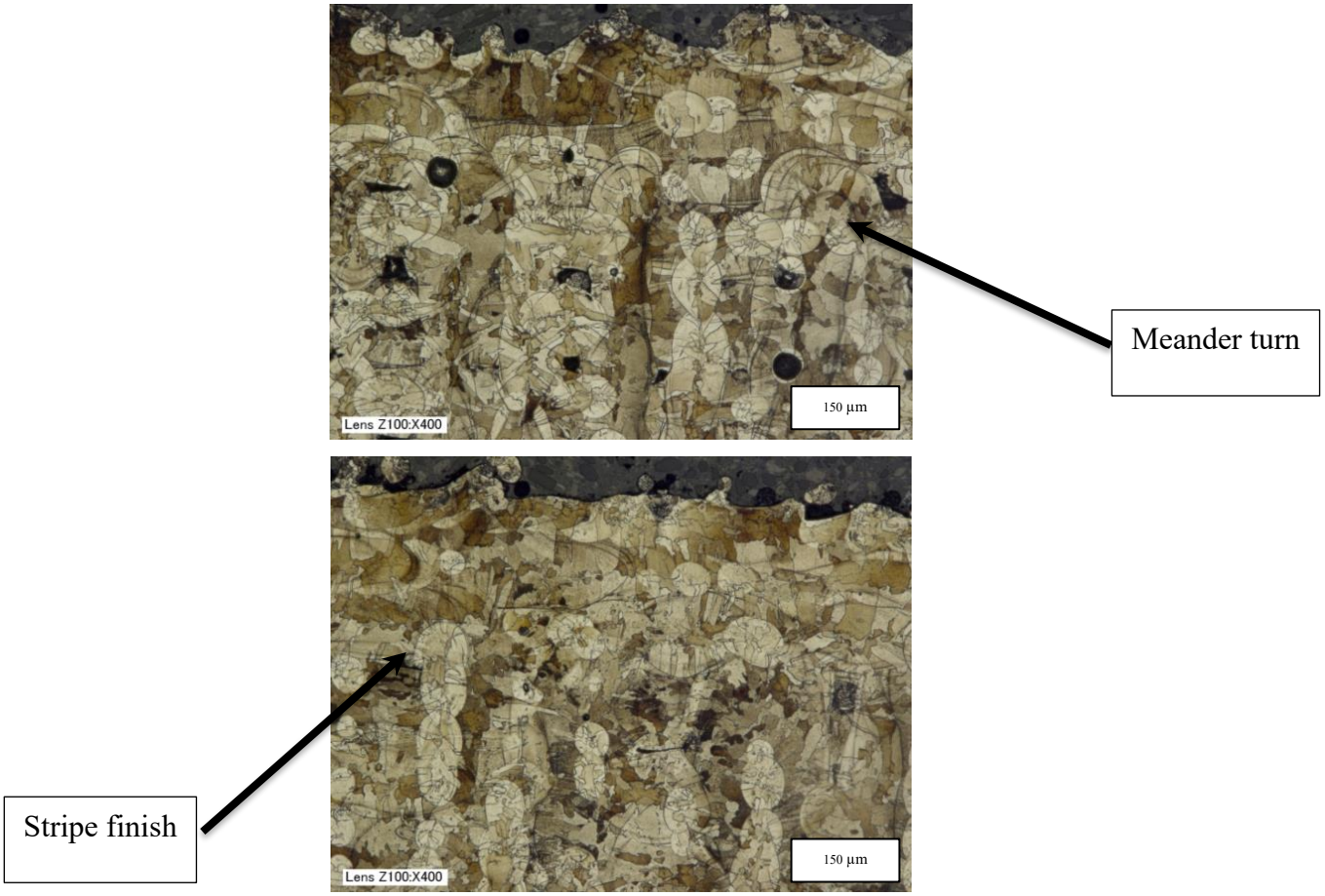

Figure 4:106: The difference between (a) Meander and (b) Stripe laser patterns

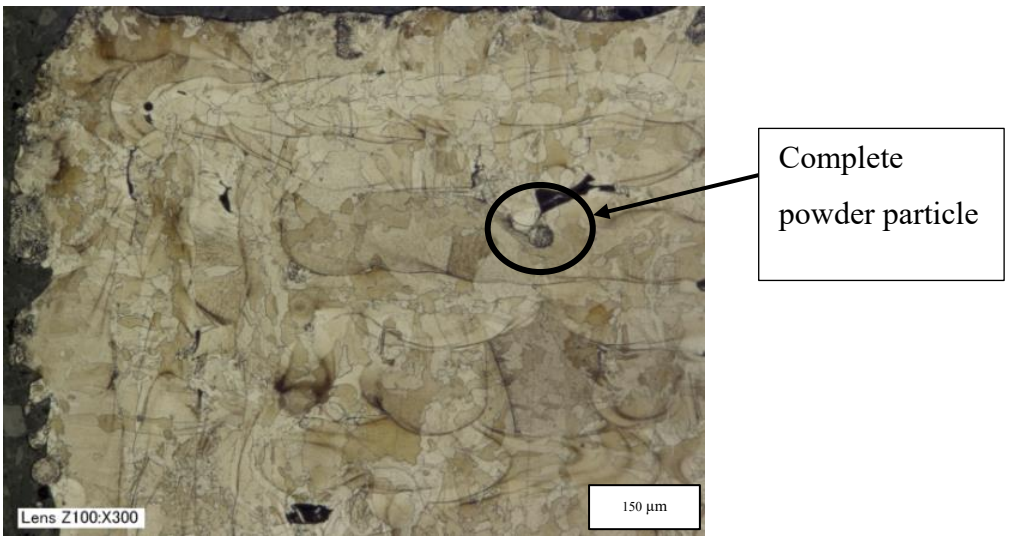

Figure 4:107: Etched cross sections of the 90° Meander Cubes 80µs exposure time and 160W laser power

Figure 4:107 shows the cross section of an etched meander sample, from the image it is possible to see how the laser path moves across the sample and how the grains tend to grow within the melt track and its adjoining tracks. It is also possible to see complete powder particles, as circled, that have not solidified into the laser track. This powder particle has a different microstructure to the surrounding melt tracks. Above the powder particle shown it is possible to see one of a few areas with no powder melted leading to an internal pore. These internal pores can lead to reduce UTS if a crack forms and propagates through the pore.

The microstructure of the 67° rotation samples has been studied to see if the laser pattern change could be seen and proved. Figure 4:108 confirms the angle of the layer shown is rotated from the 0/90° directions confirming the 67° rotation of the laser pattern. The laser pattern influences the microstructure so being able to see the laser pattern and establish what microstructure is produced allows for tailoring of the microstructure and in turn mechanical properties of components.

Figure 4:108: Laser Pattern of 67° Rotation Meander Cube

Figure 4:109 shows what appear to be two melt pools meeting. One of the melt pools, that the grains are growing vertically, and it is possible to see the cross section whereas in the second melt pool, the grains are growing horizontally, and you can see how the grains have grown. The different cooling rates within the melt pools shown in Figure 4:109 have led to the changes in microstructure seen. This image is from a meander build, either the left side of the right melt pool would have had reheat from the laser path that melted the left melt pool or vice versa and this would have had an effect the microstructure created.

The reheating leads to refined grains which can help to improve the isotropy of the component, improving the mechanical properties.

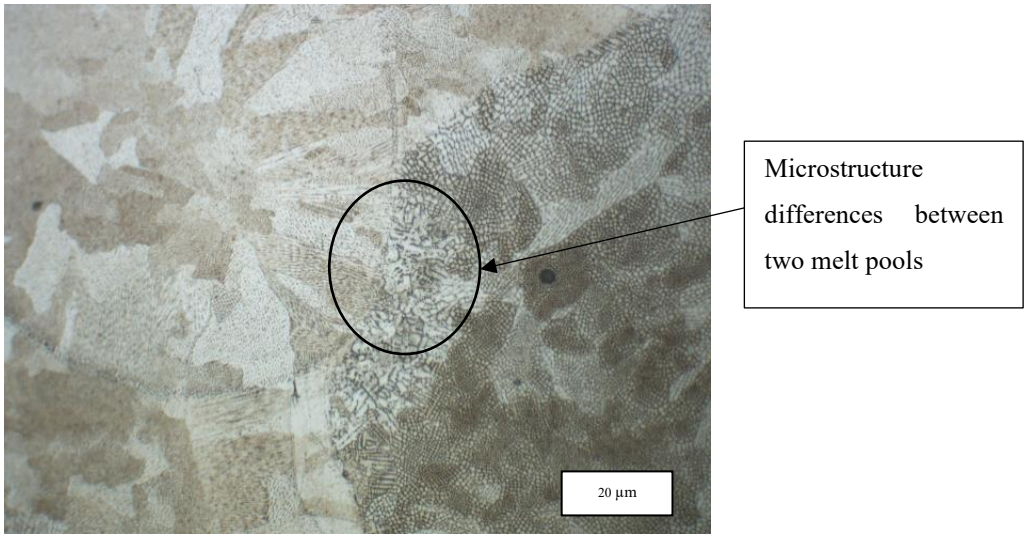

Figure 4:109: Microstructure of an AM SS316L Cube

The microstructure of the 67° rotation cubes can be seen within Figure 4:110, it is seen that the microstructure grows through the layers as they are built up but within the layers there is no consistency in the shape or sizes of the grains. It is also noted that the grains grow across the melt tracks; however, the shapes can vary from straight edges to curved edges of the grains.

Inconsistency in microstructure seen in these parts leads to anisotropy and unpredictable mechanical properties. This makes it harder to predict how parts will perform or to tailor build parameters to generate the required output properties.

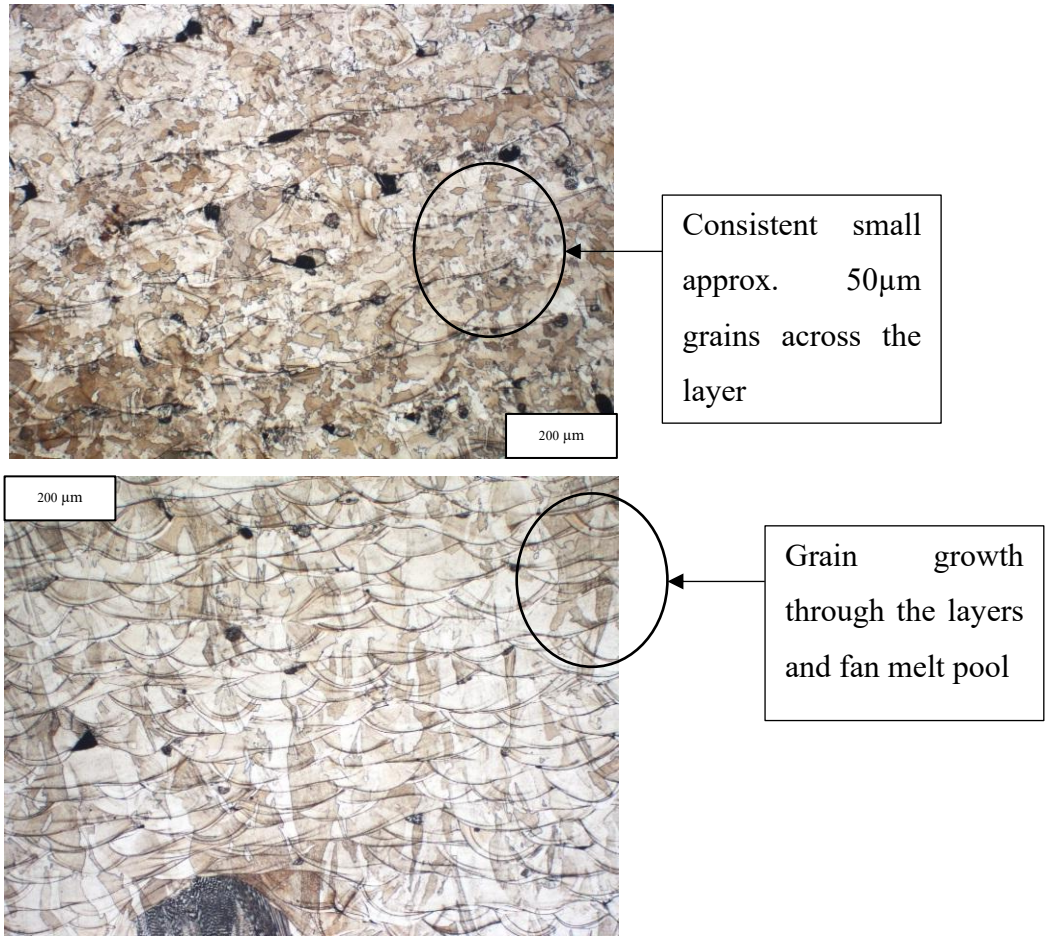

Figure 4:110: Microstructure of a 67° Rotation Cube (a) Across of Layer, (b) Through the Layers

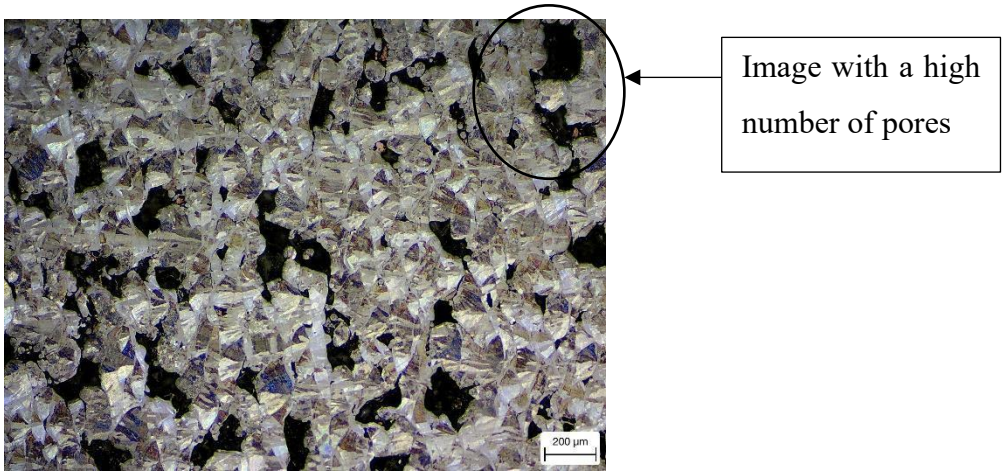

Figure 4:111: 67° Rotation, Meander Laser Path, Exposure Time 80µs, Laser Power 160W

Figure 4:111 is almost 34% pores when compared to Figure 4:112 where only 1% is pores. The lower laser power and exposure time lead to more pores within the component. Therefore although the microstructure is similar across the two parts the increase in pores leads to the reduced mechanical properties seen.

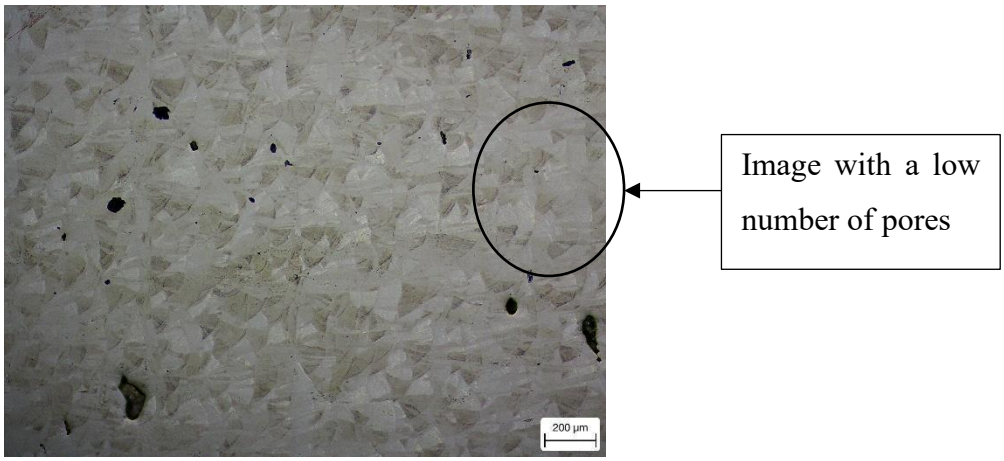

Figure 4:112: 67° Rotation, Meander Laser Path, Exposure Time 130µs, Laser Power 200W

Figure 4:111 and Figure 4:112 show the porosity within a layer and how the microstructure contains grains that are randomly distributed with consistent sizing approximately 50µm in size. The images also show how porosity is more evident in lower laser power and shorter exposure time samples which corresponds to the lower density seen within these samples. The figures show how reduced input energy is leading to poor quality parts with reduced mechanical properties. The pores are stress concentrators, can promote crack initiation and interrupt the microstructure formation

all of these reasons lead to the reduced mechanical properties that have been seen in the lower input energy components.

Comparison between Cubes and Tensile Bars

Comparison between the microstructure seen in the cubes when compared to the tensile bars has shown that these are similar with the grain growth through the layers noticeable and smaller average grain size still visible, approximately 50μm.

Aged Powder Samples

The tensile samples that were tested for the aged powder samples were then cut, mounted and polished to examine the microstructure. These samples were; as built, heat treatment 1 and heat treatment 2. Figure 4:113, Figure 4:114 and Figure 4:115 show how the microstructure has changed due to the heat treatments. It is possible to see the layers and melt pool that have been built up within the vertical samples and the layers across the horizontal samples. When comparing the as built, Figure 4:113, and heat treatment 1, Figure 4:114, samples it is possible to see how the grains have grown further through the samples and are much larger when looking at heat treated samples. When comparing heat treatment 2, Figure 4:115, to the previous images, it is possible to see that the grains have not grown any more than for heat treatment 1 and are no more refined or established within the parts.

Heat treatment helps to refine the grains, these refined grains help to increase the strength of AM components, but this comes at a cost of reduced ductility as has been seen in the results for BP2 and BP3. What is noted from these results is that there heat treatment hasn’t been excessive where the grains would have begun to grown again reducing the UTS.

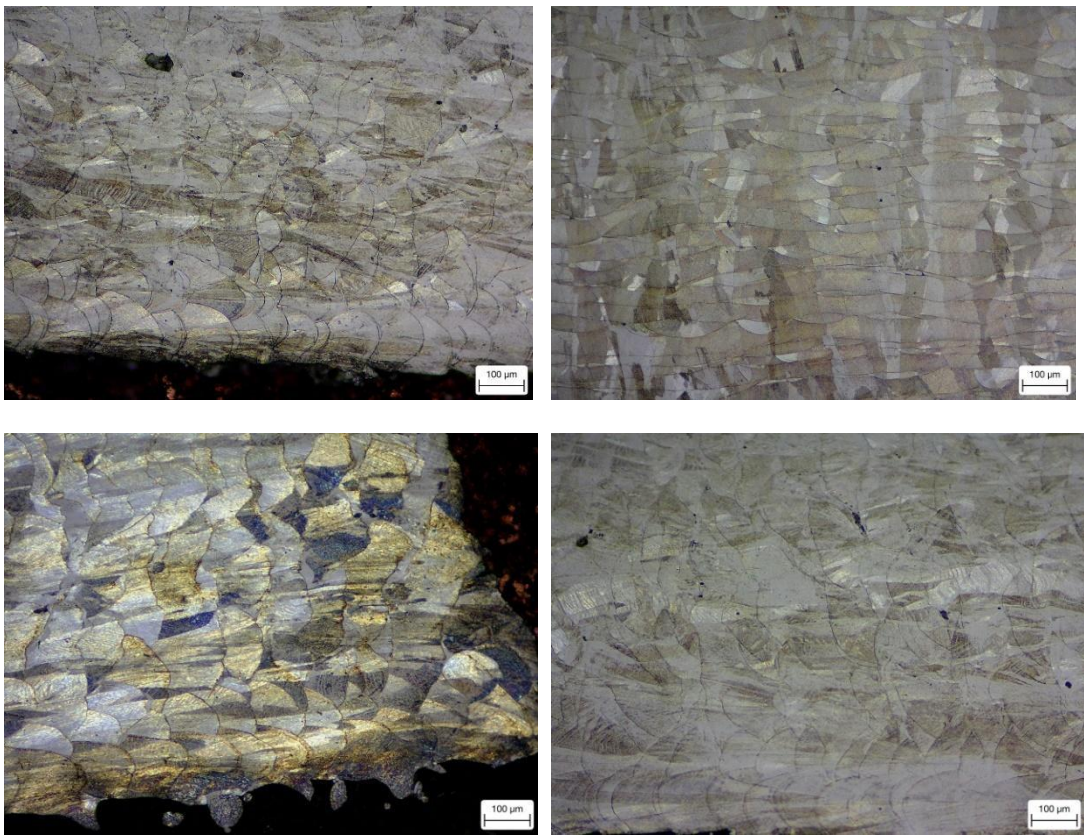

Figure 4:113: Meander Laser Path, Exposure Time 80µs, Laser Power 200W, As Built, x10 mag (a) Build 17 Vertical, (b) Build 18 Horizontal, (c) Build 18 Vertical, (d) Build 21 Vertical

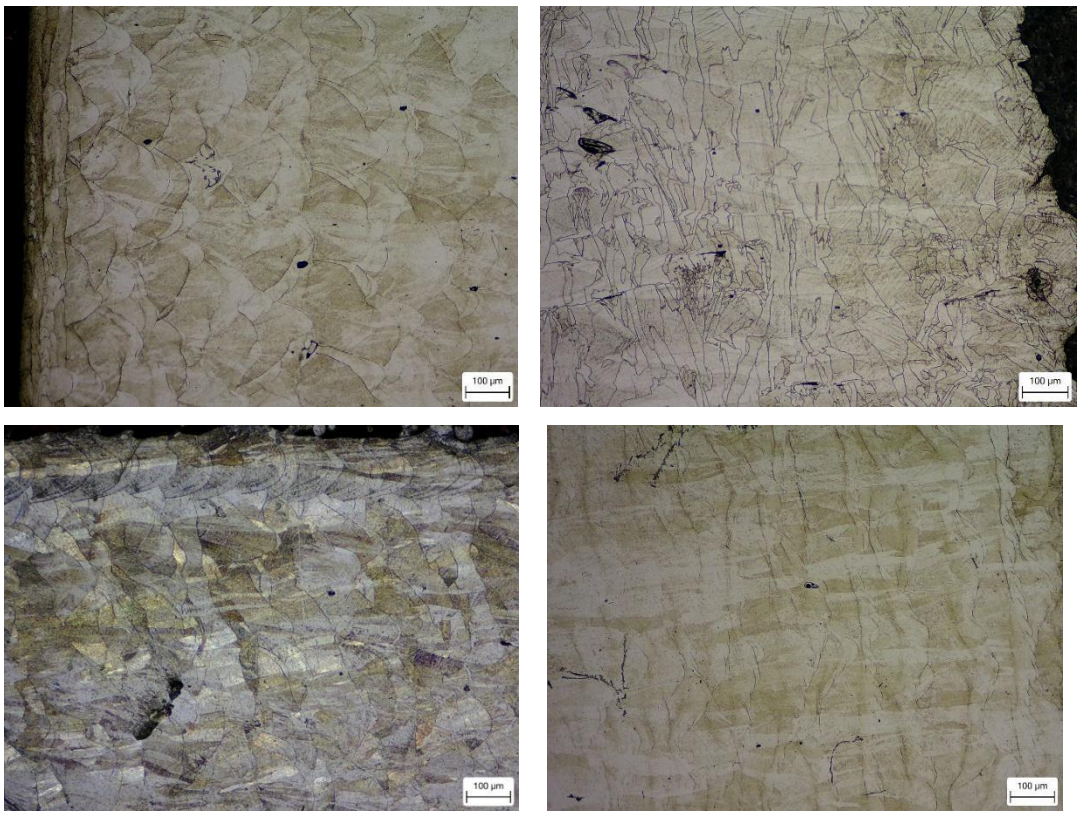

Figure 4:114: Meander Laser Path, Exposure Time 80µs, Laser Power 200W, Heat Treatment 1 Applied, x10 mag (a) Build 17 Vertical, (b) Build 18 Horizontal, (c) Build 18 Vertical, (d) Build 21 Vertical

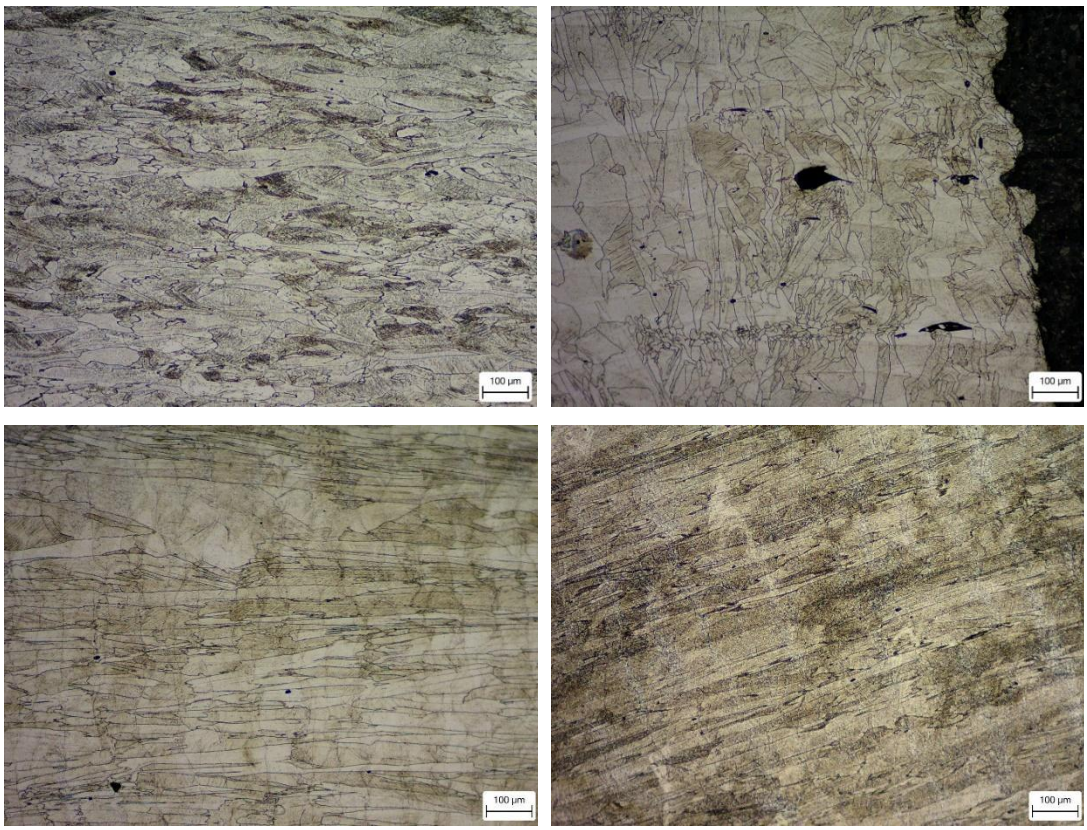

Figure 4:115: Meander Laser Path, Exposure Time 80µs, Laser Power 200W, Heat Treatment 2 Applied, x10 mag (a) Build 17 Vertical, (b) Build 18 Horizontal, (c) Build 18 Vertical, (d) Build 21 Vertical

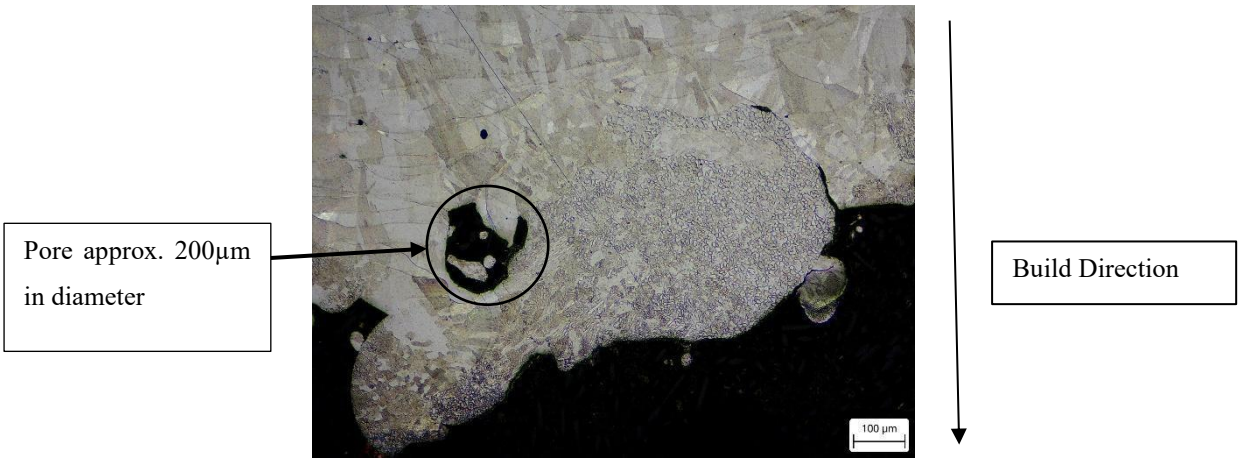

Figure 4:116: Build 18, Horizontal, As Built, x10

Figure 4:116 shows a transition between the main body of the material and the top layers. This shows how as it gets towards the top of the build the microstructure changes form larger grains 50 to 100 µm in size to fine grains 10 – 20 µm in size. It is also possible to see a pore near the surface approximately 200 µm in size containing what appear to be unattached powder particles. The changes in microstructure seen

here show the effect that reheating the layers has on the microstructure. The top layer of a part has a second laser run over it to produce a smoother more appealing surface finish. This is called the up-skin. The second laser run remelts the surface and this is what causes the change in microstructure. This has been shown by Griffiths et al [161]. This second pass by the laser is used to improve the surface roughness, reduce the number of pores and defects at the surface, improve the microstructure with increased grain density in this area and improve the mechanical properties.

Further work by Ramakrishnan et al [162] looked at the effect of laser remelting and saw similar fine grains on the top of the laser path. The highest cooling rate is found on the top surface after remelting due to there being no further heating and nothing on top of the final layer. This high cooling rate leads to a fine grain microstructure like seen in Figure 4:116.

4.6 Sizing

The literature review found that dimensional changes are an issue with AM parts. The work here has confirmed this showing that the sizing of parts produced do not match the original CADs as shown in Figure 4:117, Figure 4:118 and Figure 4:119.

For the 90° rotation samples it was found that the meander parts are bigger in all directions bar the tensile bar widths and the stripe parts were smaller in all directions. Heights have been ignored due to the excess support affecting the result. For the 67° rotation samples it is again seen that the meanders come up bigger and the stripe smaller.

All of the results appear to show no correlation between changing the parameters and the effect on the variation of size seen, this has shown that predicting the size of AM parts may not be that easy and this is rather unreliable to use to ensure accurate parts.

The standard deviation of the sizing shows that the results show statistical correlation due to the standard deviation being low and consistent across measurement directions. There is little variation in the results obtained and although it is not possible to predict which build parameters effect parts size you do know that the effect each parameter set has is consistent across a build if you investigate one part.

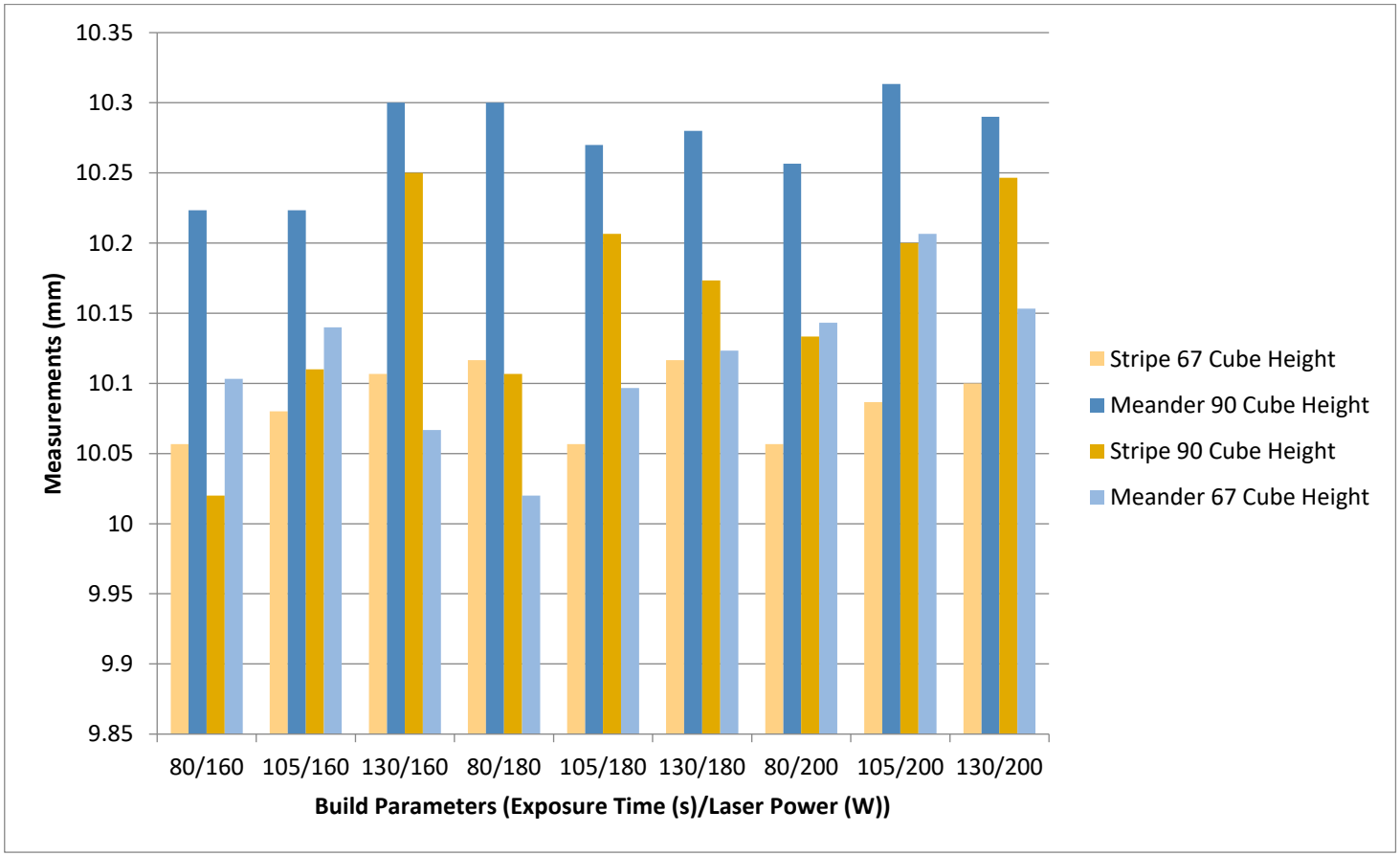

Figure 4:117: Comparison of Cube Sizing - Height

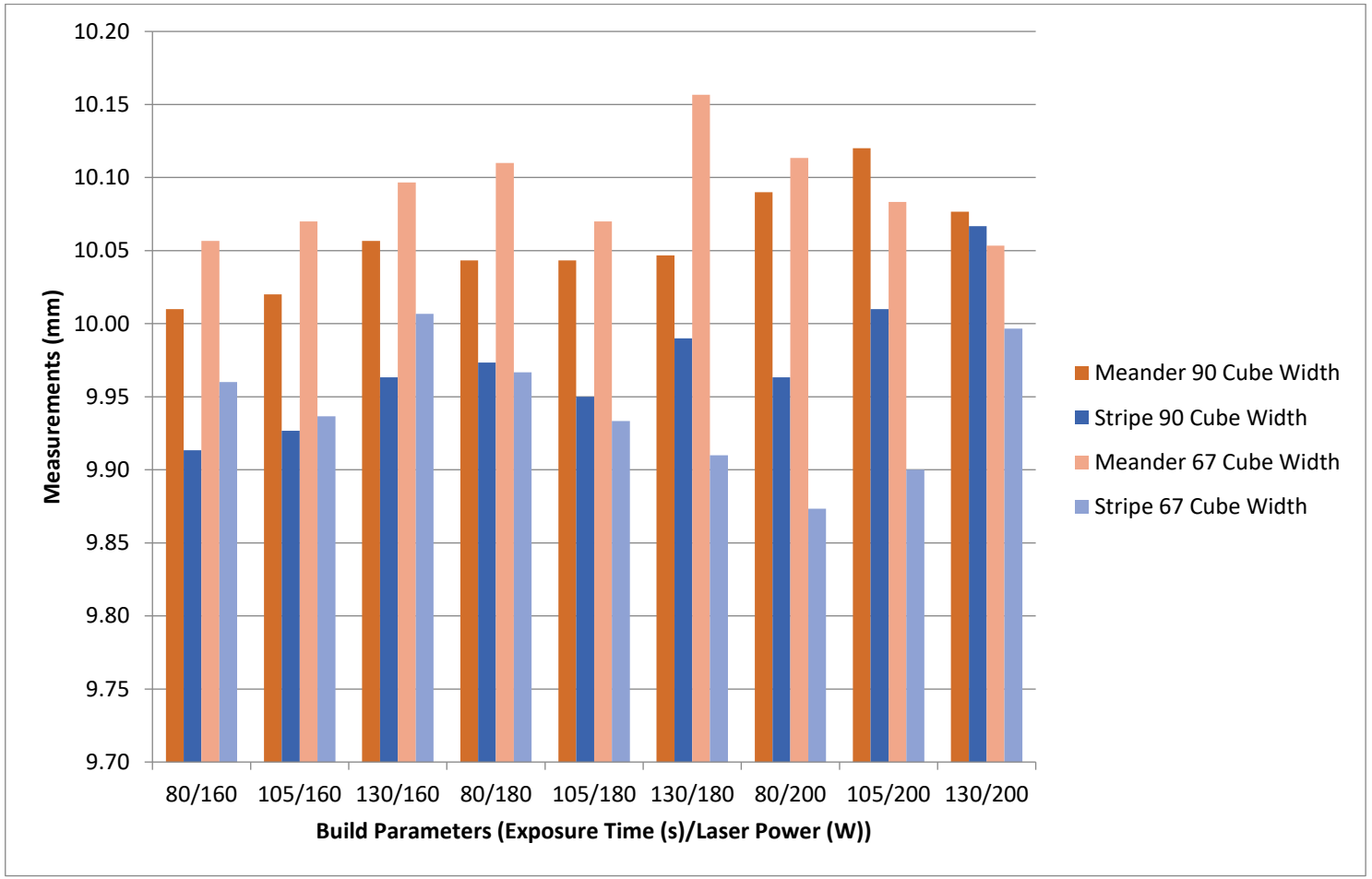

Figure 4:118: Comparison of Cube Sizing - Width

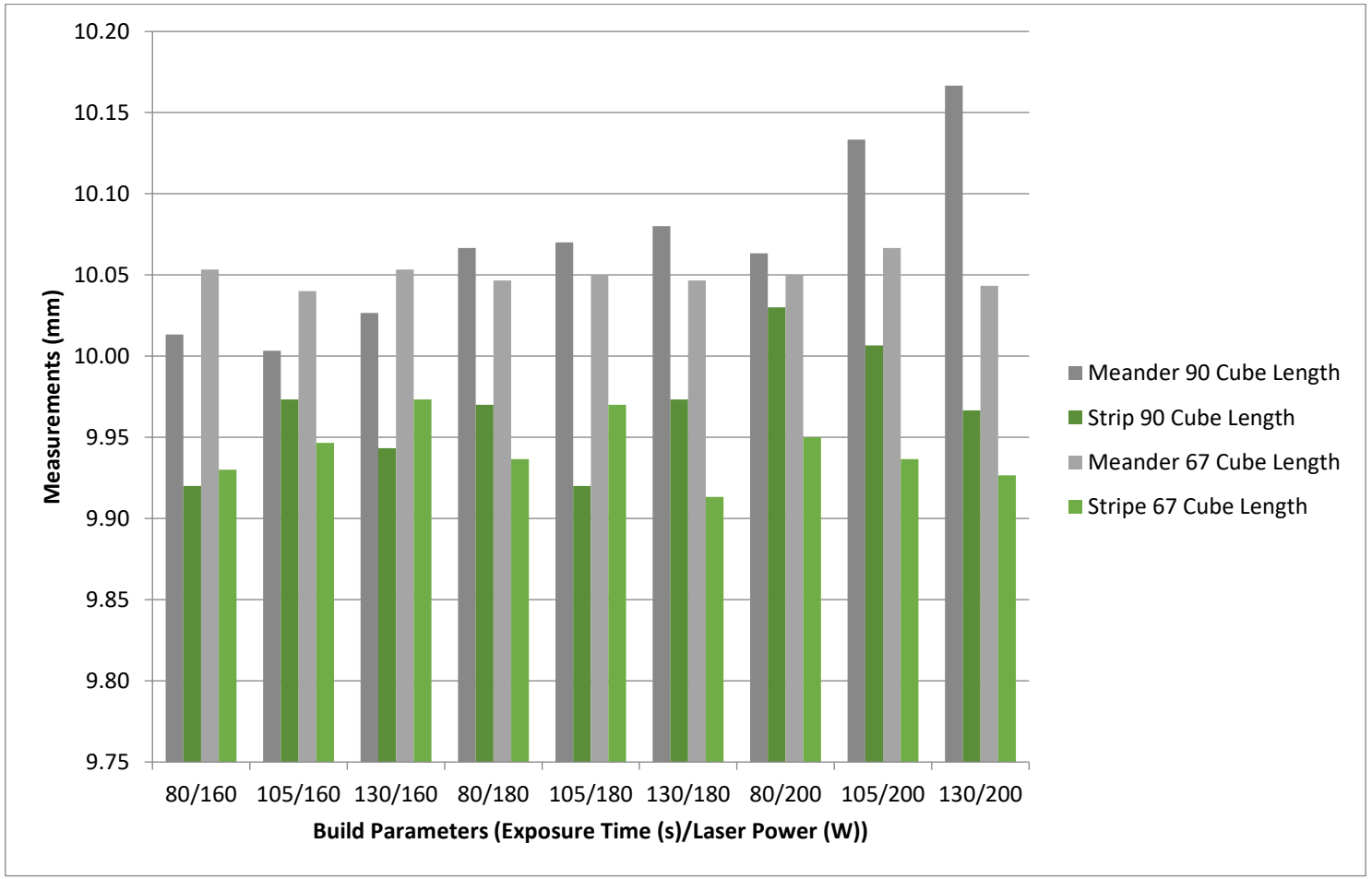

Figure 4:119: Comparison of Cube Sizing - Length

4.7 Hardness

The results from the testing show that there is a change in hardness as the laser power is increased and this is the same for both laser patterns. These results are shown in Table 5:1 and Table 5:2.

The results show Figure 4:120 that the hardest 90° rotation sample is 130µs exposure time, 200W laser power for the meander laser pattern, with a hardness value of 211.16HV. The hardest stripe laser pattern sample is in fact the hardest sample of all samples tested built using settings of 130µs exposure time and 160W laser power, giving a value of 249.49HV.

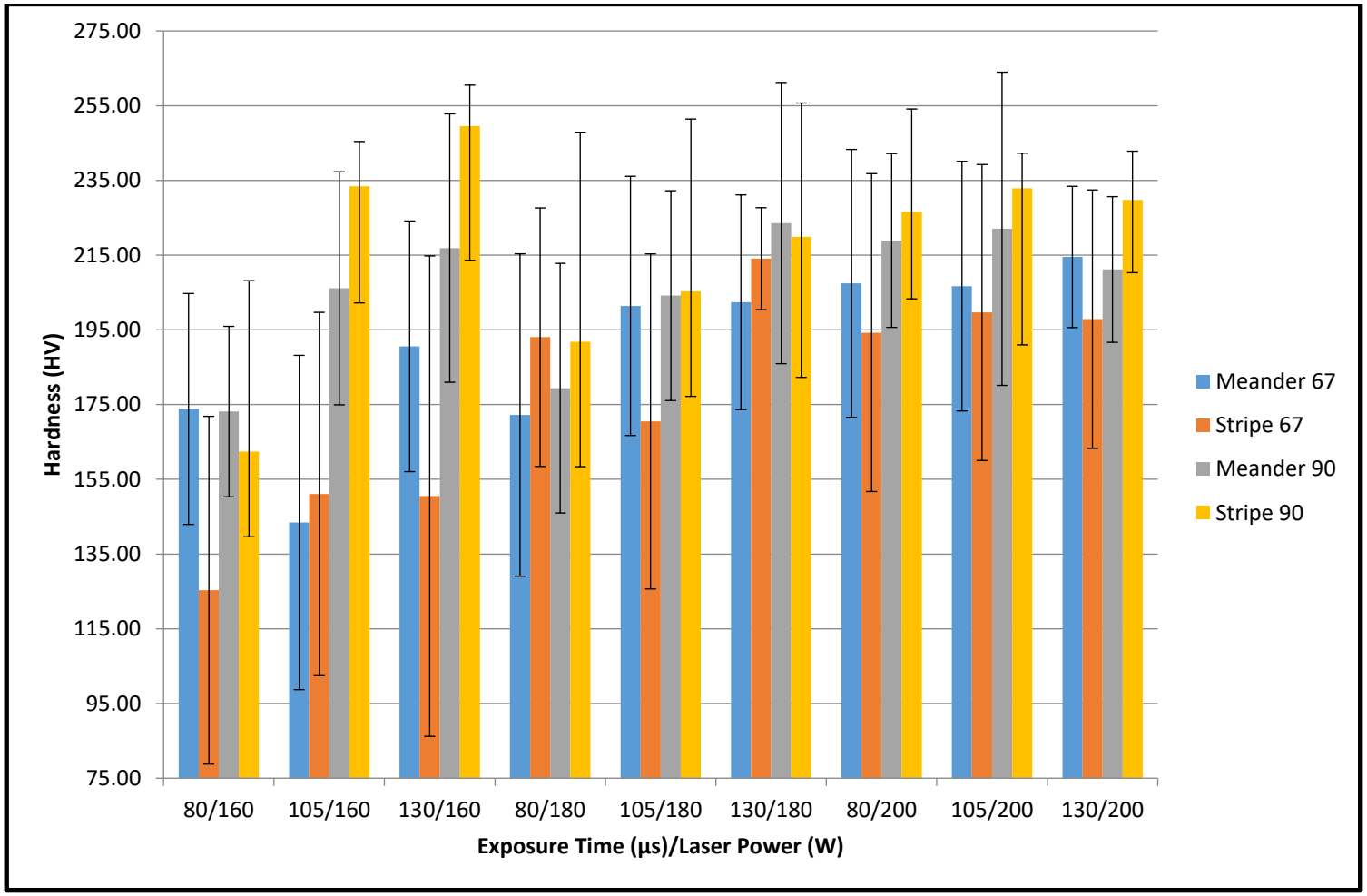

Figure 4:120: Comparison of Hardness Value between Laser Patterns and the Different Laser Rotations

The results for the 67° rotation show that the hardest sample out of all the samples tested is the 130µs exposure time, 200W laser power for the meander laser pattern, with a hardness value of 214.51HV. The hardest for the stripe cubes is just below this at 214.05HV this is again for the 130µs exposure time but for 180W laser power.
Figure 4:121 illustrates a typical indent created by the hardness indenter that is used to calculate the hardness value of the samples.
The standard deviation of the hardness test shows that for the higher laser powers although the deviations are larger, they are consistent across the samples whereas for the 160W laser power the deviations vary greatly showing a lot of variation in the results found. This variation in standard deviations shows that the results are not statistically accurate and there is variation in the hardness seen across the surface of the sample.
During the hardness testing the surface was checked before the test to ensure that the indenter did not hit a surface pore during the test, as this would have affected the results.

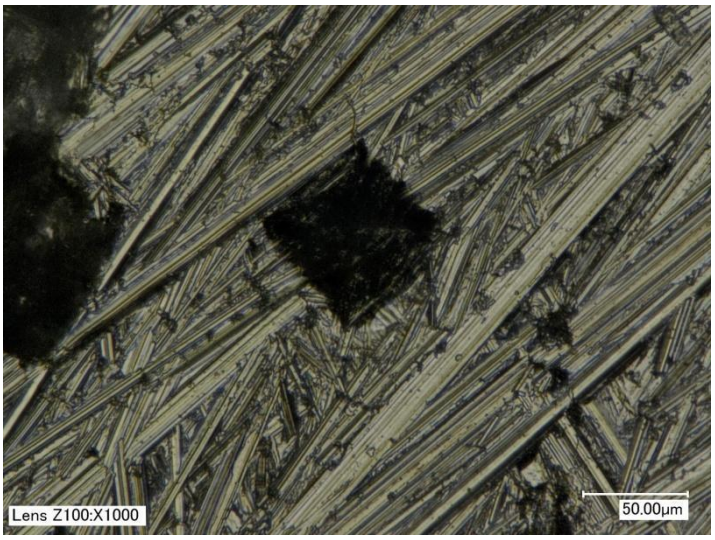

Figure 4:121: Indent caused by the hardness testing on the surface of the 67° rotation cubes 130µs exposure time and 200W laser power and meander laser power

The hardness found across the surface of a cube was measured to see if there was any suggestion of where the residual stresses may be found. This was performed as it has been seen that residual stress has an effect on the hardness of a sample [164]. The paper states that the larger the stress the lower the hardness.

Summary

The hardness testing results show that the hardest sample is from the stripe laser pattern samples using settings of 130μs exposure time, 160W laser power and 90° rotation at 249.49HV. The hardest sample for the 67° rotation is using settings of 130μs exposure time, 200W laser power with the meander laser pattern and this gives a value of 214.51HV, this shows a decrease of 15% from the best 90° rotation samples. The best sample has an increase of 6% on the value of HV for SS316L AM parts found in the literature.

4.8 Comparison between As Built and Heat-Treated Parts

Figure 4:122, Figure 4:123, Figure 4:124 and Figure 4:125 show the graphs comparing as built samples stress vs strain to those with heat treatment 1 and 2 applied. These graphs show the effect of heat treatment on the tensile strength of SS316L. Heat treatment 1, 60 minutes at 450°C, has been seen to have little effect on the results the UTS and yield stress are comparable to as built, but, heat treatment 2 of 4 hours at 1150°C has greatly reduced the yield stress and had an effect on the UTS as well also lowering this. These effects can be seen across all four builds in both the horizontally built and vertically built samples. It should be known that the heat treatment used here hasn't been optimised for this material.

Heat treatment removes dislocations therefore slip can occur easier. It also removes pores and increases ductility and this affects the UTS of the samples.

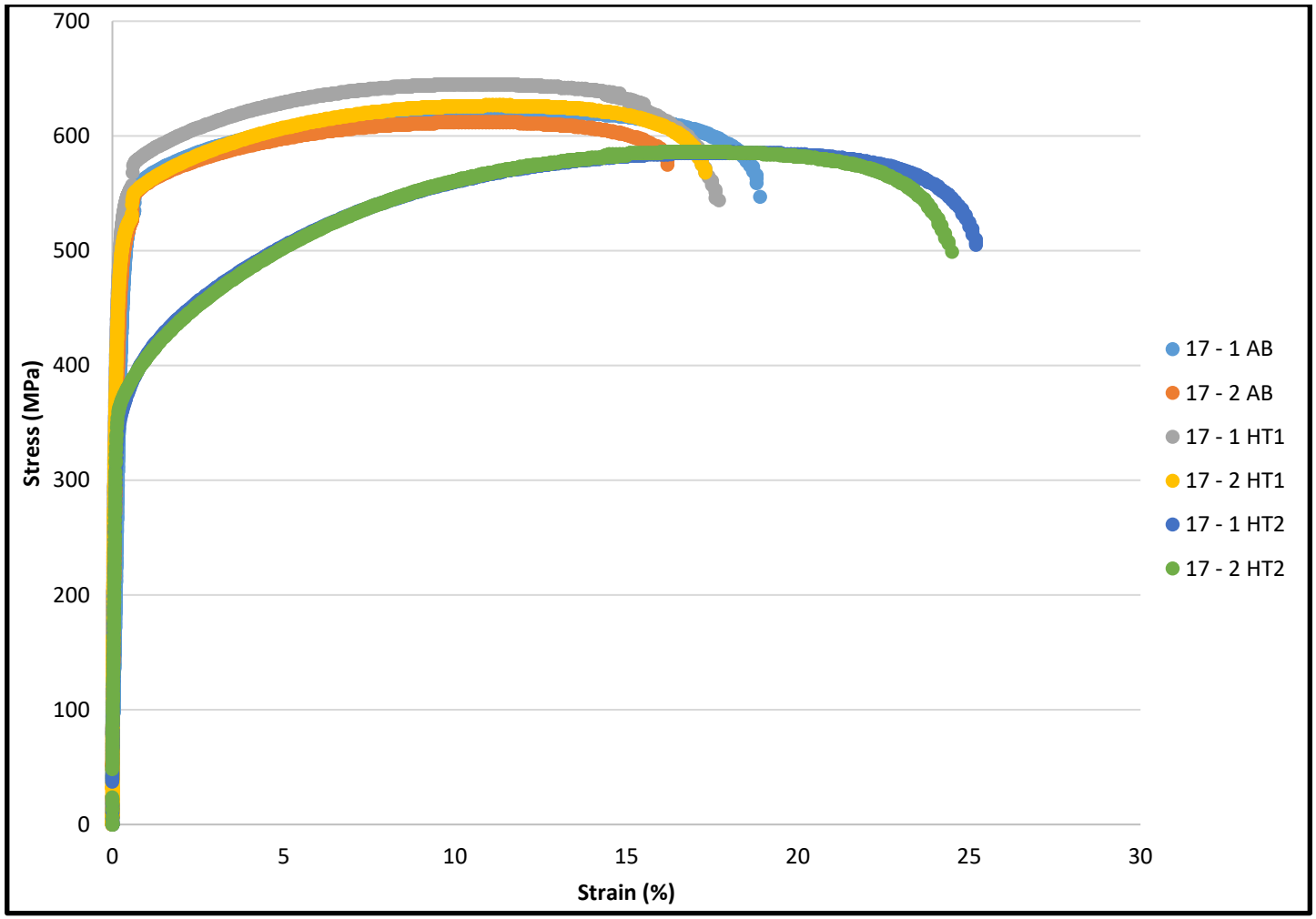

Figure 4:122: Stress vs Strain for Build 17 Samples

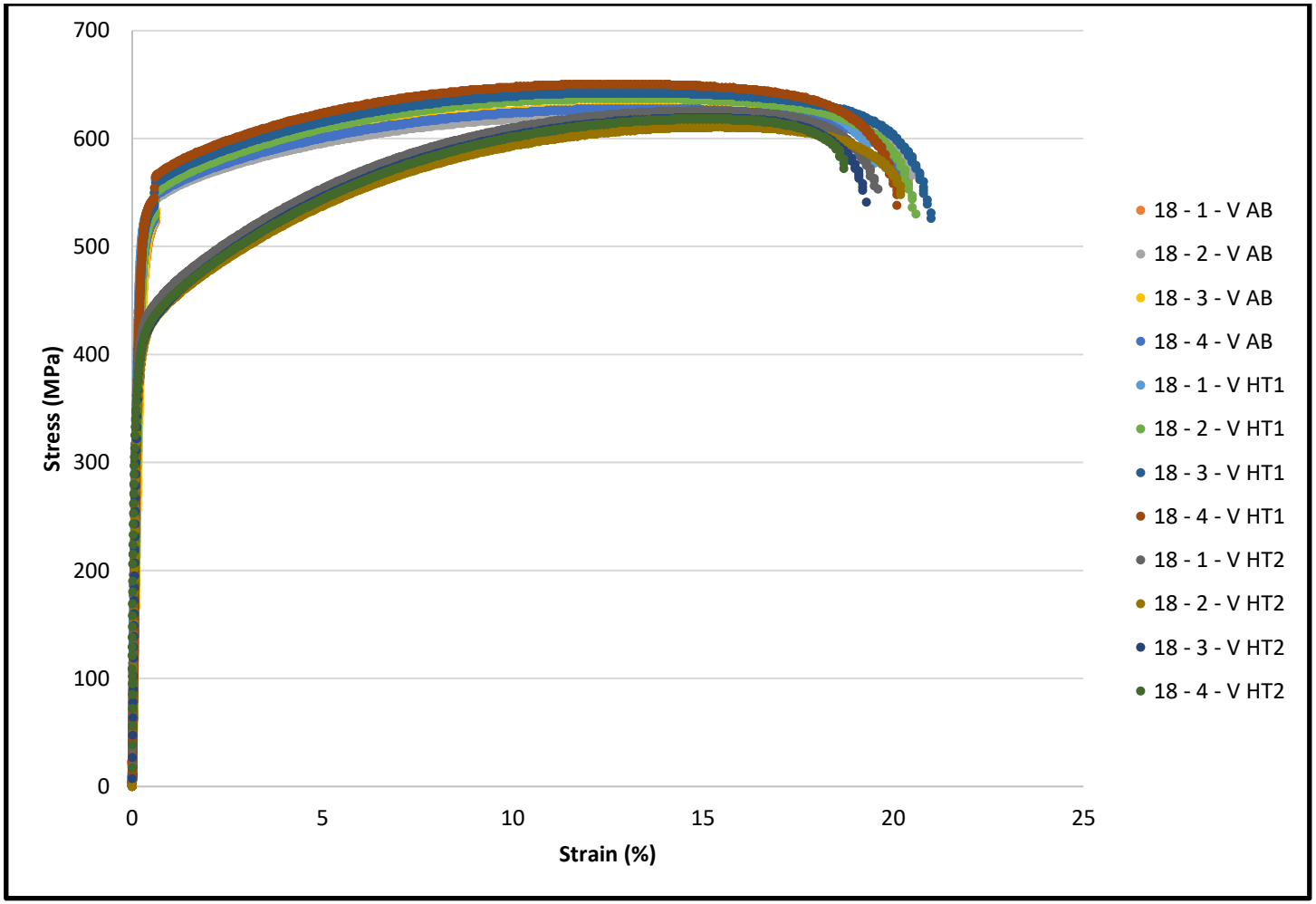

Figure 4:123: Stress vs Strain for Build 18 Vertical Samples

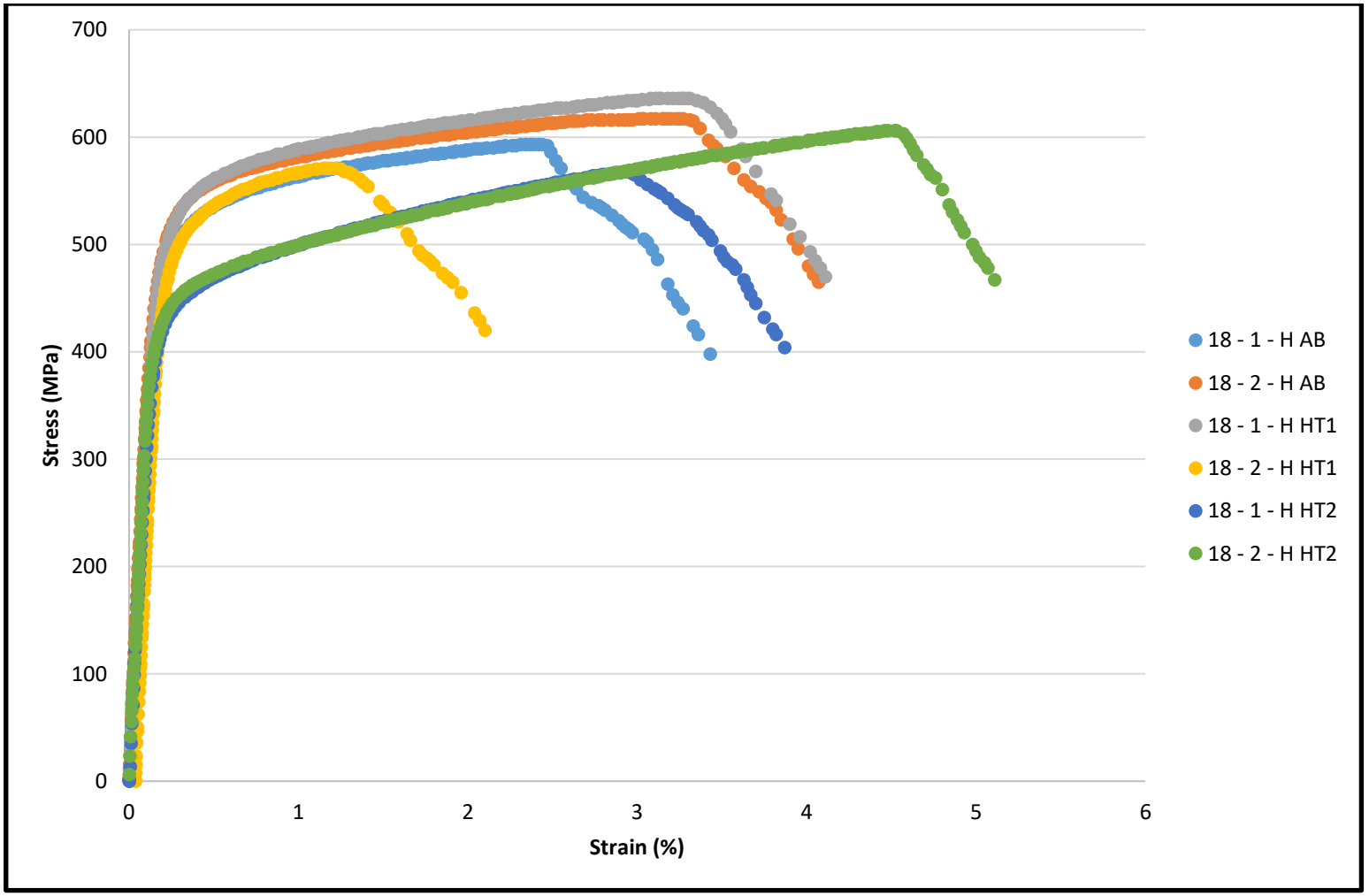

Figure 4:124: Stress vs Strain for Build 18 Horizontal Samples

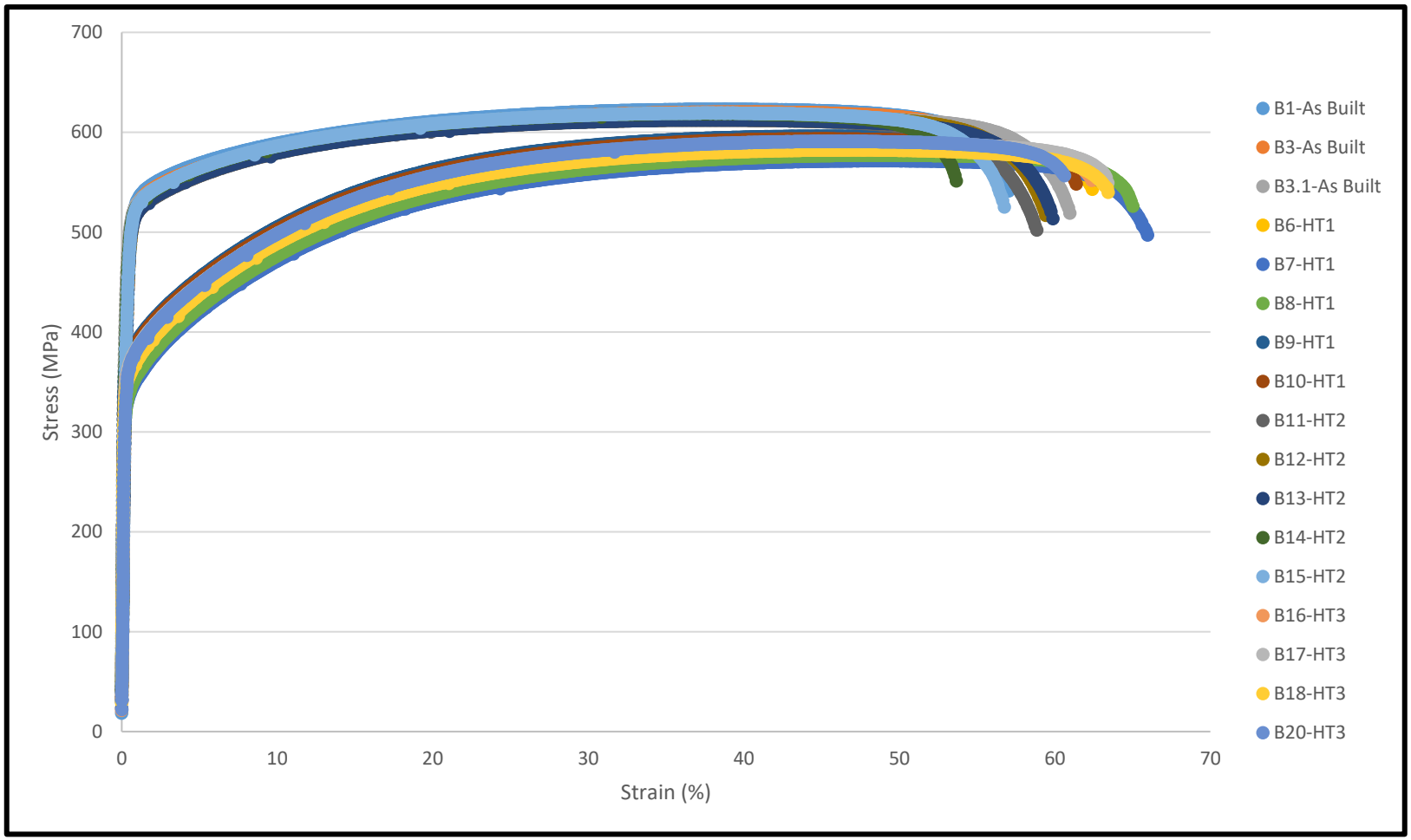

Figure 4:125 Stress vs Strain for Build Programme 3 Samples

A further build, BP3, carried out comparing as built with three different heat treatments:

- HT1 360 minute ramp to 1150°C, hold for 240 minutes and 360 minute ramp down,
- HT2 90 minute ramp to 450°C, hold for 2 hours and 90 minute ramp down,
- HT3 420 minute ramp to 1125°C, hold for 250 minutes and 240 minute ramp down.

It can be seen that as built samples and HT2 are comparable with higher UTS out of all samples tested but reduced strain to failure whereas HT1 and HT3 have a reduced UTS but increased strain to failure when compared to as built samples.

4.9 Comparison between HIPped and UnHIPped Parts

Work carried on SS316L tensile bars built at different angles has been performed. The work looked at HIPping the bars and seeing what effect this had on the tensile properties of the bars. From this work, it has been found that the UTS of tensile bars is reduced after HIPping. The average Young's Modulus is shown to increase with HIPping. The highest UTS of 592 MPa is found to occur for an unHIPped part built 45° to the horizontal.

Further work has been carried out that looked in more detail at the effect of HIPping on the microstructure and mechanical properties of SS316L [165]. The results of this work are shown in Table 4:7. These results show how the UTS is only minimally affected by the HIP treatment but the strain to failure is improved greatly. The strain to failure has gone from below 0.1 to between 0.35 and 0.5, this is up to a five times improvement.

Figure 4:126 is a graph showing the extent of the improvement made by HIPping parts. Here it can be seen that that strain to failure has dramatically improved for a comparable UTS.

Table 4:7: Comparison between HIPped and UnHIPped Samples

		UTS (MPa)	Strain to Failure
UnHIPped	**1**	554	0.09
	2	538	0.06
	3	505	0.02
HIPped	**1**	564	0.475
	2	542	0.36
	3	562	0.44

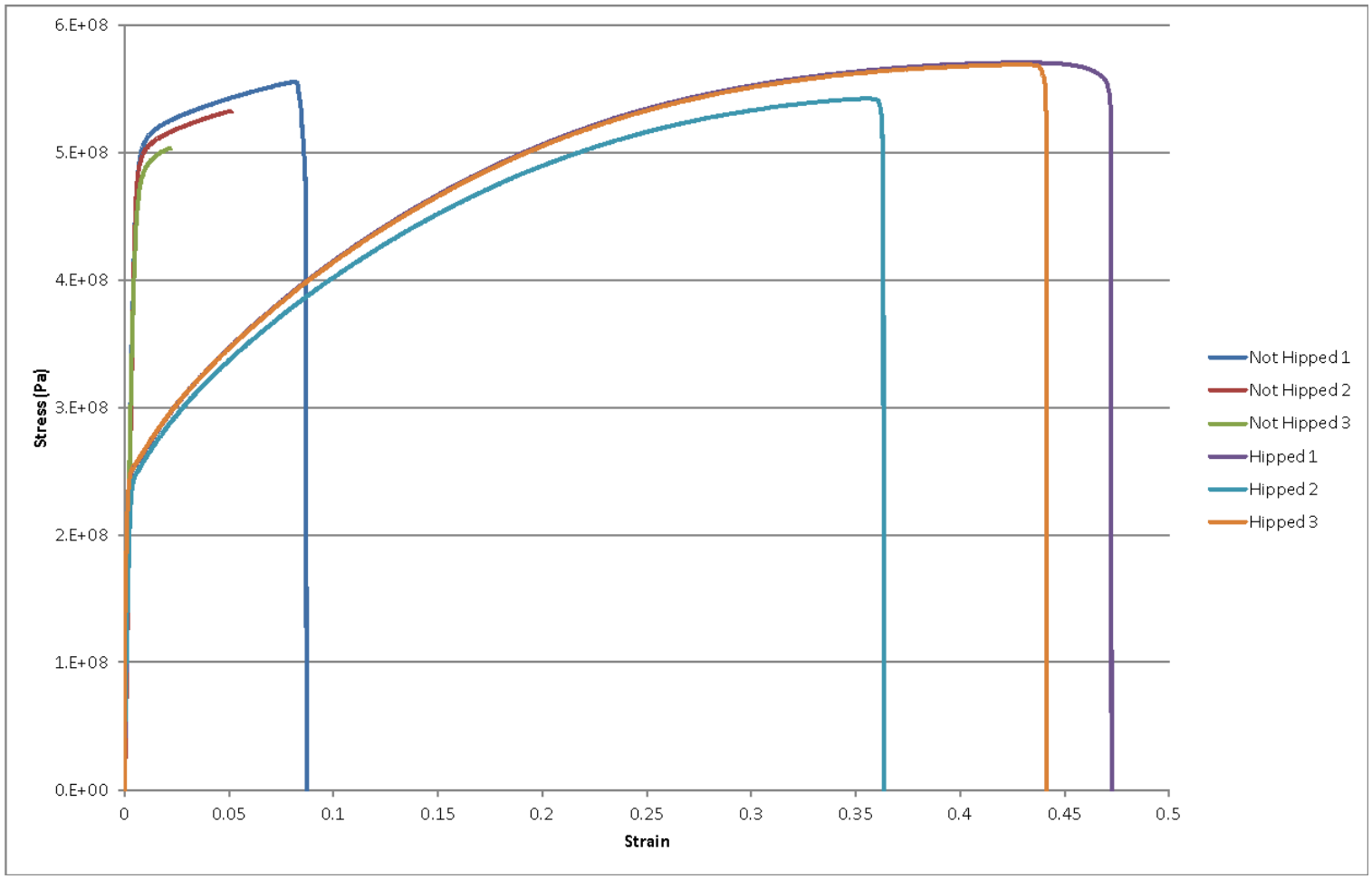

Figure 4:126: Tensile test results using rectangular cross-section test bar, and HIPped versus UnHIPped

4.10 Comparison between As Built, Heat Treated and HIPped Parts

BP3 allowed for samples manufactured in the same build to undergo different treatments before tensile testing. Parts were tested as built, following one of three heat treatments, HT1, HT2 or HT3, or after a HIP cycle. From the results it is possible to see that HIPping produced a slight reduction in strain to failure. But the various heat treatments do not show consistency between effect on strain to failure and UTS.

4.11 Comparison between Build Direction

HIPped and unHIPped parts that had been built at 0°, 45° and 90° in the horizontal and vertical angle have been tested. These samples show that for horizontal samples that there is little effect on the UTS or yield for either HIPped or unHIPped but there is on the Young's modulus. For unHIPped the 0° orientation gave the best Young's modulus, whereas for HIPped it was the 45° orientation. For vertical samples, there is more variation in the UTS and yield whereas the Young's modulus is consistent for unHIPped samples.

4.12 Comparison between 90° and 67° Laser Pattern Rotation

The experimental work has been carried out to see how changing the build parameters when building AM parts has an effect on the parts properties and also how AM parts compare to the minimum requirements of SS316L.

The experimental results have shown the best results are found when using the 90° rotation and the meander laser pattern.

4.13 Comparison between Aged and Unaged Powder

The experimental work carried out has looked at if parts built using powder that had been through the build process in a number of times had comparable properties to those that were built using 'virgin' or limited reuse powder. These samples were built using 67° rotation: meander laser pattern, 80μs exposure time and 200W laser power. These properties were used as they gave the best density when compared to the UTS of the samples and so it is believed that these were the best properties to take forward for further examination.

The results have shown that when comparing parts that have the same build properties but have been built using fresher powder the properties are comparable.

When comparing the builds manufactured using aged powder to the corresponding original samples made with a mixture of 'virgin' and fresh powder it is possible to see that in the as built state for all aged samples the UTS exceeds that of the original samples. The results comparing aged and 'mixed' powder samples have shown that powder reuse does not have a detrimental effect on the samples UTS and has increased the strain to failure seen by 50%. Figure 4:127 shows a stress strain graph for a comparable sample to the aged powder samples. From this graph the similarities between the how the sample has reacted to the applied force can be seen but what is noticed is that the sample takes longer than other samples investigated here to reach its yield and the fracture is very close to the UTS.

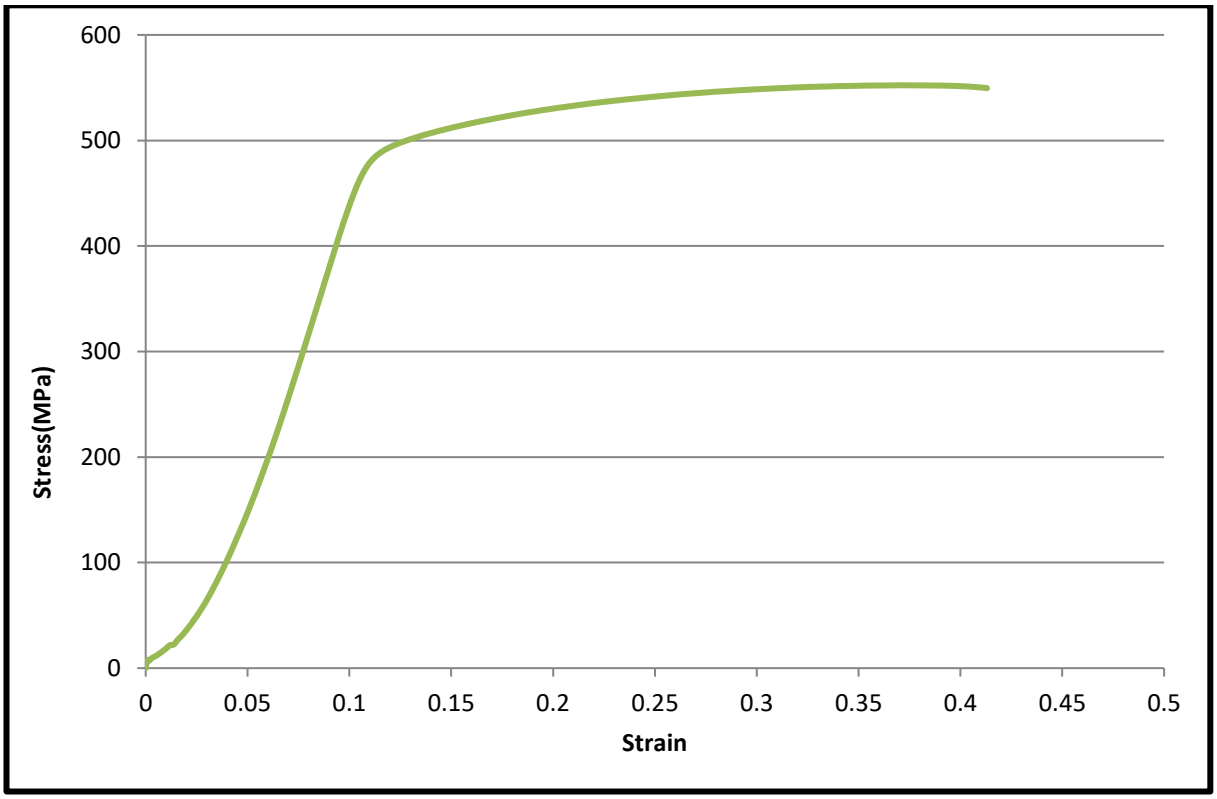

Figure 4:127: Stress Strain Graph for 67° Rotation, Meander Laser Path, Exposure Time 80µs, Laser Power 200W

4.14 Parameter Effects

This work has shown that build parameters and therefore input energy has an effect on the mechanical properties and microstructure. Optimised processing parameters lead to consistent compliance with minimum standards.

- Laser power and exposure time strongly affect density, UTS, and elongation. Higher energy input generally increases density and mechanical properties.

- Laser pattern rotation influences surface roughness and density, while meander patterns outperform stripe patterns for UTS, hardness, elongation, and density.
- Increasing laser power improves UTS, with maximum values achieved using aged powder at higher power settings.
- 90° rotation gives unpredictability in elongation.
- Heat treatment was shown to reduce UTS as the temperature was increased but has no noticeable effect on yield strength. Likely due to the fact heat treatments modifies the microstructure. Lower temperature heat treatment reduces elongation but as temperature increases further so does ductility.
- HIP improves strain to failure for comparable UTS.
- Aged powder improves UTS and elongation likely due to the smaller particle size distribution.
- Porosity limits ductility, large pores lead to brittle failures.
- The microstructure present governs yield strength.
- The AM process and heating pattern affect the grains present when compared to rolled SS316L.

4.15 Future Test Methodology

The testing that has been performed in this chapter has shown that the best parameters for building SS316L parts on the AM250 AM machine can be found and these produce parts that have properties that exceed the minimum required properties of SS316L [47]. It is believed that these can be brought closer still by using finishing processes, including HIPping and heat treatments after the parts have been removed from the base plate. This can be seen from the tensile test results of HIPped parts, which are shown in Section 4.9, Comparison between HIPped and UnHIPped Parts.

What can be drawn from this work is a test methodology that can be set up to allow for testing of other materials to be performed to establish the best parameters to use for similar materials.

The methodology that is being suggested from the work carried out is to run a series of systematic tests; testing the density, tensile strength and hardness value of the part. Added to this should be fatigue and creep testing to understand the parts service life.

To continue the experimentation on aged powder samples a set needs to be HIPped, time has not allowed that during this work, but the samples are ready to be sent off for HIPping and testing.

4.16 Summary

This chapter has looked at the analysis of the experimental tests to see how the properties of the SS316L AM parts vary due to changes in the build parameters and the powder used. Along with how these parts compare to the minimum required properties of SS316L. It has been looking to establish the best build parameters for SS316L AM parts using a variety of different parameters over an extended period of time to ensure the optimum output is achieved. What has been found during the three programmes of work is that the optimum parameters defined in BP1 have been used in BP2 and BP3 and have shown consistent high quality parts that prove the parameters defined do produce good repeatable AM components which exceed the minimum dictated in the ASTM standard.

The results that have been found here are discussed in Chapter 5, Discussion.

Chapter 5 Discussion

This chapter is a discussion of the results of the experiments performed in Chapter 4, Results, to establish the best parameters to use when building AM SS316L parts. The conclusions drawn from this analysis will be outlined in Chapter 6, Conclusions. This chapter will interpret results, considering the work here against what has been reported in the literature.

5.1 Experimental Results

The results found from this work will be compared to conventional SS316L mechanical properties, Section 4.1 [47] [159] [97] along with other, published research results. The present work has found that the results here correspond to others' works with some interesting results relating to the heat treatment of SS316L samples going beyond published work. As this work has developed through the three build programmes the initial findings have been further proved with consistent results.

There is one point that should be noted that some of the samples tested in this work had been post machined. The results have not been included as post machining improves the UTS of AM parts [171].

5.2 Summary Tables

5.2.1 Unaged Powder Samples

The mechanical and physical characterisation of the unaged powder builds Table 5:1 and Table 5:2 provides a coherent picture of how process parameters, particularly exposure time, laser power, and scan strategy, influence the resulting material performance. When viewed collectively, several consistent behavioural trends emerge that demonstrate the interplay between energy input, melt pool formation, and defect generation.

A clear and overarching observation is that increasing exposure time leads to a progressive increase in surface roughness, density, ductility, strength, and hardness. This behaviour is characteristic of higher energy input producing wider, deeper, and more stable melt pools, resulting in better consolidation but also more pronounced surface waviness as bead height and overlap increase.

These results show that:

- Roughness varies greatly with it being at least 11µm up to a value of 21µm. The roughness shows a correlation with the exposure time increasing as the exposure time increases.
- Density increases with exposure time, the maximum density obtained was 7.66g/cm^3 and the lowest found was 6.76g/cm^3.
- Extension increases with exposure time the lowest extension was an increase of only 0.75% whereas the highest was 39.57%.
- UTS increases with exposure time to a maximum of 588MPa which is higher than the value for the UTS given in ASTM A240/A250M [47] for SS316L.
- Hardness increases with exposure time to a maximum found of 249.49HV, which exceeds the known value for hardness of a SS316L AM part.

The standard deviation results shown in Table 5:1 and Table 5:2 show that there is a lot of variation in the properties of the samples data. The densities have very small standard deviations, the largest seen was a standard deviation of 0.0337 in one case with over 50% of the results have a standard deviation of 0.0, thus they have not been shown in the table, indicating that density varies little between builds and statistical correlations have been shown. This means that density from subsequent builds will be reliable and as designed.

The standard deviations of the UTS show more variation than density, majority of the input parameters show little variation and reliable results, however, there are certain input parameters where there is large variation. For example, Meander, 67°, 180W, 80µs or Stripe, 67°, 200W, 130µs, both of which have high standard deviations when compared to the UTS value which would suggest that these build parameters would give materials properties that are less predictable and may not be as designed.

The standard deviation of the Young's Modulus is similar to that of the UTS. Many of them are smaller deviations showing reliable results but there are a few anomalies where the deviations are higher, Meander, 67°, 200W, 130µs or Stripe, 67°, 160W, 80µs, and so those results are less reliable. These parameters are best avoided when hoping to achieve consistent mechanical properties across the parts produced.

The standard deviation of the Yield Stress shows variations again, the majority of the samples have low standard deviations showing the reliability of the results. There are a few parameters, Meander, 67°, 180W, 105µs or Stripe, 67°, 180W, 80µs, that show large standard deviations showing these parameters do not produce consistent properties. The large standard deviations seen for the Yield Stress do not correspond

to the larger standard deviations seen for the UTS or Young's Modulus. This shows that different build parameters have different effects on the different mechanical properties and further investigation would be needed.

The higher standard deviations all appear for 67° rotation samples, suggesting these samples will always be harder to predict the mechanical properties that are seen.

The standard deviation for UTS, Young's Modulus and Yield Stress used a population size of three samples per results. For hardness and density, a population size of nine was used producing a more representative standard deviation result.

The surface roughness ranges roughly 11–21 μm (side/top) and increases with exposure time. Therefore, it is seen that higher exposure times increase melt pool width/overlap and can spur higher bead height/surface waviness; meaning you get higher roughness even as density/strength improve.

The density is seen to increase with exposure time. The lowest found was 6.76 g/cm³ (Stripe, 67°, 160 W, 80 μs) and highest was 7.66 g/cm³ (Meander, 90°, 200 W, 130 μs). Higher energy input reduces lack-of-fusion porosity leading to higher density.

A broad span is seen in ductility (extension / strain-to-failure). The lowest is 0.75% (some early low-energy settings) to highest 39.6% (Stripe 90°, 200 W, 105 μs or Meander 90°, 200 W, 105/130 μs class). Showing that ductility generally improves with exposure time as porosity decreases and interlayer defects reduce.

The UTS is seen to increase with exposure time to 588 MPa (Meander, 90°, 200 W, 130 μs) which is higher than listed values for wrought SS316L bar in ASTM A240/A240M. Showing higher energy leads to higher density an therefore higher UTS, until you begin to trade-off with roughness.

Higher energy density can refine substructures and reduce defects, and therefore increasing the hardness seen.

Mechanical properties show broader variability, both in average values and in standard deviations. Ductility (extension/strain-to-failure) ranges from extremely brittle responses around 0.75% to highly ductile outcomes approaching 40%, indicating that even small variations in energy density can strongly influence defect structures such as interlayer lack-of-fusion or pore morphology. As defects diminish with increased energy input, ductility improves correspondingly.

Both UTS and hardness exhibit the expected positive correlation with energy input. UTS increases up to 588 MPa, surpassing the typical wrought SS316L values provided in ASTM A240/A240M, highlighting the strengthening effect of refined

microstructures typical in AM builds. Hardness similarly rises to ~250 HV, higher than commonly reported for AM 316L, again reflecting higher energy density, reduced porosity, and finer substructures.

However, the standard deviation analysis reveals that not all parameter combinations produce reliable properties. Several 67° rotation builds show disproportionately large deviations in UTS, Young's modulus, and yield stress, indicating reduced repeatability. These inconsistencies likely stem from altered thermal histories and scan-vector interactions unique to the 67° rotation, suggesting that such configurations introduce microstructural variability. Notably, the parameters with the highest deviations differ across mechanical properties, implying that each property is sensitive to different process-induced features (e.g., porosity for ductility, sub grain structure for hardness).

Overall, the unaged powder results demonstrate that:

- Density is the most consistent property, even across different scan patterns.
- Mechanical properties are more variable, particularly for 67° rotations.
- Higher exposure times consistently produce denser, stronger, harder, and rougher components, highlighting a trade-off between surface quality and mechanical performance.

Table 5:1: Summary of Experimental Results Meander Laser Pattern

Rotation (°)	Laser Pattern	Laser Power (W)	Exposure Time (µs)	Roughness Side (µm)	Roughness Top (µm)		Theoretical Density (g/cm³)	Archimedes Density (g/cm³)	Extension (mm)	Strain to Failure (%)		UTS (MPa)		Hardness (HV)		Porosity (%)	Young's Modulus (GPa)		Yield Stress (MPa)	
						SD					SD		SD		SD			SD		SD
90	M	160	80	11.94	21.45	0.76	6.86	6.90	0.25	0.83	0.59	304	22.59	173	22.8	6.01	47.60	5.32	214	1.54
90	M	160	105	12.28	22.38	0.42	7.41	7.42	3.84	12.75	2.59	524	16.86	206	31.1		101.11	1.08	160	3.85
90	M	160	130	11.69	19.73	1.45	7.7	7.59	8.14	27.05	4.64	582	4.74	216	35.9		22.66	3.68	171	5.99
90	M	180	80	12.62	22.84	1.12	7.15	7.19	1.02	3.39	0.99	417	0.54	179	33.4		51.37	3.45	312	20.04
90	M	180	105	13.04	20.62	0.55	7.58	7.54	7.65	25.42	10.35	567	0.59	204	28.1	3.29	69.95	0.36	456	3.53
90	M	180	130	13.28	15.53	0.53	7.71	7.66	14.22	47.24	3.58	578	23.02	223	37.6		110.28	2.49	233	15.85
90	M	200	80	14.1	24.4	0.70	7.25	7.22	1.97	6.54	3.30	459	28.08	218	23.2		144.72	0.52	191	6.39
90	M	200	105	14.9	19.37	2.62	7.63	7.48	7.01	23.29	3.59	550	10.61	222	41.9		79.13	1.53	254	10.66
90	M	200	130	16.01	18.27	1.74	7.76	7.66	13.15	43.68	9.96	588	4.69	211	19.4	4.56	73.3	6.78	494	1.72
67	M	160	80	15.94	25.96	3.72	7.12	7.03	1.07	3.58	3.17	312	11.36	173	30.9	5.21	181.48	5.68	196	12.68
67	M	160	105	18.36	17.57	5.46	7.39	7.19	0.99	3.29	0.77	352	4.49	143	44.7		46.82	9.26	245	3.50
67	M	160	130	16.57	17.72	3.31	7.6	7.46	2.35	7.83	0.38	452	6.25	190	33.5		54.87	3.28	275	17.47
67	M	180	80	18.93	15.84	5.96	7.57	7.42	1.12	3.73	0.92	398	52.11	172	43.1		177.72	1.48	189	2.83
67	M	180	105	19.34	13.72	3.25	7.75	7.61	2.08	6.94	4.81	500	24.16	201	34.6	2.54	61.3	6.40	434	37.89
67	M	180	130	19.16	13.05	2.45	7.85	7.65	4.28	14.26	2.67	518	21.88	202	28.7		88.57	3.79	292	10.89
67	M	200	80	20.1	14.4	3.14	7.8	7.62	7.67	25.58	2.51	543	14.70	207	35.8		91.2	2.49	451	5.82
67	M	200	105	20.21	14.73	2.54	7.87	7.66	6.13	20.43	17.10	390	8.03	206	33.4		232.74	7.18	135	1.68
67	M	200	130	18.02	11.33	0.55	7.91	7.55	8.48	28.26	3.42	556	2.04	214	18.9	0.87	83	12.76	481	14.79

Table 5:2: Summary of Experimental Results Stripe Laser Pattern

Rotation (°)	Laser Pattern	Laser Power (W)	Exposure Time (µs)	Roughness Side (µm)	Roughness Top (µm)		Theoretical Density (g/cm^3)	Archimedes Density (g/cm^3)	Extension (mm)	Strain to Failure (%)		UTS (MPa)		Hardness (HV)		Porosity (%)	Young's Modulus (GPa)		Yield Stress (MPa)	
						SD					SD		SD		SD			SD		SD
90	S	160	80	12.49	20.78	1.93	7.08	6.95	0.13	0.43	0.74	290	16.57	162	45.7	7.49	75.64	1.47	160	10.52
90	S	160	105	11.88	18.3	1.01	7.59	7.46	1.64	5.46	4.63	477	10.74	233	12.0		86.96	0.26	157	4.81
90	S	160	130	12.43	17.01	1.73	7.79	7.67	5.19	17.23	1.99	547	19.04	249	10.9		135.36	10.39	103	5.75
90	S	180	80	14.33	19.93	2.87	7.4	7.21	0.89	2.96	1.23	383	12.87	191	56.0		78.81	5.70	187	1.49
90	S	180	105	13.65	13.5	1.98	7.74	7.59	2.36	7.83	3.33	493	15.57	205	46.1	5.63	88.59	3.69	120	16.20
90	S	180	130	14.25	12.87	2.76	7.83	7.69	9.36	31.10	2.43	530	30.59	219	35.8		144.82	22.54	354	3.85
90	S	200	80	12.96	19.05	5.71	7.5	7.31	0.48	1.59	1.45	383	14.83	226	27.5		109.29	6.79	133	7.26
90	S	200	105	16.78	16.55	2.41	7.83	7.58	1.89	6.29	10.23	492	11.57	232	9.3		64.16	2.85	396	11.83
90	S	200	130	16.83	14.76	2.96	7.79	7.61	7.75	25.75	3.08	518	24.48	229	13.0	4.38	146.78	17.02	247	3.69
67	S	160	80	15.44	26.85	3.07	6.67	6.76	0.58	1.94	1.74	211	30.94	125	46.5	11.09	46.09	36.21	127	2.84
67	S	160	105	16.85	22.52	2.20	6.85	6.80	0.79	2.64	1.83	237	48.69	151	48.6		76.57	22.50	109	5.29
67	S	160	130	18.59	24.21	3.64	6.95	6.79	1.43	4.77	1.21	297	17.21	150	64.2		26.27	7.07	217	3.74
67	S	180	80	16.84	17.74	2.72	7.04	6.95	1.00	3.34	1.07	311	9.30	193	34.5		85.46	3.89	158	24.81
67	S	180	105	16.25	18.19	1.49	7.19	7.18	1.43	4.78	3.55	347	9.13	170	44.8	0.63	57.06	14.59	117	10.73
67	S	180	130	17.96	20.39	3.69	7.23	7.34	1.40	4.66	0.84	350	17.32	214	13.6		35.16	3.60	267	6.25
67	S	200	80	17.98	22.11	1.83	7.4	7.41	1.90	6.34	2.65	313	1.06	194	42.5		49.39	12.47	289	15.29
67	S	200	105	17.55	26.17	2.83	7.48	7.53	2.44	8.13	4.39	459	5.14	199	39.6		70.84	1.28	403	2.74
67	S	200	130	21.09	26.63	1.99	7.54	7.59	3.00	10.00	6.20	403	73.40	197	34.5	1.52	47.12	3.40	295	5.39

5.2.2 Aged Samples

Table 5:3: Summary of Experimental Results As Built

Build	Rotation (°)	Laser Pattern	Laser Power (W)	Exposure Time (µs)	Build Direction	Extension (mm)	Strain to Failure (%)	UTS (MPa)	Young's Modulus (GPa)	Yield Stress (MPa)	Roughness (µm)
17	67	Meander	200	80	Vertical	10.33	34.43	615	3584.221	195	11.9
17	67	Meander	200	80	Vertical	8.2	27.33	612	4031.413	223	
18	67	Meander	200	80	Vertical	10.76	35.87	625	3084.583	194	10.39
18	67	Meander	200	80	Vertical	10.64	35.47	623	3161.676	191	
18	67	Meander	200	80	Vertical	10.3	34.33	629	1975.975	329	
18	67	Meander	200	80	Vertical	10.97	36.57	627	2877.177	247	
18	67	Meander	200	80	Horizontal	2.2	7.33	593	3317.391	212	
18	67	Meander	200	80	Horizontal	1.92	6.40	617	3646.147	274	13.54
21	67	Meander	200	80	Vertical	10.79	35.97	628	2838.297	216	
21	67	Meander	200	80	Vertical	11.76	39.20	622	2054.334	271	
21	67	Meander	200	80	Vertical	11.63	38.77	630	2183.728	159	
21	67	Meander	200	80	Vertical	10.38	34.60	634	2043.751	312	9.97
21	67	Meander	200	80	Vertical	10.52	35.07	624	3720	120	
21	67	Meander	200	80	Vertical	11.57	38.57	637	5315.789	167	13.25
21	67	Meander	200	80	Vertical	11.06	36.87	628	3105.424	185	10.37
21	67	Meander	200	80	Vertical	10.81	36.03	633	3105.769	249	
21	67	Meander	200	80	Vertical	12.3	41.00	620	2991.291	149	
21	67	Meander	200	80	Vertical	11.6	38.67	628	3396.525	144	

Table 5:4: Summary of Experimental Results Heat Treatment 1

Build	Rotation (°)	Laser Pattern	Laser Power (W)	Exposure Time (µs)	Build Direction	Extension (mm)	Strain to Failure (%)	UTS (MPa)	Young's Modulus (MPa)	Yield Stress (MPa)	Roughness (µm)
17	67	Meander	200	80	Vertical	10.95	36.50	645	7420.494	227	6.69
17	67	Meander	200	80	Vertical	9.73	32.43	627	6299.941	198	
18	67	Meander	200	80	Vertical	10.5	35.00	646	4453.672	122	
18	67	Meander	200	80	Vertical	12.06	40.20	637	2884.939	144	8.26
18	67	Meander	200	80	Vertical	11.31	37.70	642	3559.01	180	
18	67	Meander	200	80	Vertical	11.02	36.73	650	2827.392	156	
18	67	Meander	200	80	Horizontal	2.41	8.03	636	2819.621	259	9.14
18	67	Meander	200	80	Horizontal	1.52	5.07	571	3363.034	294	
21	67	Meander	200	80	Vertical	11.44	38.13	636	2299.734	353	
21	67	Meander	200	80	Vertical	11.77	39.23	634	3259.593	124	
21	67	Meander	200	80	Vertical	11.3	37.67	642	2450.413	340	7.57
21	67	Meander	200	80	Vertical	10.97	36.57	648	2859.824	323	7.52
21	67	Meander	200	80	Vertical	11.32	37.73	560	3028.673	246	
21	67	Meander	200	80	Vertical	10.19	33.97	629	4842.993	130	
21	67	Meander	200	80	Vertical	9.63	32.10	640	2450.575	265	
21	67	Meander	200	80	Vertical	11.02	36.73	642	2879.432	205	10.22
21	67	Meander	200	80	Vertical	8.79	29.30	641	3422.742	273	
21	67	Meander	200	80	Vertical	11.76	39.20	635	3045.659	231	

Table 5:5: Summary of Experimental Results Heat Treatment 2

Build	Rotation (°)	Laser Pattern	Laser Power (W)	Exposure Time (µs)	Build Direction	Extension (mm)	Strain to Failure (%)	UTS (MPa)	Young's Modulus (MPa)	Yield Stress (MPa)	Roughness (µm)
17	67	Meander	200	80	Vertical	15.63	52.10	586	3237.212	264	7.91
17	67	Meander	200	80	Vertical	15.71	52.37	586	3457.925	186	
18	67	Meander	200	80	Vertical	10.73	35.77	626	4636.079	269	
18	67	Meander	200	80	Vertical	12.25	40.83	611	3289.315	213	6.35
18	67	Meander	200	80	Vertical	12.82	42.73	619	3119.881	255	9.99
18	67	Meander	200	80	Vertical	12.31	41.03	622	3428.21	245	
18	67	Meander	200	80	Horizontal	3.22	10.73	568	3178.697	211	
18	67	Meander	200	80	Horizontal	3.85	12.83	606	3415.864	325	
21	67	Meander	200	80	Vertical	13.31	44.37	591	7575.488	129	
21	67	Meander	200	80	Vertical	15.01	50.03	592	5247.674	254	10.1
21	67	Meander	200	80	Vertical	13.8	46.00	582	4084.405	220	10.7
21	67	Meander	200	80	Vertical	14.25	47.50	601	3736.046	223	
21	67	Meander	200	80	Vertical	12.47	41.57	576	2967.801	155	
21	67	Meander	200	80	Vertical	13.39	44.63	568	3456.2	165	
21	67	Meander	200	80	Vertical	13.68	45.60	565	3569.653	192	
21	67	Meander	200	80	Vertical	14.47	48.23	573	3375.979	156	9.16
21	67	Meander	200	80	Vertical	14.06	46.87	593	3278.664	271	
21	67	Meander	200	80	Vertical	13.99	46.63	580	3389.536	258	

The results from aged powder Table 5:3, Table 5:4 and Table 5:5 show a contrasting picture, where powder aging appears to have minimal influence on core mechanical properties such as UTS, yield stress, and Young's modulus. This reinforces that AM 316L powder is resilient to aging effects under the conditions tested, and that microstructural consolidation remains predominantly governed by build parameters rather than powder history.

The standard deviation for the density was negligible and has not been shown here.

These results from the aged powder investigation show heat treatments introduce clear behavioural changes:

- Heat treatment 1 at 450°C has a stress relief effect having little effect on ductility, slight increase in the UTS and yield stress and reduced roughness. Showing low temperature temper mitigates residual stress with little microstructure change.
- Heat treatment that matches HIPping, without the pressure, has an effect on the UTS and yield stress reducing both of these.
- Heat treatment 2 reduces the UTS but increases the strain to failure and extension. Showing a high temperature treatment softens the microstructure and removes the grain boundaries and heals defects.

Overall, these treatments reveal a fundamental trade-off:

- Lower-temperature treatments favour strength and surface finish,
- High-temperature treatments favour ductility and defect healing,

illustrating the dual role of heat treatment in both microstructure evolution and mechanical tailoring.

5.2.3 Build Programme 3

The results that have been achieved during BP3 are shown in Table 5:6. These extend the earlier observations by evaluating heat treatments more systematically and introducing elevated-temperature tensile tests.

It was intended during this build programme to also carry out high temperature tensile testing (500°C) but due to machine issues only one successful test was carried out. Therefore, although these results have been included, no further investigation has been carried out as there are no comparisons available. B2 and B4 results are also missing due to machine data loss. As three samples were still pulled for as built which allows

for a SD to be calculated. These results have been included and can be compared to the as built samples previously tested. Despite some data loss and limited high-temperature testing, several consistent patterns emerge.

First, the as-built samples show the lowest variability, reinforcing earlier findings that the baseline process produces stable mechanical properties when parameters are fully controlled. The standard deviations (SD) are low for the strain to failure with HT1 samples showing the biggest SD. This is the same for the UTS and HT1 having the biggest deviation, these results show the largest variation and suggest these aren't consistent. Low standard deviation means consistency of results and therefore these are the parameters and treatments that produce the most consistent components from manufacture.

Heat treatments, although beneficial in some respects, introduce additional sources of variability, particularly for Young's modulus, where standard deviations range from 30–82%. This suggests that heating cycles alter microstructure in ways that are not fully uniform across samples.

The most notable behavioural trends include:

- High-temperature treatments (1125–1150°C) reduce UTS but significantly affect ductility. Interestingly, the ductility reductions seen here contradict those from BP2, indicating that the outcomes are sensitive to subtle differences in build history, thermal exposure, or even location-specific microstructures.
- HIP-type cycles mirror this behaviour, reducing strength and lowering strain to failure relative to as-built, again highlighting potential discrepancies from the earlier programme.
- Surface roughness remains almost entirely unaffected by heat treatment, suggesting that roughness is governed almost exclusively by build parameters. The consistent average roughness of ~7.74 μm reflects strong stability in surface morphology across treatments.

Table 5:6 Summary Table Build Programme 3

Rotation (°)	Laser Pattern	Laser Power (W)	Exposure Time (µs)	Heat Treatment	Extension (mm)	Strain to Failure (%)	Average Strain to Failure (%)	UTS (MPa)	Average UTS (MPa)	Young's Modulus (MPa)	Average Young's Modulus (MPa)	Yield Stress (MPa)	Average Yield Stress (MPa)	Roughness (µm)
90	M	200	80	As Built	13.2	52.8	52.0933 (SD 4.11)	623	619 (SD 4.04)	1049.5	1771.53 (SD 1050)	331	338 (SD 52.32)	7.3
90	M	200	80	As Built	11.92	47.68		620		1288.4		393		8.33
90	M	200	80	As Built	13.95	55.8		615		2976.7		289		7.5
90	M	200	80	HTTT (500°)	4.59	18.36								9.86
90	M	200	80	HT1			47.29 (SD 7.89)	579	583 (SD 10.93)	1845.6	2080.1 (SD 501)	322	302 (SD 17.14)	7.74
90	M	200	80	HT1	14.06	56.24		571		1676		299		7.81
90	M	200	80	HT1	12.16	48.64		576		1725.9		292		8.03
90	M	200	80	HT1	9.26	37.04		596		2867.5		317		7
90	M	200	80	HT1	11.81	47.24		593		2285.5		281		8.78
90	M	200	80	HT2			51.21 (SD 3.52)	612	615 (SD 3.36)	1525.6	1568.38 (SD 186)	339	336 (SD 31.54)	7.58
90	M	200	80	HT2	13.5	54		617		1562.6		303		6.54
90	M	200	80	HT2	13.6	54.4		612		1341.7		387		9.21
90	M	200	80	HT2	11.85	47.4		618		1860.3		331		7.1
90	M	200	80	HT2	12.26	49.04		619		1551,7		320		6.61
90	M	200	80	HT3	14.64	58.56	53.08 (SD 3.83)	588	587 (SD 3.11)	1981.1	2109.1 (SD 196)	322	292 (SD 31.32)	6.82
90	M	200	80	HT3				589		2059.9		311		7.59
90	M	200	80	HT3	12.4	49.6		582		2399.8		283		7.24
90	M	200	80	HT3	12.97	51.88		587						8.96
90	M	200	80	HT3	13.07	52.28		590		1995.6		252		7.86
90	M	200	80	HIP Cycle			50.76 (SD 4.17)							7.82
90	M	200	80	HIP Cycle	14.16	56.64								7.31
90	M	200	80	HIP Cycle	12.61	50.44								7.09
90	M	200	80	HIP Cycle	12.25	49								7.84
90	M	200	80	HIP Cycle	11.74	46.96								7.83

In summary, Build Programme 3 demonstrates that:

- Heat treatments improve property consistency (lower SDs), even when average properties shift.
- High-temperature cycles have the most profound effect, softening microstructures and moderating strength.
- Surface quality is dominated by build conditions, not post-processing.

5.2.4 Overall Comparison of Results

To achieve maximum strength & density, with acceptable roughness, the following parameters are best Meander laser pattern, 90° rotation, 200 W laser power and 130 µs exposure time. Giving an expected UTS around 585–590 MPa, density 7.6–7.7 g/cm³ and top surface roughness between 15–18 µm.

To achieve the highest ductility, you need to use a higher exposure time and high-temp anneal, HT2,) generally increasing elongation up to 25%.

If you need the tightest mechanical consistency, use 90° rotation to achieve this.

Yield stress is affected by heat treatment, HT3 was most detrimental to yield stress reducing but 22% when compared to as built. HT2 and as built keep yield stress similar; HT1 reduces yield stress by 12% in BP3. Therefore, you need to choose the heat treatment route carefully based on your yield stress requirement.

Roughness is dominated by build parameters, not heat treatment. Across BP3, roughness averaged 7.4–8.0 µm and showed little shift with heat treatment. In the broader unaged set, exposure time drives roughness upward; address via post-processing or scan strategy tuning.

5.3 UTS and Mechanical Performance

For tensile testing the known typical UTS for SS316L at room temperature is 565 MPa [169]. It is known that for the vertical samples, the tensile strength is lower when the force being applied is normal to the layer formation [141]. Previous work has found that SLM samples have much higher yield strength and UTS when compared to wrought samples [144]. This does not match with what was found for most of the original samples tested which is believed to be due to the variations in build parameters. But it does match with what was found within the second and third set of samples all built during this work using the best parameters, again reinforcing the importance of selecting the correct build parameters.

AM SS316L components were produced under varied build strategies encompassing the scan pattern, meander and stripe, and layer rotations, 90° and 67°, with comparative studies of virgin and aged/recycled powder and post-build heat treatments. Input energy was used as a practical integrator for comparing process settings with different point distances and hatch spacings, acknowledging that it is an incomplete descriptor of melt-pool dynamics. Density was assessed by Archimedes and theoretical estimations, and porosity by metallography, with tensile testing aligned to assess UTS, yield strength, and ductility. Fracture surfaces were examined to interpret failure mechanisms.

5.3.1 Influence of Build Strategy (Pattern and Rotation)

For the 90° rotation samples the result for the best meander sample is 588.9MPa. This is comparable to rolled SS316L. This comparable result suggests that the parameters of 90° layer rotation, meander laser pattern, 200W laser power and 130µs produce a centre of the tensile bar, which has minimal if not zero pores and high strength between grains. A potential reason for this could be the increased re-melting of the lower layers due to the pattern the laser follows.

The tensile test results showed there is a difference in the UTS between the two different laser patterns. The results also show that the meander pattern has two results that show comparable UTS to rolled material whereas the stripe pattern has none that are higher.

For the 67° rotation samples the UTS for the best meander sample was 556MPa for the first set of samples and this is almost the same as rolled SS316L, but not as high as the 90° rotation samples. When looking at the results for BP2 and BP3 an improvement in UTS was achieved to 650MPa and 620MPa respectively, showing the need for optimum parameters to achieve best performance. Figure 4:58 and Figure 4:72, look at the fracture surface of two different samples. Both show cohesion between particles rather than scan tracks, this is likely to show that using the higher exposure time and laser power has led to increased melting of the powder and stronger cohesion between layers, explaining the increased UTS. These results show that almost all of the samples tested exceed the minimum yields stress and UTS stated by ASTM 240 [47], but the consistency across all parameters needs to be carefully considered so that all parameters are met.

When looking at the density compared to the UTS Figure 4:38, it is possible to see that as the density increases the UTS also increases for the 90° layer rotation. This

trend is not seen for the 67° layer rotation samples. This may be due to inclusions, unmelted powder particles or lack of fusion within the 67° layer rotations builds that have caused the samples to fail earlier than the samples with the higher density.

Figure 4:122, Figure 4:123, Figure 4:124 and Figure 5:1 show stress vs strain graphs for the aged powder samples.

From these graphs, it is possible to see how the UTS and yield stress has increased with builds. As the build numbers increase a corresponding increase in the UTS is noticeable. Renishaw's investigation into this shows this is a given due to the increase in interstitial oxygen and nitrogen levels as the powder has been re-used as described [40].

Figure 4:68 shows a sample that failed before reaching its UTS. This sample failed between the layers and the maximum stress found shows the maximum UTS between those layers had been exceeded. This result shows that although there is incomplete melting between certain layers there is still sufficient bonding between these particles for the strength of the sample to exceed the minimum required UTS from ASTM A240/A240M [47].

It has been previously mentioned that there may be an effect on the properties of parts with variations seen between different areas of the build plate. Work carried out in [170] drew the conclusion that tensile properties are consistent independent of build location on the plate.

5.3.2 Input Energy's Effect

When looking at different build parameters the easiest way to cross-reference is to look at the laser's energy applied to the parts. Due to the changes in point distance and hatch spacing there is not an exact match between laser energies used for all of the build programmes and samples tested, 48.048 J/mm^3, this was the value used for BP2 and BP3, when comparing to the original samples but if you compare to the closest input energies it is possible to see that the new samples still exceed the UTS found for those. In fact, the BP2 samples are more than 10% better than the original samples and the BP3 samples 6% better.

Table 5:7: Input Energy vs UTS

Input Energy (J/mm³)		46.90	48.048 BP2	48.048 BP3	51.91
UTS (MPa)	**Meander 90**	567	N/A	N/A	582
	Stripe 90	493	N/A	N/A	547
	Meander 67	500	650	619	542
	Stripe 67	347	N/A	N/A	297

Table 5:7 shows that the variation in UTS obtained from similar input energies can vary substantially, with BP2 and BP3 showing a variation of 30MPa. It shows that although most exceed 500MPa only two exceed 600MPa and two are below 400MPa. This observation shows that input energy is not the only factor affecting the variations in UTS seen.

5.3.3 Density and Porosity Effects on UTS

As expected [220] the theoretical densities do not match the measured Archimedes densities but the trends shown in the results are the same for both density measurements, as seen in Table 5:1, Table 5:2, Table 5:3, Table 5:4, Table 5:5 and Table 5:6. The theoretical density tends to be larger than the Archimedes density with the 67° rotation samples showing higher densities for both Archimedes and theoretical density. The highest density found was 7.69g/cm^3, which is only 0.31g/cm^3 lower than expected but equates to a porosity of 3.9%. This reduction from conventional material is to be expected due to the gas pores found within AM parts, the powder packing before solidification and the shrinkage that occurs during the build process.

The porosity of the cubes has been shown not to correspond to the densities found. This could be because the porosity was hard to accurately measure as it varied so much across one sample. Only one layer of the sample was studied to obtain the porosity, whereas the Archimedes density is an average of the entire cube. To obtain a higher accuracy porosity, an in-depth study taking the average of a number of layers would need to be performed, the greater the number of slices the higher would be the accuracy of the results. As the density reduced the porosity was not seen to reduce at the same rate. The porosity was seen to be up to 8% higher than the density suggested it should be.

When looking at the reasons for the change in density and porosity for the different samples within the build sets, the 90° rotation samples shown in Figure 4:8, Figure 4:13 and Figure 4:80 help to explain them. Some of the images show why there is a

higher porosity within the samples and why the samples' densities are lower than those of conventionally manufactured SS316L. From Figure 4:39 and Figure 4:40, the laser pattern is not completely defined and in particular, it can be seen in Figure 4:39 that the pattern is not continuous and it is variable. The top layer contains pores through the layers and between the melt tracks suggesting that using these build parameters will give parts with lower mechanical properties than the ones of rolled SS316L with a higher porosity.

Figure 4:41 of the lowest density parts shows the gaps between the tracks in a microstructure image. It can also be seen here that these layers contain large amounts of unmelted powder and air pockets. These pores are highlighted in Figure 4:41. What needs to be understood about the pores present is what size matters and what size can we see. Although we have studied all pores seen in these images it may be that the smaller pores don't influence the parts performance and so don't need to be investigated or counted.

The comparison between the percentage size change and the density percentage change shows no correlation, with a number of parts being larger than expected, Table 5:1 and Table 5:2. This is due to the percentage size change in most cases producing parts that have a volume larger than the comparison size whereas the density change has been shown to be lower in all cases when comparing to the density of a 10mm cube of SS316L. This is likely to be as the pores within the parts are affecting the density, but they do not affect the overall size of the cube.

When comparing the surface of AM SS316L and sheet SS316L, Figure 4:39, Figure 4:40, Figure 4:1 and Figure 4:2, it is possible to see why the properties change as the surface of the sheet metal shows none of the voids, which can be clearly seen on the AM cubes.

Figure 4:38 shows how the densities of the samples have varied when compared to the achieved UTS. This shows that as the density improves so does that UTS. This is expected since lower density means more pores and defects which would lead to reduced UTS [221]. Increases in the density has led to samples closer in composition to conventional SS316L and therefore increases UTS.

Archimedes and theoretical densities, Tables 4.4 to 4.8 showed consistent trends: higher density correlated with higher UTS Figure 4:38. The highest measured density was 7.69 g/cm³ (≈3.9% porosity). Micrographs Figure 4.97, Figure 4.98 and Figure 4.99 reveal that discontinuous or poorly defined tracks, unmelted particles, and

inter-track voids reduce density and thus UTS. Notably, this correlation was strong for 90° rotation but weaker for 67°, likely due to localised inclusions, lack-of-fusion defects, or unmelted particles dominating failure in some specimens.
The 2D metallographic porosity sometimes exceeded Archimedes inferred porosity by up to 8%, underscoring the need for multi-slice quantification to reduce sampling error.

5.3.4 Effect of Powder History (Aged vs Virgin)

The results show that using aged powder has led to an increase in the UTS of the samples produced. The results show that except for one horizontal sample all samples' UTSs exceeded 600MPa, i.e., they all exceed UTS values of conventionally manufactured SS316L. These results for aged powder, using what has been seen to be the best build parameters all exceed those produced using 'virgin' powder which had a maximum of 588.9MPa. The results also show that the third (build 21) of the aged (recycled) powder builds showed increased UTS when compared to the first (build 17) of the aged powder builds. The results increased from 612MPa (build 17) to between 620MPa to 637MPa (build 21).

This increase in UTS could have been caused by the continual sieving without the introduction of 'virgin' powder leading to more particles that are smaller in size which in turn means they are able to pack better as each layer is laid down. Although the PSD showed the powder distribution did not vary greatly between each build, but this doesn't show fines. Also continual reuse has been shown to remove fines that are present in 'virgin' powder [171]. It was seen in this work that there was an observable reduction in fines, but the powder morphology showed very little change. With this happening there are going to be less pores present within the parts which in turn will give a high strength to the part. This theory is further validated by the microstructure images, Figure 4:113, Figure 4:114 and Figure 4:115 where it is possible to see that there are little to no pores present within the samples when compared to the previous samples including Figure 4:111.

Tang et al. [170] saw that for powder reuse the oxygen content increased, the PSD reduced and that although the powder changed shape there were fewer satellite particles and powder flowability was improved. It was concluded from this research that there was no measurable undesired effect on AM parts. This matches with what has been found in this work where the UTS has increased which is a desirable effect

resulting in stronger material. These findings are also noted by Sartin et al. [161] who reused powder 12 times to produce 31 builds. It found that powder that had been affected by the process was removed by sieving and there was no consistent statistical variation in the properties observed.

The results have shown that recycled powder used within this work has improved the UTS slightly, approximately 20MPa. This is likely due to the number of times it has been reused being low enough to not significantly affect the powder quality and the powder degradation being minimal. Images show that there is little variation in the microstructure across the builds confirming there hasn't been significant powder degradation and explaining why the UTS has remained consistent.

5.3.5 Heat Treatment (HT) Influence on UTS

The variations in UTS seen for the samples following heat treatment helps to prove that heat-treating can produce parts with improved properties. The UTS for the samples with heat treatment 1 applied has led to an increase from the as built aged powder samples. The increases are higher in the first set of as built samples (build 17), increasing from 612MPa to 627MPa, than for the other two builds where an increase was still seen for most samples, but this was not as significant an increase.

Figure 4:122 and Figure 5:1 show how the yield strength has decreased with the heat treatment but strain to failure has increased. When looking at Figure 4:64 and Figure 4:65 which shows similar fracture initiation sites across HT1 and HT2 samples, it's also possible to see how the necking is more pronounced and the fracture occurs at a steep angle across the part when HT2 has been applied. Heat treatment helps refine grains which can reduce the strength but improves the ability to withstand long-term deformation under a constant load increasing the strain to failure.

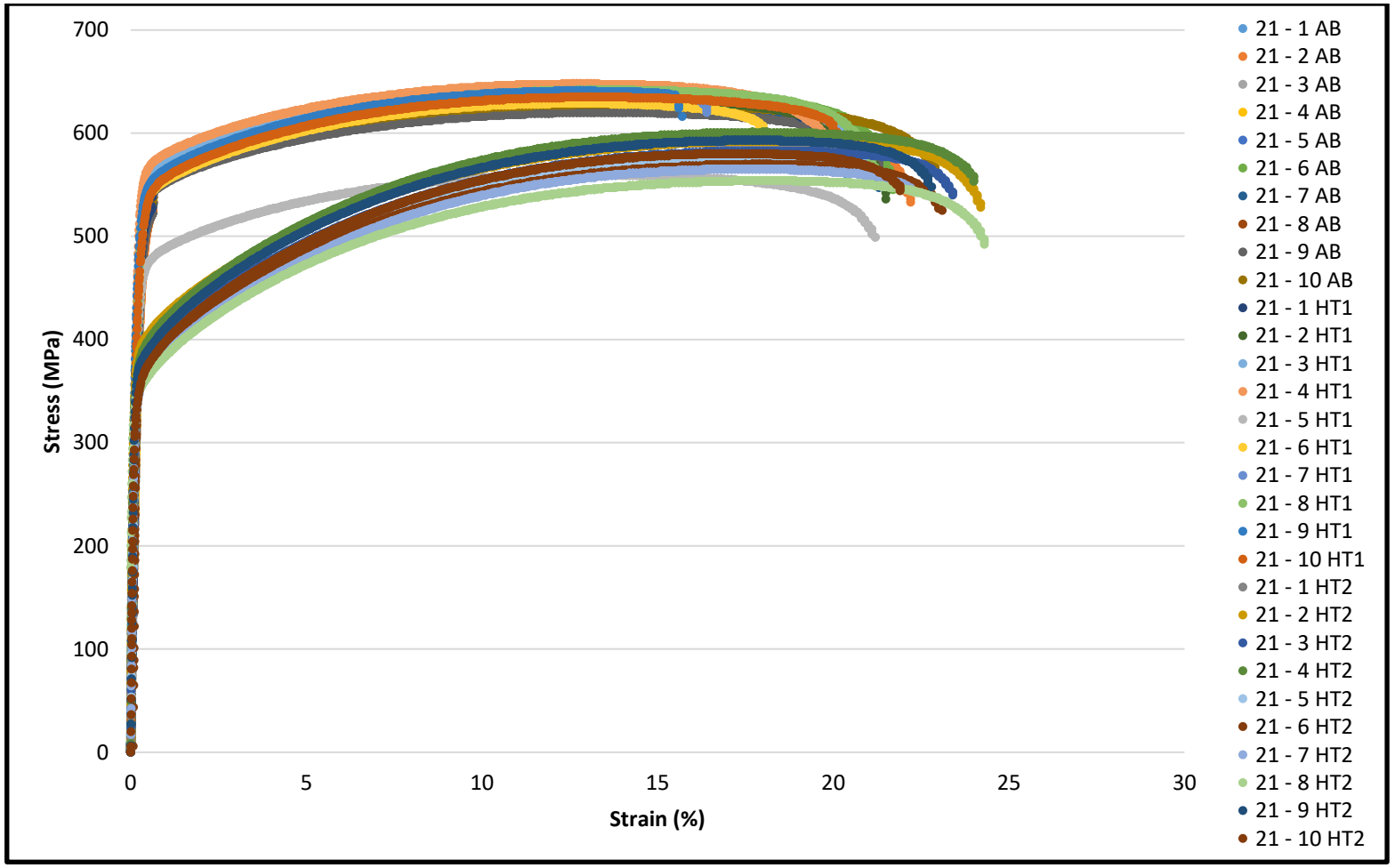

Figure 5:1:Stress vs Strain for Build 21 Samples

The microstructure in Figure 4:114 and Figure 4:115 show that after heating the grains sizes have grown in length when compared to Figure 4:113 and the grains are longer in the build direction. In this case using consistent laser settings during the build process it has been found that all samples produced in the vertical direction have been shown to have a yield stress and UTS that exceeds the minimum required by ASTM 240 [47]. The six samples tested that have been manufactured in the horizontal direction have been found to exceed these minimums; however, the extension has been shown to be much lower than the minimum of 40%. This is likely to have occurred because these samples have been found to fracture at an initial failure point where there is already a defect on the surface due to remnants from the build support. This shows that all horizontal built samples should have a finishing process applied to them to ensure that these initiation points are not present during testing.

Appling heat treatment 2 to the samples has lowered the yield stress meaning these samples will elastically deform less and require lower energy to cause plastic deformation, meaning these samples are more likely to deform. The microstructure for these samples, Figure 4:115 shows elongated grains in the build direction showing the heat treatment has allowed the grains to recrystallise in the direction of manufacture and therefore testing.

The larger grain sizes are in line with the direction of the applied force, seen within the heat-treated samples; grain sizes in this orientation are likely to be the reason for the reduced yield stress and UTS. Dislocations move easily through grains but once the dislocations reach a barrier like a grain boundary there is nowhere for it to go [172]. This then slows down the rate of propagation of the crack as it changes direction and tries to continue growing [129]. Therefore, in the larger grains, especially when the grain is long in the direction of the applied stress, these dislocations will move freely causing a greater amount of plastic deformation.

Macroscopic plastic deformation as seen in Figure 4:71 and Figure 4:72 is the result of movement of a large number of dislocations. This is because the ability of a metal to deform plastically requires dislocations to move [129]. To improve the tensile strength and hardness of a part the dislocations ability to move needs to be reduced.

Dislocations are introduced during solidification, they move along the slip planes during failure [129]. It is likely occurring in AM samples that there are a higher number of slip planes due to the layers built up during the process. A critical resolved shear stress is then required to initiate a slip plane and cause failure. Dislocations are

a sign of a ductile material and lead to plastic deformation; they require low energy to move them but higher energy to fracture them.

The decrease from heat treatment 1 in yield stress with heat treatment 2 is suggested to be caused by a decline in α' fine needles to a more coarse α and β mix [90]; these may mean that the α' fine needles were acting as a dislocation barrier and the now more coarse α and β mix is less of a barrier.

When comparing to heat treated parts all failures look like ductile failures when studying the fracture surface. When looking at the stress vs strain graphs there are differences though. Although these consistencies in failure modes are likely due to consistent build parameters, it shows that variations across the build plate may not affect the microstructure and failure mode.

Investigations by other groups into the effect of heat treatment have shown similar results to those found here. Montero Sistiaga et al [144] noted that with heat treatment the microstructure was affected as was seen in this work but found that the yield stress reduced whereas in this work the yield stress was seen to increase slightly with heat treatment 1.

Strain hardening is the hardening of a metal in the plastic regime of deformation, the microstructure which affect strain hardening, can be modified by heat treatment. It would be interesting to see if the strain hardening behaviours of the material are being adversely affected when using heat treatment to adjust the yield stress of a part.

During BP3 HT1 reduced the parts elongation whereas HT2 and HT3 increased it. This is due to the changes to the microstructure not occurring during HT1 and the slip movement being decreased.

When looking at the surface particles, it is possible to see that as a heat treatment has been applied it has affected the particles and the surface condition has changed from the smooth surface seen on unheated powder to a mottled effect, Figure 4:34, Figure 4:35 and Figure 4:36. This is likely due to the effect of the heating. If this is happening on the surface and the particles start to shrink due to heating it is also likely to be happening within the samples. This could lead to the closure of pores and be the reason for increasing the UTS of heat-treated parts [168].

5.3.6 HIP vs Heat Treatment vs As-Built

Section 4.9 talks about samples that have been HIPped and the comparison to unHIPped parts. In [165] it was shown that HIPping a part has an effect on the properties and that further work needs to be carried out on this. Current theory is that

pores collapse, reducing the bulk porosity to below 1%, creates a more supportive microstructure [165]. Figure 4:126 when compared to Figure 4:122, Figure 4:123, Figure 4:124 and Figure 5:1, show that when comparing HIPped to heat treated samples the UTS is increased for HIPped samples. This is likely due to the pressure applied during the HIPping process and this fully closing any pores within the material.

This work will need to include the aged powder study in the future. The samples for HIPping are not available to test currently. The heat treatment used here has not been optimised for these SS316L AM parts.

5.3.7 Anomalies and Early Failure

Some specimens, for example Figure 4:56, failed between layers before reaching material UTS, indicating that the interlamellar UTS was exceeded while bulk microstructure remained intact. While this emphasises the importance of interlayer bonding, many such samples still exceeded the ASTM A240/A240M minimum UTS [47]. Prior work [170] suggests tensile properties are consistent across build-plate locations; the present results support that process parameters dominate over location effects.

5.3.8 Practical Implications, Parameterisation and Quality Control

When looking at the results found in this work you are able to see and understand what controls what and how to optimise the build parameters for the best component properties.

The scan strategy it's preferred to use meander over stripe and use inter-layer rotation (90° or 67°) with exposure sufficient for track overlap and partial remelting of the prior layer, minimising lack-of-fusion.

For energy tuning, treat input energy as a screening variable, then refine point distance, hatch spacing, and scan order to suppress discontinuities in melt tracks.

On the powder lifecycle, it is necessary to implement controlled reuse and sieving; track oxygen/nitrogen and PSD; expect stable or improved UTS at moderate reuse counts when fines are reduced and flowability is maintained.

For post-processing, apply HT1/HT2-type treatments where increased ductility and stable UTS are required; monitor yield changes and fracture morphology for qualification.

For metrology, it is necessary to pair Archimedes density with multi-slice porosity and fractography; to correlate density/defect metrics with UTS to validate process windows.

5.3.9 Summary

Across all parameters, the mechanical response of AM SS316L reflects a complex interplay between; the scan strategy (pattern, rotation), thermal input, material condition (powder reuse) and post-processing (heat treatment).

The strongest materials emerged from combinations that:

- maximise re-melting between layers,
- minimise porosity and unmelted particles,
- and maintain stable powder characteristics over multiple build cycles.

Overall, with process optimisation, AM SS316L can reliably meet or exceed the performance of conventionally manufactured material.

5.4 Microstructural Influence on UTS

Figure 4:101, Figure 4:102, Figure 4:113, Figure 4:114 and Figure 4:115 show the microstructure found within AM parts and the extent to which it differs from that found in rolled SS316L, Figure 4:1. In contrast, rolled SS316L has a homogeneous microstructure where all grains are below 50μm in size. The AM parts however have an irregular grain size and shape with some being over 50μm in size.

It is also possible to see that the grains in the AM parts grow between melt pools showing that the melt track is solidifying after the next melt pool has been created. This could cause microstructural defects leading to the reduced UTSs observed in this work. The microstructure has been seen to vary across the layer of a selection of samples, Figure 4:101 and Figure 4:102. For the lower laser powers, the images do not show the melt pool, whereas for the higher laser power and exposure time images, this is clearly defined. It is also possible to see that the grains vary in size and shape and with no consistent pattern, although the larger grains appear to be present when using the lowest laser power and exposure time. This suggests that these parts took the longest to cool and have the lowest UTS. This proves that larger grains lead to lower strength, and it corresponds to the known fact that strength is increased by reducing grain size [129].

5.4.1 Through-Layer Grain Growth and Texture

The microstructure shown in Figure 4:104 and Figure 4:105, shows how the microstructure grows through the layers, this growth through the layers is likely affecting the properties of samples built in different directions. Where there are fully formed grains growing through the layers and across the layer, the UTS has been seen to increase and this is likely due to this “three dimensional” grain formation. Where grains have been shown to be confined to individual layers, the increase in UTS has not been seen. Again, the lower laser power and exposure time samples have been shown to the have larger wider grains and lower UTS values. Thus, for improved UTS then one must ensure that grain growth must encompass multiple build layers, however, one must be careful not to enlarge grains to the point of detriment of the UTS of the material. When comparing the microstructure of samples manufactured using aged powder, Figure 4:113, Figure 4:114 and Figure 4:115, it is possible to see that the grains grow through the layers and are still varied in size and shape.

It is commonly understood that high cooling rates produce cellular microstructures and low cooling produces columnar grains. Looking at the microstructure images, Figure 4:113, Figure 4:114 and Figure 4:115, it is possible to see that heat treatment has caused a thinning and elongation of grains through the samples. Heat treatment allows grains to grow because the temperature of the material is raised above the sub solvus temperature allowing the grains to grow and recrystallise. Recrystallisation is the formation of strain free new grains with lower dislocation densities, improving the quality of the material [129]. These samples had been left in the furnace to cool and so after recrystallisation had finished the grains could continue to grow while the samples remained at temperature.

Figure 4:116 shows some of the changes in microstructure seen within this work. These changes in grains match the known fact that reheating of grains helps them to grow and recrystallise [129]. Therefore, this grain growth in lower layers confirms the belief that reheating of lower layers occurs during the build process.

The variations in microstructure and grain orientations seen within these samples explains that there is more than one phase present as otherwise the texture would have been uniform [129].

5.4.2 Cooling Rate, Melt Pools and Scan Strategy

The cooling rate of the melt pools within these parts will vary due to the laser pattern. On the stripe parts the cooling rate and time between laser passes will remain

consistent whereas for the meander laser pattern the ends will receive double heating and then a double cooling period whilst the centre of the scan track will receive more spread out heating and cooling. The melt pool is dependent on the time of one scan and the distance between laser paths. As can be seen from Figure 4:68 (a) the microstructure within the meander part shows grains that are growing between the melt paths and that there is a different microstructure seen in the melt path when compared to the areas between the paths. Figure 4:68 (b) shows the stripe laser path and here it can be seen that the grains are much smaller and do not grow into neighbouring melt paths.

The faster the cooling rate the quicker the melt pool will solidify. Thus, there will be remelting of the solidified area when the laser repasses inducing cellular structures. When there is a slower cooling rate the melt pools will not need to be remelted when the laser repasses, and that energy can instead be used to melt the surrounding powder yielding columnar grains. The variation in faster and slower colling alters the strength and ductility trade-off.

5.4.3 Fracture Behaviour and Failure Modes

Fractures initiate at a point with a high stress concentration, this crack propagates across the sample until failure occurs when the crack reaches a critical length.

What can be seen from the images of fracture surfaces in Section 4.5.6 is that the images exhibit ductile failure with no extended slow growth regions. All of the ductile fractures show rapid crack propagation.

Layered construction introduces planes of weakness when bonding is incomplete, particularly at low energy input.

5.4.4 Optical Microscopy of Failed Specimens

When looking at fractured samples it is possible to see from Figure 4:52, Figure 4:54, Figure 4:56 and Figure 4:58, how the layers within the AM parts have started to pull apart during the fracturing process. This is due to defined layers built up during the process. As the samples are tested, the force applied overcomes the bond between the layers and thus the layers part from each other. This has been very evident especially when a lower laser energy was used and thus an incomplete bonding of the layers has taken place. This is shown in Figure 4:69 and Figure 4:71, where these layers separate during testing and initiate the fracture. This has led to a smaller strain to failure and

less necking of the samples and subsequently a reduction in the extension of the sample.

Looking at Figure 4:60 and Figure 4:61, it is possible to see two of the failure paths found within the samples. The first image shows how there is the beginning of a 45° shear failure as would be expected. However, the crack seems to jump down 2mm and propagate on a different plane, similar to a lamella failing. This failure had a UTS of 615MPa, and shows similarities to conventional failures with comparable UTS, suggesting these build parameters produce parts similar to conventional SS316L parts. The second image once again shows a ductile failure where necking has occurred, however the crack path has been a more direct route across the specimen. This would be expected from testing conventionally manufactured specimens. These images exemplify the diversity of AM failure paths and the challenge of in-service prediction.

Figure 4:64 and Figure 4:65 show tensile samples that have failed in a ductile manner. These failures both show different angles of failure but have a notch or stress raiser in the right hand side that has initiated the sample to failure.

5.4.5 Fracture Surface Observations and Stress-Strain Signatures

Figure 4:61 appears to be an anomaly compared to all other samples that were tested. All specimens failed across the lamella layers but have maintained an average UTS of 524 MPa, which is above the average for all samples tested. The reason that this is significant because the failure of the specimens is across the layers and the scan tracks are visible. However, when analysing the stress vs strain graph, Figure 4:68, of the two samples shown the results show that the speciemen permaturly fails and thus the strain to failure is lower when compared to the specimen with the highest UTS. When comparing this to Figure 4:66 and Figure 4:67 it is possible to see that there is a different structure within the samples and thus it is likely to have been the reason why the strain to failure is so much lower for sample 2 than for sample 1. Figure 4:66 specimen has been shown to have a stronger bond between the layers and thus the failure is reliant on the microstructure and not the build process.

Figure 4:66 and Figure 4:72 show cohesion between particles rather than scan tracks. This is likely to show that using the higher exposure time and laser power has led to melting of the powder and stronger cohesion between layers, consistent with increased UTS.

Where there are seen to be less pores between the scan tracks Figure 4:17 (c) there is a corresponding higher UTS of 556 MPa suggesting that there is more bonding between the layers and individual scan tracks.

What can also be seen from Figure 4:72 is the large number of powder particles adhearing to the surface of the tensile bar, the laser power for this sample was 160W and this along with the reduced exposure time, 80µs, could have meant that the outer layer of powder did not have sufficient time to melt the surrounding layer but melted enough to allow it to stick to the outer surface.

5.5 Additional Outcomes

5.5.1 Strain to Failure (Ductility)

The strain to failure of AM parts was found to be lower than that of rolled SS316L [47] parts. For the 90° rotation parts the max elongation found was 42.8% elongation compared to the typical elongation of 64.5% [169] for rolled SS316L, whereas for 67° rotation parts the extension is only half of the extension found within rolled SS316L at 28.26%.

This reduction of strain to failure is most likely to be due to the higher percentage of pores within the parts compared to conventional manufacturing techniques. These pores act as local stress raisers. The local stress around the pores would then increase to beyond the strength of the material and initiate a crack that would then subsequently propagate and cause catastrophic failure of the component [129].

This decrease in strain to failure for civil use would potentially not be an issue, as it is very rare that a component is designed to the limit of strain to failure. Most components are designed so that during their life so that they would not deform plastically.

5.5.2 Hardness

The hardness value for AM manufactured SS316L has been found by Tolsoa et al. to be 235 HV [46], Vickers hardness. This value of 235HV has been used to compare to the experimental results obtained.

The hardest sample tested was for the stripe laser pattern using a 90° rotation with settings of 130µs exposure time, 160W laser power giving a value of 249.49HV. This is shown to be an increase of 6% over the comparison AM material [46]. These results

show that the 90° rotation samples can have a hardness value that exceeds the hardness value taken from the literature.

However, for the 67° rotation samples the results show that the hardness value does not surpass the standard hardness value that these results have been compared too; there is a 9% decrease when compared to the standard hardness showing that the 67° rotation samples do not reproduce as hard a sample as the 90° rotation samples.

The hardness results are seen to correlate with the strength with the same trends as would be expected as the hardness increases the UTS also increases [177].

The hardest sample for the 90° rotation samples is likely to be due to the indenter being placed directly on a scan track and the build process ensuring that every other layer is built directly above the lower layer. As the indenter was moved to different locations on the surface of the sample during testing, this suggests that the compactness is increased by this building method. For 67° rotation, samples the gaps between layers will be filled with each rotation melting a new area of the sample but there is no consistency of scan tracks between layers. This is what is causing the lower hardness values.

The size of the indent is larger than the average pore size to ensure that the overall value is found, and it is not affected by localised effects as shown in Figure 4:121. There can also be issues where the residual stress affects the hardness reading. There are models to compensate for this but these have not be used here so this must be factored into the examination of the results [178] and would make good future work.

5.6 Surface and Dimensional Characteristics

5.6.1 Surface Morphology

All of the images presented in Chapter 4 show that it is easily possible to observe the scan tracks, Figure 4:8, Figure 4:13, Figure 4:14, Figure 4:15, Figure 4:16, Figure 4:17 and Figure 4:18, these are similar images to those seen in literature including [103]. What is noted is that there are certain cases where the tracks are better defined than for other settings. Figure 4:17 and Figure 4:18 show the laser tracks on the samples surface. From studying the size of the laser tracks it is possible to see that as the definition of the tracks is improved with laser power there is also an increase in the size of the track as would be expected covering more of the surface between laser scans and minimising the number of pores visible.

Where the laser pattern lines are more clearly defined, it is also possible to study the raised laser tracks with a dip between the two melt tracks. The top surface of the samples with the most defined tracks are also the samples where the meander turns are the clearest. These turns are shown in Figure 4:7, which has been found to capture these best. Where the laser tracks are larger and more defined this leads to an increase in surface roughness [222].

Figure 4:7 shows how the laser path moves towards the front of the sample, performs a loop to rotate almost 180° and then the laser path moves back up towards the back of the sample. This continuous track only occurs using the meander laser pattern. This research has not been able to show a link between the visibility of the laser path to the yield strength and UTS, suggesting that no correlation can be made from visual inspection of the macro images and the final mechanical properties of the material.

Figure 4:7 also shows one of the defects that has been found to occur during the AM build process, balling. Balling is when small particles or balls of powder stick to the surface of the AM part. Balling occurs because of two reasons, the laser power is too low or the laser scan speed [60] is too high. It is seen to occur most in the samples with the lowest laser power (160W). Balling can be reduced by increasing the laser power, lowering the scan speed or decreasing layer thickness [60].

Figure 4:4 and Figure 4:5 show lose powder both before and after a build. The loose powder contains satellite particles in both the 'virgin' and used powder, however more on the used powder. This agglomeration of powder particles on the larger samples will occur due to the ambient heating of the powder during the build process. One of the issues found is that there are no smaller particles present in Figure 4:4, although it is believed there should be. The reason for this could be that all of the smaller particles or 'fines' did not have the surface area to stick to the stub for investigation within the SEM, further investigation is required to evaluate this. However, when they have formed satellites on larger particles, they are not lost in the SEM preparation process. Powder shown in Figure 4:4 and Figure 4:5, when compared to those seen in [106] show similar characteristics. This work found that larger particles sizes led to higher elongation whilst fines lead to smoother surfaces. This is shown in the results found here where the extension is improved for the aged powder samples which will have less fines present due to the reuse of powder numerous times.

Further images, Figure 4:30 and Figure 4:31 show particles on the surface of an AM part as taken by the SEM. These are shown at a lower magnification in Figure 4:19,

Figure 4:20, Figure 4:21 and Figure 4:22. A selection of particles can be seen on the surface that appear to have either not melted or have melted and then solidified into balls, due to surface tension, this matches what has been seen in literature [154]. These particles also show defects, including; surface scales, pitting and high roughness, on the surface that will need further study. The particles have a scale type surface, indicating that when the pool is solidifying there was movement and so the skin has not solidified completely before further movement has occurred, specifically the highlighted area in Figure 4:30 shows this type of outcome. These images correlate with the used powder shown in Figure 4:5, although the particles attached to parts show less of the satellites attached than are seen in the lose powder removed after a build.

The particles on the surface of the sample shown in Figure 4:30, could be an example of balling as mentioned earlier [60] or they could be unmelted powder. The unmelted powder around the edge of the part from during the build process has then been drawn into the surface of the part as it has solidified. The images show that generally the surface of these particles are smooth but in some cases there is an undulating surface. This change in surface conditions could be an indication of unmelted powder or a solidified particle not integrated into the part. The smoother surface particle could be a good indicator that it has melted and re-solidified. This effect can also be seen in Figure 4:14, where there are a number of particle balls stuck to the scan track.

The SEM was also used to study some of the particles on the surfaces using a higher magnification. Figure 4:32 and Figure 4:33 show a selection of balled particles on the surface of one of the cubes. With these particles, it is possible to see that the surface of these particles shows defects. It has been questioned if these defects are present within the powder before the AM process or if this is caused by partial laser melting. Figure 4:33 shows a selection of surface particles, for one of these particles it is possible to observe smaller particles within the larger particle.

With relation to the powders surface, shown in Figure 4:32, initially it was thought to be caused by the AM process and the melting and solidifying of the powder. Further work, however, showed ‘virgin’ powder was also found to contain particles of powder that appear to contain smaller powder particles within them. This is most likely to be satellite powder that is formed during the solidification phase of the powder manufacturing process, where smaller particles stick to a larger particle before it has fully solidified [166]. As the powder is formed using a gas atomisation process,

powder generated using this method can comprise smaller scale particulate that are 'agglomerated' into larger spherical particles as seen in [167] and Figure 4:32.
Along with looking at specific particles on the surface of as built and heat-treated parts, Figure 4:27, Figure 4:28 and Figure 4:29 look at a larger area of the surface and the overall effect on particles. From these figures, it is possible to see how the particles on the surface have melted further into the material due to the reheating process. Figure 4:28 and Figure 4:29 show how increasing the time and temperature has led to a more mottled surface thus reducing their overall height off the surface but increasing their diameters.

5.6.2 Roughness

As discussed in section 4.5.2 the roughness varies between the sides and the top. The top of the cubes has a higher roughness than the sides. This is likely to be due to the powder sitting on top of the part, which is drawn into the melt pools creating a higher surface roughness average (Ra). These results are in Table 5:1 and Table 5:2. It can be seen that the top roughness is on average 50% greater than that of the sides.
It is interesting to note the optimum roughness results do not coincide with the highest UTS, Density and Hardness values. The parameters that provide the worst properties in most other areas, lead to the lowest surface roughness. This may be due to a lower laser power and exposure time. Less powder at the interface between the solidified part and powder bed is melted and less unmelted powder is drawn into the melt pool and melted but stays in place on the surface of the part. If this occurs, less powder is drawn into the sides of the cubes. It could also be as there is not enough power to generate a large melt pool and therefore surface tension to hold the excess powder so when the part is lifted off the base plate most of the excess powder falls off reducing the average surface roughness of the sides. When looking at the top surface, the roughness is higher for the samples with the worst properties as would be expected.
Figure 4:23 and Figure 4:24 show a comparison between top surface roughness's. Figure 4:23 shows the lowest top surface roughness whereas Figure 4:24 shows the highest top surface roughness. From the comparison of the images, the highest surface roughness samples have a laser pattern that is less defined and larger pits are present. This suggests that increasing the laser power or exposure time leads to increased melting of the particles and better-defined surface tracks. These better-defined tracks will increase the surface roughness of the samples [222].

Figure 5:2 and Figure 5:3 show how the roughness has varied as a function of input energy. It is possible to see that increasing the input energy has increased the average roughness of the sides whereas in all except the stripe 67° samples it has decreased the average roughness of the top of the samples. To low an input energy leads to lack of fusion and partially melted particles adhering to the surface and this is what is seen on the top of the samples in Figure 4:15(a) and Figure 4:16 (a). The increase in roughness seen on the sides could be due to too high an input energy where spatter ejection could solidify on the part surface, or the melt pool becomes too large.

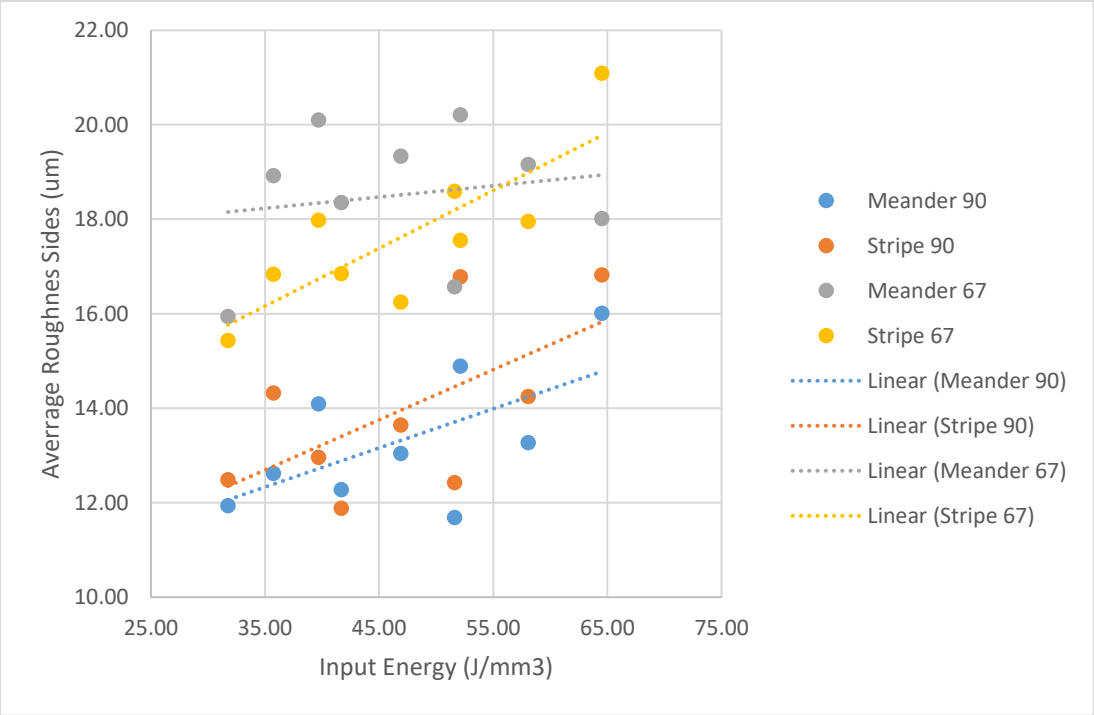

Figure 5:2: Graph Showing Average Roughness of Sides Against Input Energy

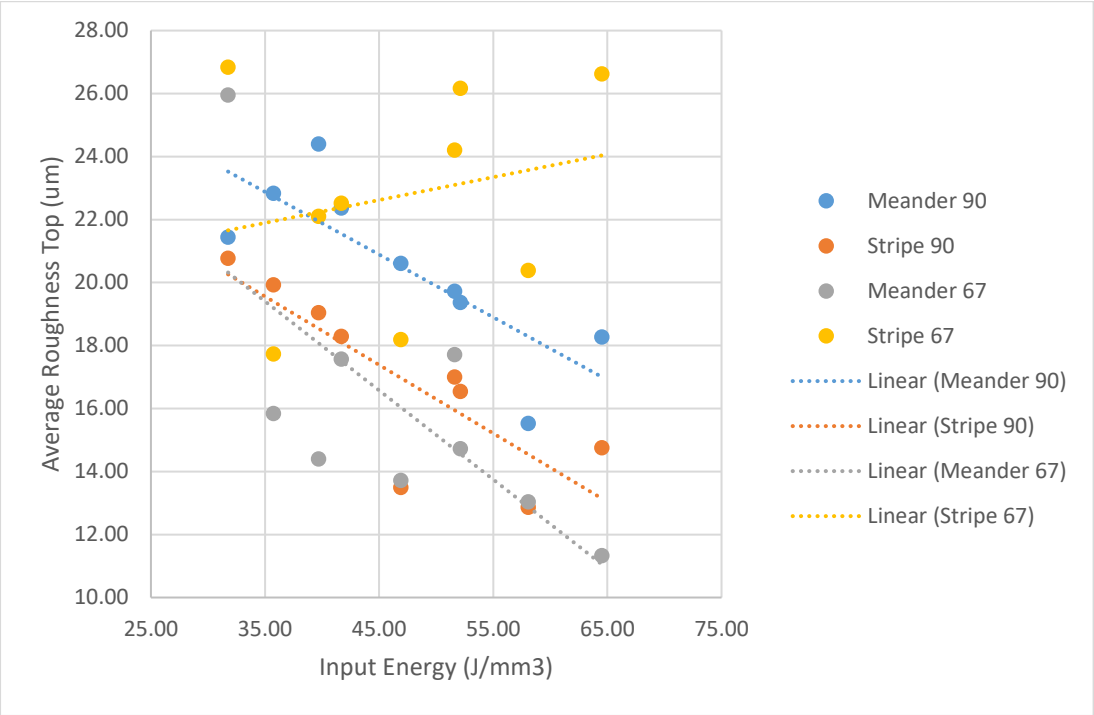

Figure 5:3: Graph Showing Average Roughness of Tops vs Input Energy

When studying the surface roughness of aged powder samples, it was found that the roughness was lower than for the samples produced with a mixture of used and 'virgin' powder. This is likely due to the continued sieving without the introduction of 'virgin' powder, which has removed the larger powder particles. Therefore there are fewer or none of these larger particles, which only partially melt during the process and then adhere to the surface, as seen in Figure 4:35, Figure 4:36 and Figure 4:37.

When investigating the roughness of the aged samples when the heat treatment is applied, the surface roughness has decreased, Table 5:1, Table 5:2, Table 5:3, Table 5:4, Table 5:5 and Table 5:6. Furthermore, there is no further decrease due to a longer hotter heat treatment suggesting that an increased length of time at higher temperature has no further effect.

When looking at samples built on the AM400 (BP3), rather than the AM250 it is clear to see that the surface roughness is improved, and that heat treatment has no effect on improving this further. The AM400 has improved gas flow and the new optical system, which has been used at the same power, which have led to these improvements in surface quality [207].

5.6.3 Dimensional Changes and Shrinkage

Geometrical testing indicates that AM part volumes can shrink by up to 1.2% when using a stripe laser pattern with a 67° rotation, whereas they can increase by up to 5.8% relative to the CAD model when a meander laser pattern with a 90° rotation is applied, as shown in Section 3.4.2.

The meander laser pattern is considered more suitable for establishing sizing parameters, as it is generally easier for manufacturers to remove excess material than to compensate for undersized parts. Accordingly, components should be designed with an intentional oversize to account for the shrinkage observed in this study. Nevertheless, tolerance must still be incorporated into all builds, as post-processing and surface finishing will further reduce the final dimensions.

Part height is influenced by unmelted powder on the upper surface, which may be drawn into the melt pool during solidification. In addition, incomplete removal of support structures can lead to an uneven base, further affecting the final height.

Variations in cooling rate associated with different laser patterns [173] may contribute to the observed dimensional changes. Cooling rate influences the microstructure, which in turn affects shrinkage behaviour. Previous studies [174] identify two primary solidification-related mechanisms that impact part dimensions: solidification shrinkage, which can introduce cavities and porosity, and linear contraction, which generates thermal stresses, cracking, and dimensional inaccuracies. Linear contraction has been shown to increase when cooling rates decrease.

5.6.4 Warpage

The warpage of AM components has been documented in the literature, such as for instance in [175].This issue only occurred at the front of one plate during one build. There is a possible reason why this may have occurred. It could be that the supports had not been fully secured to the base plate and therefore as the powder has solidified it has pulled those supports away from the base plate. But it is more likely that this occurred due to residual stress present within the bars during deposition that pulled the material away from the cold substrate [218]. This issue can be reduced by heating the powder bed [219]. Whichever of these is the reason it is something that needs to be understood and minimised as it is affecting the shape of the final parts.

5.7 Limitations

During this programme of work there were a number of limitations faced by the author including a lack of machine access. The machine was purchased as part of a larger project and so access to getting builds manufactured was spread around other work programmes as well as this work. This meant that not all of the builds that had been hoped for could be built and the number of available components for testing during this work were restricted. This limitation was controlled by building as many samples as possible when the machine was available to ensure that at least a limited number of samples were available for the second phase of this work. Part of this work was to ensure that when samples were available these were extensively tested so as to provide as much information as possible that could be used to produce valuable data for this work.

Chapter 2, the Literature Review, identified several challenges commonly encountered when manufacturing parts using AM. All of these issues were observed during the work undertaken for this study:

- Dimensional deviations were present in every part produced.
- Warpage occurred at the front of the build plate when long, thin components were manufactured, though it did not appear under other conditions.
- Stochastic surface tracks were visible on many parts, with their size and appearance varying according to the build parameters.
- Balling phenomena were detected on the surfaces of numerous cube specimens.
- Material properties of the AM components were found to fluctuate depending on the selected build parameters.

AM is a developing technology and there are still issues and problems that occur during manufacture. These issues are not fully characterised and understood by the wider community. This work has provided an explanation to these problems and the reasons behind why they occur. Showing where they occur, what parameters lead to their development and how to remove them or minimise their effect on final components, as well as their effect on final component mechanical properties.

To minimise warpage of parts before a build is carried out it needs to be ensured that the build plate is level and plane. This will ensure that the laser can melt completely through the powder layer to ensure the part fully joins with the build plate.

5.8 Proposed Optimum Parameters

It has been seen that whilst the suggested best conditions, 105µs exposure time and 180W laser power, have not been found to be the best through this work, 130µs exposure time and 200W laser power using the 90° laser rotation provided the highest UTS for mixed powder. Although these conditions do not have the best surface roughness due to most parts having a surface finish applied after they are removed from the machine and thus does not matter. Therefore, having the best UTS and density may be what is required for certain parts, which would be from the following settings: 67° rotation, meander laser pattern, 80µs exposure time and 200W laser power, the parameters used for BP2 and BP3 to corroborate these findings.

The results found for mixed powder have been found lacking when compared to the aged powder study. This showed that properties that are comparable to conventionally manufactured can be achieved consistently across a build plate. Further work has found that the suggested parameters to take forward are 200W laser powder and 80µs exposure time. With further investigation into the quantity of aged powder used within a build.

5.9 Summary

This chapter has discussed the results of the experimental testing and shown the properties of the SS316L AM parts built using Additive Manufacturing. It was found that:

- UTS increases with exposure time to a maximum of 588MPa,
- hardness increases with exposure time to a maximum of 249.9HV,
- aged powder has minimal effect on UTS, yield stress of Young's modulus, and
- strain to failure and extension are both increased by heating at 1150°C for 6 hours.

It has also been looking to establish the best build parameters for SS316L and these have been found and listed for further use and testing by other engineers.

Chapter 6 Conclusions

The work carried out has been an in-depth study into how the properties of metal parts built using additive manufacturing on Renishaw AM250 and AM400 machines for SS316L are affected by the build parameters and powders used and the changes seen through imaging of the fracture surfaces and microstructures.

6.1 Contribution to Knowledge

This work has developed an extensive experimental test programme investigating power properties and build parameters and their influence on AM parts properties and quality including testing of laser power, exposure time, laser pattern and rotation angle.

Carried out material and component analysis

- Established component properties of AM parts,
- Investigated failure mechanisms and documented them,
- Studied microstructure variations due to build parameters and heat treatment,
- Documented heat treatment effects on SS316L.

Defined a test process to establish the optimum test parameters. In this work these were found to be 200W laser power, 67° rotation between later, exposure time of 80μs. This is an input energy of 39.7 J/mm^3.

Disseminated this learning at ECCOMAS 2012 in Vienna, Airbus Technology Day and an article in Materials Science and Engineering Journal.

6.2 Conclusions

This work has helped advance the scientific understanding of Additive Manufactured (AM) components by systematically testing and recording the output of built components.

The following key conclusions can be drawn:

- When using the optimum parameters (input energy) this ensures all samples tested met the ASTM requirement for minimum tensile strength of 515MPa (ASTM F3184-16) [158].

6.2.1 Summary of Generic Conclusions

Ultimate Tensile Strength (UTS)

- UTS is primarily influenced by build parameters and input energy. Optimized processing conditions lead to consistent compliance with minimum standards, whereas non-optimized conditions can result in failures.
- Heat treatment temperature has a negative effect on UTS, with higher temperatures generally reducing strength.

Yield Strength

- Yield strength is largely controlled by build parameters, with optimized conditions ensuring compliance with standards.
- Heat treatment shows negligible impact on yield strength.

Elongation (Ductility)

- Elongation is sensitive to build parameters, powder condition, and heat treatment sequence.
    - Initial heat treatment tends to slightly reduce elongation compared to as-built, while subsequent treatments increase ductility.
    - Powder aging improves elongation compared to virgin or mixed powders.
    - Laser scan strategy (e.g., 90° rotation) introduces variability in elongation.
- HIP processing significantly enhances strain-to-failure for comparable UTS.

Porosity and Microstructure

- Porosity limits ductility, while microstructure governs yield strength.
- Large pores within fracture surfaces are associated with brittle failure modes.

Powder Condition

- Aged powder improves UTS and elongation compared to virgin or mixed powders, likely due to smaller particle size distribution.

Microstructure Characteristics

- AM parts exhibit irregular grain shapes and sizes (27–110 μm), differing from rolled SS316L.
- Heat treatment modifies microstructure, reducing yield stress and UTS.

Build Parameters and Laser Strategy

- Laser power and exposure time strongly affect density, UTS, and elongation. Higher energy input generally increases density and mechanical properties.
- Laser pattern rotation influences surface roughness and density, while meander patterns outperform stripe patterns for UTS, hardness, elongation, and density.
- Increasing laser power improves UTS, with maximum values achieved using aged powder at higher power settings.

Porosity and Powder Reuse

- Lower laser power and reused powder increase porosity due to incomplete melting, reducing density and ductility.
- Mixed virgin/reused powders result in lower elongation compared to aged powder.

Failure Modes

- Both ductile and brittle failures occur under similar UTS and microstructural conditions, indicating that porosity and defect distribution play a key role.

6.3 Contribution to Science

This work has helped develop the scientific understanding and optimisation of the AM process of SS316L, and of AM components through a rigorous and systematic test of builds, optical analysis and mechanical tests. This has used a wide data set varying process parameters, powder condition, heat treatment and laser strategies to narrow down the options and define a set of parameters to give the optimum input energy of 39.7 J/mm^3 for optimum performance after investigation into effect on microstructure, defects and mechanical performance.

It has shown that it is possible to control the microstructure and mechanical properties of AM components as well as:

- New understanding of how AM parameters control microstructure and strength
    - Larger grains means a lower UTS
    - Three dimensional grain growth across the layers means a higher UTS
    - Stripe and meander laser patterns produce different microstructures
- Novel insight into surface defects and their origins

    - Defects arise from insufficient laser energy, high scan speeds, powder ageing and powder morphology
- Demonstrated that powder reuse can improve mechanical properties
    - Aged powder can increase UTS likely due to removal of fines and improved powder packing
- Evidence that heat treatment has predicable, controllable effects
    - Heat treatment refines the grain structure improving the UTS
    - Heating at 1150°C for 6 hours improves ductility and increases strain to failure
- Clarification of build direction and scan strategy effects
    - Study confirms build orientation changes density, hardness, UTS, porosity and fracture modes
- Significant contribution to understanding fracture mechanisms in AM SS316L
    - Analysis shows failures in AM samples are mostly ductile
    - Layer delamination occurs and dominates low energy densities
    - Fracture paths differ radically depending on bonding quality and melt pool overlap
- Quantitative analysis of part sizing deviations due to laser pattern and cooling rate
    - Shows that part volume can shift from -1.2% to +5.8%
- Identification of AM process limitations and how to mitigate them by using an optimised input energy

This work provides a comprehensive, experimentally validated map linking AM processing parameters to microstructural evolution, surface morphology, mechanical properties, and dimensional outcomes for SS316L.

It delivers new scientific insights into powder reuse, defect formation, heat-treatment effects, and melt-pool mechanics, and it identifies parameter sets capable of producing wrought-equivalent properties.

Overall, the research advances both the scientific understanding and the practical application of metal additive manufacturing.

6.4 Future Work

The work and results presented here have contributed significantly to advancing knowledge on the manufacture and the resulting properties of AM parts. The research has provided novel insights into how varying build parameters influence the resulting material properties.

The conclusions have shown future directions of work:

- Range of parameter: The first aspect to consider is to continue testing using a wider range of parameter variations to ensure what has been found here is validated. The work carried out here was using a 200W laser with 67° rotation between layers and an exposure time of 80μs giving the best results. These are suggested starting parameters for future investigations and component manufacture. This is an input energy of 39.7 J/mm3 and it would be good to test different exposure times and laser powers that produce the same input energy to ensure that these are the best parameters moving forward.
- Heat treatment and the HIPping: This work has begun investigations into heat treatment and the HIPping. This should be continued. The parts would then need to be tested, and the results compared to those within this work. For SS316L it has been shown in Section 6.1, that many properties are linked to the density when compared to the expected density.
- Density: Therefore, further work would also need to be done by investigating if the density can be improved by post processing parts including heat treatment and HIPping. Heat treatment has shown that it could improve the grain size and further investigation into how it can be used to refine the grain size and orientation to enhance the material performance should be done.
- Mechanical Testing: This work has looked at basic mechanical testing. To continue to investigate AM parts, further mechanical tests would need to be conducted including but not limited to compression, fatigue, creep and shear, possibly different temperature levels. The parts studied have undergone no machining after being built. To fully understand if machining affects properties of the parts, further testing would need to be undertaken to see if this is the case.

- Microstructure: Investigations of the microstructure of AM parts has begun with this work and this would need to be further developed to by looking at EBSD and the orientation of the grains and easy slip grains to see if these have an effect on the reduced properties seen in certain samples. The work has developed a better understanding of the link between microstructure and mechanical properties. It shows a more consistent microstructure delivers better properties for AM components and this needs to be further investigated to see if it a certain microstructure can deliver certain properties consistently and this be predicted.

6.4.1 Recommendations

When purchasing a new machine, even though it will be provided as calibrated and ready for use, it is suggested that the process discussed in Section 4.14 be followed to ensure the machine is calibrated and the best parameters are used to manufacture parts that have the best properties. This test method is summarised below:

- Select best settings.
- Build five builds using these settings.
- Build and test tensile bars, compression pads (if necessary) and density cubes.
- Study the variation across the build plate.

In addition, to the above initial plan a calibration or benchmark build, should be set up and checked on a regular basis to verify the machine still performs to its maximum potential. Running this build regularly allows any out of spec changes to be caught and the machine to be recalibrated to its best performance conditions, ensuring the best part properties are also obtained with each build.

6.4.2 Test Programme

The suggested test programme to be undertaken when installing a new machine and using a new material would be as follows.

- To build cubes to investigate the surface condition, density, and porosity of a number of different parameters.
- To choose the best three samples and study the microstructure of these.
- To build tensile bars and if necessary, compression pads for the best three settings.

- This work should produce parts with the best properties.
- Repeat five builds of the best settings to ensure there are no issues across the plate.
- Ensure that when calibration is carried out further test samples of the parameters used are tested to ensure the machine is still performing at its best. Modifications may need to be made at this point.

References

[1] Science Direct "Stereolithography System," [Online] Available: https://www.sciencedirect.com/topics/engineering/stereolithography-system. Accessed: 01/02/2026.

[2] Y. Yan *et al.*, "Rapid Prototyping and Manufacturing Technology: Principle, Representative Technics, Applications, and Development Trends," *Tsinghua Sci. Technol.*, vol. 14, no. June, pp. 1–12, Jun. 2009.

[3] G. Tromans, "Introduction to Additive Technologies," in *TCT Live 19-20th Oct 2010*, 2010.

[4] EOS GmBH, "EOSINT M 270." [Online]. Available: eos_m-270_dental_2017_en_web.pdf. Accessed: 01/02/2026.

[5] J. Woodcock, "Additive Manufacturing in Metals," *TCT Magazine - June 2011*, pp. 27–32, 2011.

[6] Shapeways, "Fused Deposition Modeling[FDM]." [Online]. Available: https://www.shapeways.com/3d-print-material-technology/fused-deposition-modeling-fdm?srsltid=AfmBOorgNAY6pxnOAiTrE0aiOSc037rL_T-ok_H9U9R3E9MbBI1cFykD Accessed: 01/02/2026.

[7] Renishaw, "Laser Melting (metal 3D printing) Systems," 2014. [Online]. Available: http://www.renishaw.com/en/laser-melting-metal-3d-printing-systems--15240. Accessed: 01/02/2026.

[8] R. Noe, "What's the Difference Between Selective Laser Sintering, Direct Metal Laser Sintering, Laser Melting and LaserCusing?" [Online]. Available: http://www.core77.com/blog/materials/production_methods_whats_the_difference_between_selective_laser_sintering_direct_metal_laser_sintering_laser_melting_and_lasercusing_26457.asp. Accessed: 01/02/2026.

[9] N. K. Tolochko, M. K. Arshinov, A. V. Gusarov, V. I. Titov, T. Laoui, and L. Froyen, "Mechanisms of selective laser sintering and heat transfer in Ti powder," *Rapid Prototyp. J.*, vol. 9, no. 5, pp. 314–326, 2003.

[10] Science Direct, "Selective Laser Melting (SLM)," [Online]. Available: https://www.sciencedirect.com/topics/materials-science/selective-laser-melting. Accessed: 01/02/2026.

[11] J. Excell and S. Nathan, "The Rise of Additive Manufacturing," *The Engineer - 24th May*, 2010.

[12] B. Sampson, "3D Printing takes to the skies," *Professional Engineering*, 2013.

[13] J. Dawes, R. Bowerman, and R. Trepleton, “Introduction to the Additive Manufacturing Powder Metallurgy Supply Chain,” *Johnson Matthey Technol. Rev.*, vol. 59, no. 3, pp. 243–256, 2015.

[14] P. J. Bartolo, *Stereolithography*. 2011.

[15] R. Haridy, “Get over it: Madrid gets world’s first 3D-printed footbridge,” 2017. [Online]. Available: https://newatlas.com/3d-printed-bridge-madrid/47650/. Accessed: 01/02/2026.

[16] M. Tomlin and J. Meyer, “Topology Optimization of an Additive Layer Manufactured (ALM) Aerospace Part,” in *The 7th Altair CAE Technology Conference*, 2011, pp. 1–9.

[17] Renishaw, “QuantAM build preparation software.” [Online]. Available: http://www.renishaw.com/en/quantam-build-preparation-software--35455. Accessed: 01/02/2026.

[18] Stratasys, “GrabCAD.” [Online]. Available: https://grabcad.com/. Accessed: 01/02/2026.

[19] EOS GmbH, “EOSINT M 280.” [Online]. Available: https://www.eos.info/systems_solutions/metal/systems_equipment/eosint_m280. Accessed: 17/10/2013.

[20] Engineershandbook.com, “Rapid Manufacturing - Rapid Prototyping,” *Engineershandbook.com*, 2004. [Online]. Available: http://www.engineershandbook.com/rapidprototyping/index.htm. Accessed: 15/03/2015.

[21] Engineershandbook.com, “Rapid Prototyping - Selective Laser Sintering,” 2004. [Online]. Available: http://www.engineershandbook.com/rapidprototyping/sls.htm. Accessed: 15/03/2015.

[22] J. J.-P. Kruth *et al.*, “Binding mechanisms in selective laser sintering and selective laser melting,” *Rapid Prototyp. J.*, vol. 11, no. 1, pp. 26–36, 2005.

[23] S. Das, M. Wohlert, J. J. Beaman, and D. L. Bourell, “Producing Metal Parts with Selective Laser Sintering/Hot Isostatic Pressing,” *JOM*, vol. 50, no. 12, pp. 17–20, 1998.

[24] S. Das U, M. Wohlert, J. J. Beaman, and D. L. Bourell, “Processing of titanium net shapes by SLS/HIP,” *Direct*, pp. 115–121, 1999.

[25] R. Knight, J. Beaman, and D. Freiteg, “Metal processing using selective laser

sintering and hot isostatic pressing (SLS/HIP)," in *Solid Freeform Fabrication Symposium*, pp. 349–354, 1996.

[26] M. Shiomi, A. Yoshidome, F. Abe, and K. Osakada, "Finite element analysis of melting and solidifying processes in laser rapid prototyping of metallic powders," *Int. J. Mach. Tools Manuf.*, vol. 39, no. 2, pp. 237–252, 1999.

[27] M. M. Dewidar, J. Lim, and K. W. Dalgarno, "A Comparison between Direct and Indirect Laser Sintering of Metals," *Test*, vol. 24, no. 2, pp. 227–232, 2008.

[28] B. Xiao and Y. Zhang, "Numerical Simulation of Direct Metal Laser Sintering of Single-Component Powder on Top of Sintered Layers," *J. Manuf. Sci. Eng.*, vol. 130, no. 4, p. 041002, 2008.

[29] CRDM, "Direct Metal Laser Sintering," 2010.

[30] "Laser Sintering of Titanium gains importance.," *Ind. Laser Solut.*, no. November 2009, pp. 19–20, 2009.

[31] F. Miani, "Recent Developments of Direct Metal Selective," *Evaluation*, 1992.

[32] M. Khaing, J. Fuh, and L. Lu, "Direct metal laser sintering for rapid tooling: processing and characterisation of EOS parts," *J. Mater. Process. Technol.*, vol. 113, no. 1–3, pp. 269–272, 2001.

[33] "Direct Metal Laser Sintering," *Am. Mach.*, no. February 2008, p. 61, 2008.

[34] ARCAM, "ARCAM EBM." [Online]. Available: http://www.arcam.com/. Accessed: 01/02/2026.

[35] Engineershandbook.com, "Rapid Prototyping - Electron Beam Melting," 2004. [Online]. Available: http://www.engineershandbook.com/rapidprototyping/ebm.htm. Accessed: 15/03/2015.

[36] Neway, "Electron Beam Melting 3D Printing: An Overview," [Online]. Available: https://www.neway3dp.com/de/knowledge-hub/electron-beam-melting-ebm-3d-printing-an-overview. Accessed: 01/02/2026.

[37] M. F. Zäh and S. Lutzmann, "Modelling and simulation of electron beam melting," *Prod. Eng.*, vol. 4, no. 1, pp. 15–23, Dec. 2009.

[38] Materialise.com, "Rapid Prototyping - Why chose Fused Deposition Modeling,"2010. [Online]. Available: http://www.materialise.com/why-fused-deposition-modelling. Accessed: 15/03/2015.

[39] Engineershandbook.com, "Rapid Prototyping - Fused Deposition Modeling," 2004. [Online]. Available:

http://www.engineershandbook.com/rapidprototyping/fdm.htm. Accessed:

[40] Renishaw, “Investigating the effects of multiple re-use of Ti5Al4V powder in additive manufacturing (AM),” *White Pap.*, 2016.

[41] L. Loeber *et al.*, “Comparison of selective laser and electron beam melted titanium aluminides,” *22nd Annu. Int. Solid Free. Fabr. Symp. - An Addit. Manuf. Conf. SFF 2011*, pp. 547–556, 2011.

[42] S. Sever, “Introduction to Powder Metallurgy,” in *Constantin Brancusi University 8th International Conference - 24th - 26th May*, 2002.

[43] Sculpteo, “SLM (Selective Laser Melting) : 3D Printing Metal,” 2017. .

[44] J. P. Kruth *et al.*, “Assembly Automation Lasers and materials in selective laser sintering"Absorptance of powder materials suitable for laser sintering" Lasers and materials in selective laser sintering,” *Assem. Autom. Rapid Prototyp. J. Iss Rapid Prototyp. J. Iss Rapid Prototyp. J.*, vol. 2315, no. 5, pp. 357–371, 2003.

[45] A. Riemer, S. Leuders, M. Thöne, H. A. Richard, T. Tröster, and T. Niendorf, “On the fatigue crack growth behavior in 316L stainless steel manufactured by selective laser melting,” *Eng. Fract. Mech.*, vol. 120, pp. 15–25, 2014.

[46] I. Tolosa, F. Garciandía, F. Zubiri, F. Zapirain, and A. Esnaola, “Study of mechanical properties of AISI 316 stainless steel processed by ‘selective laser melting’, following different manufacturing strategies,” *Int. J. Adv. Manuf. Technol.*, vol. 51, no. 5–8, pp. 639–647, Apr. 2010.

[47] ASTM International, *A240/A240M - 16 Standard Specification for Chromium and Chromium-Nickel Stainless Steel Plate, Sheet and Strip for Pressure Vessels and for General Applications*. 2016.

[48] GKN, “6 Unique Benefits Of Selective Laser Melting,” 2017.

[49] “EADS novel bicycle is the wheel deal,” *The Engineer - 14th March*, p. 7, 2011.

[50] S. Lott, “On the edge of design,” *Aerospace Manufacturing - April*, pp. 24–26, 2011.

[51] T. Kellner, “How 3D Printing will Change Manufacturing,” 2017. .

[52] J. Foster, “Making Sparks Fly,” *UP to Planet EADS - June 2010*, pp. 20–23, 2010.

[53] “Laser Sintering reduces number of components.,” *Ind. Laser Solut.*, no. September/October 2010, pp. 4–5, 2010.

[54] M. Campbell, “Just print me out that robofly to go, please...,” *New Scientist - 30th July*, p. 19, 2011.

[55] E. Sallica-Leva, A. L. Jardini, and J. B. Fogagnolo, “Microstructure and mechanical behavior of porous Ti–6Al–4V parts obtained by selective laser melting,” *J. Mech. Behav. Biomed. Mater.*, vol. 26, pp. 98–108, 2013.

[56] C. Körner, E. Attar, and P. Heinl, “Mesoscopic Simulation of Selective Beam Melting Processes,” *J. Mater. Process. Technol.*, vol. 211, no. 6, pp. 978–987, Dec. 2010.

[57] S. Harris, “Aerospace Additive Ambitions Take Off,” *The Engineer - 25th April*, 2014.

[58] Encyclopaedia Britannica, “Sintering,” 2015. [Online]. Available: http://www.britannica.com/EBchecked/topic/546309/sintering. Accessed: 23/03/2015.

[59] D. Wang, Y. Yang, R. Liu, D. Xiao, and J. Sun, “Study on the designing rules and processability of porous structure based on selective laser melting (SLM),” *J. Mater. Process. Technol.*, vol. 213, no. 10, pp. 1734–1742, 2013.

[60] D. Gu and Y. Shen, “Balling phenomena in direct laser sintering of stainless steel powder: Metallurgical mechanisms and control methods,” *Mater. Des.*, vol. 30, no. 8, pp. 2903–2910, Sep. 2009.

[61] K. Alrbaey, D. Wimpenny, R. Tosi, W. Manning, and A. Moroz, “On optimisation of surface roughness of selective laser melted stainless steel parts: A statistical study,” *J. Mater. Eng. Perform.*, vol. 23, no. 6, pp. 2139–2148, 2014.

[62] “Rapid Manufacturing - Rapid Prototyping,” *Engineershandbook.com*, 2011. .

[63] B. S. S. Association, “The Basic Information about Stainless Steel,” *Technical Information - BSSA*, 2010. [Online]. Available: http://www.bssa.org.uk/about_stainless_steel.php. Accessed: 01/02/2026.

[64] EOS GmbH, “Material Data Sheet - EOS StainlessSteel 17-4 for EOSINT M 270,” 2006.

[65] “ASM Material Data Sheet - Vasco 17-4 Percipitation Hardening Steel,” *asm.matweb.com*. [Online]. Available: http://asm.matweb.com/search/SpecificMaterial.asp?bassnum=NALL81. Accessed: 01/02/2026.

[66] Titaniumexposed.com, “Titanium density - the key property that gives titanium its miraculous qualities,” 2009. [Online]. Available: http://www.titaniumexposed.com/titanium-density.html. Accessed:

01/02/2026.

[67] EOS GmbH, “Material Data Sheet - EOS Titanium Ti64 for EOSINT M 270,” 2008.

[68] MatWeb, “ASM Material Data Sheet - Titanium Ti-6Al-4V (Grade 5), Annealed.” [Online]. Available: http://asm.matweb.com/search/SpecificMaterial.asp?bassnum=MTP641. Accessed: 01/02/2026.

[69] R. Duncan and B. Hanson, *The Selection and Use of Titanium: Engineering Design Guide*. Oxford University Press, 1980.

[70] ChemSoc, “Visual Elements - Aluminium.” [Online]. Available: http://www.rsc.org/chemsoc/visualelements/pages/data/aluminium_data.html. Accessed: 01/02/2026.

[71] “ASM Material Data Sheet - Aluminium 6061,” *asm.matweb.com*. [Online]. Available: http://asm.matweb.com/search/SpecificMaterial.asp?bassnum=MA6061t6. Accessed: 01/02/2026.

[72] EOS GmbH, “Material Data Sheet - EOS Aluminium AlSi10Mg,” 2010.

[73] Mcor Technology, “How Paper-based 3D Printing Works.”

[74] BBCNews, “Printer produces personalised 3D chocolate,” *BBC Technology News - 5th July 2011*, 2011. [Online]. Available: http://www.bbc.co.uk/news/technology-14030720. Accessed: 01/02/2026.

[75] R. Borsion, “From Oreos to Nutella - The Latest 3D Printed Foods are all 100% Edible,” *Business Insider*, 2014. [Online]. Available: http://www.businessinsider.com/3d-printed-foods-2014-9?op=1&IR=T. Accessed: 01/02/2026.

[76] “Castable Wax Material Information,” *Shapeways*. [Online]. Available: http://www.shapeways.com/materials/wax. Accessed: 04/01/2015.

[77] M. Stone, “3D Printed Dresses are Radically Changing the Meaning of Haute Couture,” *Business Insider*, 2014. [Online]. Available: http://www.businessinsider.com/3d-printed-fashion-2014-8?IR=T. Accessed: 01/02/2026.

[78] OxfordCorpus, *Concise Oxford English Dictionary, Luxury 11th Edition*. 2009.

[79] B. Sampson, “Light Work,” *Professional Engineering*, p. 28.

[80] “The Printed Word,” *The Economist (Online)*, 2011.

[81] S. Ucsnik, M. Scheerer, S. Zaremba, and D. H. Pahr, “Experimental investigation of a novel hybrid metal–composite joining technology,” *Compos. Part A Appl. Sci. Manuf.*, vol. 41, no. 3, pp. 369–374, Mar. 2010.

[82] S. Harris, “Looking the Part,” *The Engineer - 25th April*, no. 25th April, pp. 38–42, 2011.

[83] A. Rangesh and W. O’Neil, “Free Space Deposition in Metals,” *TCT Magazine - June 2011*, pp. 54–55, 2011.

[84] B. Hargreaves, “Green, Clean and Lean,” *Professional Engineering - July*, pp. 36–39, 2011.

[85] H. Lipson, “This will change everything,” *New Scientist - 30th July*, p. 20, 2011.

[86] Lasersintering.com, “SLS & DMLS Finishing Classes,” 2011. .

[87] A. Yadollahi, N. Shamsaei, S. M. Thompson, A. Elwany, L. Bian, and M. Mahmoudi, “Fatigue Behavious of Selective Laser Melted 17-4 PH Stainless Steel,” pp. 721–731, Sep. 1998.

[88] E. Brandl and D. Greitemeier, “Microstructure of additive layer manufactured Ti-6Al-4V after exceptional post heat treatments,” *Mater. Lett.*, vol. 81, pp. 84–87, 2012.

[89] B. Vracken, L. Thijis, J.-P. Kruth, and J. Van Humbeeck, “Heat treatment of Ti6Al4V produced by selective laser melting:Microstructure and mechanical properties,” *J. Alloy. Compd.*, vol. 541, pp. 177–185, 2012.

[90] Avure-Technologies, “Todays HIPs: Fast, Precise, Cost-Efficient,” 2008.

[91] AzoMaterials, “Hot Isostatic Pressing,” 2010. [Online]. Available: http://www.azom.com/details.asp?articleid=924. Accessed: 01/02/2026.

[92] Arcam, “Grade 2 Titanium: Fact Sheet.”

[93] Arcam, “Ti6Al4V Titanium Alloy: Fact Sheet.”

[94] C. Qiu, N. J. E. Adkins, and M. M. Attallah, “Microstructure and tensile properties of selectively laser-melted and of HIPed laser-melted Ti–6Al–4V,” *Mater. Sci. Eng. A*, vol. 578, pp. 230–239, 2013.

[95] Avure-Technologies, “Cold Isostatic Pressing (CIP) Applications,” 2008. [Online]. Available: http://www.avure.com/iso/applications/cold-isostatic-pressing.asp. Accessed: 01/02/2026.

[96] ASTM, “ASTM A480/A480M Standard Specification for Flat-Rolled Stainless and Heat-Resisting Steel Plate, Sheet and Strip,” 2016.

[97] Edmmachining.com, “Wire EDM Machining Process,” 2011. .

[98] C. Yan, L. Hao, A. Hussein, and D. Raymont, “Evaluations of cellular lattice structures manufactured using selective laser melting,” *Int. J. Mach. Tools Manuf.*, vol. 62, pp. 32–38, 2012.

[99] Metal AM, “Metal powders – the raw materials,” 2017.

[100] LPW Technology, “LPW Additive Manufacturing.” [Online]. Available: https://www.lpwtechnology.com/. Accessed: 10/05/2015.

[101] LPW, “Plasma Spheroidisation for improved metal powder flow and packing properties,” vol. 44, no. 0. 2016.

[102] J. A. Slotwinski, E. J. Garboczi, P. E. Stutzman, C. F. Ferraris, S. S. Watson, and M. A. Peltz, “Characterization of Metal Powders Used for Additive Manufacturing,” *J. Res. Natl. Inst. Stand. Technol.*, vol. 119, p. 460, 2014.

[103] W. E. Luecke and J. A. Slotwinski, “Mechanical Properties of Austenitic Stainless Steel Made by Additive Manufacturing,” *J. Res. Natl. Inst. Stand. Technol.*, vol. 119, p. 398, 2014.

[104] G. Jacob, C. U. Brown, M. A. Donmez, S. S. Watson, and J. Slotwinski, “Effects of powder recycling on stainless steel powder and built material properties in metal powder bed fusion processes,” 2017.

[105] A. T. Sutton, C. S. Kriewall, M. C. Leu, and J. W. Newkirk, “Powders for Additive Manufacturing Processes: Characterization Techniques and Effects on Part Properties,” *Solid Free. Fabr. Proc.*, pp. 1004–1030, 2016.

[106] I. Global Market Insights, “Additive Manufacturing with Metal Powders Market worth $1.1bn by 2024,” 2018. .

[107] V. Seyda, N. Kaufmann, and C. Emmelmann, “Investigation of aging processes in Ti-6Al-4V powder material in laser melting,” *Phys. Procedia*, vol. 39, pp. 425–431, 2012.

[108] J.-P. Kruth, M. Badrossamay, E. Yasa, J. Deckers, L. Thijs, and J. Van Humbeeck, “Part and material properties in selective laser melting of metals,” in *16th International Symposium on Electromachining*. 2010.

[109] E. Yasa and J. P. Kruth, “Microstructural investigation of selective laser melting 316L stainless steel parts exposed to laser re-melting,” *Procedia Eng.*, vol. 19, pp. 389–395, 2011.

[110] P. Mercelis and J.-P. Kruth, “Residual stresses in selective laser sintering and selective laser melting,” *Rapid Prototyp. J.*, vol. 12, no. 5, pp. 254–265, 2006.

[111] S. Berumen, F. Bechmann, S. Lindner, J.-P. Kruth, and T. Craeghs, “Quality

control of laser- and powder bed-based Additive Manufacturing (AM) technologies," *Phys. Procedia*, vol. 5, no. 2009, pp. 617–622, 2010.

[112] J. Kruth, M. Leu, and T. Nakagawa, "Progress in Additive Manufacturing and Rapid Prototyping," *CIRP Ann. - Manuf. Technol.*, vol. 47, no. 2, pp. 525–540, 1998.

[113] M. Speirs, J. Van Humbeeck, J. Schrooten, J. Luyten, and J. P. Kruth, "The effect of pore geometry on the mechanical properties of selective laser melted Ti-13Nb-13Zr scaffolds," *Procedia CIRP*, vol. 5, pp. 79–82, 2013.

[114] J. Kruth, G. Levy, F. Klocke, and T. Childs, "Consolidation phenomena in laser and powder-bed based layered manufacturing," *CIRP Ann. - Manuf. Technol.*, vol. 56, no. 2, pp. 730–759, 2007.

[115] K. Alrbaey *et al.*, "The study of the laser parameters and environment variables effect on mechanical properties of high compact parts elaborated by selective laser melting 316L powder," *Mater. Sci. Eng. A*, vol. 584, no. 3, pp. 21–31, Sep. 2013.

[116] L. Thijs, F. Verhaeghe, T. Craeghs, J. Van Humbeeck, and J.-P. Kruth, "A study of the microstructural evolution during selective laser melting of Ti–6Al–4V," *Acta Mater.*, vol. 58, no. 9, pp. 3303–3312, May 2010.

[117] M. Matthew, G. Guss, S. Khairallah, A. M. Rubenchik, P. Depon, and W. E. King, "Denudation of metal powder layers in laser powder bed fusion," *Acta Mater.*, vol. 114, pp. 33–42, 2016.

[118] W. E. King *et al.*, "Observation of keyhole-mode laser melting in laser powder-bed fusion additive manufacturing," *J. Mater. Process. Technol.*, vol. 214, pp. 2915–2925, 2014.

[119] M. Ruffo, C. Tuck, and R. Hague, "Cost estimation for rapid manufacturing - laser sintering production for low to medium volumes," *Proc. Inst. Mech. Eng. Part B J. Eng. Manuf.*, vol. 220, no. 9, pp. 1417–1427, Jan. 2006.

[120] M. Ruffo and R. Hague, "Cost estimation for rapid manufacturing — simultaneous production of mixed components using laser sintering," *Proc. Inst. Mech. Eng. Part B J. Eng. Manuf.*, vol. 221, no. 11, pp. 1585–1591, Jan. 2007.

[121] M. Au, "Mechanical Behavior and Fractography of 304 Stainless Steel with High Hydrogen Concentration," no. 865.

[122] J. . Cherry, H. . Davies, S. Mehmood, N. . Lavery, S. G. . Brown, and J. Sienz,

"Investigation into the effect of process parameters on microstructural and physical properties of 316L stainless steel parts by selective laser melting," *Int. J. Adv. Manuf. Technol.*, vol. 76, no. 5, pp. 869–879, 2014.

[123] X. H. Chen, J. Lu, L. Lu, and K. Lu, "Tensile properties of a nanocrystalline 316L austenitic stainless steel," *Scr. Mater.*, vol. 52, no. 10, pp. 1039–1044, 2005.

[124] A. B. Spierings, T. L. Starr, and K. Wegener, "Fatigue performance of additive manufactured metallic parts," *Rapid Prototyp. J.*, vol. 19, no. 2, pp. 88–94, 2013.

[125] T. M. Mower and M. J. Long, "Mechanical behavior of additive manufactured, powder-bed laser-fused materials," *Mater. Sci. Eng. A*, vol. 651, pp. 198–213, 2016.

[126] I. Yadroitsava and I. Yadroitsev, "Evaluation of residual stress in selective laser melting of 316L steel," in *Progress in Additive Manufacturing*, 2014.

[127] W. Callister, *Materials Science and Engineering An Introduction*. 2006.

[128] T. Davidson, "An Introduction to Failure Analysis for Metallurgical Engineers," *TMS*, pp. 1–20, 1999.

[129] G. Ziółkowski, E. Chlebus, P. Szymczyk, and J. Kurzac, "Application of X-ray CT method for discontinuity and porosity detection in 316L stainless steel parts produced with SLM technology," *Arch. Civ. Mech. Eng.*, vol. 4, pp. 2–8, 2014.

[130] K. Mutombo, "Metallurgical evaluation of laser additive manufactured Ti6Al4V components," pp. 4–6. 2013.

[131] D. Boisselier and S. Sankaré, "Influence of Powder Characteristics in Laser Direct Metal Deposition of SS316L for Metallic Parts Manufacturing," *Phys. Procedia*, vol. 39, pp. 455–463, 2012.

[132] E. Brandl, U. Heckenberger, V. Holzinger, and D. Buchbinder, "Additive manufactured AlSi10Mg samples using Selective Laser Melting (SLM): Microstructure, high cycle fatigue, and fracture behavior," *Mater. Des.*, vol. 34, pp. 159–169, 2012.

[133] T. Niendorf, S. Leuders, A. Riemer, H. A. Richard, T. Troster, and D. Schwarze, "Highly Anisotropic Steel Processed by Selective Laser Melting," *Metall. Mater. Trans. B Process Metall. Mater. Process. Sci.*, vol. 44B, pp. 794–796, 2013.

[134] K. Senthilkumaran, P. M. Pandey, and P. V. M. Rao, "Influence of building

strategies on the accuracy of parts in selective laser sintering," *Mater. Des.*, vol. 30, no. 8, pp. 2946–2954, Sep. 2009.

[135] P. Fischer, V. Romano, H. . Weber, N. . Karapatis, E. Boillat, and R. Glardon, "Sintering of commercially pure titanium powder with a Nd:YAG laser source," *Acta Mater.*, vol. 51, no. 6, pp. 1651–1662, Apr. 2003.

[136] B. Zhang, L. Dembinski, and C. Coddet, "The study of the laser parameters and environment variables effect on mechanical properties of high compact parts elaborated by selective laser melting 316L powder," *Mater. Sci. Eng. A*, vol. 584, pp. 21–31, 2013.

[137] R. M. Mahamood and E. T. Akinlabi, "Effect of laser power on surface finish during Laser Metal Deposition process," *Lect. Notes Eng. Comput. Sci.*, vol. 2, pp. 965–969, 2014.

[138] K. Antony, N. Arivazhagan, and K. Senthilkumaran, "Numerical and experimental investigations on laser melting of stainless steel 316L metal powders," *J. Manuf. Process.*, vol. 16, pp. 345–355, 2014.

[139] K. Guan, Z. Wang, M. Gao, X. Li, and X. Zeng, "Effects of processing parameters on tensile properties of selective laser melted 304 stainless steel," *Mater. Des.*, vol. 50, pp. 581–586, 2013.

[140] H. Brodin, O. Andersson, and S. Johansson, "Mechanical testing of a selective laser melted superalloy," in *13th International Conference on Fracture*, 2013.

[141] K. Antony, N. Arivazhagan, and K. Senthilkumaran, "Studies on wettability of stainless steel 316L powder in laser melting process," *J. Eng. Sci. Technol.*, vol. 9, no. 5, pp. 533–540, 2014.

[142] M. L. Montero Sistiaga, S. Nardone, C. Hautfenne, J. Van Humbeeck, and J. Van Humbeeck, "Effect of Heat Treatment Of 316L Stainless Steel Produced by Selective Laser Melting (SLM)," *27th Annu. Int. Solid Free. Fabr. Symp. - An Addit. Manuf. Conf. Solid Free. Fabr. Symp.*, pp. 558–565, 2016.

[143] P. Fischer, "Temperature measurements during selective laser sintering of titanium powder," *Int. J. Mach. Tools Manuf.*, vol. 44, no. 12–13, pp. 1293–1296, Oct. 2004.

[144] Y. Gao, J. Xing, J. Zhang, N. Luo, and H. Zheng, "Research on measurement method of selective laser sintering (SLS) transient temperature," *Opt. - Int. J. Light Electron Opt.*, vol. 119, no. 13, pp. 618–623, Oct. 2008.

[145] T. Nakamoto, N. Shirakawa, Y. Miyata, and H. Inui, "Selective laser sintering

of high carbon steel powders studied as a function of carbon content," *J. Mater. Process. Technol.*, vol. 209, no. 15–16, pp. 5653–5660, Aug. 2009.

[146] P. Stavropoulos and P. Foteinopoulos, "Modelling of additive manufacturing processes: a review and classification," vol. 2, 2018.

[147] BSI Standards, "BS EN ISO 6892-1:2009," 2009.

[148] LPW Technology, "Powder degradation," no. 0, 2015.

[149] "Introduction to Taguchi Method," *Ee.iitb.ac.in*, 2000. .

[150] N. Raghunath and P. Pandey, "Improving accuracy through shrinkage modelling by using Taguchi method in selective laser sintering," *Int. J. Mach. Tools Manuf.*, vol. 47, no. 6, pp. 985–995, May 2007.

[151] S. Athreya and Y. D. Venkatesh, "Application Of Taguchi Method For Optimization Of Process Parameters In Improving The Surface Roughness Of Lathe Facing Operation," *Int. Ref. J. Eng. Sci.*, vol. 1, no. 3, pp. 13–19, 2012.

[152] H. L. Wei, J. Mazumder, and T. DebRoy, "Evolution of solidification texture during additive manufacturing," *Sci. Rep.*, vol. 5, pp. 1–7, 2015.

[153] J. Jhabvala, E. Boillat, T. Antignac, and R. Glardon, "Study and simulation of different scanning strategies in {SLM}," *Innov. Dev. Des. Manuf.*, no. October, pp. 369–375, 2010.

[154] Coherent, "Measuring Laser Power and Energy Output," pp. 1–5.

[155] D. R. J. Scalise, "Archimedes' Principle," *SMU Physics*, 2002. [Online]. Available: http://www.physics.smu.edu/~scalise/mechmanual/archimedes/lab.html. Accessed 01/02/2026.

[156] P. Belton, "Fast Factories," Professional Engineering, pp. 20–25, 2019.

[157] J. L. Bartlett and X. Li, "An overview of residual stresses in metal powder bed fusion," Additive Manufacturing, vol. 27, no. March, pp. 131–149, 2019.

[158] ASTM F3184-16 'AM Stainless Steel Alloy (UNS S31603) with Powder Bed Fusion (PBF)' 2017.

[159] ASTM F3001-14 'AM Titanium-6 Aluminium-4 Vanadium ELI (Extra Low Interstitial) with PBF' 2021.

[160] MTC, "Powder Qualification for Powder Bed Fusion Report," 2020.

[161] Granutools, "How can you follow powder ageing in Additive Manufacturing?," 2018. .

[162] N. E. Gorji, R. O'Connor, and D. Brabazon, "XPS, XRD, and SEM

characterization of the virgin and recycled metallic powders for 3D printing applications," IOP Conference Series: Materials Science and Engineering, vol. 591, no. 1, 2019.

[163] A. Sidambe, "SLM of Refractory Metals," Liverpool University, 2020.

[164] S. Srinivas, "NASA technical note Survey of Properties of T-111," Nasa Tn D-7855, 1975.

[165] D. E. Etter and W. H. Smith, "Effect of oxygen contamination on the tensile properties of T-111 (tantalum-8tungsten-2hafnium) at 1204 °C," Journal of the less-common Metals, vol. 27, pp. 109–122, 1972.

[166] J. Jhabvala, E. Boillat, T. Antignac, and R. Glardon, "Study and simulation of different scanning strategies in {SLM}," Innovative Developments in Design and Manufacturing, no. October, pp. 369–375, 2010.

[167] Renishaw, "Meander stripe and chessboard hatchings pattern." [Online]. Available: https://resources.renishaw.com/en/details/Meander stripe and chessboard hatchings pattern (95492). Accessed: 03/01/2020.

[168] A. Kudzal et al., "Effect of scan pattern on the microstructure and mechanical properties of Powder Bed Fusion additive manufactured 17-4 stainless steel," Materials and Design, vol. 133, pp. 205–215, 2017.

[169] H. Ali, H. Ghadbeigi, and K. Mumtaz, "Effect of scanning strategies on residual stress and mechanical properties of Selective Laser Melted Ti6Al4V," Materials Science and Engineering A, vol. 712, no. October 2017, pp. 175–187, 2018.

[170] B. Cheng, S. Shrestha, and K. Chou, "Stress and deformation evaluations of scanning strategy effect in selective laser melting," Additive Manufacturing, vol. 12, pp. 240–251, 2016.

[171] H. Y. Wan, Z. J. Zhou, C. P. Li, G. F. Chen, and G. P. Zhang, "Effect of scanning strategy on mechanical properties of selective laser melted Inconel 718," Materials Science and Engineering A, vol. 753, no. June 2018, pp. 42–48, 2019.

[172] D. Ramos, F. Belblidia, and J. Sienz, "New scanning strategy to reduce warpage in additive manufacturing," Additive Manufacturing, vol. 28, no. April, pp. 554–564, 2019.

[173] A. M. Philo, C. J. Sutcliffe, S. Sillars, J. Sienz, S. G. R. Brown, and N. P. Lavery, "A Study into the Effects of Gas Flow Inlet Design of the Renishaw

AM250 Laser Powder Bed Fusion Machine Using Computational Modelling," Solid Freeform Fabrication Symposium 2017.

[174] M. Cloots, A. B. Spierings, and K. Wegener, "Assessing new support minimizing strategies for the additive manufacturing technology SLM." 2013.

[175] R. J. Williams et al., "In situ thermography for laser powder bed fusion: Effects of layer temperature on porosity, microstructure and mechanical properties," Additive Manufacturing, vol. 30, no. March 2019, 2019.

[176] N. A. Fleck and R. A. Smith, Effect of density on tensile strength, fracture toughness and fatigue crack propagation behaviour of sintered steel, Powder Metallurgy, No. 3, p. 121 – 125, 1981.

[177] H. Gong, K. Rafi, H. Gu, T. Starr, and B. Stucker, "Analysis of defect generation in Ti-6Al-4V parts made using powder bed fusion additive manufacturing processes," Additive Manufacturing, vol. 1, pp. 87–98, 2014.

[178] Engineering "7 Issues to Look Out for in Metal 3D Printing ." . Available: https://www.engineering.com/7-issues-to-look-out-for-in-metal-3d-printing/. Accessed: 01/02/2026.

[179] M. T. Todinov, "Generic Solutions for Reducing the Likelihood of Overstress and Wearout Failures," Risk-Based Reliability Analysis and Generic Principles for Risk Reduction, pp. 239–263, 2007

[180] C. Li, Z. Y. Liu, X. Y. Fang, and Y. B. Guo, "Residual Stress in Metal Additive Manufacturing," Procedia CIRP, vol. 71, pp. 348–353, 2018.

[181] D. Barba, C. Alabort, Y. T. Tang, M. J. Viscasillas, R. C. Reed, and E. Alabort, "On the size and orientation effect in additive manufactured Ti-6Al-4V," Materials & Design, vol. 186, p. 108235, 2019.

[182] A. S. Wu, D. W. Brown, M. Kumar, G. F. Gallegos, and W. E. King, "An Experimental Investigation into Additive Manufacturing-Induced Residual Stresses in 316L Stainless Steel," Metallurgical and Materials Transactions A: Physical Metallurgy and Materials Science, vol. 45, no. 13, pp. 6260–6270, 2014.

[183] R. Williams, "Process Conditions and the Integrity of 316L Stainless Steel Parts Manufactured by Laser Powder Bed Fusion," PhD 2020.

[184] A. Sola and A. Nouri, "Microstructural porosity in additive manufacturing: The formation and detection of pores in metal parts fabricated by powder bed fusion," Journal of Advanced Manufacturing and Processing, vol. 1, no. 3,

2019.

[185] J. Robinson, I. Ashton, P. Fox, E. Jones, and C. Sutcli, “Determination of the effect of scan strategy on residual stress in laser powder bed fusion additive manufacturing,” vol. 23, no. February, pp. 13–24, 2018.

[186] L. A. Parry, I. A. Ashcroft, and R. D. Wildman, “Geometrical effects on residual stress in selective laser melting,” Additive Manufacturing, vol. 25, no. September 2018, pp. 166–175, 2019.

[187] B. Vrancken, L. Thijs, J. P. Kruth, and J. van Humbeeck, “Heat treatment of Ti6Al4V produced by Selective Laser Melting: Microstructure and mechanical properties,” Journal of Alloys and Compounds, vol. 541, no. 0, pp. 177–185, 2012.

[189] D. H. Herring, “Grain Size and Its Influence on,” The Heat Treat Doctor, no. August, pp. 1–2, 2005.

[190] Y. M. Arısoy, L. E. Criales, T. Özel, B. Lane, S. Moylan, and A. Donmez, “Influence of scan strategy and process parameters on microstructure and its optimization in additively manufactured nickel alloy 625 via laser powder bed fusion,” International Journal of Advanced Manufacturing Technology, vol. 90, no. 5–8. pp. 1393–1417, 2017.

[191] W. E. King et al., “Observation of keyhole-mode laser melting in laser powder-bed fusion additive manufacturing,” Journal of Materials Processing Technology, vol. 214, no. 12, pp. 2915–2925, 2014.

[192] A. A. Martin et al., “Dynamics of pore formation during lasebed fusion additive manufacturing,” Nature Communications, no. 2019, pp. 1–10, 2019.

[193] B. C. Salzbrenner, “High-Throughput Tensile Testing Reveals Stochastic Properties in Additively Manufactured Steel,” 2017.

[194] T. Rothenburg, “The influence of microstructure and defects on the mechanical behaviour of stainless steel manufactured by laser powder bed fusion,” PhD 2021.

[195] J. A. Cherry, H. M. Davies, S. Mehmood, N. P. Lavery, S. G. R. Brown, and J. Sienz, “Investigation into the effect of process parameters on microstructural and physical properties of 316L stainless steel parts by selective laser melting,” The International Journal of Advanced Manufacturing Technology, vol. 76, no. 5, pp. 869–879, 2014.

[196] J. A. Harris and G. J. Mcshane, “Metallic stacked origami cellular materials :

additive manufacturing , properties , and modelling," 2019.

[197] F. Bartolomeu et al., "316L stainless steel mechanical and tribological behavior—A comparison between selective laser melting, hot pressing and conventional casting," Additive Manufacturing, vol. 16, pp. 81–89, 2017.

[198] T. Mukherjee, J.W. Elmer, H. Wei, Control of grain structure, phases, and defects in additive manufacturing of high-performance metallic components, Progress in Materials Science, June 2023.

[199] P. A. Hooper, "Melt pool temperature and cooling rates in laser powder bed fusion," Additive Manufacturing, vol. 22, no. May, pp. 548–559, 2018.

[200] T. G. Spears and S. A. Gold, "In-process sensing in selective laser melting (SLM) additive manufacturing," Integrating Materials and Manufacturing Innovation, vol. 5, no. 1, pp. 16–40, 2016.

[201] Quality-One, "Introduction to Statistical Process Control (SPC)," 2019. [Online]. Available: https://quality-one.com/spc/. Accessed: 08/11/2019.

[202] L. D. Sturm, M. I. Albakri, P. A. Tarazaga, and C. B. Williams, "In situ monitoring of material jetting additive manufacturing process via impedance based measurements," Additive Manufacturing, vol. 28, no. May, pp. 456–463, 2019.

[203] C. Li, C. H. Fu and Y. B. Guo, A multiscale modelling approach for fast prediction of part distortion in selective laser melting J Materials Processing Technology 229, 703, 2016.

[204] B. Marr, "What is digital twin technology - and why is it so important?," Forbes, 2017. [Online]. Available: https://www.forbes.com/sites/bernardmarr/2017/03/06/what-is-digital-twin-technology-and-why-is-it-so-important/#64d4893a2e2a. Accessed: 01/02/2026.

[205] M. Letenneur, A. Kreitcberg, and V. Brailovski, "Optimization of Laser Powder Bed Fusion Processing Using a Combination of Melt Pool Modeling and Design of Experiment Approaches: Density Control," Journal of Manufacturing and Materials Processing, vol. 3, no. 1, p. 21, 2019.

[206] TCT Magazine, 'Renishaw introduces two new metal 3D printer models and software,' [Online] Available: https://www.tctmagazine.com/renishaw-two-metal-3d-printing-systems-software-formnext/. Accessed: 05/11/2015.

[207] R.A. Garcia-Leon, J.A. Gomez-Camperos, H.Y. Jaramillo, Scientometric

Review of Trends on the Mechanical Properties of Additive Manufacturing and 3D Pritning, Journal of Materials Engineering and Performance, vol 30, p. 4724-4734, Octoer 2021.

[208] Wholers Associates, Wholers Report 3D Printing and Additive Manufacturing Global State of the Industry, 2022.

[209] I. S. Ramirez, F. P. G. Marquez and M. Papaelias, Review on additive manufacturing and non-destructive testing, Journal of Manufacturing Systems, vol 66 p. 260-286, February 2023.

[210] P. Witherell, Emerging Datasets and Analytics Opportunities in Metals Additive Manufacturing, NIST, 2018.

[211] S. Alkunte et al., "Porosity in Additive Manufacturing: influence on mechanical, thermal and electrical properties – a review." The International Journal of Advanced Manufacturing Technology, 140(5-6):2397-2421, 2025.

[212] S. Sinha, T. Mukherjee, "Mitigation of Gas Porosity in Additive Manufacturing Using Experimental Data Analysis and Mechanistic Modelling," Applications of Modelling and Machine Learning in Additive Manufacturing, Vol 17, 2024.

[213] Inside Metal Additive Manufacturing, "Practical Solutions for Metal AM Industrialisation" [Online]. Available: https://insidemetaladditivemanufacturing.com/. Accessed 14/012/2026.

[214] K. Zhang et al., "Influences of the scanning strategy on the quality, accuracy, microstructure and performance," Journal of Materials Research and Technology, vol 26, pp1962-1983. 2023.

[215] A. Soltani, M. S. Yasin, S. Shao, N. Shamsaei, Effects of Stripe Width on the Porosity and Mechanical Performance of Additively Manufactured Ti-6Al-4V Parts," Solid Freeform Fabrication, 2021.

[216] J. Robinson, I. Ashton, P. Fox, E. Jones, C. Sutcliffe, "Determination of the effect of scan strategy on residual stress in laser powder bed fusion additive manufacturing," Additive Manufacturing, vol 23, pp 13-24, 2018.

[217] H. Yeung, B. Lane, J. Fox, F. Kim, J. Heigel, J. E. Neira, "Continuous laser scan strategy for faster build speeds in laser powder bed fusion system," Solid Freeform Fabrication Symposium, 2017.

[218] C. Chen et al., "Residual Stress of Typical Parts in Laser Powder Bed Fusion," Journal of Manufacturing Processes, vol 59, pp 621-628, 2020.

[219] T. Bera, S. Mohanty, "A Review of Residual Stress in Metal Additive

Manufacturing," 3D Print Additive Manufacturing, vol 11(4), pp 1462-1470, 2024.

[220] E. Westphal, H. Seitz, "Porosity and density measurements of AM components: A comparative analysis of measurement methods across processes and materials", Materials Science in Additive Manufacturing, vol 4, 2025.

[221] R. Hayes, "Effect of Porosity Content on the Tensile Strength of Porous Materials," Powder Metallurgy, vol 14, issue 27, 1971.

[222] D. Wang, et al, Surface Characteristics and Roughness of Laser Powder Bed Fusion Processed Parts, Laser Powder Bed Fusion of Additive Manufacturing Technology, pp 179-222, 2023.

[223] W. Wcislik, R. Pata, "Some Microstructural Aspects of Ductile Fracture of Metals." Materials, 2021.